

Reduction of HIV-virion Transport
for Prevention of HIV Transmission

by

Bonnie E. Lai

Department of Biomedical Engineering
Duke University

Date: _____

Approved:

David F. Katz, Ph.D., Supervisor

S. Munir Alam, Ph.D.

David C. Montefiori, Ph.D.

George A. Truskey, Ph.D.

Fan Yuan, Ph.D.

Dissertation submitted in partial fulfillment of
the requirements for the degree of Doctor
of Philosophy in the Department of
Biomedical Engineering in the Graduate School
of Duke University

2010

ABSTRACT

Reduction of HIV-virion Transport
for Prevention of HIV Transmission

by

Bonnie E. Lai
Department of Biomedical Engineering
Duke University

Date: _____

Approved:

David F. Katz, Ph.D., Supervisor

S. Munir Alam, Ph.D.

David C. Montefiori, Ph.D.

George A. Truskey, Ph.D.

Fan Yuan, Ph.D.

An abstract of a dissertation submitted in partial
fulfillment of the requirements for the degree
of Doctor of Philosophy in the Department of
Biomedical Engineering in the Graduate School
of Duke University

2010

Copyright by
Bonnie E. Lai
2010

Abstract

This dissertation explores strategies for reducing HIV-virion transport to mucosal surfaces to prevent HIV infection. Infection requires contact between HIV and an infectable cell, so any means of inhibiting this step could contribute to HIV prevention. Our goals were to quantify the effects of strategies that reduce transport of HIV virions and to evaluate them in the context of HIV prevention. We used fundamental transport theory to design two basic strategies: (1) modifying the effective radius of virions; and (2) modifying the native medium through which virions diffuse. We proposed to implement these strategies using (1) anti-HIV antibodies that would bind and aggregate virions and (2) topically-applied semi-solid gels that coat vaginal epithelial surfaces.

We measured diffusion coefficients of HIV virions and HIV-like particles in the presence of antibodies and within semi-solid gels. In experiments with antibodies, we did not observe reductions in the diffusion coefficients. In experiments using particle tracking to measure the diffusion coefficients of virions in vaginal gels, we found that the diffusion coefficients in gels were approximately 10,000 times lower than those in water.

We proceeded to evaluate the potential for semi-solid gels to prevent HIV transmission at mucosal surfaces. From previous experiments in our lab that characterized the topical deployment of vaginal gels *in vivo*, we know that vaginal gels form an uneven coating on the epithelium with gel layer thicknesses of the order of hundreds of microns. Thus, we determined whether semi-solid gels could function as physical barriers to HIV when deployed as thin, incomplete layers on the epithelium.

We developed an experimental system to test the barrier functioning of thin gel layers. We applied thin gel layers to the porous membrane of a Transwell system, and added a solution of HIV to the top compartment. After incubation, samples were assayed for levels of HIV. We found that thin gel layers reduced levels of HIV in the bottom compartment compared to controls where no gel had been applied: There was a log reduction in levels of HIV in conditions where gel layers of approximately 150 μm thickness had been applied to the membrane after 0-, 4-, and 8-hour incubation. Thus, it appears possible for gel layers of thicknesses found *in vivo* to function as physical barriers to HIV over biologically-relevant time scales.

We studied how nonuniform deployment of semi-solid gels affects accumulation of virions in tissue using a mathematical model. We used transport theory to develop a model of HIV diffusing from semen, through gel layers where present, to tissue. Our findings suggest that comprehensive coating of over 80% of the tissue surface area and gel layer thicknesses over 100 μm are crucial to the barrier functioning of topical gels. Under these conditions, the level of viral restriction makes a significant contribution to increasing the time required for virions to reach tissue.

Overall, the work presented here applies transport theory in the context of HIV transmission and prevention. Results contribute to theoretical and experimental frameworks that can help understand events in HIV transmission and to design and evaluate new technologies for HIV prevention.

For my father, who dedicated his dissertation to me.

Contents

| | |
|---|--------|
| Abstract..... | iv |
| List of Tables | xiv |
| List of Figures..... | xvii |
| List of Abbreviations | xxviii |
| Acknowledgements..... | xxix |
| 1. Introduction..... | 1 |
| 1.1 The need for new biomedical technologies for HIV prevention..... | 1 |
| 1.2 Biomedical technologies for HIV prevention..... | 2 |
| 1.3 HIV/AIDS transmission via the female reproductive tract..... | 4 |
| 1.4 Targets for inhibiting HIV | 10 |
| 1.5 Transport phenomena in HIV transmission and prevention | 13 |
| 1.5.1 Transport of cell-associated HIV | 16 |
| 1.5.2 Transport of HIV virions | 21 |
| 1.6 Using transport theory to design and evaluate strategies for HIV prevention..... | 26 |
| 2. Reduction of HIV-virion diffusion coefficients by antibody binding and aggregation | 30 |
| 2.1 Introduction..... | 30 |
| 2.1.1 Possible roles of antibodies in HIV prevention | 30 |
| 2.1.2 Antibody isotypes within the female reproductive tract | 32 |
| 2.1.3 Mechanisms of antibody action | 33 |
| 2.1.3.1 Neutralization..... | 34 |
| 2.1.3.2 Blocking epithelial attachment and transcytosis..... | 37 |

| | |
|---|----|
| 2.1.3.3 Fc-mediated effector functions | 37 |
| 2.1.3.4 Immune exclusion..... | 38 |
| 2.1.4 A model system of HIV-like liposomes..... | 39 |
| 2.1.5 Theoretical effects of antibody binding and aggregation | 41 |
| 2.2 Materials and Methods..... | 43 |
| 2.2.1 Experiments measuring diffusion coefficients of liposomes in the presence of antibodies | 43 |
| 2.2.1.1 Materials | 43 |
| 2.2.1.2 Liposome preparation | 44 |
| 2.2.1.3 Experimental conditions | 45 |
| 2.2.1.4 Postphotoactivation scanning experiments..... | 47 |
| 2.2.1.5 Characterization of liposomes..... | 51 |
| 2.2.2 Mathematical model of aggregation | 51 |
| 2.2.2.1 Binding of antibodies to spikes on virions..... | 53 |
| 2.2.2.2 Dissociation of antibodies from spikes on virions and aggregates..... | 56 |
| 2.2.2.3 Aggregation resulting from crosslinking | 56 |
| 2.3 Results..... | 67 |
| 2.3.1 Experiments measuring diffusion coefficients of liposomes in the presence of antibodies | 67 |
| 2.3.2 Mathematical model of aggregation | 77 |
| 2.3.2.1 Sensitivity to ratio of epitope-binding sites on antibodies to epitopes | 85 |
| 2.3.2.2 Sensitivity to rate constant of crosslinking and concentration..... | 88 |
| 2.4 Discussion..... | 91 |
| 2.5 Conclusions..... | 97 |

| | |
|---|-----|
| 3. Reduction of HIV-virion diffusion coefficients by semi-solid gels..... | 99 |
| 3.1 Introduction..... | 99 |
| 3.1.1 Semi-solid gels used in vaginal drug delivery | 100 |
| 3.1.2 Particle transport in semi-solid gels | 102 |
| 3.1.3 Methods for quantifying diffusion coefficients | 105 |
| 3.2 Materials and Methods..... | 110 |
| 3.2.1 Microbicide placebo gels from clinical trials..... | 110 |
| 3.2.2 Particle tracking | 110 |
| 3.2.2.1 Preparation of fluorescently-labeled HIV-1..... | 110 |
| 3.2.2.2 Sample preparation | 111 |
| 3.2.2.3 Microscopy | 112 |
| 3.2.2.4 Analysis..... | 113 |
| 3.2.3 Postphotoactivation scanning of HIV-like liposomes..... | 117 |
| 3.2.3.1 Preparation of HIV-like liposomes | 117 |
| 3.2.3.2 Sample Preparation | 121 |
| 3.2.3.3 Imaging fluorescent profiles | 121 |
| 3.2.3.4 Analysis..... | 122 |
| 3.3. Results..... | 124 |
| 3.3.1 Particle tracking of HIV virions in HEC and MC..... | 124 |
| 3.3.2 Accuracy of diffusion coefficients obtained via particle tracking | 128 |
| 3.3.3 Postphotoactivation scanning of HIV-like liposomes in HEC and MC dilutions | 131 |
| 3.4 Discussion..... | 137 |

| | |
|--|-----|
| 3.4.1 Summary of measured diffusion coefficients | 137 |
| 3.4.2 Comparison to diffusion coefficients of HIV in other gels..... | 137 |
| 3.4.3 Comparison to theoretical predictions for diffusion coefficients | 138 |
| 3.4.3 Effect of dilution | 142 |
| 3.4.5 Interpretation using mathematical model of virion diffusion | 145 |
| 3.4.6 Context of placebo gels <i>in vivo</i> | 146 |
| 3.5 Conclusions..... | 148 |
| 4. Evaluation of physical barrier functioning of semi-solid gels using experimental model of HIV transmission..... | 149 |
| 4.1 Introduction..... | 149 |
| 4.1.1 Experimental models of HIV transmission..... | 150 |
| 4.1.2 Assay for testing physical barrier function of thin gel layers | 153 |
| 4.2 Materials and Methods..... | 154 |
| 4.2.1 Gels | 155 |
| 4.2.2 Thin gel layers..... | 156 |
| 4.2.3 Viruses | 157 |
| 4.2.4 Transwell experiment..... | 157 |
| 4.2.5 TZM-bl assay | 158 |
| 4.2.6 Analyses..... | 160 |
| 4.3 Results..... | 161 |
| 4.3.1 Evaluation of two commonly-used vaginal gels | 161 |
| 4.3.2 Evaluation of gel layers of varying thickness | 163 |
| 4.3.3 Characterization studies | 164 |

| | |
|---|-----|
| 4.3.3.1 Thickness and distribution of gel layers | 164 |
| 4.3.3.2 Linear range of TZM-bl assay | 166 |
| 4.3.3.3 Dose-dependent neutralization by placebo gels..... | 168 |
| 4.3.3.4 HIV-1 viability over time..... | 168 |
| 4.3.3.5 Comparison of experimental results to mathematical model of 1D diffusion | 170 |
| 4.4 Discussion | 174 |
| 4.5 Conclusions..... | 178 |
| 5. Mathematical model for kinetics of HIV diffusion to tissue surfaces in the presence of realistically deployed semi-solid gels | 179 |
| 5.1 Introduction..... | 179 |
| 5.1.1 Pharmacokinetic and pharmacodynamic models in HIV/AIDS | 179 |
| 5.1.2 Stochastic model of microbicide functioning | 180 |
| 5.1.3 Deterministic model of microbicide functioning..... | 181 |
| 5.2 Materials and Methods..... | 184 |
| 5.2.1 Governing equations | 186 |
| 5.2.2 Boundary conditions | 186 |
| 5.2.3 Initial conditions | 188 |
| 5.2.4 Parameters..... | 188 |
| 5.2.4.1 Diffusion coefficients..... | 189 |
| 5.2.4.2 Geometry..... | 190 |
| 5.2.4.3 HIV viral load and threshold..... | 191 |
| 5.2.5 <i>In vivo</i> imaging studies | 192 |
| 5.2.6 Numerical methods | 193 |

| | | |
|---------|--|-----|
| 5.2.6.1 | Modeling of surface entirely coated at constant thickness | 194 |
| 5.2.6.2 | Using model to evaluate trade-offs between coating thickness and fractional area coated | 195 |
| 5.2.6.3 | Application to data from <i>in vivo</i> experiments..... | 196 |
| 5.3 | Results..... | 197 |
| 5.3.1 | Initial modeling of complete coating with constant thickness..... | 197 |
| 5.3.2 | Modeling of conserved volume of gel | 199 |
| 5.3.3 | Trade-offs between thickness and area coated..... | 200 |
| 5.3.4 | Effect of reducing virion diffusion coefficient | 201 |
| 5.3.5 | Application of model to <i>in vivo</i> data..... | 202 |
| 5.4 | Discussion | 208 |
| 5.5 | Conclusions..... | 214 |
| 6. | Conclusions..... | 215 |
| 6.1 | Summary | 215 |
| 6.2 | Context..... | 218 |
| 6.2.1 | Significance of hindering HIV transport at mucosal surfaces | 218 |
| 6.2.2 | Trends in microbicides development | 219 |
| 6.2.3 | Efficacy of placebo gels in microbicides clinical trials | 222 |
| 6.3 | Future directions | 225 |
| 6.3.1 | Recommendations for preclinical testing of microbicide gels..... | 225 |
| 6.3.2 | Pharmacokinetic and pharmacodynamic models for microbicide functioning | 227 |
| 6.3.3 | Design of advanced materials that act as topical barriers to HIV | 227 |
| 6.3.4 | Design of a true placebo for microbicides clinical studies | 228 |

| | |
|---|-----|
| 6.3.5 Furthering understanding of mechanisms of transport and relationship between viral inoculum and infection | 229 |
| 6.4 Theoretical and experimental methods for HIV/AIDS research..... | 229 |
| Appendix. Postphotoactivation scanning with multiple diffusing species | 231 |
| A.1 Example of analysis assuming multiple diffusing species..... | 231 |
| A.2 Experimental validation using a solution with multiple diffusing species | 236 |
| A.2.1 Fluorescein | 237 |
| A.2.2 Dextrans | 238 |
| A.2.3 Multiple diffusing species | 242 |
| A.3 Characterization of lower limit of detection and resolution | 245 |
| A.3.1 Experimental characterization of noise | 246 |
| A.3.2 Simulations to determine lower limit of detection..... | 248 |
| A.3.3 Comparison of simulated and experimental results | 253 |
| References..... | 256 |
| Biography..... | 279 |

List of Tables

| | |
|--|----|
| Table 1. Values for the diameter of HIV virions previously reported in the literature.... | 23 |
| Table 2. Scenarios of HIV binding by immunoglobulins (Ig) and resulting effective diffusion coefficients. Hydrodynamic radii of HIV and Ig were obtained from the literature. The radii of HIV bound by Ig, R_{HIV+Ig} , was estimated by summing the radius of HIV and the diameter of the Ig. This assumes that the HIV virion is completely coated by Ig binding, and that the resulting particle is effectively a sphere. Diffusion coefficients were estimated using the Stokes-Einstein equation assuming spherical particle geometry. Time required to diffuse 100 μm was estimated assuming diffusion in 2D for which $t \sim l^2/4D$. We assumed temperature of 37°C and medium viscosity of 1 cP. | 42 |
| Table 3. Scenarios of HIV aggregation by polymeric Ig and resulting effective diffusion coefficients. Diffusion coefficients were estimated using the Stokes-Einstein equation assuming spherical particle geometry unless otherwise noted. Time required to diffuse 100 μm was estimated assuming diffusion in 2D for which $t \sim l^2/4D$. We used temperature of 37°C and medium viscosity of 1 cP. | 42 |
| Table 4. Summary of parameters used in experiments: peptide:lipid ratio (P:L ratio); dilution of dextran stock solution expressed in terms of the ratio of volume of stock solution to volume of PBS; antibody isotypes tested; antibody:epitope ratios (A:E ratios); incubation protocol; liposome dilution used in postphotoactivation scanning experiments expressed in terms of the fraction of volume of liposome solution to total sample volume; and the time course of acquiring images in postphotoactivation scanning including the number of images acquired, the average time elapsed between images and the average time elapsed from the first image to the final image. | 46 |
| Table 5. Variables used in mathematical model of virion aggregation by IgA. | 66 |
| Table 6. Constants used in mathematical model of virion or liposome aggregation by IgA. *Values were derived from literature except for the constant of crosslinking, which is currently unknown..... | 66 |
| Table 7. Diffusion coefficients (mean \pm SE, n = 4 replicates unless otherwise noted) of liposomes in the presence of 2F5 IgG, IgA, and IgM..... | 71 |
| Table 8. Diffusion coefficients (mean \pm SE, n = 4 replicates unless otherwise noted) of liposomes in the presence of different concentrations of IgA. For liposomes with 2F5 epitope peptide, the peptide:lipid ratio (P:L) was 1:420..... | 72 |

| | |
|---|-----|
| Table 9. Diffusion coefficients (mean \pm SE, n = 4 replicates unless otherwise noted) of liposomes in the presence of different concentrations of IgA. For liposomes with 2F5 epitope peptide, the peptide:lipid ratio (P:L) was 1:100..... | 75 |
| Table 10. Table of polymers commonly used in vaginal formulations and microbicides. | 101 |
| Table 11. Comparison of methods for measuring diffusion coefficient (D)..... | 107 |
| Table 12. Concentrations of gels for which diffusion coefficients (D) were measured. | 109 |
| Table 13. Lipid composition of HIV, from [101]. | 118 |
| Table 14. Synthetic liposome formulation based on composition of HIV-1 Env (designed by Dr. Patrick Kiser, University of Utah). | 119 |
| Table 15. Values of diffusion coefficient for HIV virions and 100-nm beads in HEC and MC. | 129 |
| Table 16. Diffusion coefficients (mean \pm SE, n = 3) in glycerol solutions. Experiments were performed at 37° C. Theoretical values for diffusion coefficient were calculated using Stokes-Einstein, assuming spherical particle of 126-nm diameter. | 130 |
| Table 17. Diffusion coefficients obtained (mean \pm SE) from postphotoactivation scanning of HIV-like liposomes in HEC and MC dilutions, and PBS. | 136 |
| Table 18. Examples of cell-based assays used in evaluation of microbicide candidates. | 151 |
| Table 19. Thicknesses of gel layers (mean \pm SE) for different collar heights and gel volumes (n = 12 for HEC, n = 6 for MC). | 165 |
| Table 20. Parameters used in model of HIV-virion diffusion from semen through microbicide gel..... | 189 |
| Table 21. Summary measures for <i>in vivo</i> deployment data. The numbers “1” and “2” represent data from two independent experiments for each gel/ protocol. K = KY Jelly, R = Replens. +/- simulated coitus..... | 205 |
| Table 22. Comparison of diffusion coefficients measured here to values published in the literature. Diffusion coefficients ($D_{\text{experiment}}$) of fluorescein and dextrans in PBS were measured by postphotoactivation scanning. All experiments were performed at room | |

temperature, approximately 24-25° C. Literature values for the diffusion coefficient were obtained using FRAP or *diffusion into slab..... 236

List of Figures

| | |
|--|----|
| Figure 1. Sites of HIV transmission in the female genital tract. (A) HIV transmission most likely occurs via vaginal and cervical tissues. (B) HIV transmission across vaginal and ectocervical tissues. HIV is introduced via semen. The outermost layer of ectocervical and vaginal tissues consists of multi-layered squamous epithelium. The stroma contains immune cells that may be infected by HIV, including T lymphocytes, macrophages, and Langerhans cells. (C) Endocervical tissue consists of a single-layered columnar epithelium covered by cervical mucus..... | 5 |
| Figure 2. Course of HIV infection (A) in cervicovaginal tissue and (B) systemically. Figures adapted from [14, 18]..... | 8 |
| Figure 3. Potential targets for inhibiting the HIV life cycle. HIV virions diffuse to bind with the CD4 receptor and CCR5 or CXCR4 co-receptor on the target cell membrane. This dissertation focuses on reducing diffusion of HIV virions. After binding, receptor-mediated fusion of the virion and target cell occurs. A recent study suggests that HIV may require endosome-mediated fusion [65]. Within the cytoplasm, reverse transcriptase catalyzes the reverse transcription of viral RNA to cDNA. To date, most microbicide agents have targeted free virions, entry, fusion, or reverse transcription. Vaccines use neutralizing antibodies to target extracellular virions and inhibit attachment, entry, and fusion. T-cell vaccines target cell-associated virus. Figure adapted from [66-68]..... | 11 |
| Figure 4. Proposed mechanisms of cell-associated HIV transport. (A) HIV is introduced to the vaginal lumen via semen as both cell-associated HIV and cell-free virions. HIV virion diffusion can be described by random walk. Cell migration can be described by random walk with persistence. (B) Cells may migrate to the epithelium, where they bud virions that diffuse through gaps in the epithelium. (C) Cells may migrate through the epithelium, perhaps through ulcers, to the stroma or into the lymphatic system. (D) Direct cell-to-cell transmission of HIV occurs through nanotubes. | 17 |
| Figure 5. Probability of infection per exposure event as a function of viral load (in blood) according to Equation 3. We used two sets of estimated values for baseline probability and viral load: $\beta_0 = 0.0005$, $V_0 = 10^{4.5}$ copies/ml [97]; $\beta_0 = 0.1$, $V_0 = 10^7$ copies/ml [88]. | 22 |
| Figure 6. HIV virion structure and components. | 24 |
| Figure 7. Diffusion coefficients predicted by the Stokes-Einstein equation (Equation 6) for varying left: particle diameter and right: effective viscosity of medium. | 26 |
| Figure 8. Topics presented in this dissertation..... | 27 |

| | |
|---|----|
| Figure 9. Antibodies can be used to modify effective radii via specific (A) binding or (B) aggregation of virions. | 30 |
| Figure 10. Relevant antibody isotypes, with molecular weights (MW) [117] and hydrodynamic radii (R). References for R are listed in Table 2. (A) IgG: The Fab portion binds antigens. The Fc region is responsible for effector functions such as opsonization and antibody-dependent cell-mediated cytotoxicity. (B) Dimeric IgA: The J chain is a polypeptide that covalently links IgA monomers. (C) Secretory IgA: The secretory component of secretory IgA is derived from the receptor that transports the IgA across epithelial cells. (D) Pentameric IgM contains five monomers linked by disulfide bonds. | 33 |
| Figure 11. Mechanisms of antibody action: (A) neutralization; (B) blocking epithelial attachment or transcytosis; (C) Fc-mediated effector functions such as antibody-dependent cell-mediated cytotoxicity (ADCC); and (D) immune exclusion..... | 33 |
| Figure 12. HIV-1 spike interacting with cell membrane receptor CD4 and co-receptor CCR5. Binding is mediated by gp120 and fusion is mediated by gp41. Reproduced with permission from Macmillan Publishers Ltd: <i>Nature Reviews Microbiology</i> from Ref. [122] © (2008) and from <i>Nature</i> Ref. [102] © (2006). | 35 |
| Figure 13. HIV-1 envelope spike with binding sites of broadly neutralizing antibodies. Antibodies b12 and 2G12 bind gp120 whereas 4E10 and 2F5 bind gp41. Reproduced with permission from Bentham Science Publishers Ltd: <i>Current Pharmaceutical Design</i> from Ref. [128] © (2007). | 36 |
| Figure 14. Liposomes used in postphotoactivation scanning experiments. The lipid composition is POPC:POPE:DMPA:chol (45:25:20:1.33). The ratio of 2F5 epitope (Sp62-GTH1) peptide to lipid was 1:100 or 1:420. | 40 |
| Figure 15. Slide preparation for postphotoactivation scanning: (A) A spacer is adhered to a glass slide; (B) The sample is applied within the spacer; (C-D) The chamber is sealed with a glass cover slip. | 47 |
| Figure 16. Apparatus used for uncaging: (A) A metal stencil with slit width of 200 μm is used to uncage a linear region of the sample; (B) The slide is placed underneath the stencil within an apparatus used to ensure proper alignment; (C) An additional UV filter is placed on top of the assembly; (D) A mercury arc lamp provides the UV light source. | 48 |
| Figure 17. Chemical structure of caged fluorescein used in postphotoactivation scanning. Upon exposure to UV light, the caged-fluorescein becomes fluorescent. (Adapted from invitrogen.com.)..... | 48 |

| | |
|---|----|
| Figure 18. The kinetics of three processes are described in the mathematical model: (A) binding of antibodies to spikes on virions; (B) dissociation of antibodies from spikes on virions; and (C) aggregation resulting from crosslinking. | 52 |
| Figure 19. Aggregation reaction. The concentration of aggregates with i number of particles increases due to aggregation of particles with j and $i-j$ particles. The concentration decreases due to further aggregation with aggregates of j particles..... | 57 |
| Figure 20. Diffusion problem used to calculate the collision frequency. | 59 |
| Figure 21. Surface Plasmon Resonance (SPR) results showing interaction of 2F5 antibodies with 2F5 epitope peptide liposomes. Response of control liposomes (no peptide) was subtracted from response of peptide liposomes. Antibodies were injected at concentrations of 100 $\mu\text{g/ml}$ at flow rate of 20 $\mu\text{l/min}$ for 2 minutes. SPR measurements were performed by Kara Anasti..... | 67 |
| Figure 22. Examples of results from postphotoactivation scanning of liposomes with 2F5 epitope peptide with different isotypes of 2F5 antibody. For each condition, top: images over time (red = high intensity, blue = low intensity); bottom left: $\alpha(D)$; and bottom right: intensity profiles fit to diffusion model. | 70 |
| Figure 23. Diffusion coefficients of liposomes in the presence of 2F5 IgG, IgA, and IgM (mean \pm SE, $n = 4$ replicates unless otherwise noted). | 70 |
| Figure 24. Diffusion coefficients of liposomes in the presence of different concentrations of IgA (mean \pm SE, $n = 4$ replicates unless otherwise noted). For liposomes with 2F5 epitope peptide, the peptide:lipid ratio (P:L) was 1:420..... | 72 |
| Figure 25. Examples of results from postphotoactivation scanning of liposomes with 2F5 epitope peptide and 2F5 dimeric IgA antibody. For each condition, top: images over time (red = high intensity, blue = low intensity); bottom left: $\alpha(D)$; and bottom right: intensity profiles fit to diffusion model. Here, the peptide:lipid ratio (P:L) was 1:420. | 74 |
| Figure 26. Diffusion coefficients of liposomes in the presence of different concentrations of IgA (mean \pm SE, $n = 4$ replicates unless otherwise noted). For liposomes with 2F5 epitope peptide, the peptide:lipid ratio (P:L) was 1:100..... | 75 |
| Figure 27. Examples of results from postphotoactivation scanning of liposomes with 2F5 epitope peptide with 2F5 dimeric IgA antibody. For each condition, top: images over time (red = high intensity, blue = low intensity); bottom left: $\alpha(D)$; and bottom right: intensity profiles fit to diffusion model. Here, the peptide:lipid ratio (P:L) was 1:100. . | 77 |

| | |
|---|----|
| Figure 28. Mathematical model results for portion of spikes bound by antibody on each liposome over time and normalized concentration of antibody over time. The antibody concentration is normalized to the initial concentration of antibodies. | 78 |
| Figure 29. The probability of crosslinking over time in the mathematical model..... | 78 |
| Figure 30. Mathematical model results for concentration of individual liposomes over time. Concentration is normalized to the initial concentration of liposomes. | 79 |
| Figure 31. Mathematical model results for concentration profiles of liposome aggregates over time. Concentrations are normalized to the initial concentration of liposomes..... | 80 |
| Figure 32. Distribution of diffusion coefficients resulting from mathematical model of liposome aggregation. | 81 |
| Figure 33. Example of simulated postphotoactivation scanning results from inputting the distribution of diffusion coefficients from the mathematical model of liposome aggregation for t = 0 (Figure 32). At t = 0 h, none of the liposomes are aggregated, so this also represents the control condition. Left: $\alpha(D)$; Right: intensity profiles fit to diffusion model. | 82 |
| Figure 34. Example of simulated postphotoactivation scanning results from inputting the distribution of diffusion coefficients from the mathematical model of liposome aggregation for t = 4 h (Figure 32). Left: $\alpha(D)$; Right: intensity profiles fit to diffusion model..... | 83 |
| Figure 35. Example of simulated postphotoactivation scanning results from inputting the distribution of diffusion coefficients from the mathematical model of liposome aggregation with free label and noise for t = 0. At t = 0 h, none of the liposomes are aggregated, so this also represents the control condition. Left: $\alpha(D)$; Right: intensity profiles fit to diffusion model. | 84 |
| Figure 36. Example of simulated postphotoactivation scanning results from inputting the distribution of diffusion coefficients from the mathematical model of liposome aggregation with free label and noise for t = 4 h. Left: $\alpha(D)$; Right: intensity profiles fit to diffusion model. | 84 |
| Figure 37. Comparison of aggregation model results for (A) low and (B) high antibody:epitope (A:E) ratios. The A:E ratio refers to the ratio of the number of epitope-binding sites on antibodies to the number of epitopes. Note that plots have different time scales. | 87 |

| | |
|---|-----|
| Figure 38. Example of simulated postphotoactivation scanning results from inputting the distribution of diffusion coefficients from the mathematical model of liposome aggregation for A:E ratio = 5 and t = 4 h (Figure 37B5) with free label and noise. Controls are shown in Figure 33 (without noise and free label) and Figure 35 (with same levels of noise and free label). Left: $\alpha(D)$; Right: intensity profiles fit to diffusion model. | 88 |
| Figure 39. Comparison of aggregation model results for (A) reduced $k_{crosslink}$ and (B) reduced C_{v0} | 90 |
| Figure 40. Scenarios of particle size in relation to gel structures. (A) Size of diffusing particles is much smaller than mesh size. (B) Size of diffusing particles is similar to mesh size. (C) Size of diffusing particles is much greater than mesh size. | 103 |
| Figure 41. Scheme for calculating the diffusion coefficient from single-particle tracking. | 114 |
| Figure 42. Liposome labeled for use in postphotoactivation scanning..... | 118 |
| Figure 43. Cryo-electron microscopy tomography characterizing the spatial distribution of Env spikes on (a) SIV and (b-d) HIV-1. These surface-rendered models of virions suggest that spikes cover only a small portion of the HIV-1 virion surface, leaving much of the lipid portion exposed. Scale bar = 50 nm. Reproduced with permission from Macmillan Publishers Ltd: Nature from Ref. [102] © (2006)..... | 120 |
| Figure 44. Examples of tracks obtained for fluorescently-labeled HIV virions in HEC and MC, and for 100-nm bead dried to glass slide. Particles were tracked for 41s..... | 125 |
| Figure 45. Examples of plots for MSD vs. τ for HIV in HEC and MC. Data represent different virions within single experiments. | 126 |
| Figure 46. Diffusion coefficients (mean \pm SE, n = 3 independent experiments) obtained using particle tracking of fluorescently-labeled HIV in HEC and MC undiluted, diluted to 50% (v/v) in PBS, and diluted to 20% (v/v) in PBS. Values are given in Table 15..... | 127 |
| Figure 47. Comparison of diffusion coefficients (mean \pm SE) for HIV and 100-nm beads in HEC and MC (n = 3). Diffusion coefficients were not significantly different except for in 20% HEC (t-test, p < 0.05) | 129 |
| Figure 48. Example plot of MSD vs. τ for 100-nm beads dried to glass slide from one experiment. Data represent MSDs of different particles. | 131 |

| | |
|--|-----|
| Figure 49. Examples of results from postphotoactivation scanning of HIV-like liposomes in MC dilutions (A-E) and PBS (F). For each condition, top: images over time (red = high intensity, blue = low intensity), bottom left: plot of $\alpha(D)$, and bottom right: intensity profiles fit to diffusion model. | 135 |
| Figure 50. Diffusion coefficients (mean \pm SE) obtained from postphotoactivation scanning of HIV-like liposomes in HEC and MC dilutions, and PBS. See Table 17 for detailed results. | 136 |
| Figure 51. Comparison of cone-and-plate viscosities for undiluted HEC and MC and effective viscosities calculated from measured diffusion coefficients of HIV virions and 100-nm beads in HEC and MC (Table 15). To calculate the effective viscosity, we used the Stokes-Einstein relation (Equation 6), temperature of 37° C, and particle diameters of 125 nm and 126 nm for HIV and 100-nm beads, respectively. Cone-and-plate viscometry data were collected by Jennifer Peters. | 140 |
| Figure 52. Summary of diffusion coefficients of HIV-like liposomes and HIV virions in HEC and MC. Values for undiluted, 50%, and 20% (v/v) gel in PBS were obtained using particle tracking. Values for 10%, 5%, 2% (v/v) gel in PBS were obtained using postphotoactivation scanning of HIV-like liposomes. | 144 |
| Figure 53. Interpretation of experimentally-measured diffusion coefficients using mathematical model of diffusion of HIV virions from semen, through microbicide layer, to tissue compartment. (A) Schematic of mathematical model. Measured diffusion coefficients were input to the model. Plots show percent of virions in the tissue compartment, as a function of time, for various concentrations of (B) HEC and (C) MC. | 145 |
| Figure 54. (A) Idealized scenario of HIV transmission in the presence of a microbicide. (B) Transwell system for evaluating barrier function of topical gels. | 153 |
| Figure 55. Transwell system to evaluate barrier functioning of thin gel layers. | 155 |
| Figure 56. (A) Applicator used to apply thin gel layers to Transwell membrane. (B) Gel is applied to tip of rod. (C) Gel layer thickness is controlled by adjusting gel volume and collar depth. | 156 |
| Figure 57. Levels of HIV-1 in bottom compartment of Transwell for two semi-solid gels, HEC and MC ($n \geq 4$ independent experiments). Experimental results are normalized to controls where no gel was applied to the membrane, such that % control = $RLU_{bottom,experiment}/RLU_{bottom,control}$. Additional control experiments were performed in | |

which an equivalent amount of gel was mixed in to solutions. For 0-, 4-, and 8-hour incubations, there was a log reduction in levels of HIV-1 in the bottom compartment. 162

Figure 58. Transwell assay results for various thicknesses of HEC gel ($n \geq 4$ independent experiments). Experimental results are normalized to controls where no gels were applied to the membrane, such that $\% \text{ control} = RLU_{bottom,experiment}/RLU_{bottom,control}$. Characterization of gel layer thickness is shown in Table 19 (p. 165). 164

Figure 59. Standard curves relating fluorescence intensity and thickness for Left: HEC and Right: MC labeled with fluorescein. 165

Figure 60. Examples of gel distributions applied to membranes in Transwell system.. 166

Figure 61. Linear range of TZM-bl assay for HIV-1 strains used in Transwell experiments ($n = 4$). Levels of luminescence are expressed as Relative Luminescence Units, RLU..... 167

Figure 62. Luminescence values (mean \pm SE) for experimental conditions and controls are within the linear range of the TZM-bl assay shown in Figure 61. Data are pooled from various conditions in $n = 14$ independent experiments. Levels of luminescence are expressed as Relative Luminescence Units, RLU. 167

Figure 63. Neutralization of HIV-1 DU156 and TRO by HEC and MC gels ($n = 4$). Equivalent concentrations used in the Transwell are annotated to the plot. HEC and MC did not neutralize HIV-1 at the concentrations used in the Transwell..... 168

Figure 64. Levels of HIV in the bottom compartment of no-gel controls (mean \pm SE, $n \geq 4$). 169

Figure 65. Total levels of HIV in the Transwell (mean \pm SE, $n \geq 4$). RLU values were calculated according to Equation 58. Data were fit to exponential curves to calculate half-life..... 170

Figure 66. Mathematical model of HIV transport in Transwell experiments..... 171

Figure 67. Comparison of theoretical predictions and experimental results (mean \pm SE, $n \geq 4$) for portion of HIV in the bottom compartment of no-gel controls. 172

Figure 68. Comparison of theoretical predictions and experimental results (mean \pm SE, $n \geq 4$) for Transwell with approximately 150- μm gel layer. Theoretical predictions are shown in black, gray and white. Experimental results for HEC and MC are shown in red and blue, respectively. Left: Results are expressed in terms of portion in the bottom

| | |
|---|-----|
| compartment, calculated according to Equation 59. Right: Results are normalized to no-gel control, according to Equation 57. | 173 |
| Figure 69. Idealized scenario of HIV transmission in the female reproductive tract in the presence of a microbicide gel. A microbicide gel is applied before coitus to partially coat the vaginal epithelium. Semen containing HIV virions is deposited in the lower female reproductive tract. HIV virions must diffuse from semen, through the gel layer, to reach tissue surfaces. | 182 |
| Figure 70. Diagram of mathematical model for HIV diffusion from semen, through topical microbicide, to tissue. | 185 |
| Figure 71. Schematic showing how mathematical model is used to interpret data from <i>in vivo</i> deployment experiments. | 196 |
| Figure 72. Accumulation of virions in tissue compartment over time for varying thickness of gel layer. Time to threshold is calculated by finding the time for which the number of virions in the tissue compartment is equal to the threshold value. Increasing the thickness of the gel layer increases the time to threshold. $D_{HIV,gel} = 0.5 D_{semen}$ (Table 20). | 198 |
| Figure 73. Accumulation of virions in tissue compartment over time for varying levels of viral restriction. Time to threshold is calculated by finding the time for which the number of virions in the tissue compartment is equal to the threshold value. Decreasing the diffusion coefficient of virus in gel increases the time to threshold. Here, $h_{gel} = 300 \mu\text{m}$ (Table 20). | 199 |
| Figure 74. Trade-offs between gel layer thickness and area coated when the volume of gel is conserved as described in Equation 70, for different values of viral restriction. As the fractional area coated increases, time to threshold increases. | 200 |
| Figure 75. Contour plot showing values of threshold time for different gel thicknesses and fractional areas coated. Note that fractional area coated is the more important factor for all but the thinnest gel layers. | 201 |
| Figure 76. Contour plot showing values of threshold time for different levels of viral restriction and fractional areas coated. When fractional area coated is greater than 0.80, then levels of viral hindrance contribute significantly to threshold time. | 202 |
| Figure 77. Contour plots depicting deployment data from selected <i>in vivo</i> experiments. Black represents undetectable coating (thickness $\sim 0 \mu\text{m}$), white represents coating thickness $> 500 \mu\text{m}$, and gray areas represent coating thicknesses between 0-500 μm . Axial length indicates distance from the end of the probe tube, which is placed in the | |

fornix of the vagina. Angle indicates the position of the endoscope during imaging. Data represent the first (prefix “1”) of two independent experiments for each gel/ protocol listed in Table 21. K = KY Jelly, R = Replens. +/- simulated coitus. Note that simulated coitus increased the fractional area coated for both gels. 204

Figure 78. Resulting threshold times for application of mathematical model to experimental data obtained from deployment of vaginal gels in women. The numbers “1” and “2” represent data from two independent experiments for each gel/ protocol. K = KY Jelly, R = Replens. +/- = with/ without simulated coitus. Three levels of viral hindrance were input ($D_{gel}/D_{semen} = 0.1, 0.5, 1$)..... 206

Figure 79. Comparison of the use of arithmetic and harmonic means to approximate thickness of gel coating in the mathematical model. The arithmetic and harmonic means of the thicknesses were calculated from experimental data. The calculated means and experimental fractional area coated were input to the HIV transport model to determine $t_{threshold}$. The harmonic mean better approximated the results derived from discretizing the thickness data into 50- μ m bins. The numbers “1” and “2” represent data from two independent experiments for each gel/ protocol. K = KY Jelly, R = Replens. +/- = with/ without simulated coitus. 207

Figure 80. Observed effectiveness for different values of microbicide and placebo efficacies calculated using Equation 73 [162]. 224

Figure 81. Simulated initial condition using Gaussian curve described by Equation 75. 232

Figure 82. Simulated intensity profiles for 2 diffusing species. 233

Figure 83. Simulated postphotoactivation scanning data. 233

Figure 84. Examples of sets of diffusion profiles used in analysis. Left: Set of diffusion profiles generated for D_{min} . Right: Set of diffusion profiles generated for D_{max} 234

Figure 85. Results from analysis of simulated postphotoactivation scanning data. Left: $\alpha(D)$. Red asterisks indicate diffusion coefficients used to generate simulated data. Right: intensity profiles fit to diffusion model. 236

Figure 86. Example of postphotoactivation scanning results for fluorescein diffusing in PBS. Top: images over time (red = high intensity, blue = low intensity); Bottom left: $\alpha(D)$; and Bottom right: intensity profiles fit to diffusion model..... 237

Figure 87. Examples of postphotoactivation scanning results for dextrans of various molecular weights in PBS. Top: images over time (red = high intensity, blue = low

| | |
|---|-----|
| intensity); Bottom left: $\alpha(D)$; and Bottom right: intensity profiles fit to diffusion model. | 240 |
| Figure 88. Diffusion coefficients for dextrans of various molecular weights with power law fit. | 241 |
| Figure 89. Example of postphotoactivation scanning results for mixture of 10- and 500-kD dextrans in PBS. Top: images over time (red = high intensity, blue = low intensity); Bottom left: $\alpha(D)$; and Bottom right: intensity profiles fit to diffusion model. | 243 |
| Figure 90. Example of postphotoactivation scanning results for mixture of 70- and 500-kD dextrans in PBS. Top: images over time (red = high intensity, blue = low intensity); Bottom left: $\alpha(D)$; and Bottom right: intensity profiles fit to diffusion model. | 244 |
| Figure 91. Example of postphotoactivation scanning results for mixture of 10-, 70-, and 500-kD dextrans. Top: images over time (red = high intensity, blue = low intensity); Bottom left: $\alpha(D)$; and Bottom right: intensity profiles fit to diffusion model. | 245 |
| Figure 92. Intensity profiles for caged fluorescein in epoxy. Each plot represents 9 intensity profiles over time for each of the 8 experiments performed. | 247 |
| Figure 93. Examples of simulated postphotoactivation scanning intensity profiles with varying levels of random noise added. | 249 |
| Figure 94. Simulations characterizing the lower limit of detection of postphotoactivation scanning experiments. Intensity profiles were generated using D_{input} and adding random noise with variance σ^2 . We then used postphotoactivation scanning analysis methods to solve for D_{output} (mean \pm SE, n = 10 simulations). The plot shows where results diverged from the ideal $D_{output} = D_{input}$ | 250 |
| Figure 95. Example of results from postphotoactivation scanning simulations where $D_{input} = 10^{-11}$ cm ² /s. Left: Distribution of $\alpha(D)$. Red asterisks indicate diffusion coefficients used to generate simulated data. Right: Simulated intensity profiles fit to diffusion model. | 251 |
| Figure 96. Example of results from postphotoactivation scanning simulations where $D_{input} = 10^{-12}$ cm ² /s. Left: Distribution of $\alpha(D)$. Red asterisks indicate diffusion coefficients used to generate simulated data. Right: Simulated intensity profiles fit to diffusion model. | 252 |
| Figure 97. Example of results from postphotoactivation scanning simulations where $D_{input} = 10^{-11}$ cm ² /s and $\sigma = 0.02$. Left: Distribution of $\alpha(D)$. Red asterisks indicate | |

diffusion coefficients used to generate simulated data. Right: Simulated intensity profiles fit to diffusion model. 253

Figure 98. Example of postphotoactivation scanning experimental results for HIV-like liposomes in 50% (v/v) gel in PBS with high levels of experimental noise. Left: $\alpha(D)$; Right: intensity profiles fit to diffusion model. 254

Figure 99. Example of postphotoactivation scanning experimental results for HIV-like liposomes in 50% (v/v) gel in PBS with low levels of experimental noise. Left: $\alpha(D)$; Right: intensity profiles fit to diffusion model. 255

List of Abbreviations

| | |
|-----------|---|
| A:E ratio | Ratio of epitope-binding sites on antibodies to epitopes (Antibody:Epitope ratio) |
| ADCC | Antibody-dependent cell-mediated cytotoxicity |
| AIDS | Acquired Immunodeficiency Virus |
| FRAP | Fluorescence Recovery After Photobleaching |
| gp120 | Glycoprotein 120, component of HIV-1 Env |
| gp41 | Glycoprotein 41, component of HIV-1 Env |
| HEC | Hydroxyethyl Cellulose placebo used in clinical trial of Cellulose Sulfate |
| HIV | Human Immunodeficiency Virus (Here, we use HIV to refer to HIV-1) |
| HIV-1 Env | HIV-1 Envelope |
| MC | Methylcellulose placebo used in clinical trial of Carraguard |
| P:L ratio | Peptide:Lipid Ratio for liposomes with 2F5 epitope peptide |
| PBS | Phosphate-Buffered Saline |
| RTI | Reverse Transcriptase Inhibitor |
| SHIV | Chimeric Simian Immunodeficiency Virus/ Human Immunodeficiency Virus |
| SIV | Simian Immunodeficiency Virus |
| SPR | Surface Plasmon Resonance |

Acknowledgements

I would like to express my gratitude for the many individuals and institutions that have made this work possible. Thanks to my advisor, Dr. David Katz, for his guidance and kind encouragement throughout the past several years. Thanks also to my committee members for their thoughtful advice and generous support: Dr. S. Munir Alam; Dr. David Montefiori; Dr. George Truskey; and Dr. Fan Yuan. I feel incredibly fortunate to have interacted with such a diverse group of talented scientists.

Katz lab members of past and present, official and unofficial, have provided help on a daily basis: Dr. Anthony Geonnotti; Jennifer Peters; Mike DeSoto; Dr. Marcus Henderson; Dr. Sarah Kieweg; Doug Kieweg; Dr. Derek Owen; Matt Brown; Matt Novak; Yao Quan Xie; Lori Hu; Mary Ellen Koran; Andrew Tutt; Jason Chen; Cami Parrish; and Yaijng Gao. In particular, I worked with Anthony to collect preliminary data for the Transwell experiments, Mary Ellen contributed to preliminary data for postphotoactivation scanning of liposomes, and Andrew developed analysis methods for particle tracking. Jenny, Marcus, and Dr. David Walmer collected the *in vivo* deployment data used in Chapter 5. I have also benefitted immensely from the advice and mentorship of other graduate students in Biomedical Engineering: In particular, I am grateful to Dr. C. Steve Wallace and Dr. Charles Anamelechi for their advice about progressing through graduate school.

Several individuals have contributed their expertise to specific projects. In producing HIV-like liposomes (Chapters 2, 3): Dr. Munir Alam; Dr. Moses Sekharan;

Kathy Stempel; Kara Anasti; Dr. Ji-Young Park; Dr. David Needham; and Dr. Patrick Kiser. In particle tracking (Chapter 3): Dr. Sam Johnson and Dr. Yasheng Gao of the Duke University Light Microscopy Core Facility; Dr. Jeremy Cribb, Dr. Benjamin Evans, and Dr. Richard Superfine of the Center for Computer Integrated Systems for Microscopy and Manipulation (CISMM) at the University of North Carolina, Chapel Hill; Dr. Jeffrey Lifson and Julian Bess of the National Cancer Institute at Frederick; Shetha Shukair and Dr. Tom Hope at Northwestern University; and Dr. Julie Jay at the University of Utah. In working with the TZM-bl assay and HIV (Chapter 4): Dr. David Montefiori; Barbara Sokolik-Wolak; and Dr. Gabriel Perez. I also thank Dr. Alan Gelfand for thoughtful discussions of the analyses characterizing the lower limit of detection of the postphotoactivation scanning assay presented in the Appendix.

This work was supported by grants from the National Institutes of Health (NIH U19 AI077289) and developmental grants from the Duke University Center For AIDS Research (CFAR, NIH P30 AI 64518). My graduate studies were supported by the National Science Foundation Graduate Research Fellowship, James B. Duke Fellowship, and Pratt-Gardener Fellowship. We also thank CONRAD and the Population Council for providing the placebo gels used in our studies.

Finally, I would like to thank my friends and family for their encouragement throughout my graduate school journey. Thanks to Jessica Sanders and Dr. Rebecca Kunder for their support. In particular, I owe a debt of gratitude to my boyfriend, Andy Simnick, who has endured my crabbiness admirably over these past few months.

1. Introduction

This dissertation explores reducing HIV transport to mucosal sites of infection as a mechanism for HIV prevention. We developed experimental and theoretical methodology for (1) quantifying HIV transport and (2) evaluating strategies for reducing HIV transport in terms of efficacy for HIV prevention.

1.1 The need for new biomedical technologies for HIV prevention

Since the Human Immunodeficiency Virus/ Acquired Immunodeficiency Syndrome (HIV/AIDS) pandemic was first recognized in 1981, HIV/AIDS has become a leading cause of death worldwide [1]. Globally, there are approximately 33 million individuals living with HIV [2]. In particular, women have become increasingly affected. For example, in sub-Saharan Africa, women account for 61% of adults with HIV/AIDS [2]. Of individuals living with HIV, approximately 12.6 million (approximately 38%) were infected through male-to-female sexual transmission via the female genital tract [3].

HIV prevention is needed to sustain long-term control of the HIV/AIDS pandemic. Over the past few years, worldwide access to antiretroviral therapy for treating individuals with HIV/AIDS has improved dramatically. For example, the number of people receiving antiretroviral therapy in low- and middle-income countries has increased by 10-fold over the past 6 years [2]. As a result, in the year 2008, the number of annual AIDS deaths declined for the first time since the emergence of the virus [2]. However, in 2007, for every two individuals starting antiretroviral therapy, there were five others who were newly infected with HIV [1]. Epidemiological models

have suggested that combining treatment and prevention efforts will ultimately reduce resources needed for treatment in the long term [4]. Successful prevention programs must combine behavioral [5], structural (social, economic, political, and environmental) [6], and biomedical approaches. The development of new biomedical technologies for prevention would aid significantly in efforts to curb the HIV/AIDS pandemic.

1.2 Biomedical technologies for HIV prevention

Current proven biomedical interventions for the prevention of sexual transmission of HIV include condoms and male circumcision [7]. New biomedical technologies for HIV/AIDS prevention under development include topical microbicides, vaccines, and oral antiretroviral prophylaxis. Public health experts suggest that research for new biomedical technologies for HIV prevention should be a priority. However, new technologies should not be viewed as panacea, but rather as additional tools in multi-faceted prevention programs [1]. Here, we focus on new biomedical interventions where transport at mucosal surfaces is a concern, as is the case for topical microbicides and vaccines.

Topical microbicides are agents applied at the mucosal site of sexual transmission to prevent sexually transmitted infections (STIs) [8-11]. Microbicide development has largely been motivated by (1) the fact that women are biologically and socially more vulnerable to HIV than men and (2) the lack of female-controlled methods for STI prevention that do not require male consent. The first generation microbicide candidates included surfactants, agents to maintain vaginal pH, and anionic polymer viral entry inhibitors. The recent trend for microbicide development has been toward more HIV-

specific agents, known as antiretrovirals (ARVs). These include entry inhibitors specific to HIV-1 Env or CCR5, and reverse transcriptase inhibitors. Microbicides in development are being formulated as semi-solid gels, intravaginal rings, quick-dissolve films, and tablets [12, 13]. It is likely that multiple dosage forms will be needed to accommodate women's differing social, economic, and personal preferences and needs.

Vaccines rely on host immunity to prevent infection. Efforts to develop a vaccine for HIV began in 1983 when the virus was discovered to be the cause of AIDS.

However, these efforts have not yet yielded a successful vaccine. HIV has presented a number of immunological challenges: In contrast to many other viruses, HIV quickly establishes a pool of latently infected cells that cannot be cleared; broadly neutralizing antibodies are rarely elicited, perhaps due to autoreactivity of these antibodies; and the virus exhibits great genetic diversity [14]. There also seems to be a delicate balance in eliciting the appropriate immune response. Local inflammation can render women more vulnerable to HIV infection by attracting additional targets for infection to mucosal sites. A recent study of SIV transmission in rhesus macaques suggests that using glycerol monolaurate to block production of proinflammatory cytokines prevents recruitment of target cells and, thus, blocks HIV infection [15]. It is possible that different immune responses may be needed for prevention and control of infection, and the first publicly-available vaccines for HIV may be disease-modifying rather than prophylactic [14].

Recently, a phase III clinical trial in over 16,000 volunteers in Thailand of a vaccine combining canarypox vector priming injections and recombinant gp120 subunit booster injections demonstrated statistically significant reduction in HIV infection [16].

However the rate of efficacy, approximately 31.2% fewer infections in the vaccine vs. control arm ($p = 0.04$, modified intention-to-treat analysis), is generally regarded to be too low for the vaccine to be administered widely as is. Surprisingly, the vaccine did not reduce the viral load of those infected. This suggests that the immunity conferred by the vaccine might not be the immune response needed to control systemic viremia. Future research will attempt to further understand the immune response elicited by the vaccine.

Several microbicide and vaccine candidates have failed to demonstrate efficacy in Phase III clinical trials. This points to inadequacies in our understanding of what is needed for HIV prevention and the difficulty of conducting clinical trials in HIV prevention [17]. In light of these challenges, there is a clear need for continued research and development of multiple approaches to HIV prevention.

1.3 HIV/AIDS transmission via the female reproductive tract

Understanding the early events of transmission at mucosal surfaces is crucial to designing technologies for HIV prevention. During male-to-female sexual transmission of HIV, semen containing infectious HIV is deposited in the lower female reproductive tract. HIV could be introduced as free virions and through infected T cells and macrophages. In order for infection to occur, HIV must overcome numerous barriers: It must penetrate mucosal tissues to infect target cells, establish local infection, and disseminate itself from the mucosal site of infection to lymphatic tissue to establish systemic infection [18].

The female reproductive tract presents a relatively robust barrier to infection, as the male-to-female transmission probability per exposure event is $1/200 - 1/2000$ [3].

This is much lower than blood-borne transmission, which has the transmission probability per exposure of 95/100 – 1/150 [3]. The female reproductive tract has evolved to protect against STD pathogens while accommodating reproductive processes [19], and the mucosal environment contains several defenses that reduce the likelihood of HIV transmission.

Male-to-female sexual HIV transmission most likely occurs via the lower female reproductive tract, which consists of the vagina, ectocervix, and endocervix (Figure 1A).

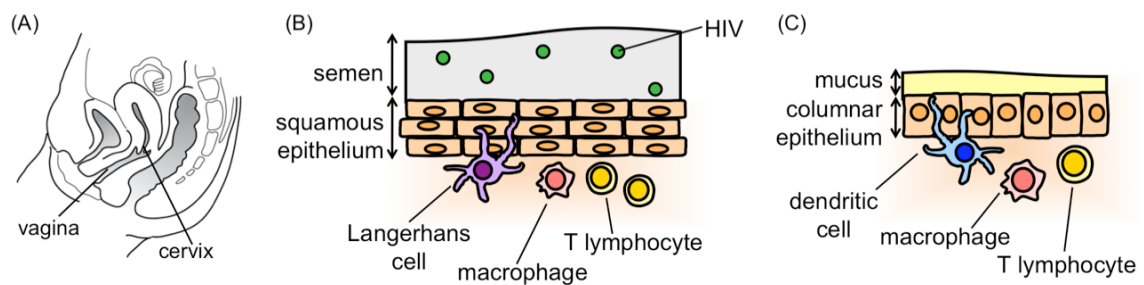


Figure 1. Sites of HIV transmission in the female genital tract. (A) HIV transmission most likely occurs via vaginal and cervical tissues. (B) HIV transmission across vaginal and ectocervical tissues. HIV is introduced via semen. The outermost layer of ectocervical and vaginal tissues consists of multi-layered squamous epithelium. The stroma contains immune cells that may be infected by HIV, including T lymphocytes, macrophages, and Langerhans cells. (C) Endocervical tissue consists of a single-layered columnar epithelium covered by cervical mucus.

The outermost tissue in the vagina and ectocervix consists of multi-layered squamous epithelium (Figure 1B). The thickness of the epithelium varies from 50 to 250 μm , depending on projections of papillae from the stroma underneath [20]. This thickness corresponds to approximately 23-28 layers of epithelial cells [21]. Mean vaginal epithelial thickness does not change substantially over the menstrual cycle [21]. The squamous epithelium serves as a physical barrier to HIV in that the epithelial cells lack the receptors needed for HIV infection, namely CD4, and CCR5 or CXCR4. Studies

have shown that epithelial cells cannot be productively infected by HIV [22] and may sequester virus [23].

Epithelial layers may also contain Langerhans cells, immature intraepithelial dendritic cells that sample antigens in the lumen. It is not completely understood how Langerhans cells participate in HIV infection [24, 25]. Although earlier studies suggested that Langerhans cells are productively infected by HIV [26-29], more recent work has shown how Langerhans cells can act to inhibit HIV infection by internalizing and degrading HIV [30].

The stroma, or lamina propria, beneath the epithelium contains immune cells that may be infected by HIV such as CD4⁺ T cells, macrophages, and stromal dendritic cells [3]. Recent microscopy studies have shown that the squamous epithelial barrier is imperfect, as HIV can move through gaps between epithelial cells to penetrate layers of vaginal tissue and come in contact with immune cells [31].

In contrast to the vagina and ectocervix, the epithelium of the endocervix is comprised of single-layered columnar cells (Figure 1C). Endocervical epithelial cells in culture form a polarized physical barrier due to the presence of tight junctions [32, 33]. The endocervical canal is approximately 2.5 cm in length and contains tubular branching invaginations known as crypts. Endocervical cells secrete the mucus that occupies the cervical lumen. Unlike other glandular tissue, there is no distinction between the mucus-secreting columnar cells that line the cervical lumen and those that line the crypts [34]. Mucus production varies depending on the menstrual cycle. Cervical mucus production is greatest just before ovulation, when estrogen levels are high and progesterone levels

are low [34]. Permeability of mucus also appears to vary with the menstrual cycle, with ovulatory mucus being most permeable to spermatozoa [35].

It remains unknown whether the vagina or the cervix is more vulnerable to HIV infection. The multi-layered squamous epithelium may provide a more robust physical barrier to HIV penetration than the single-layered columnar epithelium. However, cervical mucus has been shown to trap virions *in vitro* [36, 37], on cervical explant tissue [38], and in rhesus macaques [39]. Cervical mucus also has antimicrobial activity [40, 41]. The surface area of the vagina and ectocervix has been estimated to be approximately 15 times that of the endocervix [20]. Thus, the virus is more likely to encounter vaginal or ectocervical tissue than endocervical tissue. In this dissertation, we consider the entirety of the lower female reproductive tract to be vulnerable to HIV transmission.

There are also innate immune factors that may act to neutralize HIV at mucosal surfaces. Endogenous antimicrobial peptides and proteins present in the reproductive tract have been shown to neutralize HIV [31, 42-44]. These include secretory leukocyte protease inhibitor (SLPI) [45], defensins [46-48], lysozyme [49], and lactoferrin [50]. Some chemokines have been shown to inhibit HIV [51]. There are also innate immune factors that act against HIV intracellularly, including APOBEC3G [52, 53] and TRIM-5 α [54]. Mucosal immunity varies to accommodate sperm transport and fertilization, and there appears to be a window of vulnerability near the time of ovulation that may render women more susceptible to HIV infection [43]. The complement system and cellular innate immune responses also contribute to nonspecific defenses against HIV [44].

It has also been suggested that the acidic pH of the vagina may neutralize virions [55] and immobilize or kill lymphocytes [56]. Vaginal pH is approximately 4-4.5 [57]. Lactobacilli that colonize the vagina produce lactic acid and hydrogen peroxide (H₂O₂) to maintain the low pH of the vaginal lumen and combat pathogens [58, 59]. H₂O₂-producing lactobacilli have been shown to inhibit HIV *in vitro* [60]. Disruptions in normal flora due to disease have been associated with increased risk of HIV infection [61, 62].

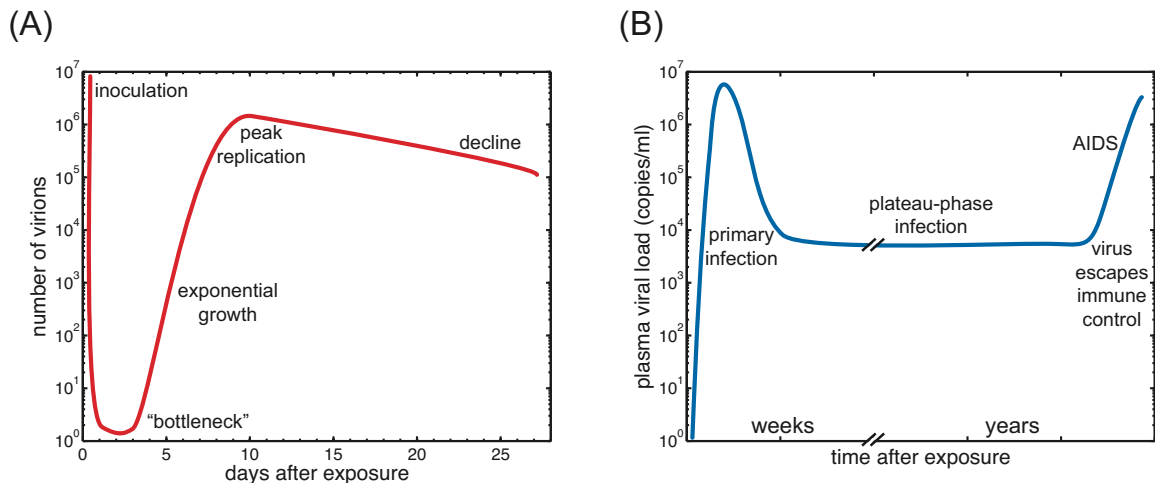


Figure 2. Course of HIV infection (A) in cervicovaginal tissue and (B) systemically. Figures adapted from [14, 18].

These many physical and biochemical defenses are effective in reducing the levels of HIV that successfully reach target cells. HIV replication in cervicovaginal tissues follows the trend shown in Figure 2A. According to experiments characterizing vaginal Simian Immunodeficiency Virus (SIV) transmission in rhesus macaques, the viral inoculum is rapidly reduced by several orders of magnitude within 24 hours [39]. Much of the virus is likely cleared by cervicovaginal fluids or trapped in cervical mucus [39]. A portion of virions traverses the epithelial barrier within minutes or hours [63]. HIV

infection is limited to low levels in the reproductive tract for 1-3 days, where replication of virus is isolated to small focal sites [39]. According to genetic analyses, in most cases, sexual HIV transmission occurs via only a single virus that is successful in establishing infection [39]. HIV is rapidly disseminated from mucosal tissues to lymphatic tissue via drainage by lymphatic vessels or transport by dendritic cells [39]. However, there is a delay in systemic infection until local infection is established. Local levels of viral replication must exceed the threshold needed to sustain productive infection, and this requires 1-3 days. Expansion of virus locally provides a constant source of virus that allows for the establishment of productive infection at other sites in the host.

The course of systemic infection is shown in Figure 2B. Primary infection begins with a burst of viremia beginning approximately 7 days after exposure, and peaking approximately 3 weeks after exposure [14]. Over the next 2-6 months, levels of virus decline one or two orders of magnitude, presumably under the control of CD8⁺ and CD4⁺ T cells. This is followed by the plateau phase, during which levels of virus are maintained at a set point for months or years. If left untreated, HIV infection eventually escapes from immune control, resulting in AIDS.

Initial rounds of viral replication may establish a permanent latent pool of HIV-infected cells that cannot be eliminated by current treatments. Thus, there is a small, crucial window of time in which HIV infection can be prevented [64]. This has led researchers to focus on early events in mucosal infection. This is the time during which the virus is most vulnerable: The number of infected cells is small compared to the number of effector cells, and the virus must expand or it will come to nothing. The low

levels of virus that take hold in the mucosal tissue suggest that moderately strengthening the barrier at mucosal surfaces may be sufficient to prevent HIV infection [39].

1.4 Targets for inhibiting HIV

At a molecular and cellular level, microbicides and vaccines could potentially act through a variety of mechanisms. There are several events in the HIV life cycle that can be targeted to prevent HIV from spreading from one cell to another (Figure 3). Inhibiting these events can potentially be used in *therapy* by preventing the spread of HIV from one cell to another within a HIV-infected individual, or in *prevention* of new infections by preventing the spread of HIV from infected cells within a HIV-infected individual to an uninfected individual or by preventing the spread of HIV from cells locally at the mucosal site of initial infection to other parts of the body.

Combining multiple strategies has proven to be most effective in therapy, and will also likely be the case for prevention [9]. Today, standard first-line therapies combine two nucleoside/nucleotide reverse transcriptase inhibitors (NRTIs) and a nonnucleoside reverse transcriptase inhibitor (NNRTI). Combinations prevent selection of drug resistant variants: Virions with mutations conferring resistance to three drugs are rare or not viable. HIV prevention may be similar in that combining multiple agents with different mechanisms of action may enhance efficacy. Some agents appear to work through multiple mechanisms of action, and thus may be more difficult for HIV to evade.

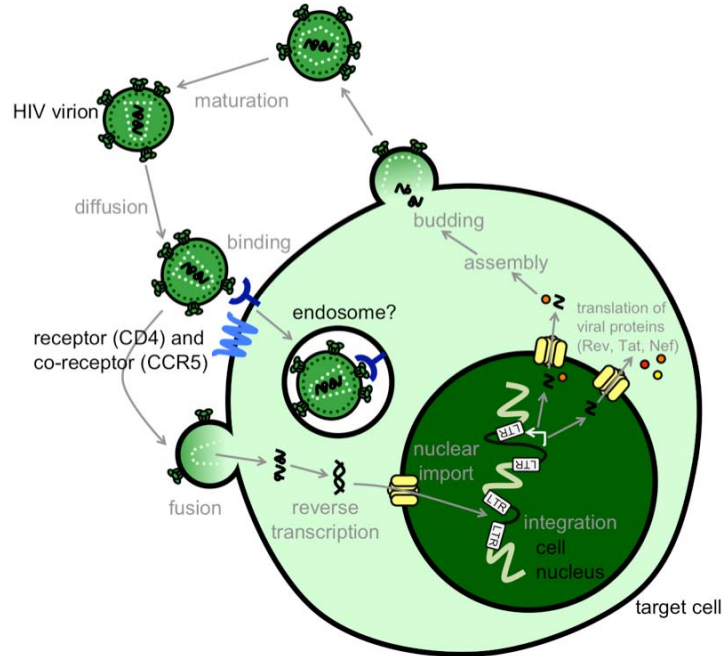


Figure 3. Potential targets for inhibiting the HIV life cycle. HIV virions diffuse to bind with the CD4 receptor and CCR5 or CXCR4 co-receptor on the target cell membrane. This dissertation focuses on reducing diffusion of HIV virions. After binding, receptor-mediated fusion of the virion and target cell occurs. A recent study suggests that HIV may require endosome-mediated fusion [65]. Within the cytoplasm, reverse transcriptase catalyzes the reverse transcription of viral RNA to cDNA. To date, most microbicide agents have targeted free virions, entry, fusion, or reverse transcription. Vaccines use neutralizing antibodies to target extracellular virions and inhibit attachment, entry, and fusion. T-cell vaccines target target cell-associated virus. Figure adapted from [66-68].

Specific targets for inhibiting HIV along its life cycle include the following:

extracellular virions or cell-associated virus, virus-cell attachment, viral entry, fusion, uncoating, reverse transcription, nuclear import, integration, and virion maturation (Figure 3) [67-69]. Currently, topical microbicides in clinical testing include entry inhibitors and reverse transcriptase inhibitors [9]. Thus far, vaccines have aimed to produce antibody and T-cell responses [14]. Antibodies could potentially act by facilitating the clearance of extracellular virions or by inhibiting virus-cell attachment,

viral entry, fusion, and uncoating. T-cell responses may control infection by killing or suppressing HIV-infected cells.

Here, we focus on hindering HIV transport as a mechanism for HIV prevention. Considering that HIV infection requires contact between HIV and an infectable cell, any means of inhibiting this step could be used for HIV prevention. One strategy for preventing HIV transmission is the use of physical barriers – this is the mechanism of action of the only current biomedical technology for HIV prevention, condoms. Physical barriers also serve as a significant component of the innate immune defenses: Epithelial tissue [22] and mucus [37] have been shown to hinder HIV transport. Barrier methods literally block the contact between HIV and vulnerable tissue. The materials that comprise condoms, primarily latex or polyurethane, are practically impermeable to HIV virions [70]. In contrast, new biomedical technologies for HIV prevention rely on HIV-neutralizing agents in the context of materials semi-permeable to HIV.

The strategy of reducing HIV-virion transport as a mechanism of HIV prevention has not been comprehensively studied. For HIV transport through materials such as semi-solid gels, epithelial tissue, or mucus, it becomes important to understand the kinetics of transport in relation to the kinetics of viral inhibition. Materials that slow viral transport can act synergistically with other agents with different mechanisms of action. For example, for entry or fusion inhibitors that target virions, it may be important for drugs to neutralize virions prior to viral contact with tissues. Thus, slowing HIV transport at mucosal surfaces can provide a valuable opportunity for neutralizing agents to act. For reverse transcriptase inhibitors, materials that delay contact of virus and tissue

may provide time needed to adequately load tissues with inhibitory concentrations of drug prior to viral entry. Thus, hindering HIV transport at mucosal surfaces can become an important consideration for topical microbicides and vaccines.

1.5 Transport phenomena in HIV transmission and prevention

Transport theory can inform our understanding of physical processes that affect the movement of HIV in the female reproductive tract. Both convection (transport arising from bulk motion of fluids) and diffusion (random motion of molecules arising from the thermal energy of molecular collisions) are present in the female reproductive tract. Active transport of HIV virions by endocytosis or other cellular mechanisms may be observed in some cells of the female reproductive tract. Transport of HIV may also occur through motility of HIV-infected cells. Numerous theoretical frameworks have been developed to quantitatively understand fluid, mass, and cellular transport phenomena. Applying these theoretical frameworks to HIV transmission and prevention can give us greater insight to biological phenomena and allow us to design strategies for intervention.

The nondistended vagina is a collapsed tube with approximate dimensions as follows: length of 6 cm; width of 2-3 cm; and surface area of 100 cm^2 [71]. Fluid in the vagina consists of vaginal transudate, exfoliated epithelial cells, and fluids from the upper reproductive tract such as cervical mucus, endometrial, and tubal fluids [57]. The rate of vaginal fluid production is approximately 2-8 ml/day [57]. The clearance time of fluid from the reproductive tract has been estimated to be 6-17 hours [72]. Fluid production has been observed to increase during sexual stimulation [73]. Convective flow of vaginal

fluids may clear a large portion of HIV from the vaginal lumen [39]. Convective transport of fluid in the vagina has previously been modeled as flow of a thin layer of fluid along a cylinder [72]. Upward convection in the female reproductive tract has also been documented: The uterus and fallopian tubes may at some times act as a pump to move fluid from the lower reproductive tract to the upper reproductive tract [74].

During male-to-female sexual HIV transmission, HIV is introduced to the female reproductive tract via semen. The average volume of human ejaculate is 3.4 ml [75]. Semen may contain cell-associated HIV and/or cell-free HIV virions. The cellular component of semen consists of sperm, polynuclear cells, immature germ cells, lymphocytes, macrophages, and epithelial cells [34]. HIV-infected T cells and macrophages may be a source of HIV during HIV transmission [76, 77]. The other component of semen, seminal plasma, contains secretions from the testes, epididymides, prostate, seminal vesicles, proximal bulbourethral glands, and distal periurethral glands [34]. The seminal plasma of HIV-infected individuals may contain HIV virions. HIV viral load in blood and semen are correlated, with viral loads in blood typically higher than those in semen [78]. Correlation may vary depending on STI infection and antiretroviral treatment [78]. It is not understood whether cell-free or cell-associated HIV contributes more significantly to HIV infection.

Some studies suggest that cell-free virions contribute more significantly to sexual HIV transmission. Virions can be rapidly dispersed through convective transport of fluids such as semen, blood, and lymph [66]. Virions are approximately 2 orders of magnitude smaller than cells and may be able to diffuse through gaps in the epithelium.

Furthermore, there appear to be many more virions than HIV-infected cells in semen. Semen viral load ranges from 10^3 - 10^5 copies/ml in HIV-positive, untreated men [79]. Semen viral load is the highest during acute HIV infection [79], and this corresponds with the observation that rates of HIV transmission are 12-fold higher during the first 2.5 months of infection compared to rates during latent infection. For men who are receiving antiretroviral therapy, semen viral load may become undetectable [80]. There are approximately 10^5 potential target cells per ml in semen: 10^4 CD4⁺ T cells/ml and 10^5 macrophages/ml in semen from HIV-positive donors [81]. Inflammation in the genital tract during HIV infection may increase the number of immune cells present in semen [76]. However, it is unclear how many of these target cells are HIV-infected. A recent review of data suggests that the median infection rate of HIV target cells in semen is 0.2% (range 0.002-16%). Assuming 10^5 total target cells per ml semen, this corresponds to 200 HIV-infected cells per ml (range 2-16,000). Thus, the number of HIV-infected cells appears to be 1-3 orders of magnitude lower than that of free virions.

One recent study of samples from men who have sex with men (MSM) suggests that HIV is more likely transmitted through free virions [82]. The study performed phylogenetic analyses of (1) the transmitted strains in recently-infected individuals and (2) the RNA from HIV virions in seminal plasma and the DNA from cell-associated virus isolated from seminal leukocytes of the source partners. The study found that transmitted strains were more closely related to RNA from virions.

On the other hand, some studies have suggested that cell-associated HIV transmission may be more efficient than cell-free HIV transmission – this has been

observed in a mouse model [83] and *in vitro* [84, 85]. Generally, cell-associated HIV may be less vulnerable than free HIV virions [66]. Free virions progressively lose infectivity over time, and are more vulnerable to innate and adaptive immune responses. Without active motility, free virions may be more prone to being trapped by some physical barriers, like mucus. Random diffusion of virions is also generally slower than the movement of motile cells. Cell-to-cell transmission allows for direct infection of target cells by cell-to-cell contact. Cell-to-cell contact recruits viral receptors to the intercellular interface, allowing for efficient entry of virus [86]. Movement of virus from one cell directly to another can protect the virus from many innate and adaptive immune defenses [66].

We have focused on HIV transmission by cell-free virions, consistent with much of current HIV/AIDS research [87]. For example, the most widely used animal model in HIV/AIDS research, the SIV/rhesus macaque model, typically uses inocula containing high doses of cell-free HIV virions [88]. However, our focus on free virions may be confounded if HIV is more frequently transmitted through cell-associated virus. Thus, for completeness, we have included a brief review of cell-associated HIV transport below.

1.5.1 Transport of cell-associated HIV

Cell-associated HIV transmission via the female reproductive tract is not fully understood; several mechanisms have been proposed (Figure 4) [76]. HIV-infected lymphocytes or macrophages may serve as a source of free HIV virions: Cells may migrate to the epithelial barrier, where they bud HIV virions that diffuse through gaps in

cells (Figure 4B). HIV-infected lymphocytes introduced in semen or host lymphocytes infected in the lumen may migrate from the lumen, through epithelium, into the lymphatic system according to the “Trojan horse” hypothesis (Figure 4C) [89]. In rhesus macaques, it is possible for SIV-infected peripheral blood monocytes to rapidly migrate from the vaginal lumen to lymphatic tissues through genital ulcers [90, 91]. HIV-infected T cells may also migrate from semen into the epithelium or stroma, where there may come in contact with and directly infect host immune cells in the mucosal tissue.

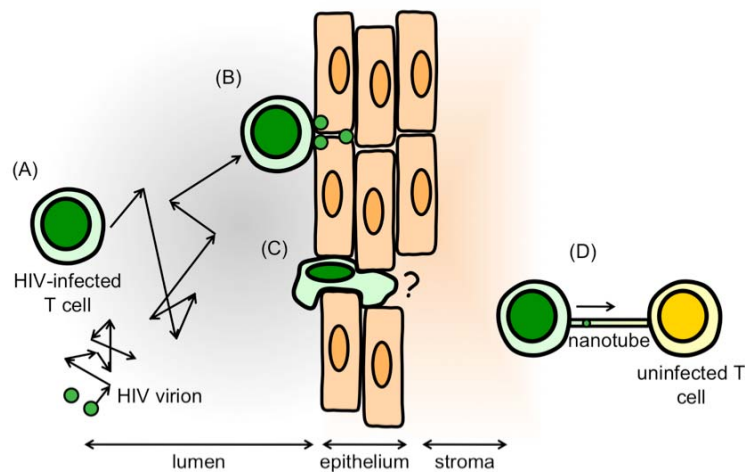


Figure 4. Proposed mechanisms of cell-associated HIV transport. (A) HIV is introduced to the vaginal lumen via semen as both cell-associated HIV and cell-free virions. HIV virion diffusion can be described by random walk. Cell migration can be described by random walk with persistence. (B) Cells may migrate to the epithelium, where they bud virions that diffuse through gaps in the epithelium. (C) Cells may migrate through the epithelium, perhaps through ulcers, to the stroma or into the lymphatic system. (D) Direct cell-to-cell transmission of HIV occurs through nanotubes.

Recently, cell-to-cell transmission between T lymphocytes has been observed using microscopy [86]. Nanotubes, cellular extensions typically of 180-380 nm in diameter and $38 \pm 8 \mu\text{m}$ (and up to 200 μm) in length, are formed between two T cells, allowing for the direct, receptor-dependent transfer of HIV (Figure 4D) [86]. The

velocity of labeled Gag moving along the nanotube was $8 \pm 3 \times 10^{-6}$ cm/s [86]. Direct cell-to-cell transmission via nanotubes is likely the dominant mode of transmission in secondary lymphoid tissue, where T cells are densely packed [66]. In contrast, T cells in the mucosa may be too disperse for frequent cell-to-cell transmission.

In all of these cases, transport of cell-associated HIV can be characterized by cell motility followed by diffusion of virions or cell-to-cell transmission (Figure 4). The motility of cells in culture has been characterized by random walk with persistence [92]. Persistence is the tendency for a cell to continue in its motion of direction. Mean square displacement, $\langle d^2(t) \rangle$, of a cell undergoing random walk with persistence can be described as follows:

$$\langle d^2(t) \rangle = 2n_d \mu \left(t - P \left(1 - e^{-\frac{t}{P}} \right) \right)$$

Equation 1

Where n_d is the number of dimensions, μ is the random motility coefficient, and P is the persistence time. For time intervals comparable to the persistence time, the relation can be simplified:

$$\langle d^2(t) \rangle = 2n_d \mu (t - P)$$

Equation 2

This simplified form allows for the use of linear regression to experimentally determine the random motility coefficient (μ) and persistence time (P) from a plot of $\langle d^2(t) \rangle$ vs. t .

Willits and Saltzman have previously studied reducing transport of cell-associated HIV as a means of HIV prevention [93]. They focused on reducing migration of HIV-infected cells through cervical mucus. They proposed that synthetic polymers could be used to inhibit cell migration through cervical mucus by altering the fiber structure of mucus [94]. They quantified migration of monocytes in the polymers polyvinyl pyridine (PVP) and polyethylene glycol (PEG) mixed with human cervical mucus or an equivalent amount of phosphate-buffered saline (PBS) as a control. Experiments recorded monocytes migrating through polymer and mucus mixtures. Data for mean square displacement vs. time, $\langle d^2(t) \rangle$, were fit to a linear regression. For 2-dimensional diffusion, the slope is equivalent to 4μ . The motility coefficients of monocytes in PVP and PEG mixed with mucus were 2.6×10^{-9} and 3.8×10^{-9} cm²/s, respectively. Surprisingly, these coefficients were slightly higher than those for the control, where an equivalent amount of PBS had been mixed with mucus: $1.4-1.8 \times 10^{-9}$ cm²/s. Thus, it seemed that the addition of PVP and PEG to cervical mucus unintentionally increased monocyte motility in cervical mucus, although the clinical implications of this small increase are unknown.

Others have explored different approaches for inhibiting cell-associated HIV transmission. For example, Olmsted et al. quantified the effect of low pH on lymphocyte, monocyte, and macrophage motility [56]. They found a sigmoidal relationship between pH and percent motility, where pH of 5.5 appeared to completely immobilize cells. They applied BufferGel, a microbicide candidate that maintains low vaginal pH, to a mouse

model with cell-associated HIV transmission. They found that BufferGel reduced the number of infections (1/12 infected) compared to controls (12/12 infected with PBS treatment, 5/7 infected with KY Jelly treatment). However, results of a phase II clinical trial for BufferGel were not as promising: The study found similar numbers of HIV infections in the BufferGel, placebo gel, and no gel arms [95].

Khanna et al. evaluated the compound 2-hydroxypropyl- β -cyclodextrin for preventing transmission of cell-associated HIV in a mouse model [83]. The compound may act to inhibit cell-associated HIV through two mechanisms: (1) It inhibits cell migration by blocking cellular polarity; and (2) It inhibits budding of virus from lipid rafts by absorbing cholesterol from cell membranes. They found a statistically significant reduction in the number of mice infected when treated with 2-hydroxypropyl- β -cyclodextrin: 1/11 mice were infected with 2-hydroxypropyl- β -cyclodextrin compared to 12/17 infected in the control group.

Mechanisms of cell-associated HIV transmission and prevention remain poorly understood [87]. Further research is needed to determine the how often cell-associated HIV contributes to new infections. If cell-associated HIV is indeed a significant factor in infection, then hindering migration of HIV-infected lymphocytes and macrophages may contribute to HIV prevention. Methods using transport theory to quantify cell migration may be useful to developers who are comparing different approaches to hindering migration.

1.5.2 Transport of HIV virions

HIV virions are introduced to the lower female reproductive tract via semen during male-to-female sexual transmission of HIV. The viral load of semen varies, depending on stage of infection, co-infection with other sexually transmitted diseases, and treatment [78]. At peak viremia during primary infection, viral load in semen can reach up to 10^5 or 10^6 copies/ml [79].

Viral load in semen is likely related to the probability of HIV transmission. Previous studies have shown a relationship between blood viral load and HIV transmission [96], and semen viral load is often correlated with blood viral load [78]. Using the data from the Rakai project [96], the probability of infection (β_1) is related to viral load in blood (V_1) as follows:

$$\beta_1 = 2.45^{\log_{10}(V_1/V_0)} \beta_0 .$$

Equation 3

Where β_0 is the probability of infection for baseline viral load, V_0 [97, 98]. Figure 5 shows a plot of probability of infection vs. viral load for male-to-female sexual HIV transmission [97]. We can ascertain from this relationship that any biomedical intervention that reduces the effective viral inoculum to mucosal tissues will reduce the likelihood of transmission. Tuckwell et al. have used the relation between viral load and likelihood of infection to develop a model of the effectiveness of microbicides [99] (Described in detail in Chapter 5).

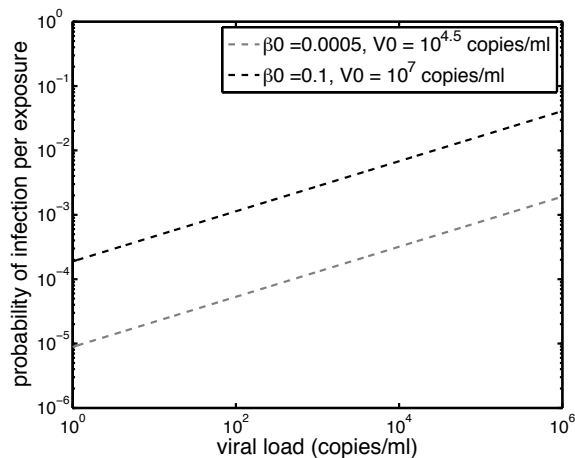


Figure 5. Probability of infection per exposure event as a function of viral load (in blood) according to Equation 3. We used two sets of estimated values for baseline probability and viral load: $\beta_0 = 0.0005$, $V_0 = 10^{4.5}$ copies/ml [97]; $\beta_0 = 0.1$, $V_0 = 10^7$ copies/ml [88].

While mechanisms of transport at the mucosal surface of the lower female reproductive tract are not fully understood, we assume that transport at these small length-scales occurs via diffusion. Near many mucosal surfaces in the body, such as the gastrointestinal and respiratory epithelium, mucus forms and maintains an adherent unstirred layer through which particles must diffuse [100]. In the cervix, the lumen is filled by cervical mucus secreted from epithelial cells. This likely creates a similar scenario in which particles must diffuse to reach tissue surfaces. In the vagina, epithelial cells do not secrete mucus. However, mucus may leak down from the cervix, particularly during maximal mucus production at midcycle. The outermost surface of the multi-layered squamous epithelium consists of sloughed cells. We suppose that vaginal fluids and sloughed squamous epithelial cells comprise a diffusive layer at the surface of the lower reproductive tract.

Physical properties of HIV virions help govern their diffusive behavior. Size, shape, charge, and surface ligands may affect how particles move through and interact

with the surrounding medium. Virions are budded from infected cells. Thus, their outer surface, or envelope, is largely comprised of a lipid bilayer membrane. The lipid membrane of HIV virions has been characterized, and appears to be enriched with sphingolipids compared to the cell membranes from which they bud [101]. This supports the hypothesis that virions bud from lipid rafts [101]. To our knowledge, the surface charge of HIV has not been measured. However, HIV virions bud from negatively-charged cell membranes, so the net surface charge of HIV virions is also likely to be negative [36].

Virions are roughly spherical with diameter of approximately 110-125 nm.

Literature values for the diameter of HIV virions are listed in Table 1.

Table 1. Values for the diameter of HIV virions previously reported in the literature.

| Reference | Diameter (nm) | Technique |
|-----------------------------|--|--|
| Zhu et al. (2006) [102] | 110 ± 8 | Cryo-electron microscopy tomography |
| Briggs et al. (2006) [103] | 125 ± 14 | Cryo-electron microscopy |
| Briggs et al. (2003) [104] | 145 ± 25 | Electron microscopy |
| Gentile et al. (1994) [105] | Min: 110.5 ± 13.1 Max: 128.8 ± 13.8 | Electron microscopy using adenovirus virions as size markers |

Each virion contains two copies of RNA, two copies of reverse transcriptase, matrix protein (p17), and capsid protein (p24) (Figure 6). The surface of each HIV virion contains approximately 14 ± 7 glycoprotein spikes [102]. These spikes consist of gp120 and gp41 trimers that mediate receptor binding and viral entry, respectively. HIV glycoproteins are the most variable of the HIV-1 gene products, evolving to escape host

immune responses [106]. The outer domain of gp120 is also densely glycosylated with host-derived N-glycans that allow the surface to be shielded from antibodies [106].

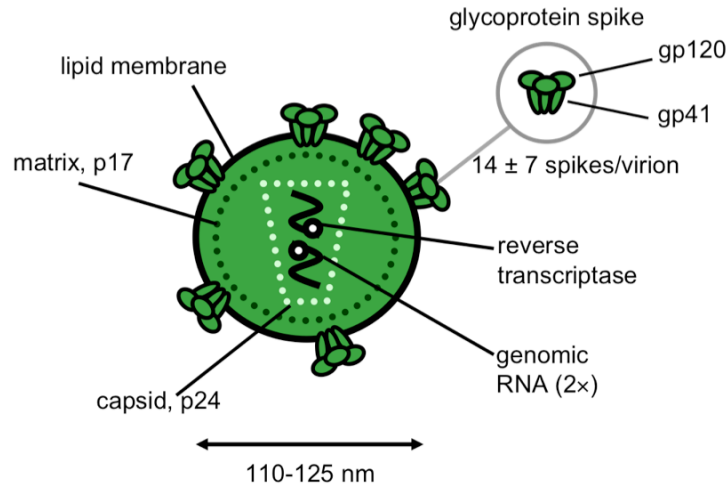


Figure 6. HIV virion structure and components.

Simple diffusion can be described using Fick's law, which relates diffusive flux (J_i) to the concentration (C_i) gradient using the diffusion coefficient [107]:

$$J_i = -D_{ij} \nabla C_i$$

Equation 4

The diffusion coefficient, D_{ij} , describes the diffusion for particle i in a given medium j .

Fick's law is an empirical relation valid for dilute binary solutions. In more complex media, like semi-solid gels and tissues, the diffusion coefficient may depend on a number of factors. However, in many cases, Fick's law may still be applied, replacing the simple diffusion coefficient by an empirically determined effective diffusion coefficient, D_{eff} .

For a given particle and medium, the diffusion coefficient can be determined through empirical measurements of concentration over space and time. In this dissertation, Fick's law for simple diffusion is used to determine the effective diffusion coefficient (D_{eff}) of

HIV-like particles using a method for measuring the diffusion coefficient developed in our lab known as postphotoactivation scanning (Chapter 2, 3). We also incorporate simple diffusion in mathematical models of pharmacodynamics in Chapter 5.

The diffusion coefficient can also be derived from the mean-square displacement, $\langle r^2 \rangle$, of a particle under Brownian motion as follows:

$$\langle r^2 \rangle = 2n_d D_{ij} t .$$

Equation 5

Where n_d is the number of dimensions in which the particle is diffusing and t is the time of observation. Using this relation, the diffusion coefficient can be determined by observing the diffusion path of a particle and calculating the mean-square-displacement as a function of time. In this dissertation, we use microscopy to observe the random motion of fluorescently-labeled HIV virions and use the observed paths to determine mean-square-displacements and diffusion coefficients (Chapter 3).

The diffusion coefficient can also be estimated using the Stokes-Einstein equation, which treats the diffusing particle as a sphere within viscous fluid and considers a force balance between force of viscous drag and force of collisions. For a sphere of radius, R , in a medium of viscosity μ , the diffusion coefficient is as follows:

$$D_{ij} = \frac{k_B T}{6\pi\mu R} .$$

Equation 6

Here k_B is the Boltzmann constant and T is the temperature. From this simple expression for the diffusion coefficient, we can ascertain that it is possible to modulate

the diffusion of a particle by altering the medium in which it is diffusing or by altering the particle itself. For example, we could reduce the diffusion coefficient of a particle by (1) increasing the effective radius of the particle or (2) increasing the effective viscosity of the medium (Figure 7).

Thus, the Stokes-Einstein equation inspired the two strategies that we propose for reducing the transport of HIV virions at mucosal surfaces: (1) increasing the effective radius of particles using antibodies that bind and aggregate virions; and (2) increasing the effective viscosity using semi-solid gels through which virions must diffuse.

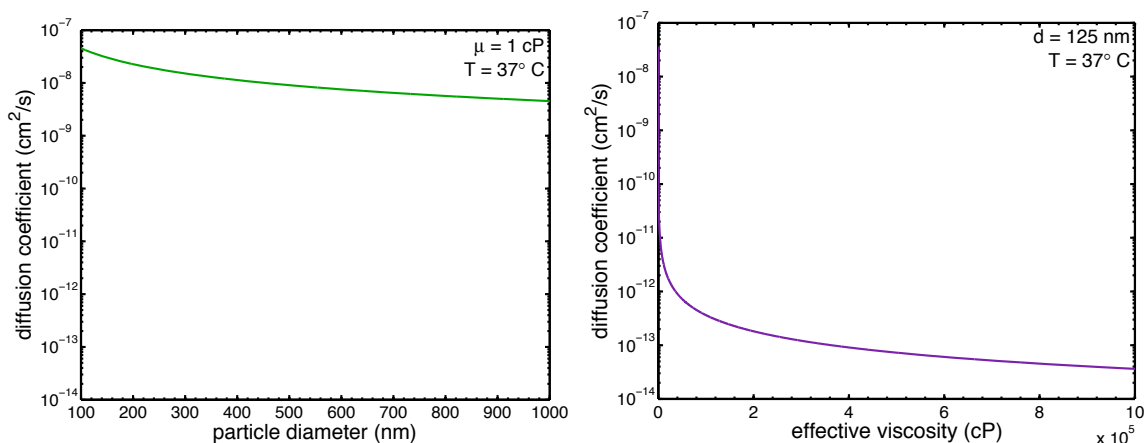


Figure 7. Diffusion coefficients predicted by the Stokes-Einstein equation (Equation 6) for varying left: particle diameter and right: effective viscosity of medium.

1.6 Using transport theory to design and evaluate strategies for HIV prevention

In this dissertation, we analyze strategies that hinder HIV transport as mechanism of preventing HIV transmission. We proposed two strategies for reducing HIV-virion diffusion coefficients, based on fundamental transport theory: (1) increasing the effective radii of particles by using anti-HIV antibodies that bind and aggregate virions; and (2)

introducing a viscous medium, semi-solid gel, through which virions must diffuse to reach tissue (Figure 8).

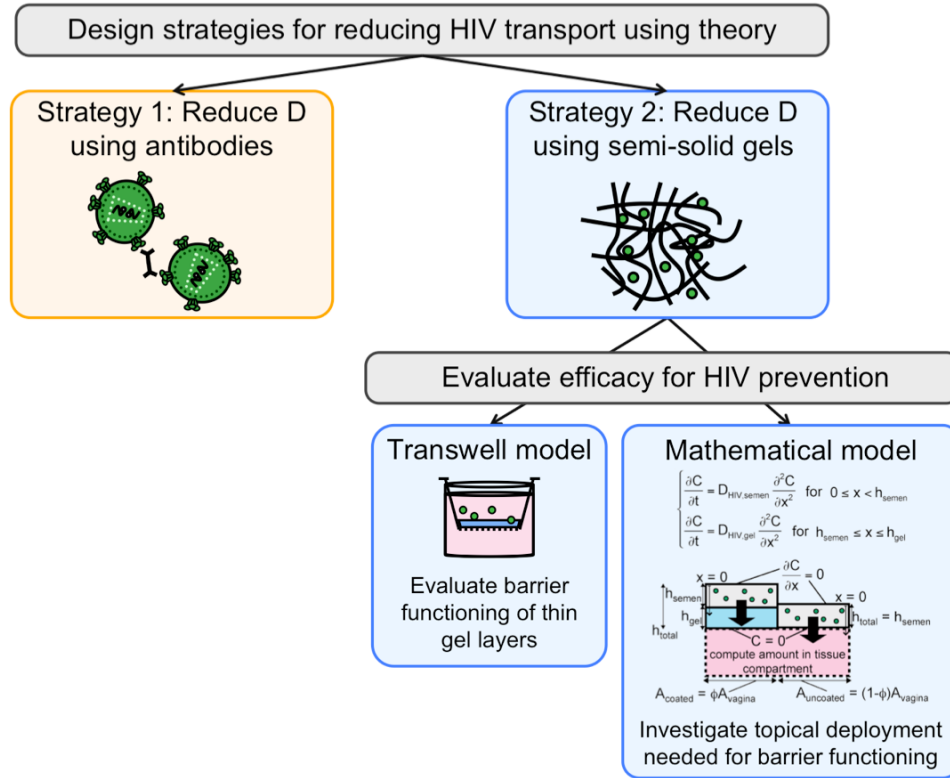


Figure 8. Topics presented in this dissertation.

We quantified the degree to which these two strategies reduced diffusion coefficients by measuring the diffusion coefficients of HIV virions and HIV-like particles in the presence of antibodies and gels. We then developed experimental and mathematical methods for evaluating the efficacy of these strategies in preventing HIV transmission.

Chapter 2. Reduction of HIV-virion diffusion coefficients by antibody binding and aggregation. We studied the effects of antibody binding and aggregation on transport by using the postphotoactivation scanning technique to measure the diffusion coefficients

of liposomes with 2F5 epitope peptides in the presence of 2F5 IgG, IgA, and IgM antibodies. In preliminary experiments, we did not observe the expected reductions in the diffusion coefficients. To further understand the problem, we developed a mathematical model of the kinetics of aggregation and conducted simulations of postphotoactivation scanning. Our results suggest that effects of aggregation in our system were small and/or experimental noise confounded the accurate measurement of diffusion coefficients.

Chapter 3. Reduction of HIV-virion diffusion coefficients by semi-solid gels. We measured diffusion coefficients of fluorescently-labeled HIV virions and HIV-like liposomes in semi-solid gels. We tested two gels used as placebos in microbicides clinical trials, hydroxyethyl cellulose (HEC) and methylcellulose (MC). We found that diffusion coefficients of HIV virions in these gels, undiluted, were approximately 10,000 times lower than those of virions in water.

Chapter 4. Evaluation of physical barrier functioning of semi-solid gels using experimental model of HIV transmission. We further explored the strategy of using semi-solid gels to hinder virion diffusion by developing an experimental system for testing the barrier function of thin gel layers. We used a Transwell system, in which thin gel layers were applied to the porous membrane. We challenged the gel layer with a solution of HIV in the top compartment, and measured levels of HIV in the bottom compartment after a given incubation period. We found that gel layers of thicknesses found *in vivo* are sufficient to act as physical barriers to HIV transport: Levels of HIV

were lower in the bottom compartment of Transwells where a thin layer of gel had been applied to the membrane, compared to control.

Chapter 5. Mathematical model for kinetics of HIV diffusion to tissue surfaces in the presence of realistically deployed semi-solid gels. We considered the topical deployment, or gel coating thickness distribution, necessary for a semi-solid gel to serve as an effective physical barrier over the entire vaginal epithelium. We developed a mathematical model of HIV diffusion from semen, through gel layers, to tissue. We found that it was necessary for the gel to coat over 80% of the tissue area in layers of at least 100 μm thick.

In Chapter 6, we conclude by summarizing our major findings. We then place these findings within the context of HIV prevention and results of recent microbicides clinical trials. We discuss ways in which methods developed here may be used as tools for developers and suggest future studies.

The Appendix describes additional studies validating and characterizing the postphotoactivation scanning method used to measure diffusion coefficient in Chapter 2 and 3.

2. Reduction of HIV-virion diffusion coefficients by antibody binding and aggregation

2.1 Introduction

One strategy for reducing transport of HIV virions is to increase the effective radii of diffusing particles. According to the Stokes-Einstein equation (Equation 6), the diffusion coefficient of a spherical particle is inversely related to its radius, $D \propto \frac{1}{R}$. Antibodies can be used to modify effective radii via specific (1) binding (Figure 9A) or (2) aggregating (Figure 9B) virions. The work described in this chapter explores the potential for HIV-specific antibodies to reduce the diffusion coefficients of virions. We analyzed this effect using experimental and theoretical models. This chapter describes (1) experiments measuring the diffusion coefficient of HIV-like liposomes in the presence of antibody and (2) a mathematical model for the kinetics of virion aggregation by dimeric IgA.

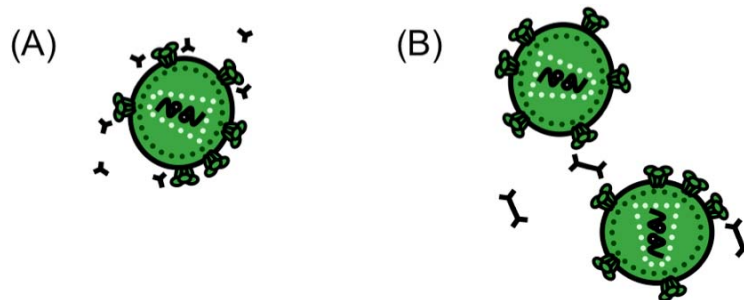


Figure 9. Antibodies can be used to modify effective radii via specific (A) binding or (B) aggregation of virions.

2.1.1 Possible roles of antibodies in HIV prevention

Antibodies are a crucial component of the adaptive immune response, and they will likely serve an important role in a successful prophylactic vaccine for HIV [108]. It

is generally recognized that antibodies are needed to block infection of target cells whereas T-cell responses are needed to control viral replication [108]. Passive immunization studies in rhesus macaques have provided proof of concept that it is possible for antibodies to prevent HIV infection [109]. Passive immunization is the acquisition of immunity from exogenous antibodies rather than those produced endogenously after exposure to antigen. These studies have shown that antibodies delivered systemically [110, 111] or mucosally [112] prior to vaginal challenge by chimeric Simian/Human Immunodeficiency Virus (SHIV) protected animals from infection.

In particular, there has been recent interest in the antibody response to HIV at mucosal sites, where HIV transmission most commonly occurs [3, 113]. Mucosal antibodies could block the initial infection of target cells within mucosal tissue, ultimately preventing systemic HIV infection. The success of passive immunization using antibodies applied intravaginally is encouraging: One study applied 5 mg of the antibody b12 prior to vaginal SHIV challenge and found that only 3/12 animals were infected compared to 12/13 of controls [112].

Ideally, vaccination could be used to induce antibodies against HIV at mucosal sites prior to exposure to the virus. However, induction of mucosal immune responses is not completely understood. In lieu of being able to induce protective antibodies mucosally using vaccination, it may also be possible to introduce antibodies topically, as microbicides. On the other hand, the cost of producing antibodies for topical administration may be prohibitive.

Antibodies have the potential to act against HIV at mucosal surfaces through several mechanisms of action [114]. However, the relative importance of these different mechanisms is still poorly understood. Furthermore, research is needed to elucidate the quantities of antibodies needed for efficacy in HIV prevention. The work presented in this chapter contributes to quantitative understanding of one mechanism by which antibodies may act.

2.1.2 Antibody isotypes within the female reproductive tract

Of the five antibody (Ig) isotypes, two are present in the female reproductive tract: IgG and IgA [115] (Figure 10). These immunoglobulins are produced by uterine, endocervical, ectocervical, and vaginal epithelial cells [115]. IgG is the most abundant isotype in blood serum. In contrast, IgA is the most abundant isotype at mucosal surfaces. IgA is found in different forms in the reproductive tract, including monomeric, polymeric, and secretory [115]. Polymeric forms of IgA contain a J chain polypeptide that covalently links the monomers (Figure 10B). Secretory IgA is a protease-resistant dimer linked by a secretory component in addition to the J chain (Figure 10C). Polymeric IgA can cross-link antigens to prevent attachment to mucosal cells. Immune complexes may then be trapped by mucus and subsequently cleared. The IgM isotype is also commonly found on mucosal surfaces, but has not been detected in significant quantities in the female reproductive tract (Figure 10D). Due to its multivalency, pentameric IgM efficiently aggregates antigens such as virions and cells with many repeating epitopes. Studies have documented HIV-specific antibodies in the female

reproductive tract, which consist mostly of IgG with low to undetectable levels of IgA [34, 113, 116].

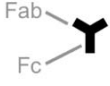



| | (A) IgG | (B) dimeric IgA | (C) secretory IgA | (D) pentameric IgM |
|----------------|---|---|--|---|
| |  |  |  |  |
| MW (Da) | 150,000 | 300,000 | 370,000 | 900,000 |
| R (nm) | 5.29 | 8.7 | 9.1 | 12.65 |

Figure 10. Relevant antibody isotypes, with molecular weights (MW) [117] and hydrodynamic radii (R). References for R are listed in Table 2. (A) IgG: The Fab portion binds antigens. The Fc region is responsible for effector functions such as opsonization and antibody-dependent cell-mediated cytotoxicity. (B) Dimeric IgA: The J chain is a polypeptide that covalently links IgA monomers. (C) Secretory IgA: The secretory component of secretory IgA is derived from the receptor that transports the IgA across epithelial cells. (D) Pentameric IgM contains five monomers linked by disulfide bonds.

2.1.3 Mechanisms of antibody action

Antibodies may act through several mechanisms to prevent HIV infection.

Proposed mechanisms include the following [109, 114, 118]: neutralization; blocking

epithelial attachment or transcytosis of virus; Fc-mediated effector functions; and

immune exclusion (Figure 11). The quality and quantity of the antibody response needed

to prevent HIV infection are currently unknown.

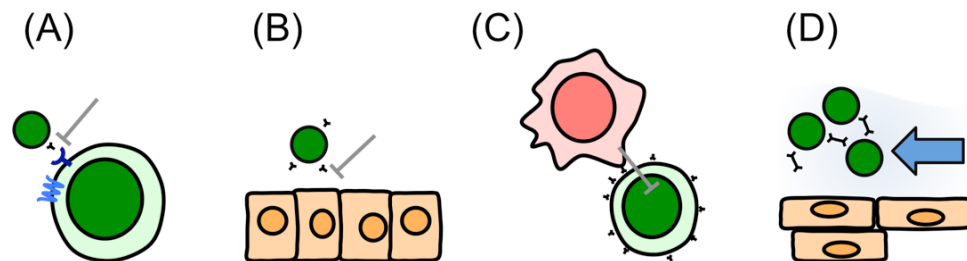


Figure 11. Mechanisms of antibody action: (A) neutralization; (B) blocking epithelial attachment or transcytosis; (C) Fc-mediated effector functions such as antibody-dependent cell-mediated cytotoxicity (ADCC); and (D) immune exclusion.

2.1.3.1 Neutralization

Neutralization refers to phenomena by which antibodies can block binding and fusion between virus and target cells. Thus far, known neutralizing antibodies operate by either (1) binding the envelope trimer to prevent receptor engagement or (2) binding epitopes exposed after virion attachment to inhibit fusion [119]. Neutralization is commonly quantified *in vitro* using assays for inhibition of viral entry to target cells [109, 120]. Neutralization is the most comprehensively studied mechanism of antibody action because it directly prevents infection of target cells. It is believed that induction of neutralizing antibodies will be needed to create a HIV vaccine that provides sterilizing immunity, the immune response needed to entirely prevent or rapidly clear infection [121].

To neutralize virions, antibodies must target the HIV envelope (Env) glycoproteins gp120 and gp41 (Figure 12). These are the only virus-encoded ligands on the virion surface. The exterior of HIV virions is otherwise comprised of lipid membrane budded from infected host cells. Thus, efforts to design HIV immunogens that elicit neutralizing antibodies have focused on the so-called glycoprotein spike [122].

HIV binding is mediated by gp120, which binds to the receptor CD4 on target cells (Figure 12). Once CD4 is bound, a number of conformational changes occur to expose the transient Membrane Proximal External Region (MPER) binding site, allowing for binding of the co-receptor CCR5 or CXCR4. Fusion of the virion and target cell membranes is then mediated by gp41. A single glycoprotein trimer is sufficient for entry [123].

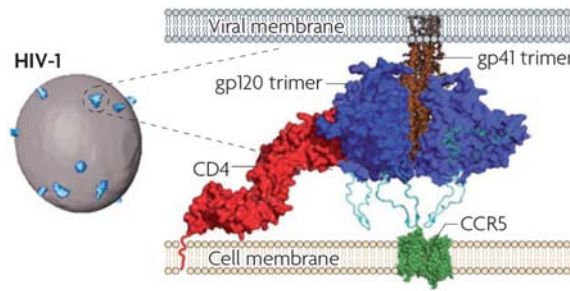


Figure 12. HIV-1 spike interacting with cell membrane receptor CD4 and co-receptor CCR5. Binding is mediated by gp120 and fusion is mediated by gp41. Reproduced with permission from Macmillan Publishers Ltd: *Nature Reviews Microbiology* from Ref. [122] © (2008) and from *Nature* Ref. [102] © (2006).

HIV glycoproteins are the most variable of the HIV-1 gene products, evolving to escape host immune responses [106]. HIV gp120 contains variable loops that can tolerate some mutation without compromising the ability of the glycoprotein spike to mediate entry [124]. The outer domain of gp120 is also densely glycosylated with host-derived N-glycans that allow the surface to be shielded from antibodies [106, 125]. Trimerization of gp120 and gp41 may obscure epitopes found on monomeric molecules [119]. Researchers have sought broadly-specific neutralizing antibodies, those that target the most conserved regions on HIV, to address the greatest number of variants.

Four broadly neutralizing antibodies have been comprehensively studied: b12, 2G12, 2F5, and 4E10 [122]. The antibodies b12 and 2G12 target gp120 whereas 2F5 and 4E10 bind gp41 (Figure 13). The binding sites of 2F5 and 4E10 are close to the viral membrane, in the hydrophobic region known as MPER. Broadly neutralizing antibodies to HIV are rarely elicited. Haynes et al. hypothesized that 2F5 and 4E10 antibodies are rarely found because they bind with phospholipids and are autoreactive [126]. Furthermore, kinetic studies have suggested the binding sites of 2F5 and 4E10 are not

readily accessible – such binding sites must be induced by conformational changes brought about by interaction of the antibody and lipid membrane [127]. Being autoreactive, these antibodies would be eliminated by B cell tolerance mechanisms.

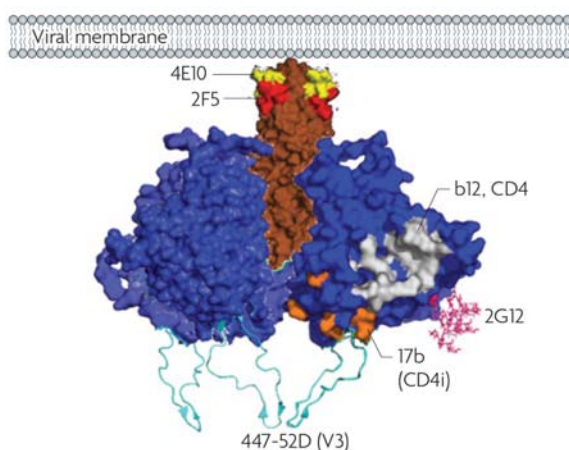


Figure 13. HIV-1 envelope spike with binding sites of broadly neutralizing antibodies. Antibodies b12 and 2G12 bind gp120 whereas 4E10 and 2F5 bind gp41. Reproduced with permission from Bentham Science Publishers Ltd: *Current Pharmaceutical Design* from Ref. [128] © (2007).

It has been unexpectedly challenging to induce anti-HIV antibodies that neutralize virus, rather than merely binding viral epitopes. Studies of passive immunization have suggested that neutralizing antibodies are necessary for protection, and antibodies that bind but do not neutralize virus are not sufficient to prevent infection [129].

Furthermore, the first HIV/AIDS vaccines tested in clinical trials used recombinant protein antigens based on the surface of gp120. Despite producing antigen-specific antibody responses, these vaccines did not prove to be efficacious for preventing HIV infection or reducing viral load [130, 131].

The topic of neutralizing antibodies is an active area of research. One emerging trend is the use of high-throughput screening of serum from HIV-infected individuals to

identify additional broadly-specific neutralizing antibodies [132]. Furthermore, researchers are working to design novel immunogens that will elicit broadly neutralizing antibodies following vaccination [133].

2.1.3.2 Blocking epithelial attachment and transcytosis

Studies of HIV-specific antibodies *in vitro* have suggested that antibodies may block epithelial attachment and transcytosis. In assays of epithelial attachment, b12 IgG and IgA have been shown to reduce the association of HIV-1 and an epithelial cell line, ME180 [134]. HIV-specific IgA and IgM have also been shown to block transcytosis of virus *in vitro* in experimental models using polarized monolayers of endocervical cell lines [135, 136]. However, the role of transcytosis *in vivo* has been controversial: Although transcytosis is observed in cell culture models, it has not yet been observed in intact tissue or *in vivo* [3].

2.1.3.3 Fc-mediated effector functions

The Fc (crystalizable fragment) portion of an antibody can mediate a number of immune effector functions. These include antibody-dependent cell-mediated cytotoxicity and complement activation (ADCC). ADCC is a phenomenon in which immune effector cells trigger apoptosis of target cells bound by antibody [117]. Immune cells that have receptors for Fc include macrophages, monocytes, natural killer (NK) cells, neutrophils, and eosinophils. These cells act through different mechanisms to induce cytotoxicity of the target cell.

The complement system consists of soluble and cell-associated glycoproteins that carry out antibody-mediated effector functions [117]. In the classical pathway of

complement-mediated activation, the formation of antibody-antigen complexes on the target cell initiates a cascade that leads to eventual formation of the membrane-attack complex. The membrane-attack complex perforates the cell, causing lysis. The complement system can also promote the phagocytosis of antigens by macrophages and neutrophils.

The effect of these Fc-mediated effector functions in mucosal HIV infection and prevention is still poorly understood. Hessel et al. investigated the significance of the Fc region in antibody protection [137]. They tested the passive immunization of rhesus macaques using variants of the antibody b12. They observed a decrease in the ability of the antibody to protect from SHIV infection when animals were treated with a b12 antibody variant that had weak ability to bind the Fc receptor and complement. A variant that was competent in binding the Fc receptor, but not in activating complement, did not diminish the effects of passive immunization. Overall, these effects suggest that effector functions mediated by Fc and the Fc receptor may have an important role in the protective effect of antibodies.

2.1.3.4 Immune exclusion

The experimental and theoretical work in this chapter focuses on the mechanism sometimes referred to as immune exclusion. Polymeric immunoglobulins function at mucosal membrane surfaces to cross-link, aggregate, or agglutinate large pathogenic antigens, allowing complexes of pathogens and Ig to be cleared with mucus or other local secretions. We expect that secretory IgA, which is dimeric, may be able to crosslink and aggregate virions in the lower female reproductive tract. Some IgG may also be capable

of aggregating virions because each IgG has two antigen binding sites. However, the ability of IgG to bind multiple virions depends on the spacing of the virion epitopes and the angle of the FAb arm with respect to the virion surface [138]. Anti-HIV IgG with the ability to aggregate virions has not yet been documented.

To our knowledge, the effects of antibody binding and aggregation on HIV transport have not been previously quantified. It is not possible to directly test the effect of immune exclusion in humans [114]. It is also difficult to study immune exclusion in cell culture because cultured epithelial cells do not produce the mucus layers and clearance found *in vivo* [114]. Here, we use a model system to quantify how anti-HIV antibodies reduce the diffusion coefficients of HIV-like liposomes.

2.1.4 A model system of HIV-like liposomes

To study the effect of antibody binding and aggregation on HIV diffusion coefficients, we used a model system that Dr. Munir Alam's group at Duke University has created for studying the binding of anti-HIV antibodies to HIV epitope peptides that associate with synthetic liposomes [127]. The model system was originally devised to study the broadly neutralizing antibodies 2F5 and 4E10 and their binding to the MPER of the HIV-1 gp41 segment of the HIV-1 envelope. The Alam lab has previously used this model system in surface plasmon resonance experiments to characterize the binding kinetics of 2F5 and 4E10 to MPER in synthetic liposomes. The group has synthesized several peptides that mimic HIV epitopes. Those peptides contain a C-terminal HIV-1 p24 gag α -helix region (GTH1) that promotes association of peptides and lipid bilayers.

In our experiments, we used a HIV-1 gp41 2F5 epitope peptide, sometimes referred to as Sp62-GTH1.

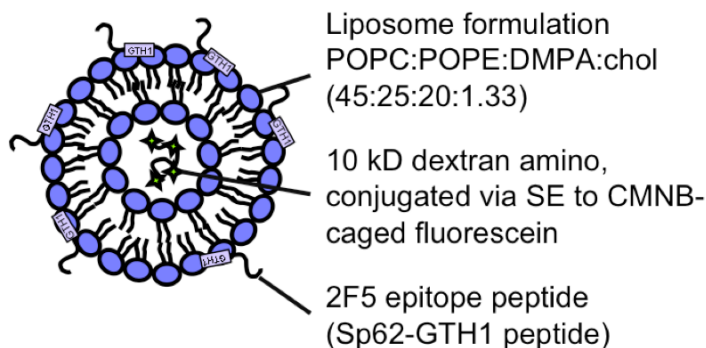


Figure 14. Liposomes used in postphotoactivation scanning experiments. The lipid composition is POPC:POPE:DMPA:chol (45:25:20:1.33). The ratio of 2F5 epitope (Sp62-GTH1) peptide to lipid was 1:100 or 1:420.

To quantify diffusion coefficients, we used a method previously developed in our lab, postphotoactivation scanning [139]. In postphotoactivation scanning, particles of interest are labeled with caged fluorophore, and the sample is placed within a sealed chamber on a glass slide. A slit-shaped region of the sample is uncaged using UV light. We obtain images of the sample over time, as the uncaged particles diffuse outward into the surrounding space. We fit the intensity profiles to the solution of the diffusion equation to obtain the diffusion coefficient.

The Alam lab's system provides an appropriate model for studying HIV virion diffusion in the presence of antibody binding and aggregation because the HIV-like liposomes can be labeled for use in postphotoactivation scanning, and the well-characterized, broadly-neutralizing 2F5 antibody has been shown to bind the 2F5 epitope peptide within these synthetic liposomes.

In collaboration with the Alam lab, we used this system and postphotoactivation scanning to quantify the effects of antibody binding and aggregation on effective diffusion coefficients of HIV-like liposomes in PBS. We chose the simple, Newtonian medium of PBS because particle diffusion can be described theoretically using the Stokes-Einstein relation (Equation 6). We expected specific antibody binding and aggregation to increase the effective radius of liposomes. We hypothesized that this increase in radius would, in turn, decrease the diffusion coefficients measured for the liposomes in postphotoactivation scanning.

2.1.5 Theoretical effects of antibody binding and aggregation

According to the Stokes-Einstein equation (Equation 6), the diffusion coefficient of a spherical particle is inversely related to its radius. To estimate the expected effects of antibody binding and aggregation on diffusion coefficients in liposome-antibody mixtures, we performed some simple calculations using the Stokes-Einstein relation and literature values for radii of virions and antibodies. Table 2 shows the expected effect of binding by antibodies. Table 3 shows the expected effect of aggregation of virions.

Based on the theoretical predictions shown in Table 2, we expected that binding by HIV-specific antibodies would only modestly decrease the effective diffusion coefficient, at most by 15-30%. We expected that postphotoactivation scanning would not be able to resolve such small changes based on our experience from previous experiments. In contrast, we expected that aggregation by antibodies would more significantly decrease the effective diffusion coefficient (Table 3). To further understand the kinetics of aggregation and the resulting distribution of aggregated species, we

developed a mathematical model of virion aggregation by dimeric IgA. To determine if we would be able to measure changes in diffusion coefficients using postphotoactivation scanning, we input distributions of diffusion coefficients from the mathematical model to mathematical simulations of postphotoactivation scanning experiments.

Table 2. Scenarios of HIV binding by immunoglobulins (Ig) and resulting effective diffusion coefficients. Hydrodynamic radii of HIV and Ig were obtained from the literature. The radii of HIV bound by Ig, R_{HIV+Ig} , was estimated by summing the radius of HIV and the diameter of the Ig. This assumes that the HIV virion is completely coated by Ig binding, and that the resulting particle is effectively a sphere. Diffusion coefficients were estimated using the Stokes-Einstein equation assuming spherical particle geometry. Time required to diffuse 100 μm was estimated assuming diffusion in 2D for which $t \sim l^2/4D$. We assumed temperature of 37°C and medium viscosity of 1 cP.

| Particle | MW (g/mol) | R (nm) | R_{HIV+Ig} (nm) | $\frac{D_{HIV+Ig}}{D_{HIV}}$ | Time to diffuse 100 μm (min) |
|----------------|---------------|-------------|-------------------|------------------------------|--|
| HIV virion | | 62.5 [103] | 62.5 | 1 | 11 |
| IgG | 150,000 | 5.29 [140] | 73.08 | 0.855 | 13 |
| IgA, monomer | 162,000 | 6.50 [140] | 75.5 | 0.828 | 14 |
| IgA, dimer | 330,000 | 8.7 [141] | 79.9 | 0.782 | 15 |
| IgA, secretory | 405,000 | 9.1 [141] | 80.7 | 0.774 | 15 |
| IgM, pentamer | 900,000 | 12.65 [140] | 87.8 | 0.712 | 16 |

Table 3. Scenarios of HIV aggregation by polymeric Ig and resulting effective diffusion coefficients. Diffusion coefficients were estimated using the Stokes-Einstein equation assuming spherical particle geometry unless otherwise noted. Time required to diffuse 100 μm was estimated assuming diffusion in 2D for which $t \sim l^2/4D$. We used temperature of 37°C and medium viscosity of 1 cP.

| Scenario of aggregation | $R_{aggregate}$ (nm) | $\frac{D_{aggregate}}{D_{HIV}}$ | Time to diffuse 100 μm (min) |
|--|----------------------------|---------------------------------|--|
| 2 HIV virions crosslinked by IgA dimer, as pictured in Figure 9B. Aggregate particle was treated as a prolate ellipsoid in the Stokes-Einstein equation. | $a = 133.7,$ $b = 62.5$ | 0.95 | 12 |
| Data of HIV-1 BaL virion aggregation by 2F5 IgA obtained by Shattock et al. using size exclusion chromatography DLS [142]. | 180 300 450 | 0.347 0.208 0.139 | 33 55 83 |
| Aggregate with effective radius 10 \times HIV | 625 | 0.1 | 115 |

2.2 Materials and Methods

2.2.1 Experiments measuring diffusion coefficients of liposomes in the presence of antibodies

2.2.1.1 Materials

Antibodies, lipids, and peptides were generously provided by the Alam Lab (Duke University, Durham, NC). We tested human monoclonal 2F5 antibodies to HIV gp41. We used the following isotypes: IgG, dimeric IgA, and pentameric IgM (Polymun Scientific, Vienna, Austria). Concentrations of stock solutions were 3.0, 1.78, and 1.07 mg/ml, respectively.

The following lipids were obtained from Avanti Polar Lipids (Alabaster, AL): 1-palmitoyl-2-oleoyl-*sn*-glycero-3-phosphocholine (POPC, Catalog number 850457); 1-palmitoyl-2-oleoyl-*sn*-glycero-3-phosphoethanolamine (POPE, Catalog number 850757); 1,2-dimyristoyl-*sn*-glycero-3-phosphate (DMPA, Catalog number 830845); and cholesterol (Catalog number 700000). Lipids were dissolved in chloroform in the molar ratio of POPC:POPE:DMPA:cholesterol 45:25:20:1.33. Lipids were mixed by vortexing and dried in the fume hood using nitrogen gas. Remaining chloroform was removed using vacuum desiccation overnight.

In our experiments here, we used the 2F5 nominal epitope peptide (QQEKNEQELLELDKWASLWN) with the GTH1 sequence (YKRWIILGNKIVRMYS) at the carboxyl terminus. The GTH1 sequence anchors the peptide epitope to the lipid (Figure 14). The peptide-liposome system has been comprehensively characterized by Dennison, Alam, et al. [143]. Peptides were added to

lipids to give the final peptide:lipid ratio of 1:420 or 1:100. These correspond to approximately 190 and 760 peptides per liposome, respectively.

2.2.1.2 Liposome preparation

Liposomes (Figure 14) were prepared using membrane extrusion [127, 143, 144] using the Avanti® Mini-Extruder (Avanti Polar Lipids, Inc., Alabaster, Alabama). Liposomes were labeled with caged-fluorescein by rehydrating the lipid film with a solution of 10-kD dextrans conjugated with CMNB-caged fluorescein via succinimidyl ester in PBS; this mixture was incubated in a water bath for 45 minutes at 50° C. The concentration of lipid was 5-6 mg lipid per ml buffer/dextran mixture. Liposomes were typically extruded in 350- μ l quantities using 250- μ l syringes in the Mini-Extruder apparatus. Dextrans were previously conjugated with caged fluorophore using 10 mg/ml amino 10-kD dextrans (Cat. No. D-1860, Invitrogen, Carlsbad, CA) and CMNB-caged fluorescein, succinimidyl ester (Cat. No. C-20050, Invitrogen, Carlsbad, CA) according to the manufacturer's instructions. Fluorescent label was conjugated to dextrans to improve solubility in PBS. Liposomes were formed by extrusion through 400-nm, 200-nm, and 100-nm nucleopore membranes in succession.

Free label was subsequently removed using two gel filtration columns (Sephadex G75, GE Healthcare, Piscataway, NJ). Gel filtration columns were prepared using 5-ml syringes with the plunger removed. A small amount of glass wool was placed inside the syringe, near the tip. The syringe was then filled with the Sephadex medium. Columns were placed in 15-ml conical tubes and centrifuged at 2000 RPM for 10 min to remove excess buffer. Columns were transferred to new conical tubes, and the sample was then

applied, drop by drop, to the Sephadex medium. Again, columns were centrifuged for 2000 RPM for 10 min. The sample was transferred to a second column and the process was repeated. The volume of the sample was noted prior to and after column filtration. We observed that excess buffer in the column typically diluted the sample by a factor of approximately 0.8.

Liposomes were prepared either on the same day as experiments or one day prior to experiments. Liposomes were stored at 4° C, capped with nitrogen gas to prevent oxidation and protected from exposure to light to prevent uncaging of the fluorophore.

2.2.1.3 Experimental conditions

Following extrusion, liposomes were mixed with antibodies. To calculate the concentration of antibody used to achieve the desired ratio of epitope-binding sites on antibodies to epitopes (A:E ratio), we converted the concentration of peptide, 0.1 mg per ml buffer, to the molar concentration using the peptide molecular weight of 4641.6 g/mol. We used the approximate antibody molecular weight per epitope-binding site of 150,000 g/mol.

We performed three independent experiments with different conditions (Table 4). We varied the experimental parameters because we did not observe the expected reductions in diffusion coefficients in any of our experiments. Thus, we tried different conditions in an attempt to find the optimal conditions for reducing diffusion coefficients. There is no obvious unique set of experimental conditions that best simulates *in vivo* conditions. Our experiments used high concentrations of liposomes and antibodies to provide proof of principle.

Table 4. Summary of parameters used in experiments: peptide:lipid ratio (P:L ratio); dilution of dextran stock solution expressed in terms of the ratio of volume of stock solution to volume of PBS; antibody isotypes tested; antibody:epitope ratios (A:E ratios); incubation protocol; liposome dilution used in postphotoactivation scanning experiments expressed in terms of the fraction of volume of liposome solution to total sample volume; and the time course of acquiring images in postphotoactivation scanning including the number of images acquired, the average time elapsed between images and the average time elapsed from the first image to the final image.

| P:L ratio | Dextran dilution | Isotypes | A:E ratios | Incubation protocol | Liposome dilution | Time of images |
|-----------|------------------|-----------|---------------|----------------------|-------------------|--|
| 1:420 | 1:1 | IgG, A, M | 1:32 | Overnight, 4° C | 9/10 | 11-12 images 31 min between 5 h 26 min total |
| 1:420 | 1:1 | IgA | 1:1, 2:1, 5:1 | Overnight, 4° C | 1/100 | 7-8 images 32 min between 3 h 23 min total |
| 1:100 | None | IgA | 1:1, 3:1, 5:1 | 4-5 hours, 24-25 ° C | 1/10 | 8 images 30 min between 3 h 26 min total |

Mixtures of liposomes and antibodies were incubated for 4-5 hours at room temperature (approximately 24-25° C) or overnight at 4° C prior to beginning postphotoactivation scanning experiments.

Slides were prepared by placing a Secure Seal Spacer (Electron Microscopy Sciences) on a glass slide, applying 13 µl of sample, and sealing with a coverslip (Figure 15). Slides and cover slips were treated with solution of 2-5% bovine serum albumin in distilled water to prevent nonspecific binding (Catalog # A9547, Sigma, St. Louis, MO). The depth of the sample was the thickness of the spacer, 120 µm.

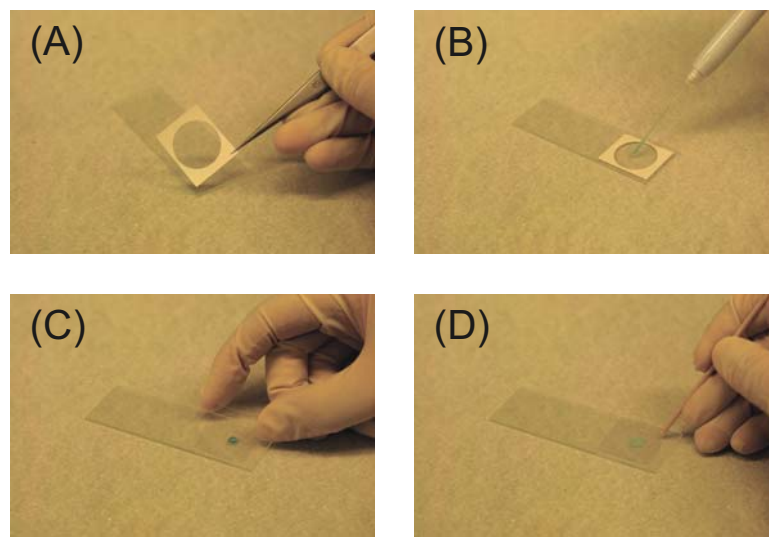


Figure 15. Slide preparation for postphotoactivation scanning: (A) A spacer is adhered to a glass slide; (B) The sample is applied within the spacer; (C-D) The chamber is sealed with a glass cover slip.

For each experiment, we prepared four replicates for each condition. We discarded replicates if any of the following occurred: (1) The sample moved within the chamber; (2) Experimental noise in the image prevented analysis; or (3) Analysis failed to detect a peak representing the liposomes. In each experiment we also included positive and negative controls for uncaging the fluorophore. In positive controls, the entire sample was uncaged to confirm that the fluorophore was uncaging under exposure to UV light. In negative controls, the sample was not exposed to UV light so that the fluorophore was not spontaneously uncaging during the course of the experiment.

2.2.1.4 Postphotoactivation scanning experiments

The postphotoactivation scanning method determines diffusion coefficients by analyzing fluorescence profiles over time [139]. Fluorescence profiles were generated by uncaging a linear region of the sample using UV light (using 500 W mercury arc lamp, Oriel, Stratford, CT and UV filter, 255-425 nm, Edmund Scientific, Barrington, NJ) and a

metal stencil with a single slit of width 200 μm (Figure 16). The CMNB-caged fluorescein used to label the liposomes becomes fluorescein upon uncaging (Figure 17).

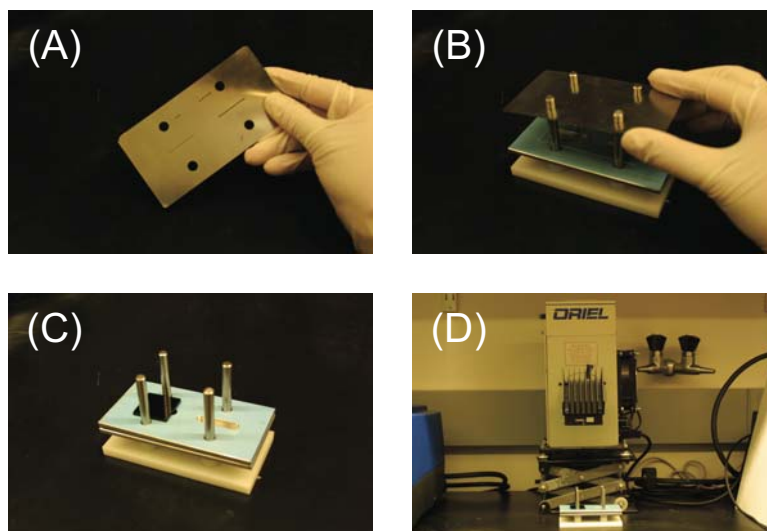


Figure 16. Apparatus used for uncaging: (A) A metal stencil with slit width of 200 μm is used to uncage a linear region of the sample; (B) The slide is placed underneath the stencil within an apparatus used to ensure proper alignment; (C) An additional UV filter is placed on top of the assembly; (D) A mercury arc lamp provides the UV light source.

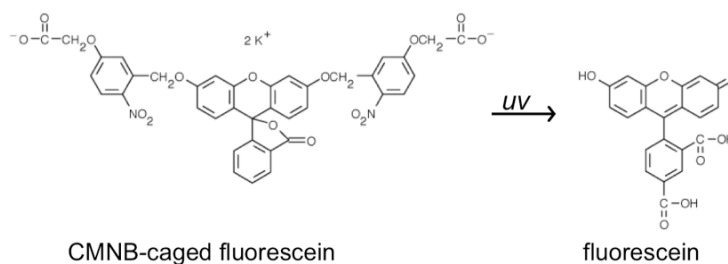


Figure 17. Chemical structure of caged fluorescein used in postphotoactivation scanning. Upon exposure to UV light, the caged-fluorescein becomes fluorescent. (Adapted from invitrogen.com.)

The fluorescent profiles were imaged over time using a microarray scanner with 532 nm laser and 20- μm pixel resolution (Genepix 4000B, Molecular Devices, Sunnyvale, CA). A single image was obtained prior to uncaging to provide background

information for image analysis. The time course of imaging during experiments is listed in Table 4. Experiments were performed at room temperature, approximately 24-25°C.

Images were saved as .tif files. Image analysis was performed using MATLAB (The MathWorks, Inc., Natick, MA). For each slide, a portion of the image containing the fluorescent region was selected by for analysis. The user selected the portion for analysis visually, using the computer cursor to highlight an area that (1) contained the entirety of the fluorescence as it diffused outward in the x direction so that the fluorescence at the boundaries was equal to the background level of fluorescence and (2) had the minimal amount of experimental noise due to spots on slide or bubbles in the sample. Slides in which the sample had moved within the chamber were excluded from analysis. Background intensity values were subtracted from the intensity profiles so that the intensity values at the boundaries were zero. Intensity values were normalized to the highest intensity value in the first image taken after uncaging.

We analyzed postphotoactivation scanning profiles accounting for multiple diffusing species, each with a distinct diffusion coefficient. This method of analysis was useful for experiments using HIV-like liposomes, in which free label was often present in solution, even after column filtration. This method of analysis allowed us to resolve distinct diffusion coefficients for liposomes and free label.

Our analysis followed one developed by Periasamy et al. [145] for analysis of Fluorescence Recovery After Photobleaching (FRAP) diffusion profiles. We assumed that diffusion profiles could be described by a distribution of diffusion coefficients, $\alpha(D)$.

The observed intensity profile ($I_{observed}$) at any given time is the sum of intensity profiles (I_i) for the multiple diffusing species:

$$I_{observed}(x,t) = \sum_i \alpha_i I_i(D_i, x, t)$$

Equation 7

Here, the index, i , refers to each species, for which α_i is the relative amplitude of the diffusing species with diffusion coefficient D_i .

To analyze the observed diffusion profiles, we discretized D at equal intervals in log space between D_{min} and D_{max} . For the experiments in this chapter, we selected $D_{min} = 10^{-10}$ cm²/s, $D_{max} = 10^{-6}$ cm²/s, and performed analyses using 100 points. We numerically solved the diffusion equation for all D_i assuming that the intensity at the boundaries was zero and using the experimental initial condition (I_0):

$$\frac{dI_i}{dt} = D_i \frac{\partial^2 I_i}{\partial x^2}, I_i(\pm\infty, t) = 0, I_i(x, 0) = I_0(x)$$

Equation 8

We then used the MATLAB optimization function “lsqnonlin” to find the distribution $\alpha(D)$ that minimizes the square of the difference between the observed and computed intensity profiles:

$$\sum [I_{observed}(x,t) - I_{computed}(x,t)]^2$$

Equation 9

Here, $I_{computed}$ is the sum of intensity profiles I_i with distribution α .

Our method differed from that developed by Periasamy et al. [145] in the following ways: (1) We analyzed diffusion profiles over both space and time, whereas Periasamy analyzed FRAP data (sum of fluorescence in a region of interest) over time; (2) We used the MATLAB “lsqnonlin” optimization scheme to solve for $\alpha(D)$, whereas Periasamy et al. used the maximum entropy method. For detailed examples, validation experiments, and characterization of the lower limit of detection and resolution of our postphotoactivation scanning analysis methods, refer to the Appendix.

2.2.1.5 Characterization of liposomes

The sizes of the liposomes were measured using dynamic light scattering (DLS) (ZetaPlus Zeta Potential Analyzer with Model B1-9000AT Digital Correlator, Brookhaven Instruments, Holtsville, NY). Surface Plasmon Resonance (SPR) was used to confirm 2F5 antibody binding to the 2F5 epitope peptide on liposomes. Measurements were performed by Kara Anasti in the Alam lab using a BIAcore 3000 with BIAevaluation 4.1 software (BIAcore, GE Healthcare). Detailed protocols for SPR measurements are described elsewhere [127, 143].

2.2.2 Mathematical model of aggregation

We did not observe reductions in diffusion coefficients in our experiments, so we developed a mathematical model to better understand the kinetics of aggregation and effects of experimental parameters. Here, we describe a mathematical model of virion aggregation in the presence of dimeric IgA. We adapted the analysis developed by Dolgosheina et al. for aggregation of bacteria by bivalent IgG [146]. Specifically, we modified the functions describing collision frequency and probability of crosslinking

upon collision and values of constants so that they reflected the conditions in our experimental system.

We considered the two types of particles in our system, HIV virions (or liposomes) and antibodies. Virions are treated as spheres with radius (R_{virion}) of 62.5 nm. Each virion has a number of envelope spikes, n_{spikes} , that can be bound by antibody. The average number of spikes on a HIV virion is 14 ± 7 [102]. The liposomes used as surrogates for HIV in our experiments are similar to HIV virions in size. Using dynamic light scattering, we determined that the radii of control liposomes and liposomes with 2F5 epitope peptide were 57 ± 2 nm ($n = 4$). Antibodies are bivalent dimeric IgA with hydrodynamic radii ($R_{antibody}$) of 8.7 nm [141]. We assumed that each antibody could bind a single spike on the virion surface and that an antibody could not bind two spikes on a single virion simultaneously.

We modeled the kinetics of three processes (Figure 18): (A) binding of antibodies to spikes on virions, (B) dissociation of antibodies from spikes on virions, (C) aggregation of virions resulting from crosslinking of virions by dimeric IgA.

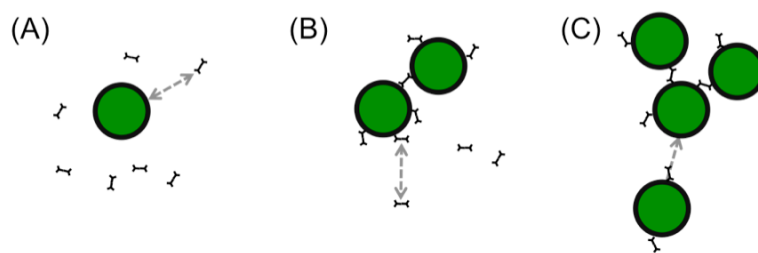
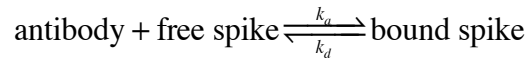


Figure 18. The kinetics of three processes are described in the mathematical model: (A) binding of antibodies to spikes on virions; (B) dissociation of antibodies from spikes on virions; and (C) aggregation resulting from crosslinking.

2.2.2.1 Binding of antibodies to spikes on virions

The binding reaction of antibodies to virions can be expressed as a second-order reversible reaction:



Equation 10

Antibodies in solution bind to free spikes on virions to produce a complex of the antibody and epitope. The association and dissociation rate constants for the reaction are k_a and k_d , respectively. According to Dolgosheina et al., it is useful to express the level of antibody binding in terms of the portion of spikes bound (P_{bound}) by antibody for each virion:

$$P_{bound} = \frac{N_{bound}}{n_{spikes}}$$

Equation 11

Here, N_{bound} is the number of bound spikes on each virion and n_{spikes} is the total number of spikes on each virion. The rate of dissociation and aggregation depend on the portion of spikes bound on each virion, so it is convenient to use this expression rather than concentration.

Following the analysis of Dolgosheina et al., we assumed that the portion of the spikes bound by ligand is dependent on time alone. This assumption is valid so long as the rate of reaction is limited by binding rather than diffusion. To confirm that this assumption is reasonable, we calculated the Thiele modulus (ϕ), which is the dimensionless group representing the ratio of diffusion time to reaction time [107]:

$$\phi = \frac{\text{diffusion time}}{\text{reaction time}} = \sqrt{\frac{kL^2C}{D}} = \sqrt{\frac{k_a \left(1 / \sqrt[3]{N_{Av} (C_{a0} - C_{v0})}\right)^2 C_{a0}}{(D_{antibody} + D_{virion})}}$$

Equation 12

Here, k is the rate coefficient, L is the characteristic length scale of the problem, C is the concentration, and D is the diffusion coefficient. In order for our assumption to be valid, we would want the diffusion time to be much less than the reaction time, so that $\phi \ll 1$.

To estimate the Thiele modulus for our problem here, we considered the time for antibody to diffuse to a virion and the reaction time of antibody binding to a virion. Thus, the effective diffusion coefficient can be estimated by summing the diffusion coefficients of antibodies and virions. We estimated the diffusion coefficient (D) using the Stokes-Einstein relation (Equation 6) and the radii of liposomes and IgA. The characteristic length scale is the average distance between antibodies and virions, or the distance over which an antibody must diffuse to reach a virion. We estimated the characteristic length scale (L) by using the concentrations of antibodies and virions to estimate the interparticle spacing, which is proportional to the inverse of the cube-root of the number of particles in a given volume [147]. The reaction time is the product of the association rate constant ($k_a = 8.45 \times 10^7 \text{ cm}^3 \text{ mol}^{-1} \text{ s}^{-1}$) and the concentration of antibody. To estimate concentrations, we used the initial concentration of antibodies (C_{a0}) and virions (C_{v0}). The values of constants used are listed in Table 6. We found $\phi = 0.009$, so our assumption that antibody binding is a function of time alone was reasonable.

Also, this assumption implies that the portion of spikes bound does not depend on the size of the aggregate. That is, the size of the aggregate does not impede antibody binding. This assumption was reasonable, as the antibody binding occurs rapidly, before aggregation can sterically hinder further binding.

The rate of reaction can be expressed as follows:

$$R_{bound} = \frac{1}{n_{spike}} \frac{dN_{bound}}{dt} = \frac{dP_{bound}}{dt} = k_a C_{antibody} [1 - P_{bound}] - k_d P_{bound}$$

Equation 13

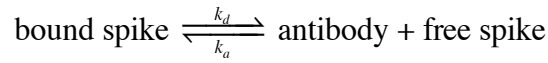
Here, the first term of the equation, $k_a C_{antibody} [1 - P_{bound}]$, is the rate of increase in the portion bound due to antibody binding. The rate of increase is dependent on the rate constant, k_a , the concentration of free antibody, $C_{antibody}$, and the portion of free spikes, $P_{free} = 1 - P_{bound}$. The second term of the equation, $k_d P_{bound}$, is the rate of decrease in the portion bound due to disassociation.

For our experimental system using 2F5 antibody and liposomes with 2F5 epitope peptide, the rate constants have been measured using SPR [143]. The binding kinetics of the antibodies 2F5 and 4E10 can be described as a two-step process [127, 148]. First, the antibody encounters the membrane proximal external region of gp41. The antibody induces conformational changes to expose the binding pocket. Then, stable docking of the antibody occurs. In our mathematical model, we simplified antibody binding kinetics by approximating the binding reaction as a single step with rate constants that correspond to the slower docking step. We used the rate constants measured previously using SPR at 30° C [143]. The binding constant of the overall reaction is $K_d = 1.75 \times 10^{-9} \text{ M}^{-1}$ and the

disassociation rate constant of docking is $k_d = 1.48 \times 10^{-4} \text{ s}^{-1}$. To calculate the association rate constant, $k_a = k_d/K_d = 8.45 \times 10^7 \text{ M}^{-1}\text{s}^{-1}$.

2.2.2.2 Dissociation of antibodies from spikes on virions and aggregates

Antibodies may dissociate from virions and aggregates according to the following reaction:



Equation 14

Here, the aggregate could consist of i virions such that $i = 1, 2, 3, \dots, N_0$.

The rate of the reaction can be expressed as follows:

$$\frac{dC_{\text{antibody}}}{dt} = k_d P_{\text{bound}} n_{\text{spikes}} \sum_{i=1}^{N_0} (iC_i) - k_a C_{\text{antibody}} [1 - P_{\text{bound}}] n_{\text{spikes}} \sum_{i=1}^{N_0} (iC_i)$$

Equation 15

The first term describes the increase in the concentration of free antibody due to disassociation of antibodies from virions and aggregates, which is the product of the dissociation rate constant and the concentration of bound spikes in the system. The second term describes the decrease in the concentration of free antibody due to binding to virions and aggregates, which is the product of the association rate constant, the concentration of antibody, and the concentration of free spikes in the system.

2.2.2.3 Aggregation resulting from crosslinking

The rate of aggregation is described using the Smoluchowski kinetic equation for diffusion-limited aggregation [147]. We considered the reaction in which aggregates of

size i are formed by the collision of smaller aggregates, j and $i-j$. At the same time, aggregates of size i are colliding with other aggregates of size j (Figure 19).

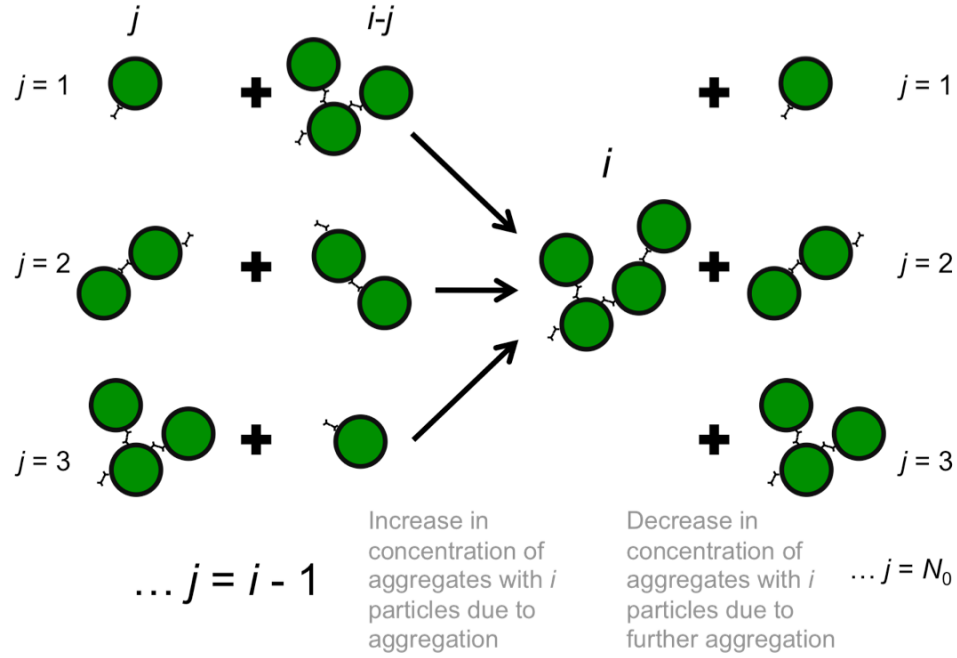


Figure 19. Aggregation reaction. The concentration of aggregates with i number of particles increases due to aggregation of particles with j and $i-j$ particles. The concentration decreases due to further aggregation with aggregates of j particles.

Assuming that there is no dissociation of aggregates, the concentration of aggregates with i number of particles can be expressed by the following equation:

$$\frac{dC_i}{dt} = \frac{1}{2} \sum_{j=1}^{j=i-1} \beta_{j, i-j} C_j C_{i-j} - \sum_{j=1}^{j=N_0-i} \beta_{ij} C_i C_j$$

Equation 16

Here, the index $i = 1, 2, 3, \dots N_0$. The first term has the coefficient of $\frac{1}{2}$ because a single particle is formed by the aggregation of two particles.

The rate constant of aggregation, β_{xy} , is determined by (1) the probability of crosslinking upon collision (P_{xy}) and (2) the molar rate of collisions (Z_{xy}) [149]. The rate of aggregation events can be expressed as follows:

$$R_{aggregation} = \beta_{xy} C_x C_y = P_{xy} Z_{xy} .$$

Equation 17

The probability of crosslinking depends on the nature of the epitopes and antibodies, their concentration, and the contact time between colliding aggregates [149]. Following Dolgosheina et al., we assumed that the probability of crosslinking does not depend on the size of the aggregate, but is proportional to the portion of spikes bound on the central particle and the portion of free spikes on the colliding particle [146]:

$$P_{xy} = P_{crosslink} = k_{crosslink} P_{bound} [1 - P_{bound}] .$$

Equation 18

Here, $k_{crosslink}$ is the constant of crosslinking. Ideally, $k_{crosslink}$ should be empirically derived [146]. However, $k_{crosslink}$ for our system is currently unknown. We propose the following mechanistic expression to estimate $k_{crosslink}$ based on parameters in our system:

$$k_{crosslink} = 4P_{max} k_{area} = 4P_{max} \frac{n_{spikes} \pi R_{spike}^2}{4\pi R_{virion}^2} = 4P_{max} \times \text{peptide:lipid ratio} .$$

Equation 19

Here, P_{max} is the maximum probability of crosslinking upon collision, or the portion of collision events that result in crosslinking. The factor of 4 is introduced so that the probability of crosslinking ($P_{crosslink}$) is maximally equal to P_{max} when the portion of bound spikes on the central particle and the portion of free spikes on the colliding particle

are both 0.5. Again, this quantity should ideally be empirically derived. In our simulations we inputted the maximum possible value, $P_{max} = 1$. The unitless constant k_{area} is the ratio of the surface area of the spikes to the surface area of the virion. For HIV, the radius of the Env spike is 5.25 nm [102]. Assuming 14 spikes per virion and a virion radius of 62.5 nm [102], we find that the k_{area} for HIV is approximately 0.025. For liposomes, we estimated k_{area} using the peptide:lipid ratio of the liposome formulation. For the liposomes used in our experiments, we tried the peptide:lipid ratios of 1:100 and 1:420 [143]. Thus, values of $k_{crosslink}$ are 0.04 and 0.01, respectively.

To derive the molar rate of collisions (Z_{xy}), we considered the situation where one fixed, central particle of size y is surrounded by particles of size x (Figure 20). When particles of size x diffuse within the interaction distance, $R_{interaction}$, the particles x and y collide and stick to form an aggregate of size $x + y$. To calculate the collision rate, we found the flux of particles to $r = R_{interaction}$. The total rate of collisions on the surface of particle y is the product of the flux and the surface area of interaction space.

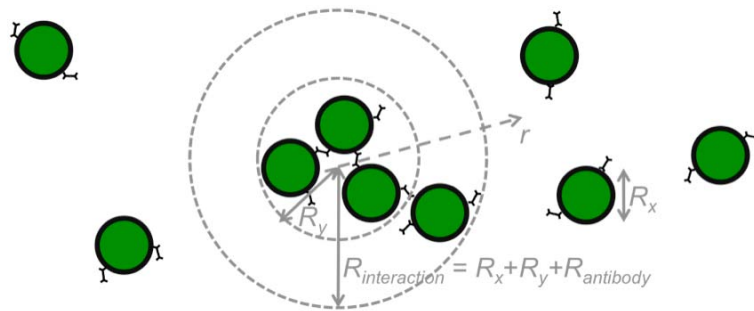


Figure 20. Diffusion problem used to calculate the collision frequency.

To derive the collision frequency function, we began with diffusion equation in spherical coordinates:

$$\frac{\partial C}{\partial t} = \frac{1}{r^2} \frac{\partial}{\partial r} \left[D r^2 \frac{\partial C}{\partial r} \right]$$

Equation 20

We solved the diffusion equation considering the initial and boundary conditions.

Initially, the concentration is C_x for r greater than the interaction distance:

$$C(r, t = 0) = C_x \text{ for } r > R_{interaction}$$

Equation 21

For $t > 0$, the boundary condition at the interaction distance is

$$C(r = R_{interaction}, t) = 0 \text{ for } t > 0$$

Equation 22

The concentration is zero because particles of size y collide with the fixed, central particle to form a particle of size $x + y$. Particles that enter the interaction space are essentially absorbed by the central particle. Far from the interaction distance, the concentration remains the same as the bulk concentration of particles of size x , C_x :

$$C(r = \infty, t) = C_x \text{ for } t > 0$$

Equation 23

The solution is that for diffusion in a semi-infinite medium [107]:

$$C = C_x \left[1 - \frac{R_{interaction}}{r} \operatorname{erfc} \left(\frac{r - R_{interaction}}{2\sqrt{Dt}} \right) \right]$$

Equation 24

At steady state, $t = \infty$, so $\operatorname{erfc}(0) = 1$. The steady-state assumption is justified as long as the concentration at the semi-infinite boundary is equal to the initial concentration. Here,

by definition, the concentration in the bulk (Equation 23) is equal to the initial concentration (Equation 21). The concentration profile as a function of radial position can be simplified to the following:

$$C = C_x \left(1 - \frac{R_{interaction}}{r} \right)$$

Equation 25

The flux of i particles at $r = R_{interaction}$ is the following:

$$J|_{r=R_{interaction}} = -D \frac{\partial C}{\partial r} \Big|_{r=R_{interaction}} = -D \frac{C_x}{R_{interaction}}$$

Equation 26

We convert the flux above to the molar flux by multiplying by Avogadro's number (N_{Av}).

The total molar rate of collisions is the product of the molar flux, the surface area of the interaction space, and the concentration of the central particle of size y :

$$Z_{xy} = -4\pi N_{Av} R_{interaction}^2 J|_{r=R_{interaction}} C_y = 4\pi N_{Av} D R_{interaction} C_x C_y$$

Equation 27

The radius of interaction is the sum of the radii of the two colliding aggregates and the antibody that links them:

$$R_{interaction} = R_x + R_y + R_{antibody}$$

Equation 28

To estimate the size of an aggregate with x number of particles, we considered the aggregate to be a random coil with x segments of length $2R_{virion}$. The root-mean-square end-to-end distance for a random coil is the following [107]:

$$\langle d_0^2 \rangle^{1/2} = n^{1/2}l$$

Equation 29

Thus, the estimated radius of an aggregate with x number of particles is

$$R_x = x^{1/2}R_{virion}$$

Equation 30

Here, we neglected the contribution of the bound antibody to the aggregate size. The random coil approximation may overestimate the radius of the aggregate because it assumes that segments can rotate freely. In reality, the rotation is likely constrained by the antibody.

To generalize our solution to account for the diffusion of the central particle, the diffusion coefficient, D , in Equation 26 should represent the sum of the diffusion coefficients of particles of size x and y :

$$D = D_x + D_y$$

Equation 31

We can estimate the diffusion coefficients of aggregates using the Stokes-Einstein relation:

$$D_x = \frac{k_B T}{6\pi\mu R_x} = \frac{k_B T}{6\pi\mu x^{1/2} R_{virion}}$$

Equation 32

Again, we used the random coil approximation for the aggregate radius in Equation 30. Substituting expressions for D and $R_{interaction}$ to Equation 26, we can express the molar rate of collision as follows:

$$Z_{xy} = \frac{2}{3} \frac{N_{Av} k_B T}{\mu} \left(\frac{1}{x^{1/2} R_{virion}} + \frac{1}{y^{1/2} R_{virion}} \right) \left[R_{virion} (x^{1/2} + y^{1/2}) + R_{antibody} \right] C_x C_y$$

Equation 33

Returning to Equation 17 for the rate of aggregation events, we can substitute the probability of crosslinking (Equation 18) and the number of collisions (Equation 33):

$$R_{aggregation} = \beta_{xy} C_x C_y = P_{xy} P_{xy} = k_{crosslink} P_{bound} [1 - P_{bound}] \times \frac{2}{3} \frac{N_{Av} k_B T}{\mu} \left(\frac{1}{x^{1/2} R_{virion}} + \frac{1}{y^{1/2} R_{virion}} \right) \left[R_{virion} (x^{1/2} + y^{1/2}) + R_{antibody} \right] C_x C_y$$

Equation 34

Thus, the aggregation rate constant is

$$\beta_{xy} = k_{crosslink} P_{bound} [1 - P_{bound}] \times \frac{2}{3} \frac{k_B T}{\mu} \left(\frac{1}{x^{1/2} R_{virion}} + \frac{1}{y^{1/2} R_{virion}} \right) \left[R_{virion} (x^{1/2} + y^{1/2}) + R_{antibody} \right]$$

Equation 35

To summarize, we have a system of N_0+2 equations (Equation 13, Equation 15, and Equation 16). We assumed the following initial conditions:

- None of the spikes on the virions are bound by antibody such that

$$P_{bound}(t=0) = 0$$

Equation 36

- The concentration of antibody is a known quantity, C_{a0} :

$$C_{antibody}(t=0) = C_{a0}$$

Equation 37

- None of the virions are aggregated so that the concentration of individual virions is a known quantity C_{v0} :

$$C_i(t = 0) = \begin{cases} C_{v0} & \text{for } i = 1 \\ 0 & \text{for } i > 1 \end{cases}$$

Equation 38

We calculated the initial concentration of liposomes in our experiments by assuming that each 100-nm liposome consisted of 80,047 lipid molecules [143]. To prepare the liposomes, we used the concentration of 5-6 mg of lipid per ml buffer. Thus, accounting for the lipid composition used, this corresponds to an extruded liposome concentration of approximately 1×10^{-10} mol/cm³. The liposome solution is further diluted by factors of 0.8 and 0.1 by column filtration and in the experiments themselves. Thus, the estimated concentration of liposomes used in postphotoactivation scanning is approximately 8×10^{-12} mol/cm³. The number of peptides on each liposome, which corresponds with n_{spikes} in the mathematical model, was 190 or 760, depending on the peptide:lipid ratio. These values were estimated previously by Dennison et al. for liposomes with the peptide:lipid ratio of 1:420 and 1:100, respectively [143].

In our experiments, we varied the concentration of antibody relative to the number of epitopes on each liposome, so that the ratio of epitope-binding sites to epitopes ranged from 1:1 to 5:1. Assuming the initial liposome concentration above and 760 peptides on each liposome, this corresponds to antibody concentrations from 3×10^{-9} to 1.5×10^{-8} mol/cm³.

To aid in solving the equations, we nondimensionalized them using the following transformations:

$$\tilde{C}_{antibody} = \frac{C_{antibody}}{C_{a0}}, \quad \tilde{C}_i = \frac{C_i}{C_{v0}}, \quad \text{and} \quad \tilde{t} = tk_a C_{a0}.$$

Equation 39

Equation 13 becomes

$$\frac{dP_{bound}}{d\tilde{t}} = \tilde{C}_{antibody} [1 - P_{bound}] - \frac{k_d}{k_a C_{a0}} P_{bound}.$$

Equation 40

Equation 15 becomes

$$\frac{d\tilde{C}_{antibody}}{d\tilde{t}} = \frac{k_d C_{v0}}{k_a C_{a0}^2} P_{bound} n_{spikes} \sum_{i=1}^{N_0} (i \tilde{C}_i) - \frac{C_{v0}}{C_{a0}} \tilde{C}_{antibody} [1 - P_{bound}] n_s \sum_{i=1}^{N_0} (i \tilde{C}_i).$$

Equation 41

Equation 16 becomes

$$\frac{d\tilde{C}_i}{d\tilde{t}} = \frac{1}{2} \frac{C_{v0}}{k_a C_{a0}} \sum_{j=1}^{j=i-1} (\beta_{j,i-j} \tilde{C}_j \tilde{C}_{i-j}) - \frac{C_{v0}}{k_a C_{a0}} \sum_{j=1}^{j=N_0-1} (\beta_{ij} \tilde{C}_i \tilde{C}_j).$$

Equation 42

The initial conditions become

$$P_{bound}(\tilde{t} = 0) = 0, \quad \tilde{C}_{antibody}(\tilde{t} = 0) = 1, \quad \text{and} \quad \tilde{C}_i(\tilde{t} = 0) = \begin{cases} 1 & \text{for } i = 1 \\ 0 & \text{for } i > 1 \end{cases}.$$

Equation 43

To numerically solve this system of equations, we used the MATLAB ordinary differential equation solver “ode15s”. Variables used in the model are summarized in Table 5. Constants input to the model are listed in Table 6. These values are used unless otherwise noted.

Table 5. Variables used in mathematical model of virion aggregation by IgA.

| Variable | Definition | Units |
|--------------------------|--|---|
| P_{bound} | Portion of spikes on each virion bound by antibodies | unitless |
| $C_{antibody}$ | Concentration of free antibody in solution | mol/cm ³ |
| C_i | Concentration of aggregates with i number of particles | mol/cm ³ |
| i, j | Number of particles in aggregate; indices used in summations | unitless |
| β_{xy} | Rate constant of aggregation for colliding particles of size x and y | cm ³ mol ⁻¹ s ⁻¹ |
| $R_{aggregation}$ | Rate of aggregation events | mol/(cm ³ s) |
| $P_{xy} = P_{crosslink}$ | Probability of crosslinking upon collision | unitless |
| Z_{xy} | Rate of collision | cm ³ mol ⁻¹ s ⁻¹ |
| $R_{interaction}$ | Interaction distance used to derive the number of collisions | cm |

Table 6. Constants used in mathematical model of virion or liposome aggregation by IgA.
*Values were derived from literature except for the constant of crosslinking, which is currently unknown.

| Constant | Definition | Input value (HIV virions) | Input value (liposomes) |
|-----------------|---|---------------------------|--|
| R_{virion} | Radius of virion | 62.5 nm[103] | 57 nm |
| n_{spikes} | Number of envelope spikes or peptide epitopes on each virion | 14[102] | 760[143] |
| $R_{antibody}$ | Radius of antibody | 8.7 nm[141] | 8.7 nm[141] |
| k_a | Association rate constant | Unknown | 8.45×10^7 cm ³ mol ⁻¹ s ⁻¹ [143] |
| k_d | Dissociation rate constant | Unknown | 1.48×10^{-4} s ⁻¹ [143] |
| N_0 | Maximum size of aggregate | Unknown | 100 |
| $k_{crosslink}$ | Constant of crosslinking | Unknown | 0.04* |
| P_{max} | Maximum probability of crosslinking upon collision | Unknown | 1* |
| k_{area} | Ratio of surface area of spikes to total surface area of virion | 0.025[102] | 0.01[143] |
| N_{Av} | Avogadro's constant | | 6.02×10^{23} mol ⁻¹ |
| k_B | Boltzmann constant | | 1.38×10^{-16} cm ² g/(s ² K) |
| T | Temperature | 37° C=310 K | 25° C=298 K |
| μ | Viscosity of medium | Unknown | 1 cP |
| C_{a0} | Initial concentration of antibody | Unknown | 3×10^{-9} mol/cm ³ |
| C_{v0} | Initial concentration of virions | Unknown | 8×10^{-12} mol/cm ³ |

2.3 Results

2.3.1 Experiments measuring diffusion coefficients of liposomes in the presence of antibodies

Dynamic Light Scattering (DLS) was used to measure the diameter of liposomes. The diameters of control liposomes and liposomes with the 2F5 epitope peptide were the same, 114 ± 4 nm ($n = 4$ independent samples). Liposomes were similar in size to HIV-1 virions (Table 1).

Surface Plasmon Resonance (SPR) was used to confirm antibody binding by 2F5 IgG and IgA (Figure 21). Results indicate that there was indeed specific binding of 2F5 antibodies to liposomes with the 2F5 epitope peptide compared to control liposomes without peptide.

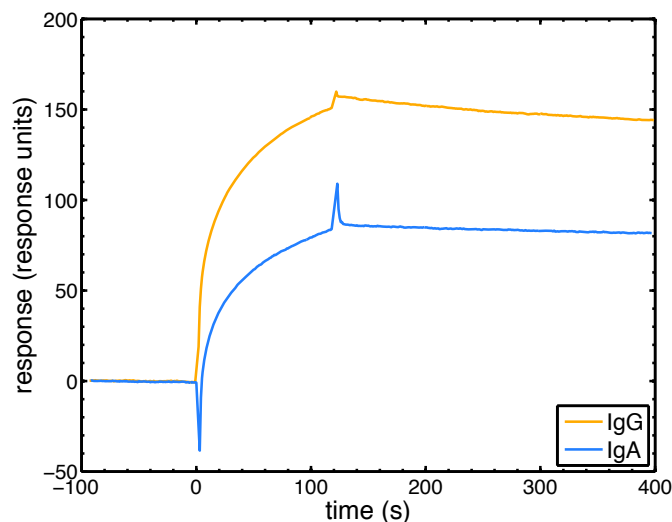
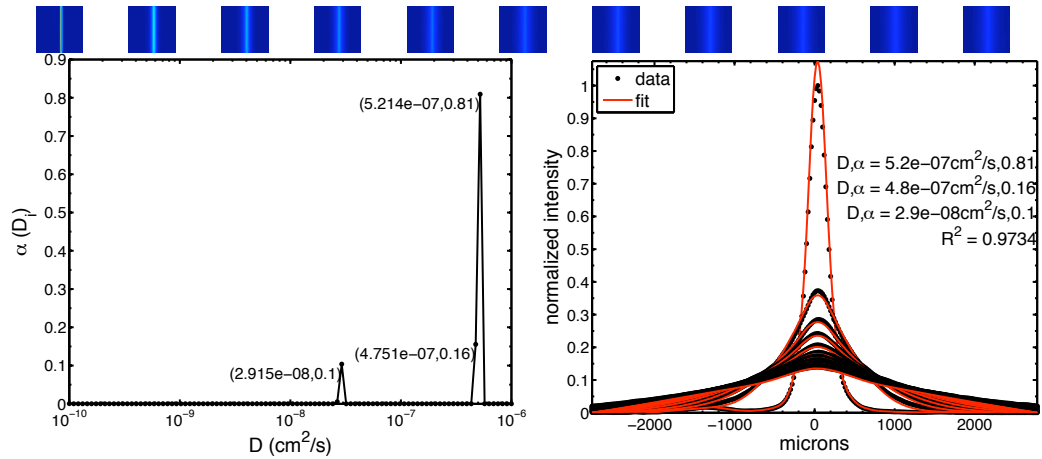


Figure 21. Surface Plasmon Resonance (SPR) results showing interaction of 2F5 antibodies with 2F5 epitope peptide liposomes. Response of control liposomes (no peptide) was subtracted from response of peptide liposomes. Antibodies were injected at concentrations of $100 \mu\text{g/ml}$ at flow rate of $20 \mu\text{l/min}$ for 2 minutes. SPR measurements were performed by Kara Anasti.

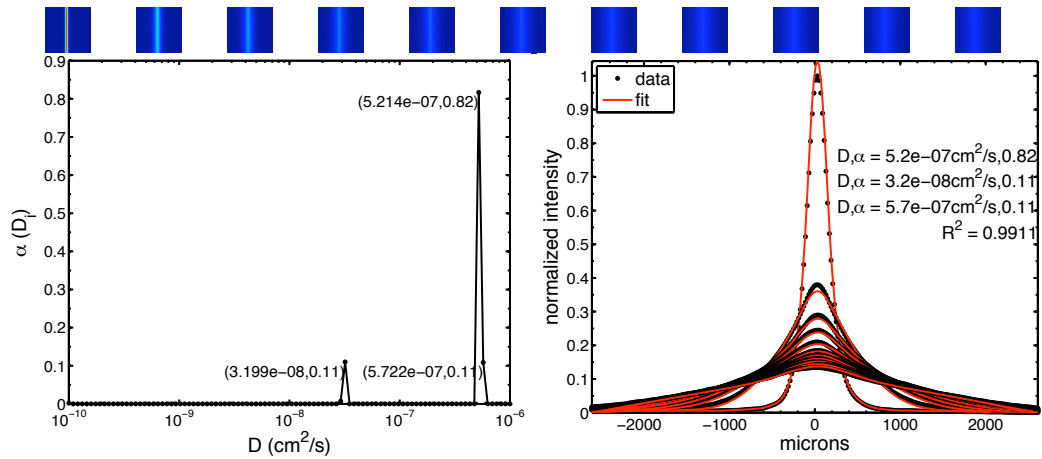
We performed three preliminary postphotoactivation scanning experiments to measure the diffusion coefficients of liposomes with 2F5 epitope peptide in the presence of 2F5 antibodies. Experimental conditions are summarized in Table 4. For each experimental condition, we performed 4 replicates. In these initial experiments with this system we did not observe the expected reduction in the diffusion coefficients in any of the experiments.

In the first experiment, we mixed liposomes with 2F5 IgG, IgA, and IgM. We used the antibody concentration of 100 $\mu\text{g}/\text{ml}$. We chose this concentration because it is the concentration typically used in SPR studies in the Alam lab. Figure 22 shows examples of images and results from postphotoactivation scanning. In this experiment, for each replicate, we obtained 11-12 images over approximately 5.5 hours. We analyzed the intensity profiles to obtain the distribution of diffusion coefficients, $\alpha(D)$. The amplitude of the peak, α , represents the fraction of diffusing species with the diffusion coefficient D_i . Each plot shows a small peak at approximately $3 \times 10^{-8} \text{ cm}^2/\text{s}$, representing liposomes. Each plot also shows a larger peak at approximately $5 \times 10^{-7} \text{ cm}^2/\text{s}$, representing free label. Figure 23 and Table 7 summarize diffusion coefficients measured for liposomes using postphotoactivation scanning. We did not observe any reductions in diffusion coefficients of liposomes with 2F5 epitope peptide in the presence of 2F5 antibodies, regardless of isotype.

(A) liposomes with 2F5 epitope peptide control (PBS)



(B) liposomes with 2F5 epitope peptide + 2F5 IgG



(C) liposomes with 2F5 epitope peptide + 2F5 IgA

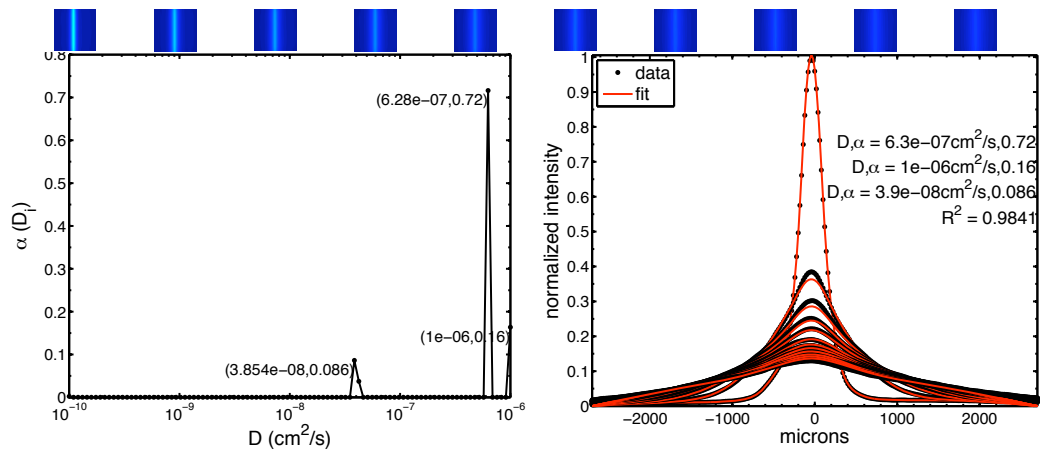


Figure 22. Examples of results from postphotoactivation scanning of liposomes with 2F5 epitope peptide with different isotypes of 2F5 antibody. For each condition, top: images over time (red = high intensity, blue = low intensity); bottom left: $\alpha(D)$; and bottom right: intensity profiles fit to diffusion model.

(D) liposomes with 2F5 epitope peptide + 2F5 IgM

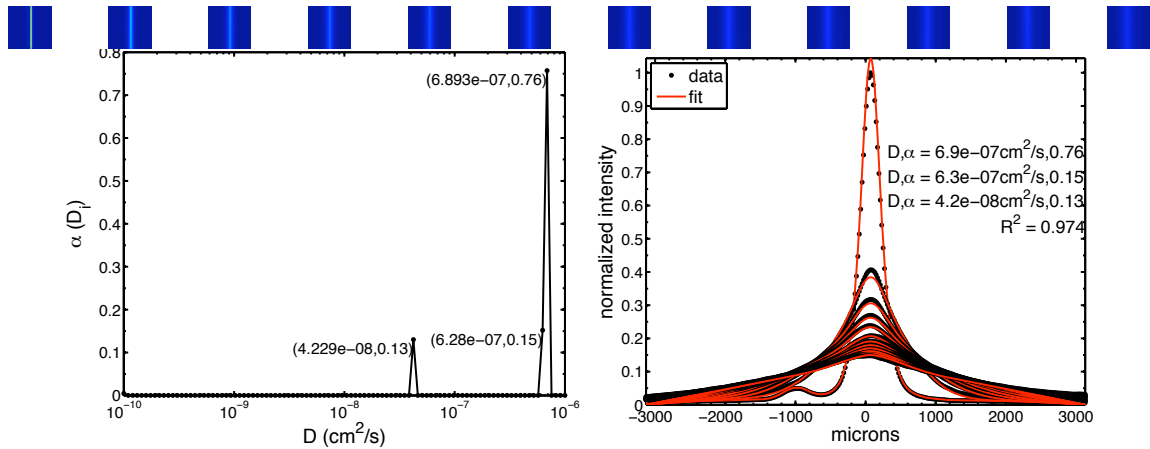


Figure 22. Examples of results from postphotoactivation scanning of liposomes with 2F5 epitope peptide with different isotypes of 2F5 antibody. For each condition, top: images over time (red = high intensity, blue = low intensity); bottom left: $\alpha(D)$; and bottom right: intensity profiles fit to diffusion model.

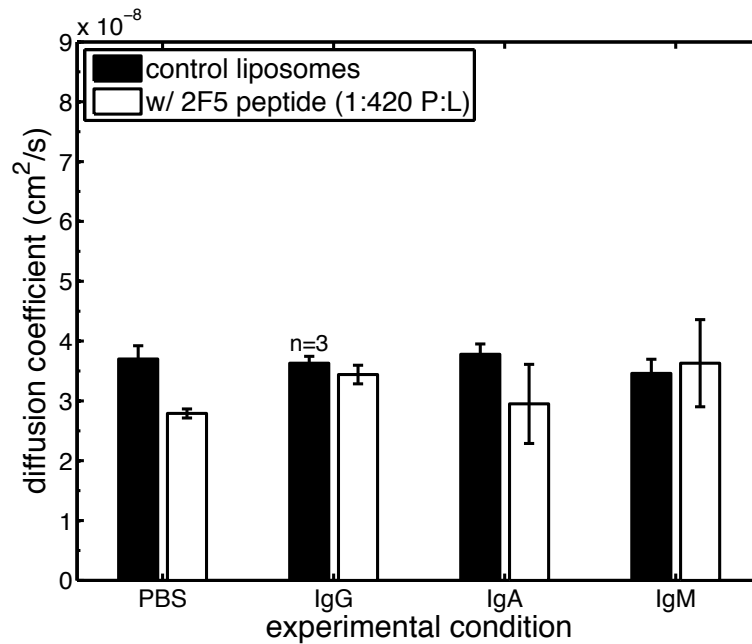


Figure 23. Diffusion coefficients of liposomes in the presence of 2F5 IgG, IgA, and IgM (mean \pm SE, n = 4 replicates unless otherwise noted).

Table 7. Diffusion coefficients (mean \pm SE, n = 4 replicates unless otherwise noted) of liposomes in the presence of 2F5 IgG, IgA, and IgM.

| | Diffusion coefficient ($\times 10^{-8} \text{ cm}^2\text{s}^{-1}$) | | | |
|--|--|--------------------------|---------------|---------------|
| | Control (PBS) | Antibody isotype | | |
| | | IgG | IgA | IgM |
| Control liposomes | 3.7 ± 0.2 | 3.6 ± 0.1 | 3.8 ± 0.2 | 3.5 ± 0.2 |
| Liposomes with 2F5 epitope peptide (1:420 P:L) | 2.79 ± 0.07 | 3.4 ± 0.2 (n = 3) | 3.0 ± 0.7 | 3.6 ± 0.7 |

For the second experiment, we increased the concentration of antibody relative to the number of epitopes so that the number of epitope-binding sites on antibodies would be equal to or in excess of the number of peptide epitopes. In the first experiment, the ratio of epitope-binding sites on antibodies to peptide epitopes (antibody:epitope ratio) was 1:32. In the second and third experiments, we varied the antibody:epitope ratio within the range of 1:1 to 5:1. We also focused on using IgA to aggregate antibodies because the aggregation of HIV virions by 2F5 dimeric IgA has been previously documented by Shattock et al. using size exclusion chromatography DLS [142].

Figure 24 and Table 8 summarize diffusion coefficients measured for liposomes in the presence of different concentrations of 2F5 IgA antibody. Even with increased concentrations of antibodies, we did not observe the expected decrease in diffusion coefficient. We did observe increased variation in our results due to noise in the images obtained. Figure 25 shows examples of postphotoactivation scanning images and intensity profiles. Images tended to be noisy because we had diluted the liposome solution 1/100 to achieve the desired antibody:epitope ratio. We have found that the postphotoactivation scanning method tends to be sensitive to noise, and that noise may

cause the experimentally-measured diffusion coefficient to appear higher than the true diffusion coefficient (see Appendix).

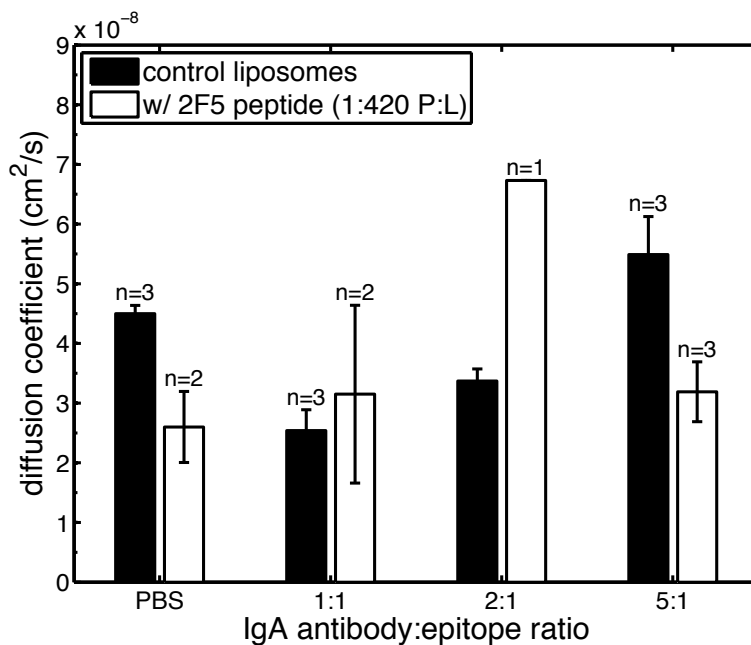
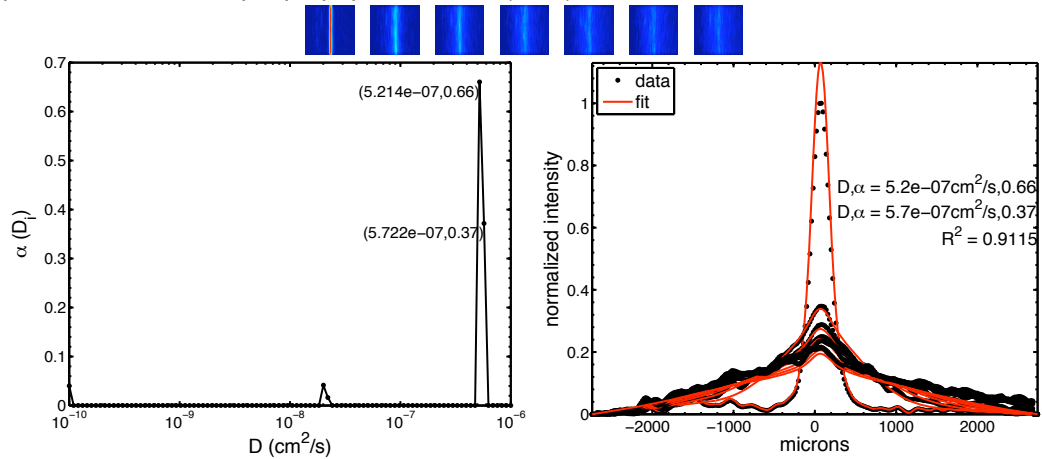


Figure 24. Diffusion coefficients of liposomes in the presence of different concentrations of IgA (mean ± SE, n = 4 replicates unless otherwise noted). For liposomes with 2F5 epitope peptide, the peptide:lipid ratio (P:L) was 1:420.

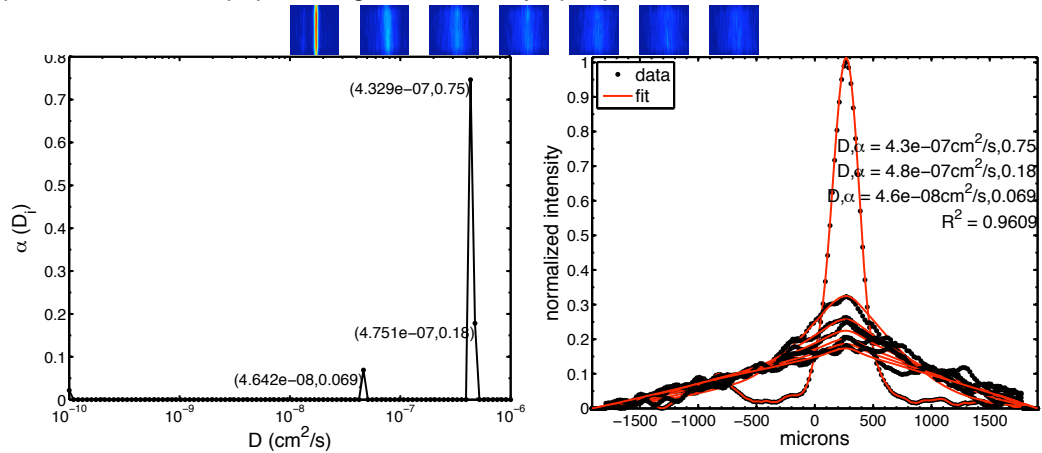
Table 8. Diffusion coefficients (mean ± SE, n = 4 replicates unless otherwise noted) of liposomes in the presence of different concentrations of IgA. For liposomes with 2F5 epitope peptide, the peptide:lipid ratio (P:L) was 1:420.

| | Diffusion coefficient ($\times 10^{-8} \text{ cm}^2 \text{ s}^{-1}$) | | | |
|--|--|----------------------------|----------------|----------------------|
| | Control (PBS) | IgA antibody:epitope ratio | | |
| | | 1:1 | 2:1 | 5:1 |
| Control liposomes | 4.5 ± 0.1 (n = 3) | 2.5 ± 0.3 (n = 3) | 3.4 ± 0.2 | 5.5 ± 0.6 (n = 3) |
| Liposomes with 2F5 epitope peptide (1:420 P:L) | 2.6 ± 0.6 (n = 2) | 3 ± 4 (n = 2) | 6.7 (n = 1) | 3.2 ± 0.5 (n = 3) |

(A) liposomes with 2F5 epitope peptide control (PBS)



(B) liposomes with 2F5 peptide + IgA 1:1 antibody:epitope ratio



(C) liposomes with 2F5 peptide + IgA 2:1 antibody:epitope ratio

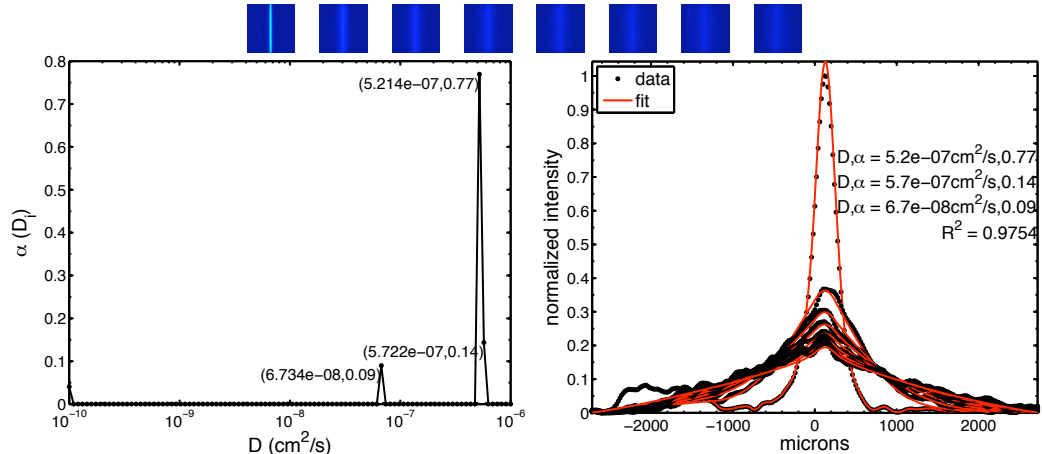


Figure 25. Examples of results from postphotoactivation scanning of liposomes with 2F5 epitope peptide and 2F5 dimeric IgA antibody. For each condition, top: images over time (red = high intensity, blue = low intensity); bottom left: $\alpha(D)$; and bottom right: intensity profiles fit to diffusion model. Here, the peptide:lipid ratio (P:L) was 1:420.

(D) liposomes with 2F5 peptide + IgA 5:1 antibody:epitope ratio

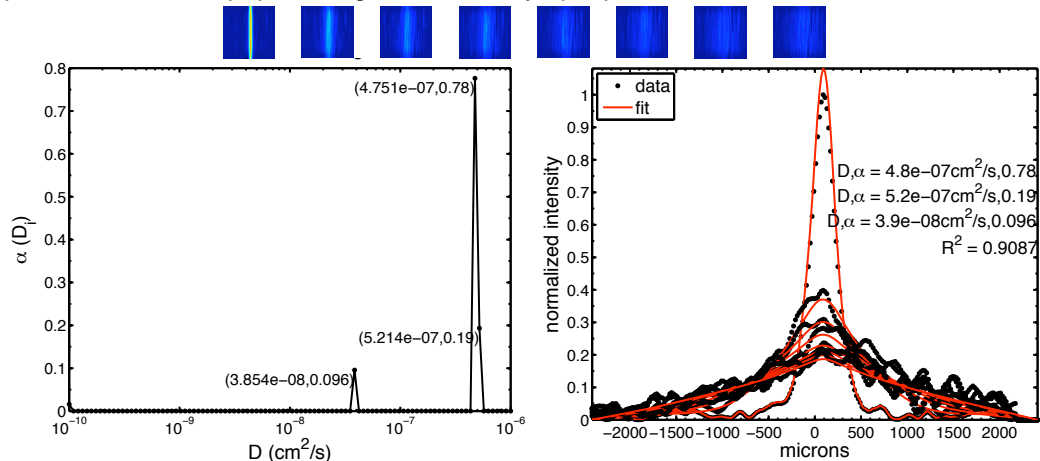


Figure 25. Examples of results from postphotoactivation scanning of liposomes with 2F5 epitope peptide and 2F5 dimeric IgA antibody. For each condition, top: images over time (red = high intensity, blue = low intensity); bottom left: $\alpha(D)$; and bottom right: intensity profiles fit to diffusion model. Here, the peptide:lipid ratio (P:L) was 1:420.

For the third experiment, we increased the number of epitopes on the liposomes from approximately 190 peptides per liposome to 760 peptides per liposome to see if this would increase the effect of aggregation. We also increased the concentration of fluorophore to improve the image quality upon dilution of the liposome solution. Again, we did not observe the expected decreases in diffusion coefficients (Figure 26). The image quality was still poor (Figure 27), and we observed high levels of variability in our results, likely due to noisy images.

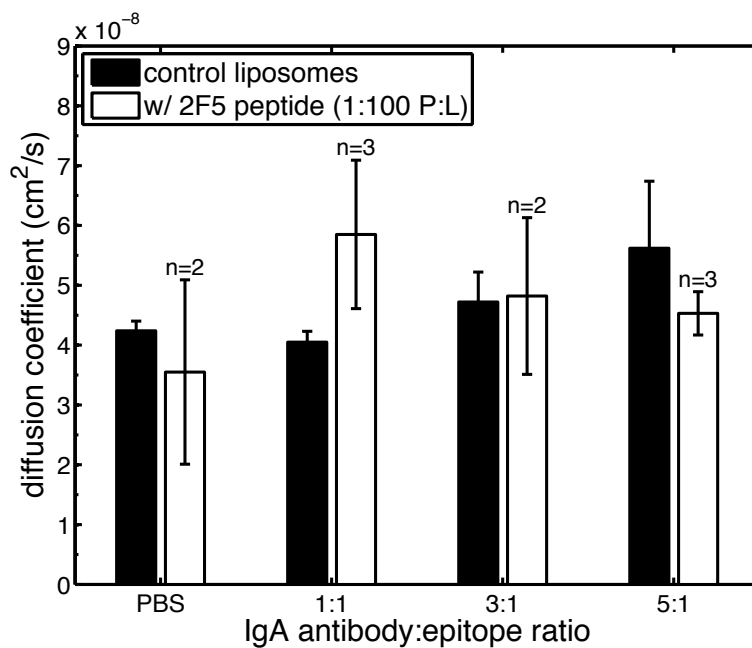
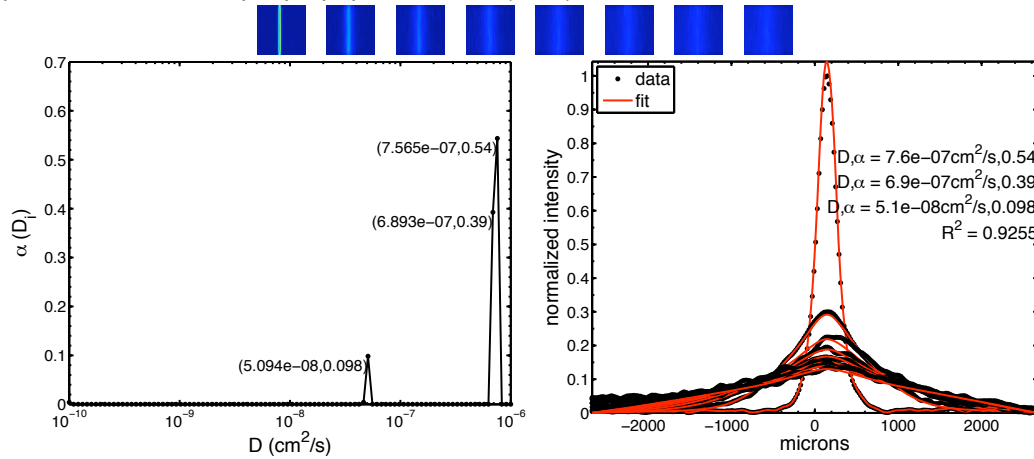


Figure 26. Diffusion coefficients of liposomes in the presence of different concentrations of IgA (mean \pm SE, n = 4 replicates unless otherwise noted). For liposomes with 2F5 epitope peptide, the peptide:lipid ratio (P:L) was 1:100.

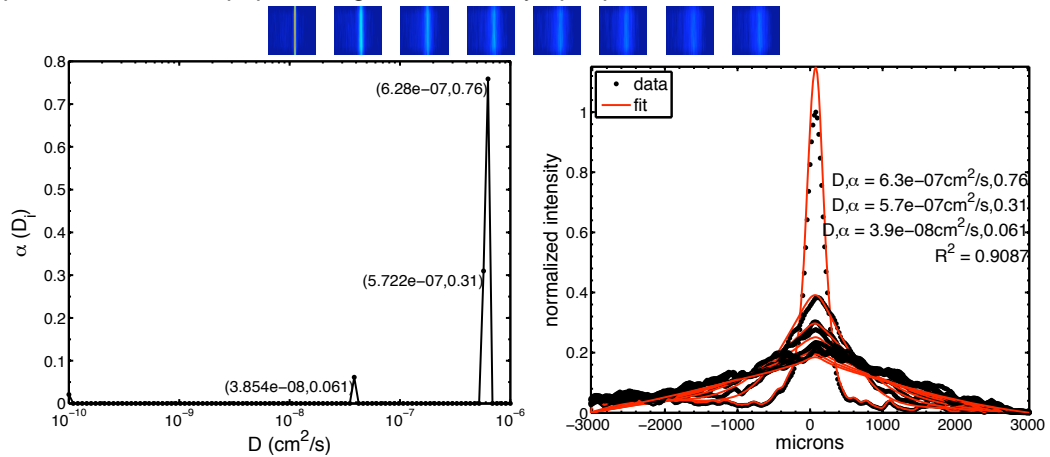
Table 9. Diffusion coefficients (mean \pm SE, n = 4 replicates unless otherwise noted) of liposomes in the presence of different concentrations of IgA. For liposomes with 2F5 epitope peptide, the peptide:lipid ratio (P:L) was 1:100.

| | Diffusion coefficient ($\times 10^{-8} \text{ cm}^2 \text{ s}^{-1}$) | | | |
|--|--|----------------------------|----------------------|--------------------------|
| | Control (PBS) | IgA antibody:epitope ratio | | |
| | | 1:1 | 3:1 | 5:1 |
| Control liposomes | 4.2 ± 0.2 | 4.1 ± 0.2 | 4.7 ± 0.5 | 6 ± 1 |
| Liposomes with 2F5 epitope peptide (1:100 P:L) | 4 ± 2 (n = 2) | 6 ± 1 (n = 3) | 5 ± 1 (n = 2) | 4.5 ± 0.4 (n = 3) |

(A) liposomes with 2F5 epitope peptide control (PBS)



(B) liposomes with 2F5 peptide + IgA 1:1 antibody:epitope ratio



(C) liposomes with 2F5 peptide + IgA 3:1 antibody:epitope ratio

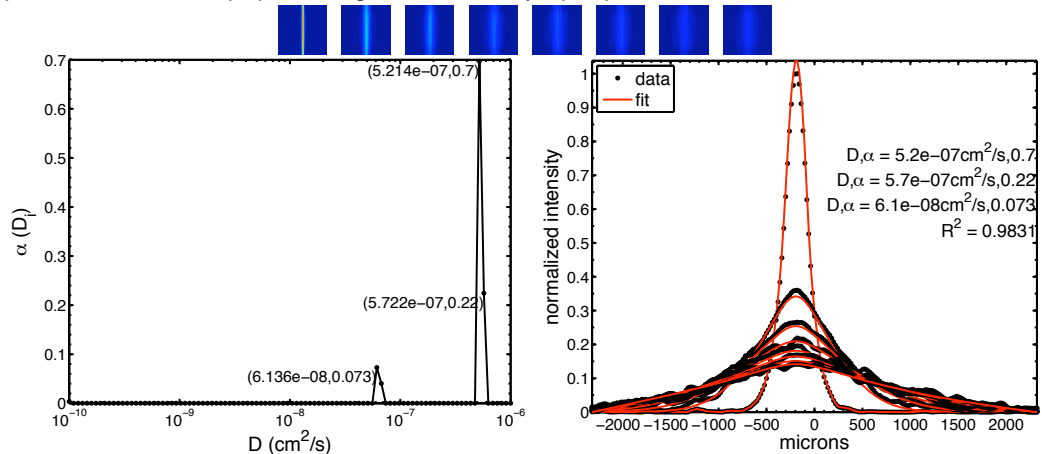


Figure 27. Examples of results from postphotoactivation scanning of liposomes with 2F5 epitope peptide with 2F5 dimeric IgA antibody. For each condition, top: images over time (red = high intensity, blue = low intensity); bottom left: $\alpha(D)$; and bottom right: intensity profiles fit to diffusion model. Here, the peptide:lipid ratio (P:L) was 1:100.

(D) liposomes with 2F5 peptide + IgA 5:1 antibody:epitope ratio

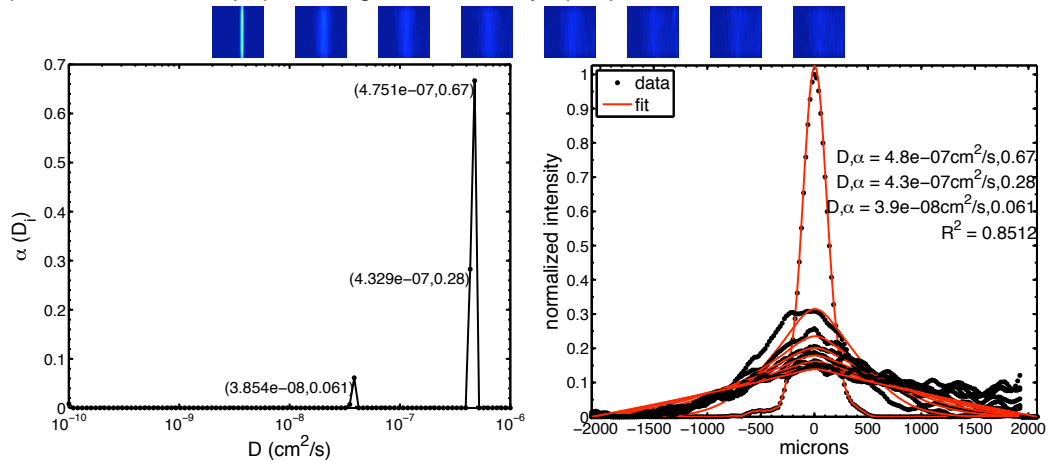


Figure 27. Examples of results from postphotoactivation scanning of liposomes with 2F5 epitope peptide with 2F5 dimeric IgA antibody. For each condition, top: images over time (red = high intensity, blue = low intensity); bottom left: $\alpha(D)$; and bottom right: intensity profiles fit to diffusion model. Here, the peptide:lipid ratio (P:L) was 1:100.

2.3.2 Mathematical model of aggregation

Since we did not observe the expected reductions in the diffusion coefficients in any of our experiments, we developed a mathematical model to better understand the kinetics of aggregation and the resulting distribution of diffusion coefficients for aggregates. We input values of constants that represent conditions used in postphotoactivation scanning experiments with liposomes and 2F5 IgA (Table 6). Inputting the high concentrations of liposomes and antibodies used in experiments, we observed that binding and aggregation reactions occur rapidly in the model, within seconds or minutes. Figure 28 shows the portion of epitopes on the liposome bound by antibody and the normalized concentration of antibody over time. The concentration of the free antibody in solution decreases and reaches equilibrium rapidly, as these antibodies bind epitopes on the liposomes. The equilibrium portion of epitopes bound is approximately the ratio of the concentration of antibodies and the concentration of spikes

on virions. Here, we input concentration values representing the 1:1 ratio of epitope-binding sites to epitopes used in experiments.

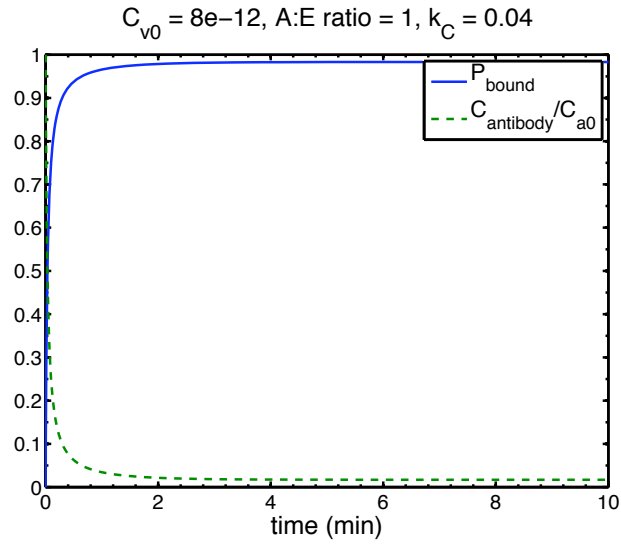


Figure 28. Mathematical model results for portion of spikes bound by antibody on each liposome over time and normalized concentration of antibody over time. The antibody concentration is normalized to the initial concentration of antibodies.

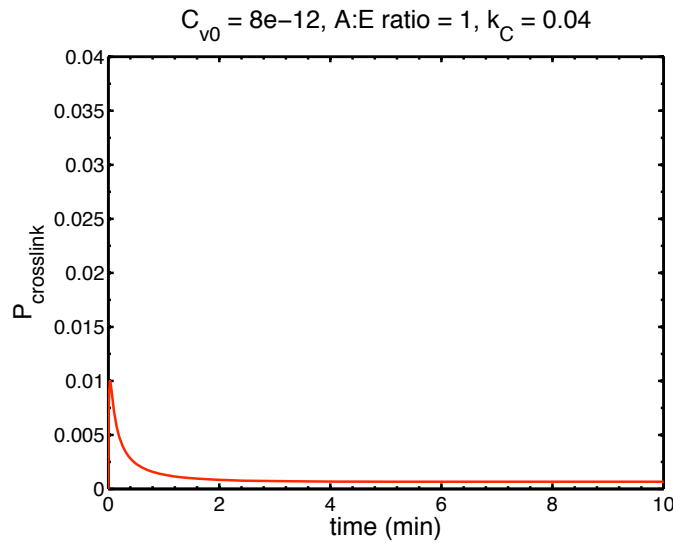


Figure 29. The probability of crosslinking over time in the mathematical model.

Figure 29 shows the probability of crosslinking over time (Equation 18). The probability of crosslinking increases rapidly to approximately 0.01 but quickly decreases

to reach an equilibrium value as P_{bound} reaches its equilibrium value. The actual value for the constant of crosslinking, $k_{crosslink}$, is unknown. The value input to the model here might be unrealistically high, causing aggregation to occur very quickly.

Figure 30 and Figure 31 show the concentration profiles of individual liposomes and aggregated liposomes over time. Again, aggregation reactions occur rapidly, within seconds or minutes.

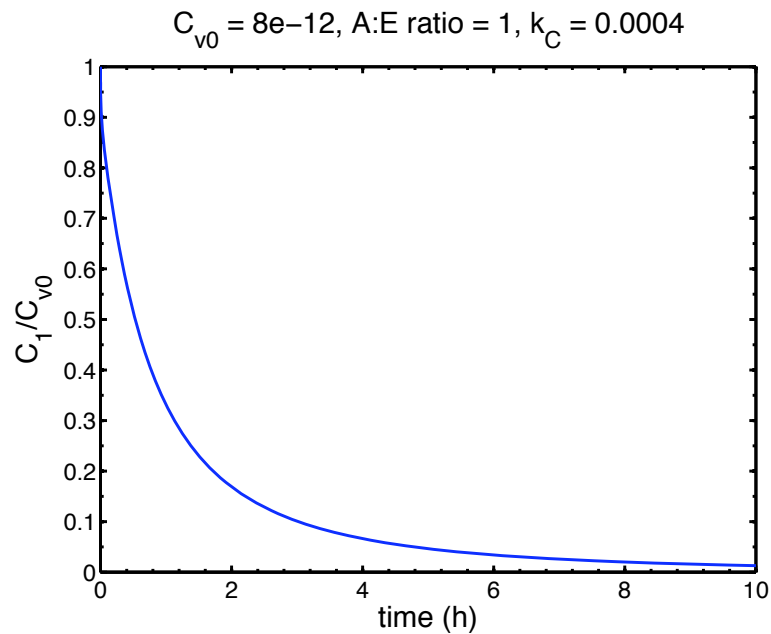


Figure 30. Mathematical model results for concentration of individual liposomes over time. Concentration is normalized to the initial concentration of liposomes.

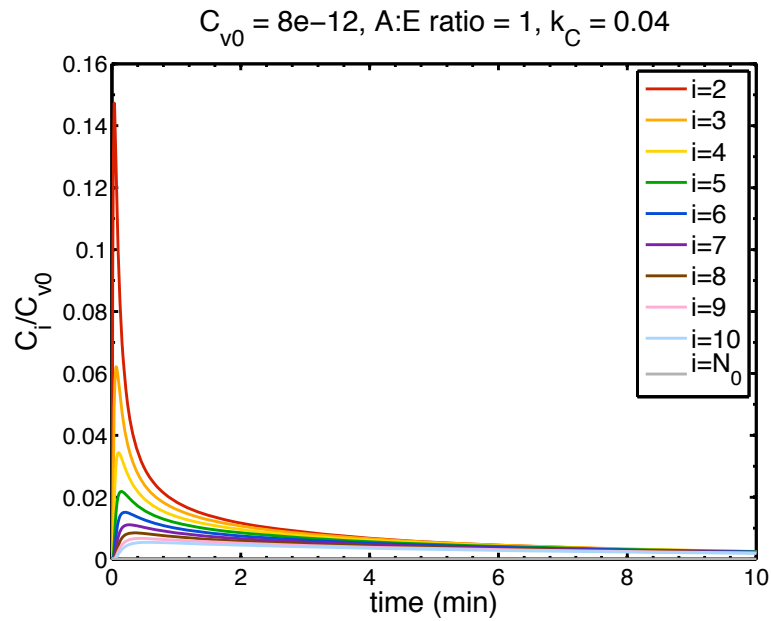


Figure 31. Mathematical model results for concentration profiles of liposome aggregates over time. Concentrations are normalized to the initial concentration of liposomes.

Figure 32 shows the distribution of diffusion coefficients that would result from the concentration profiles of aggregates. To estimate the diffusion coefficient of an aggregate with i particles, we used the Stokes-Einstein equation and the approximation for aggregate radius (Equation 32). Initially ($t=0$), none of the liposomes are aggregated, so there is a sharp peak in the distribution where $\alpha = 1$ and the diffusion coefficient is equal to that of single virions. After a few hours, the distribution rapidly spreads so that there is a range of diffusion coefficients representing the various sizes of aggregates. At the time of our experiments, after incubation for 4-5 hours or overnight, we would expect that aggregation would lead to a distribution of species with a range of diffusion coefficients.

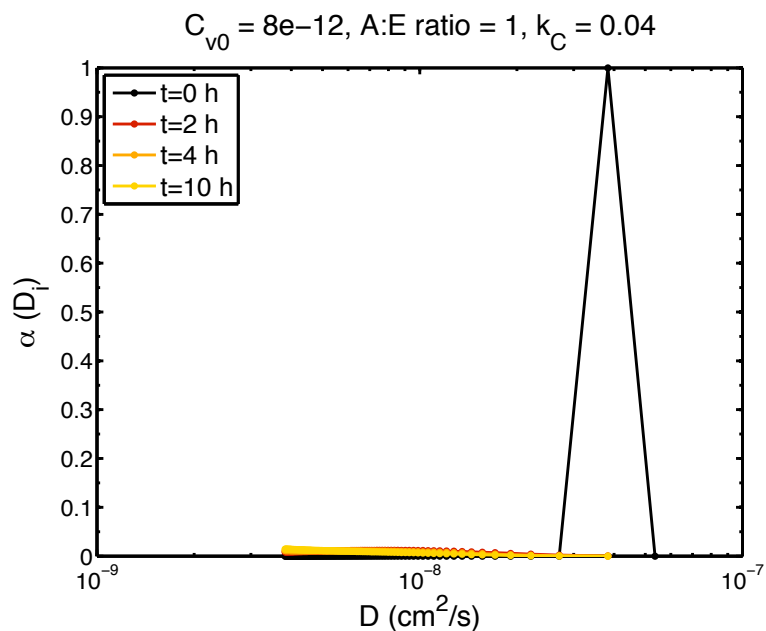


Figure 32. Distribution of diffusion coefficients resulting from mathematical model of liposome aggregation.

To determine if we would be able to detect this change in the distribution of diffusion coefficients using the postphotoactivation scanning method, we generated simulated postphotoactivation scanning profiles and used our analysis method to generate apparent results. Details of these simulation methods are described in the Appendix (§A.1).

Figure 33 and Figure 34 show simulated postphotoactivation scanning results for $t = 0$ and $t = 4$ h, respectively. At $t = 0$ h, none of the liposomes are aggregated, so this also represents the distribution of the control condition. For $t = 4$ h, we were able to detect a decrease in the apparent diffusion coefficient resulting from aggregation using simulated results. The output distribution of diffusion coefficients does not match the input distribution well, but it does reflect a decrease in the diffusion coefficients compared to control. The poor correspondence between input and output profiles is

likely due to the optimization algorithm used to solve for $\alpha(D)$. The analysis method has limited resolution, and the sum of intensity profiles resulting for several species with similar diffusion coefficients may resemble the intensity profile resulting from another, single species with disparate diffusion coefficient. This seems to have been the case here, where diffusing species with a range of diffusion coefficients from $3 \times 10^{-9} \text{ cm}^2/\text{s}$ to 3×10^{-8} appear mostly as a peak at $4.5 \times 10^{-9} \text{ cm}^2/\text{s}$, with some smaller peaks above and below this value.

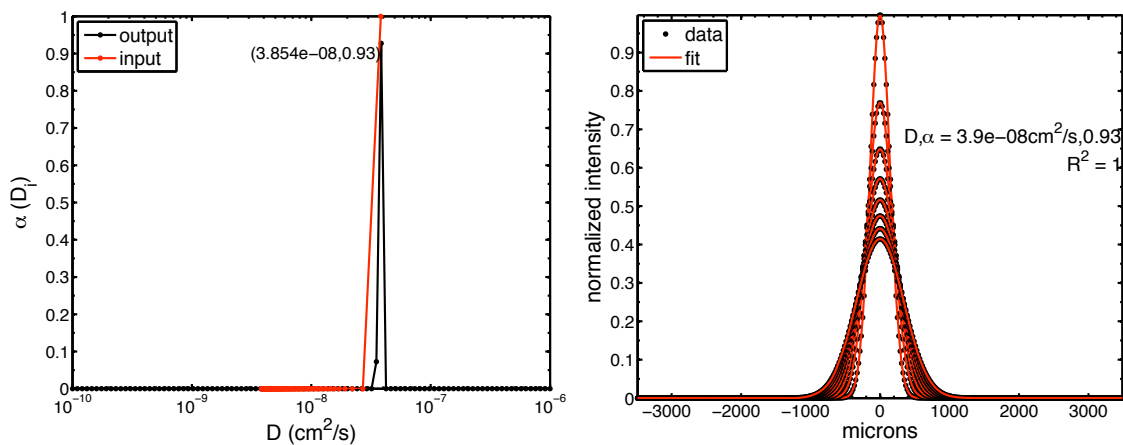


Figure 33. Example of simulated postphotoactivation scanning results from inputting the distribution of diffusion coefficients from the mathematical model of liposome aggregation for $t = 0$ (Figure 32). At $t = 0$ h, none of the liposomes are aggregated, so this also represents the control condition. Left: $\alpha(D)$; Right: intensity profiles fit to diffusion model.

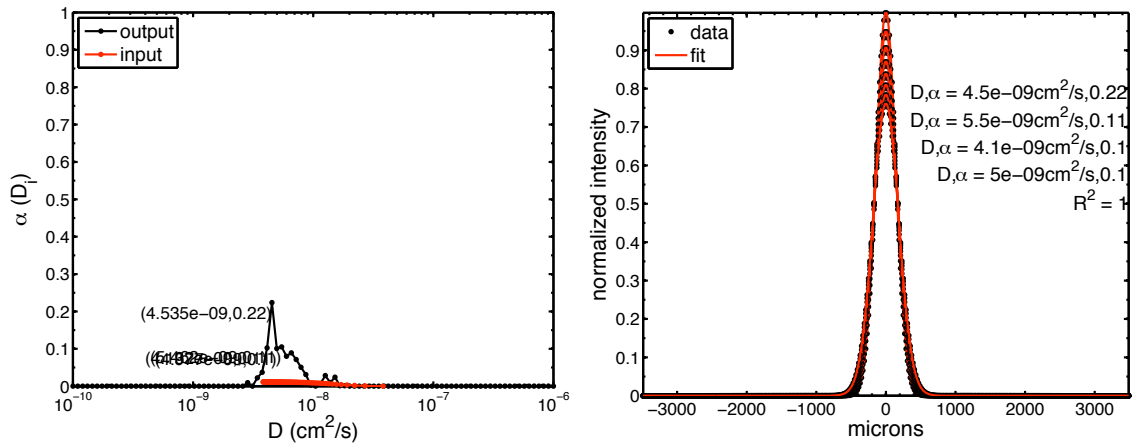


Figure 34. Example of simulated postphotoactivation scanning results from inputting the distribution of diffusion coefficients from the mathematical model of liposome aggregation for $t = 4$ h (Figure 32). Left: $\alpha(D)$; Right: intensity profiles fit to diffusion model.

Although we should theoretically be able to detect the change in diffusion coefficients caused by aggregation using postphotoactivation scanning, we encountered a number of experimental challenges, which may have affected our results. Factors included the presence of free label and noise. Thus, we conducted simulations with the addition of free label and noise. We introduced free label into simulations by inputting values typically observed for the free label peak in experiments: $\alpha = 0.9$ and $D = 5 \times 10^{-7}$ cm^2/s . We normalized the distribution of diffusion coefficients obtained from the aggregation model so that $\sum \alpha = 0.1$. Details of how noise was introduced to simulations are described in §A.3.2. Here, we used a moderate level of noise, $\sigma = 0.02$.

We found that, even despite these challenges, we should have been able to detect a decrease in diffusion coefficient if aggregation had occurred (Figure 35, Figure 36). The accuracy was diminished for the diffusion coefficient of the control case: The apparent diffusion coefficient was $5.0 \pm 0.4 \times 10^{-8}$ cm^2/s ($n = 5$ simulations), higher than

the input value of $3.8 \times 10^{-8} \text{ cm}^2/\text{s}$ (Figure 35). However, we detected reduced diffusion coefficients at $t = 4 \text{ h}$, with peaks representing aggregated liposomes at approximately $6 \pm 2 \times 10^{-9} \text{ cm}^2/\text{s}$ ($n = 5$ simulations) (Figure 36).

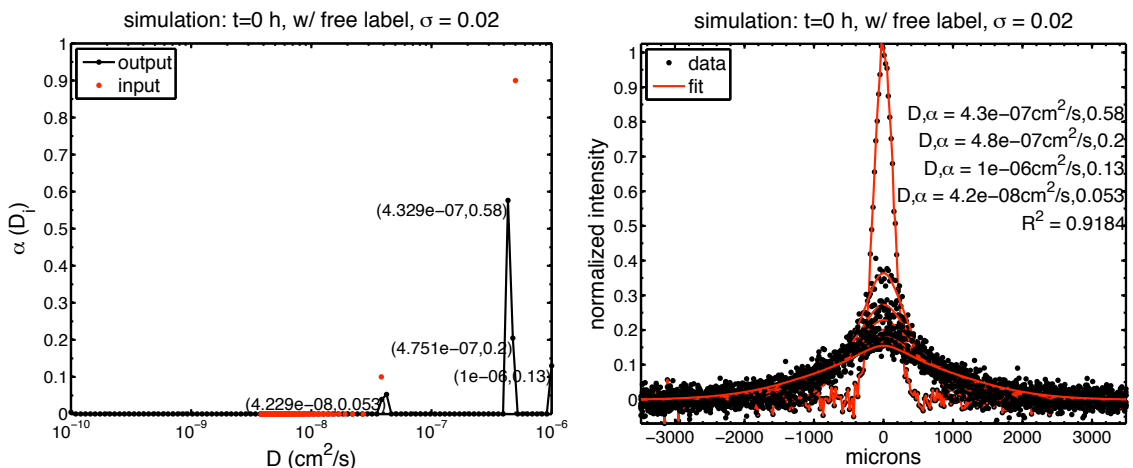


Figure 35. Example of simulated postphotoactivation scanning results from inputting the distribution of diffusion coefficients from the mathematical model of liposome aggregation with free label and noise for $t = 0$. At $t = 0 \text{ h}$, none of the liposomes are aggregated, so this also represents the control condition. Left: $\alpha(D)$; Right: intensity profiles fit to diffusion model.

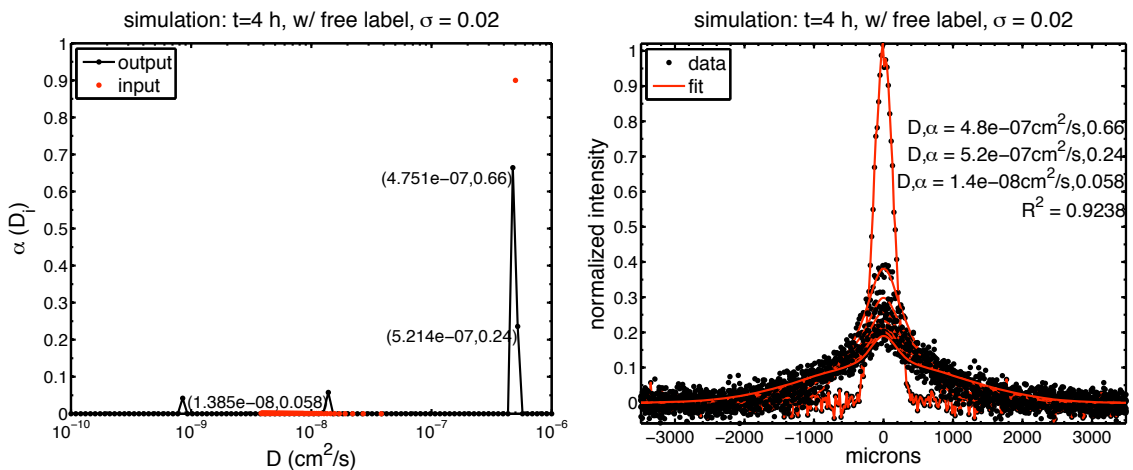


Figure 36. Example of simulated postphotoactivation scanning results from inputting the distribution of diffusion coefficients from the mathematical model of liposome aggregation with free label and noise for $t = 4 \text{ h}$. Left: $\alpha(D)$; Right: intensity profiles fit to diffusion model.

2.3.2.1 Sensitivity to ratio of epitope-binding sites on antibodies to epitopes

In our experiments, we used a range of antibody concentrations relative to the liposome concentration. We explored the effect of these different ratios in the mathematical model by inputting two extreme cases (Figure 37). In one, the number of epitope-binding sites on antibodies was much less than the number of epitopes (Figure 37A), antibody:epitope ratio = 0.0001. In the other case, the number of epitope-binding sites was in excess of the number of epitopes (Figure 37B), antibody:epitope ratio = 5. This latter condition was used in some of our experiments.

Changing the ratio of epitope-binding sites on antibodies to epitopes can dramatically affect the kinetics of aggregation (Figure 37). In both cases, we observed that the time needed for aggregation changed from the scale of minutes to hours. The antibody binding reaction, which depends on the rate constant of association (k_a) and the concentrations of antibodies and virions, occurs very rapidly: The portion of epitopes bound, normalized concentration of antibody, and the probability of crosslinking all reach equilibrium values within seconds (Figure 37A1, B1). When the antibody:epitope ratio is low (Figure 37A1), the concentration of antibody rapidly declines as all of the free antibody becomes bound to epitopes on liposomes. The portion of epitopes bound remains low because there are not enough antibodies to bind all of the epitopes. In contrast, when the antibody:epitope ratio is high, the portion of epitopes bound (P_{bound}) quickly increases (Figure 37B1). The concentration of free antibody remains high because there is an excess of antibody to epitopes.

Interestingly, there is a resulting difference between the kinetics of the probability of crosslinking in the two extreme cases: For high antibody:epitope, there is a transient period of time during which $P_{crosslink}$ increases before declining to near zero (Figure 37B2). For the low antibody:epitope case, $P_{crosslink}$ remains low at all times (Figure 37A2). This difference affects the concentration profiles of individual liposomes and aggregates over time (Figure 37A3-4, B3-4). However, the resulting distributions of diffusion coefficients, $\alpha(D)$, are similar over the timescale of hours (Figure 37A5, B5).

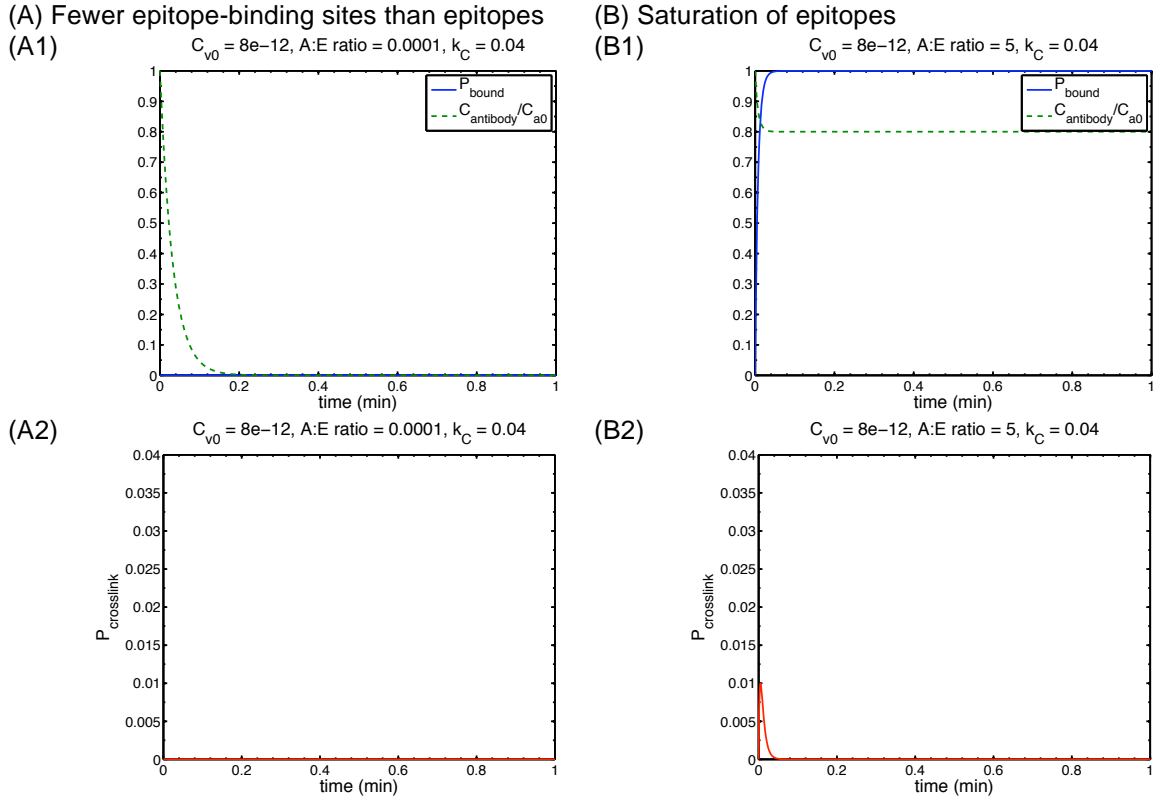


Figure 37. Comparison of aggregation model results for (A) low and (B) high antibody:epitope (A:E) ratios. The A:E ratio refers to the ratio of the number of epitope-binding sites on antibodies to the number of epitopes. Note that plots have different time scales.

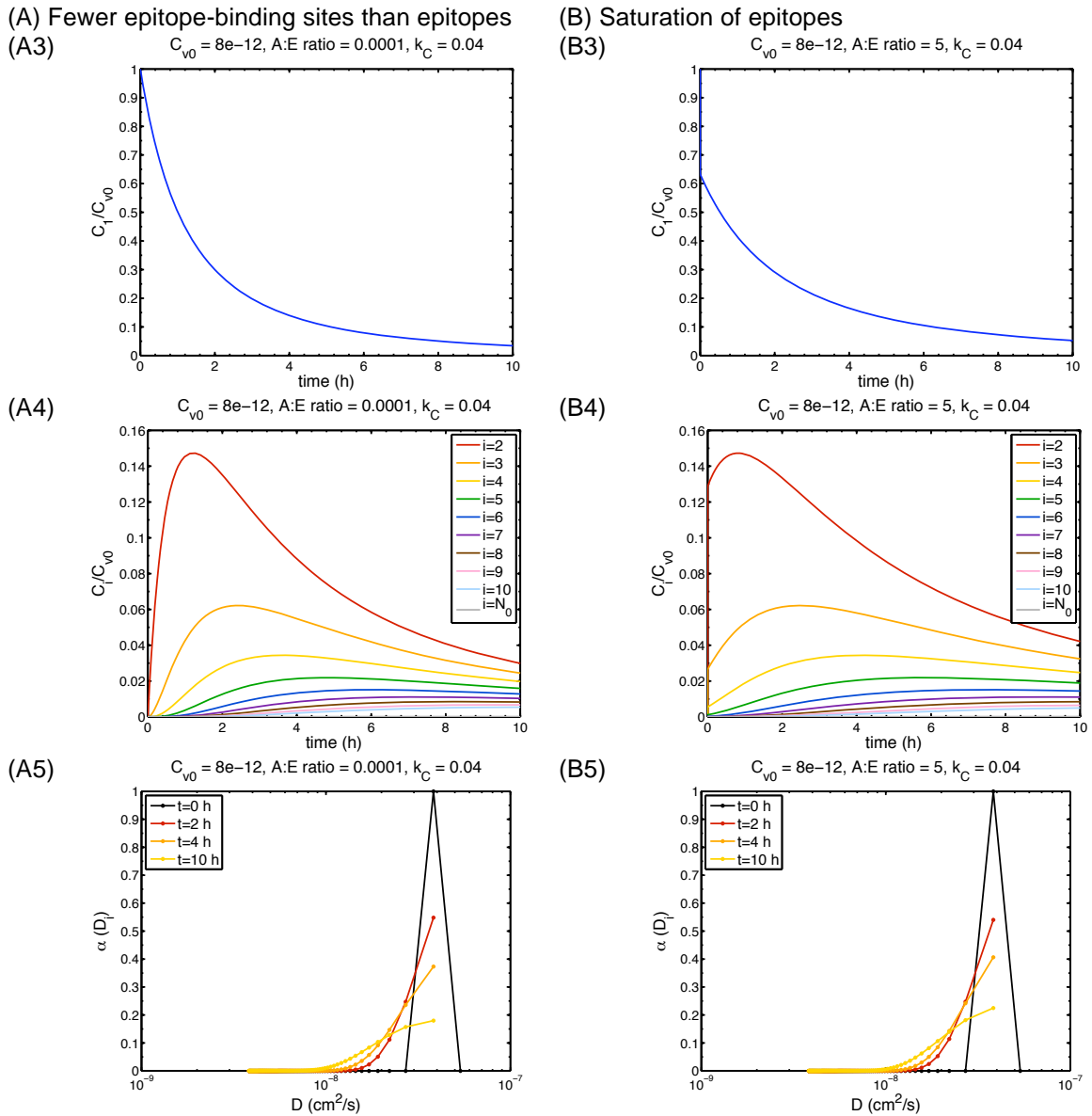


Figure 37. Comparison of aggregation model results for (A) low and (B) high antibody:epitope (A:E) ratios. The A:E ratio refers to the ratio of the number of epitope-binding sites on antibodies to the number of epitopes. Note that plots have different time scales.

Using the theory to predict if we would be able to experimentally detect changes in diffusion coefficient due to moderate aggregation, we again input the distribution of diffusion coefficients to simulations of postphotoactivation scanning. We used the distribution for A:E = 5, $t = 4$ h shown in Figure 37B5. Here, we found that the

postphotoactivation scanning assay would yield apparent diffusion coefficients of $3.1 \pm 0.3 \times 10^{-8} \text{ cm}^2/\text{s}$ ($n = 5$ simulations). This value is slightly lower than the true input diffusion coefficient of liposomes, $3.8 \times 10^{-8} \text{ cm}^2/\text{s}$. However, the reduction is more significant when compared to the apparent diffusion coefficient in the simulated control condition with free label and noise, $5.0 \pm 0.4 \times 10^{-8} \text{ cm}^2/\text{s}$ (Figure 35). This suggests that noise may lead to increases in the apparent diffusion that may obscure subtle reductions in diffusion coefficients caused by aggregation, especially when results are compared to controls with lower levels of noise.

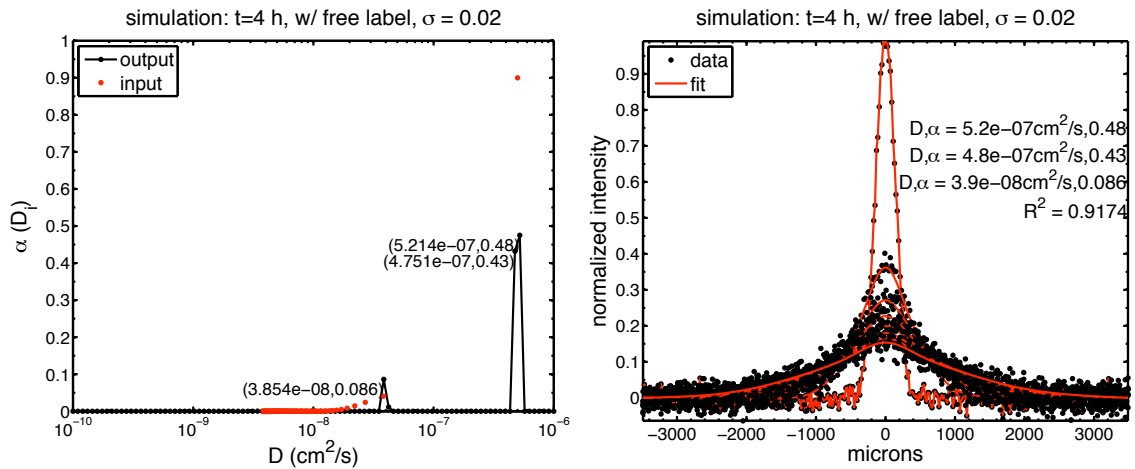


Figure 38. Example of simulated postphotoactivation scanning results from inputting the distribution of diffusion coefficients from the mathematical model of liposome aggregation for A:E ratio = 5 and $t = 4$ h (Figure 37B5) with free label and noise. Controls are shown in Figure 33 (without noise and free label) and Figure 35 (with same levels of noise and free label). Left: $\alpha(D)$; Right: intensity profiles fit to diffusion model.

2.3.2.2 Sensitivity to rate constant of crosslinking and concentration

The time course of aggregation is affected by the rate constant of crosslinking and the concentrations of antibodies and liposomes. The rate constant of crosslinking is currently unknown, and should be determined empirically, if possible. To explore the

sensitivity of our model to values of $k_{crosslink}$, we input a value reduced by a factor of 0.1 to the mathematical model (Figure 39A). Since P_{bound} and $C_{antibody}$ are not affected by $k_{crosslink}$, Figure 39A1 remains identical to the reference case in Figure 28. The shape of the $P_{crosslink}$ remains the same, but its magnitude is reduced by the decreased value of $k_{crosslink}$ (Figure 39A2). This, in turn, reduces the rate of aggregation (Figure 39A3-4).

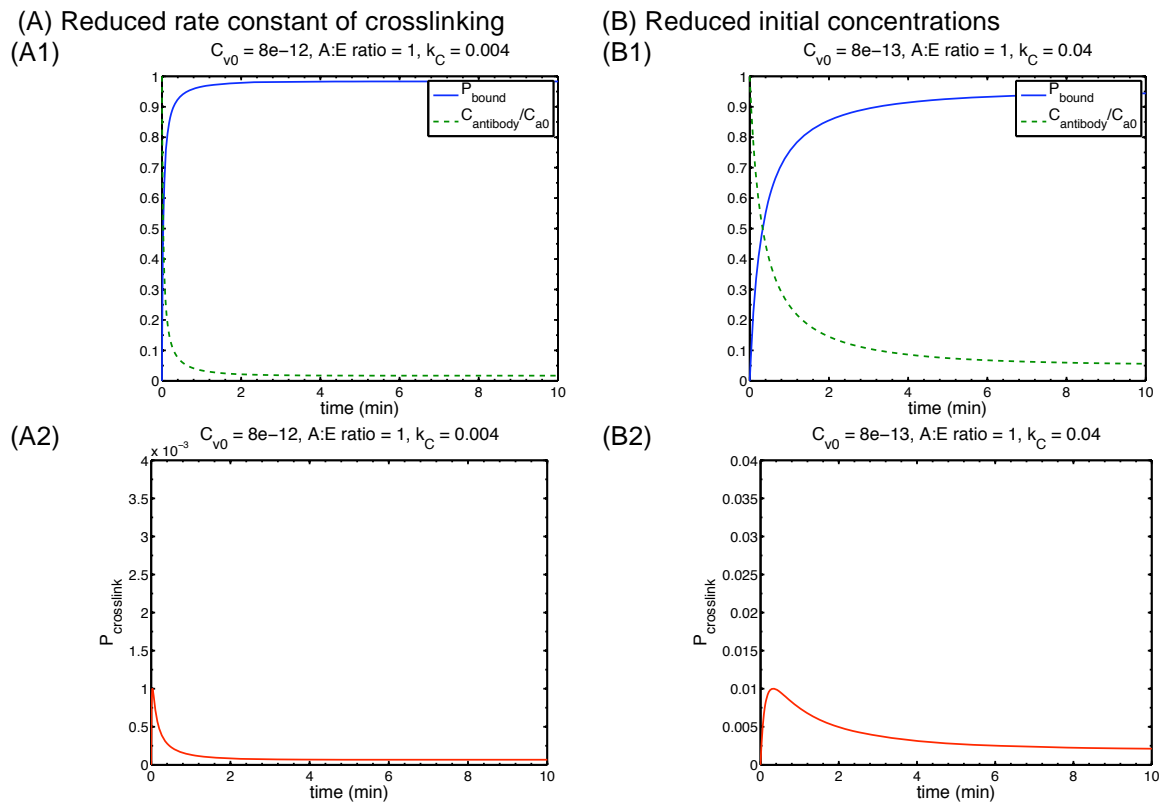


Figure 39. Comparison of aggregation model results for (A) reduced $k_{crosslink}$ and (B) reduced C_{v0} .

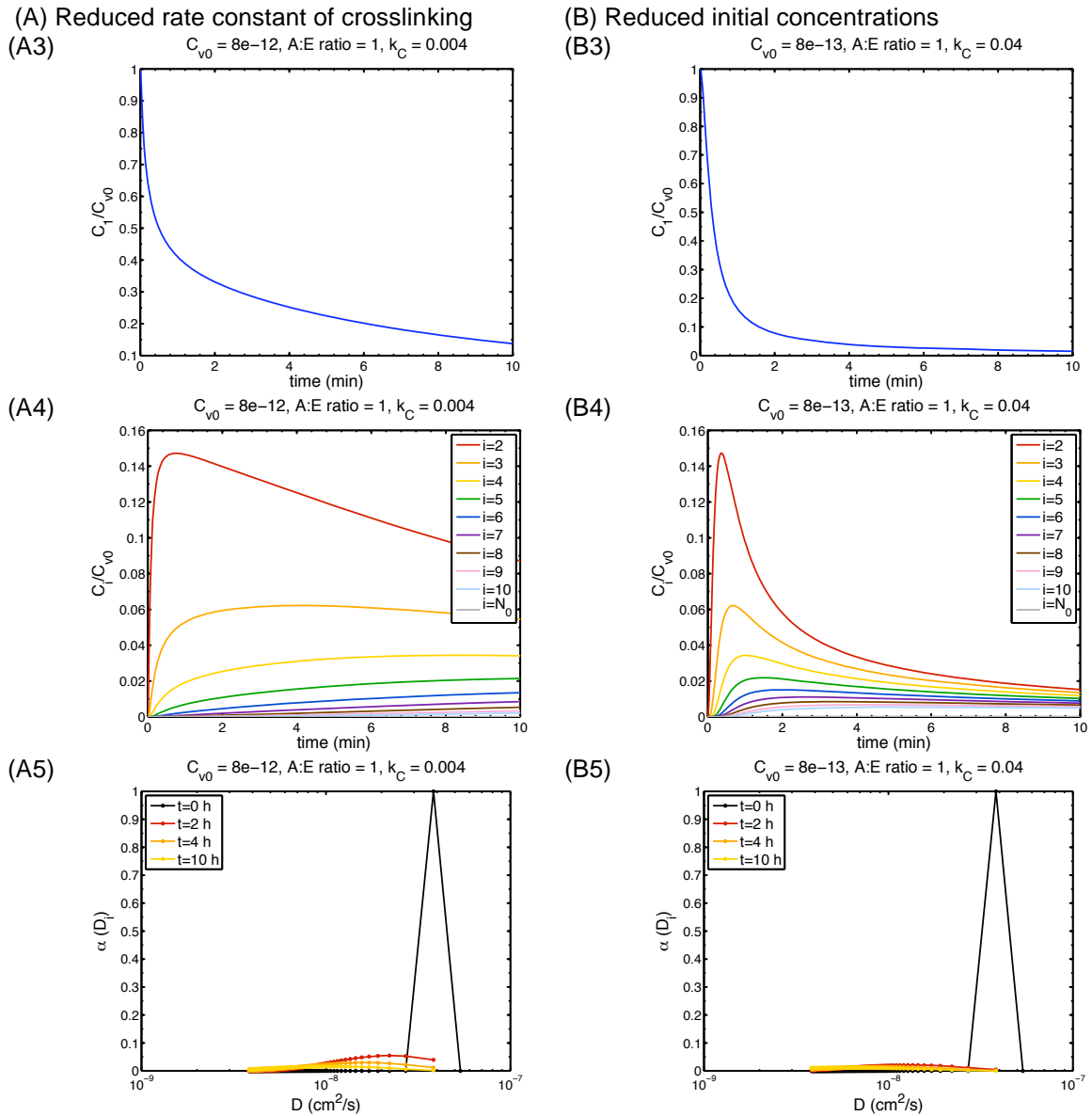


Figure 39. Comparison of aggregation model results for (A) reduced $k_{crosslink}$ and (B) reduced C_{v0} .

We also input values reduced by a factor of 0.1 for initial concentrations of liposomes and antibodies (Figure 39B). We found that this extended the time required for portion of antibody bound (P_{bound}) and concentration of free antibody ($C_{antibody}$) to reach equilibrium values (Figure 39B1). Furthermore, the equilibrium values differ from the reference condition because the rate of disassociation, which depends only on

antibody concentration, is greater relative to the rate of association, which depends on both antibody and liposome concentration. As a result, the probability of crosslinking reaches its maximum value more gradually (Figure 39B2). Overall, aggregation still occurs relatively quickly, on the time scale of minutes (Figure 39B3-4). The resulting distribution of diffusion coefficients (Figure 39B5) is similar to the reference condition (Figure 32).

2.4 Discussion

The goal of this study was to quantify the effects of antibody binding and aggregation on the diffusion coefficients of HIV virions. We hypothesized that antibody binding and aggregation would increase the effective radii of diffusing particles, thus decreasing the measured diffusion coefficients. Here, we conducted postphotoactivation scanning experiments using a model system of liposomes with 2F5 epitope peptide and 2F5 antibody. In our preliminary experiments, we did not observe the expected reductions in diffusion coefficients due to aggregation, despite trying a variety of experimental conditions. To further understand our problem, we developed a mathematical model of aggregation and performed simulations of postphotoactivation scanning. These indicated that we theoretically should have been able to detect reductions in diffusion coefficients due to aggregation using postphotoactivation scanning. Taken together, this suggests that (1) there were experimental phenomena that confounded our results and/or (2) aggregation effects in our experiments were actually small and our model does not properly account for experimental phenomena.

First, it is possible that there were experimental phenomena that confounded our results. For example, we observed high levels of noise in images, which may have caused measured diffusion coefficients to appear higher than their true values. Noise is due to (1) use of low concentrations of liposomes in experiments and (2) addition of antibodies. In our second and third experiments, we diluted liposome solutions to a much greater extent than in typical postphotoactivation scanning protocols to achieve the desired antibody:epitope ratios. The ratio of the molecular weight of each antibody epitope-binding site (150,000 g/mol) to the molecular weight of the 2F5 epitope peptide (4641.6 g/mol) was 32.3. Thus, the ratio concentration of IgA to peptide, in terms of mg/ml, should be 32.3 for 1:1 antibody:epitope ratio, 62.4 for 2:1 antibody:epitope ratio, etc. We were limited by the stock concentration of IgA, 1.78 mg/ml. The initial peptide concentration in the liposome solution was 0.1 mg/ml. Thus, it was challenging to strike a balance between the concentration of liposomes needed for postphotoactivation scanning and the desired antibody:epitope ratio. To obtain images, we needed to use the highest photomultiplier tube (PMT) and laser power settings on the scanner. In future experiments, it might be possible to use higher concentrations of liposomes in the assay if we could concentrate the antibody stock solution.

Furthermore, it is possible that the addition of antibodies also increased the level of noise in the images. We observed higher levels of background fluorescence in samples with high concentrations of antibodies, perhaps due to autofluorescence of the antibodies. This is supported by the observation that diffusion coefficients were often slightly higher for control liposomes and 2F5 peptide epitope liposomes in the presence

of antibody compared to the PBS controls (Figure 24, Figure 26). Interpretation of the results is complicated by the fact that there is currently no clearly-defined control condition. For example, our simulations in Figure 38 indicate that moderate reductions in diffusion coefficients due to aggregation may be obscured by experimental noise, which may cause diffusion coefficients to appear higher than their true values. In simulations, it is possible to compare equivalent levels of noise by simply inputting the same value for the noise coefficient. However, in experiments, the level of noise may have increased with increasing antibody concentration. Thus, it is impractical to compare the antibody treatment condition with the control in which no antibody was added. Comparison of liposomes with 2F5 epitope peptides to control liposomes with equivalent amounts of antibody added could help account for antibody-associated noise. However, it is not possible to discern any clear trends from our limited experimental data thus far. In future experiments, improved controls for antibody-associated noise could be mixtures of liposomes with 2F5 epitope peptide and antibodies that do not bind the liposomes or epitope.

Second, it may have been possible that aggregation effects in our experiments were actually small, and our model overestimated levels of aggregation. The level of aggregation in our system remains uncertain. Future work could use alternative methods to confirm aggregation, such as size exclusion chromatography. It would also be helpful to have a positive control for aggregation, such as dimeric anti-lipid antibodies. However, these were not available at the time of our experiments. The 2F5 antibodies were used here because they were available in polymeric forms. The 2F5 antibodies have

been studied comprehensively because they neutralize a broad spectrum of HIV. However, these antibodies may not be optimal aggregators of virions. Future research may uncover antibodies that are better aggregators of HIV.

Also, the optimal conditions for aggregation in our experimental system are unknown. There is likely a limited range of concentrations over which aggregation occurs. As shown by the mathematical model of aggregation, antibody:epitope ratios that are either too low or too high may lead to slow aggregation kinetics. When the antibody:epitope ratio is too low, crosslinking is slow because the reaction is limited by the small quantities of antibodies. When the antibody:epitope ratio is too high, then epitopes become saturated with antibody so that crosslinking is limited by the small number of free epitopes. The optimal number of epitopes on each liposome is also unknown.

The mathematical model of aggregation may have overestimated levels of aggregation. Some of the rate constants in the model are unknown. We inputted to the model the association (k_a) and dissociation (k_d) rate constants for 2F5 IgG because these values have been published in the literature [127, 143]. Ideally, we would have used the corresponding values for 2F5 IgA. However, these have not yet been published. The probability of crosslinking is also unknown. Ideally, empirical observations should inform the shape of the probability function (Equation 18). The constant of crosslinking ($k_{crosslink}$) should be empirically derived. Since the probability of crosslinking is a nondimensional quantity in the model, lowering its value would, in turn, lower the magnitude of aggregation. The value input here might have been unrealistically high. In

particular, at the high concentrations of antibodies and liposomes used in experiments and input to the model, the rate of crosslinking may be limited by the rate constant of the crosslinking reaction rather than diffusion. Thus, it is possible that our mathematical model overestimated the effects of aggregation.

Furthermore, our model does not account for antibody disaggregation. It is unknown if this is significant phenomenon in antibody-based aggregation of HIV virions. Disaggregation has been observed previously in biological systems: for example, in red blood cells that are aggregated by platelets [150]. If disaggregation were indeed significant, then it would be possible to account for this in the mathematical model by including additional disaggregation terms in the Smoluchowski equation (Equation 16).

While our experiments here did not detect changes in diffusion coefficients due to aggregation, we were able to uncover some deficiencies in our experimental system, develop a mathematical model of the kinetics of aggregation, and develop simulation methods that will be helpful in troubleshooting future experiments. The high levels of noise in our images and the sensitivity to noise of the postphotoactivation scanning analysis method point to the need to better account for variability caused by experimental noise, perhaps by using additional controls. Future experiments could also use alternative methods for measuring diffusion coefficients, such as Fluorescence Recovery After Photobleaching (FRAP). The length scale of imaging in FRAP is smaller than that of postphotoactivation scanning, so dilute solutions of liposomes could be used without introducing as much noise. In troubleshooting future experiments, the mathematical model can provide insights to how aggregation varies with input experimental

parameters, and simulations can help discern if changes in the distribution of diffusion coefficients can be detected using the postphotoactivation scanning method.

Overall, this work contributes to quantitatively understanding how binding and aggregation can affect diffusion of HIV virions. If hindrance of virion diffusion is indeed shown to be a possible mechanism of action for HIV prevention, then the virion diffusion coefficient in the presence of antibodies could be used as a metric for screening antibodies for topical microbicides or vaccines. The mathematical model may also serve as a tool for understanding how system parameters may affect the level of aggregation observed.

If future experiments are able to provide proof of concept for antibody-mediated reduction of diffusion coefficients, it may be interesting to investigate the phenomenon in more complex media. The biological context of our work here is the mechanism of antibody action sometimes referred to as immune exclusion: Polymeric immunoglobulins at mucosal membrane surfaces aggregate pathogens, such as virions, allowing complexes of pathogens and antibodies to be cleared with mucus or other local secretions. In the preliminary experiments in this chapter, we used a simple medium, phosphate-buffered saline (PBS). This medium, like water, may be similar in rheological and transport properties to plasma-like transudate found on epithelial surfaces of the vagina. Diffusion of particles in water is usually well described by the Stoke-Einstein relation (Equation 6). However, in future work, it may be interesting to investigate how antibody-induced aggregation may affect transport of immune complexes through more complex media like mucus or tissue. Recent studies have examined how HIV diffuses through mucus [36,

37] and interstitial spaces of epithelial tissue [31]. In these media, the effective diffusion coefficient might not be simply inversely related to the radius, as in the Stokes-Einstein relation. For example, the diffusion coefficient of particles in mucus has been described by an obstruction-scaling model [151, 152]. In tissues, transport is related to the size and connectedness pores through which particles move [153]. In these models, the increase in effective radius caused by aggregation may have an even more dramatic effect because there may be a size cutoff beyond which transport does not occur or is extremely slow.

Biomedical strategies for using antibodies to prevent HIV transmission could include vaccination to produce mucosal antibodies or topical application of exogenously produced antibodies as microbicides. One of the challenges in producing a prophylactic vaccine for HIV is the very brief window of time between HIV transmission and establishment of a pool of latently infected cells that cannot be cleared [14]. For this reason, vaccine researchers are seeking methods to use elements of adaptive immunity to trigger rapid innate immune responses to HIV [154]. Modulation of HIV transport at mucosal surfaces using antibodies could conceivably accomplish this goal: Antibody binding and aggregation could act synergistically with innate mucosal barriers like mucus and epithelial tissue.

2.5 Conclusions

The effects of antibody binding and aggregation on HIV diffusion have not been previously quantified. Here, we measured diffusion coefficients of HIV-like liposomes with 2F5 epitope peptides in the presence of 2F5 antibodies. In preliminary experiments, we did not observe reductions in diffusion coefficients by antibodies. To further

understand experimental parameters, we developed a mathematical model. This model describes the theoretical kinetics of aggregation and the resulting distribution of diffusion coefficients. Simulations suggest that it is theoretically possible to detect changes in diffusion coefficients resulting from aggregation in postphotoactivation scanning experiments. The model and simulations of postphotoactivation scanning can be used to troubleshoot future experiments.

3. Reduction of HIV-virion diffusion coefficients by semi-solid gels

3.1 Introduction

Another strategy for reducing the transport of HIV virions is to topically introduce a medium through which virions must diffuse before reaching mucosal tissue. Semi-solid polymer gels are good candidates for this purpose, as they are commonly used in vaginal drug delivery and have been used to formulate microbicides. Semi-solid gels have the potential to act as physical barriers to the diffusion of HIV virions: Polymers may hinder particle diffusion through physical obstruction, hydrodynamic drag, and/or electrostatic interactions.

In this chapter, we describe experiments for quantifying the diffusion coefficients of HIV virions and HIV-like liposomes in semi-solid gels. To our knowledge, diffusion coefficients of HIV virions in typical vaginal gels have not been previously measured. For our studies here, we selected two gels that are commonly used in vaginal drug delivery and have been used as placebos in microbicides clinical trials, hydroxyethyl cellulose (HEC) and methylcellulose (MC). As placebos, these materials are presumed to have minimal effect on virion diffusion. We hypothesized that the diffusion coefficients of HIV virions and HIV-like liposomes in these semi-solid gels would be lower than those in water. To investigate the effect of dilution on HIV transport, we also measured the diffusion coefficients of HIV virions and HIV-like liposomes in dilutions of these gels in PBS. We hypothesized that diffusion coefficients of HIV would increase with level of dilution.

This work provides proof of concept that vaginal gels, including microbicide gels, can reduce the diffusion coefficients of HIV virions. By quantifying HIV diffusion in these gels, we determined the baseline level of viral hindrance observed in typical vaginal gels. Measurements in dilutions of gels provide some preliminary idea of how dilution by fluids *in vivo* may affect the barrier functioning of these gels. Future efforts to design gels that act as physical barriers topically should out-perform these placebo gels.

3.1.1 Semi-solid gels used in vaginal drug delivery

Semi-solid gels have been used for intravaginal drug delivery [155, 156] and the formulation of topical microbicides [12, 13]. Microbicides formulated as semi-solid gels may act through several mechanisms in HIV prevention: They may deliver active pharmaceutical ingredients (APIs) to neutralize virus in fluids and/or tissue, provide lubrication to reduce trauma to the epithelium during intercourse, and slow HIV transport to mucosal surfaces by distancing infectious virions by forming a layer of gel between semen and epithelial tissue and hindering HIV diffusion through physical obstruction, viscous drag, or electrostatic interactions.

Semi-solid gels consist of low concentrations (typically 0.25-6%) of gelling agents within solvents. Polymers commonly used in vaginal gels and topical microbicide formulations are summarized in Table 10. Vaginal gels should have the following qualities: nontoxic; easy-to-use; discreet; painless; cost-effective; and widely-available [156].

Several polyanionic polymers have been evaluated as microbicide candidates: dextrin sulfate; dextran sulfate; cellulose sulfate; carrageenan; naphthalene sulfonate;

poly acrylic acid; and cellulose acetate phthalate [157]. These anionic polymers have been shown to bind HIV-1 *in vitro*, and some have formed the basis of first-generation microbicide gel candidates. However, none of these microbicide candidates has demonstrated efficacy for HIV prevention in clinical trials [158-161]. The reasons for the failures of microbicides clinical trials remain poorly understood [162]. Of these gels, those that have been shown to be safe might later be used as the basis for new microbicide formulations. For example, carrageenan-based Carraguard has been combined with other active pharmaceutical agents to form new candidate microbicide gels [163].

Table 10. Table of polymers commonly used in vaginal formulations and microbicides.

| Polymers commonly used in vaginal gels [155, 156] | Polymers used in microbicide gels |
|---|---|
| Carbopol | Carbopol (BufferGel [161]) |
| Gelatin | Carrageenan (Carraguard [159]) |
| Hydroxyethyl cellulose | Cellulose acetate phthalate [164] |
| Hydroxypropyl cellulose | Cellulose sulfate (Ushercell [158]) |
| Methylcellulose | Dextrin sulfate [165] |
| Polycarbophil | Dextran sulfate |
| Polyethylene glycol (MW < 20,000) | Hydroxyethyl cellulose (universal placebo [166]) |
| Polysaccharide hyaluronic | Methylcellulose (placebo in Carraguard trial [159]) |
| Polyvinylpyrrolidone | Naphthalene sulphonate (PRO2000[167]) |
| Sodium alginate | |
| Sodium carboxymethylcellulose | |
| Starch | |

Other next-generation microbicide candidates are also being formulated as topical gels. Some antiretroviral agents are being formulated as microbicides in semi-solid gels [12]. For example, the NNRTI Dapivirine (TMC120) is being formulated in a Carbopol gel [168]. The NNRTI UC781 is being formulated using a mixture of carbomer and

methylcellulose [169]. The NRTI Tenofovir is being formulated into a hydroxyethyl cellulose gel [170, 171].

3.1.2 Particle transport in semi-solid gels

When gelling agents are dispersed within a solvent, the molecules entangle and may associate to form three-dimensional networks. These three-dimensional structures impede the flow of fluids by trapping and immobilizing solvent molecules. Solvent molecules can be categorized as follows: (1) free, mobile molecules; (2) molecules bound as a solvation layer through hydrogen bonds; (3) molecules trapped within the gel network structure.

Mathematical models have been developed to describe particle diffusion in polymer solutions and to provide some insight about how we may conceptualize HIV virion diffusion in microbicide gels [172]. Mechanisms used in mathematical models include (1) hydrodynamic drag on particles, (2) physical obstruction by polymer chains, and (3) particle-polymer interactions such as electrostatic interactions. In hydrodynamic models, the diffusion coefficient is based on modifications to the Stokes-Einstein equation (Equation 6). Polymer chains are conceptualized as centers of hydrodynamic resistance that increase drag on the particle by slowing down the fluid near polymer chains. In physical obstruction models, polymer chains are treated as impenetrable objects that increase the path length for diffusing particles. Polymer chains allow passage of particles only when the particle is smaller than the distance between polymer chains. Some models account for electrostatic interactions or specific binding between particles and polymer chains. None of these mathematical models can perfectly predict the

empirical results for diffusion coefficients of particles in polymer solutions. In particular, many models fail to describe the dependence of diffusion coefficient on particle radius.

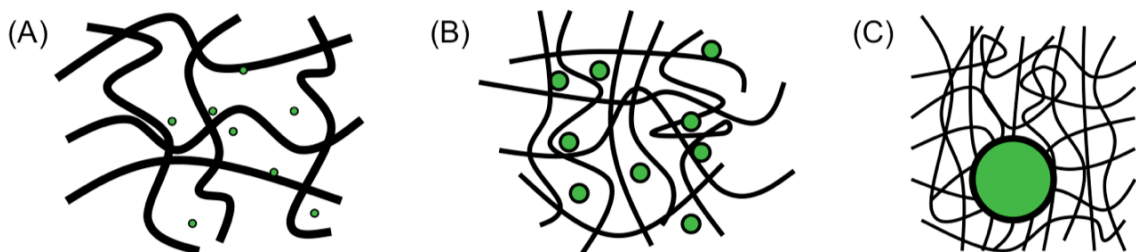


Figure 40. Scenarios of particle size in relation to gel structures. (A) Size of diffusing particles is much smaller than mesh size. (B) Size of diffusing particles is similar to mesh size. (C) Size of diffusing particles is much greater than mesh size.

Particle size in relation to gel structures is important in characterizing transport. Mesh size is defined as the average distance between polymer chains in solution. We may conceive of three general scenarios (Figure 40): (1) size of diffusing particles is much smaller than mesh size (Figure 40A); (2) size of diffusing particles is similar to mesh size (Figure 40B); and (3) size of diffusing particles is much greater than mesh size (Figure 40C). When particles are much smaller than polymer structures, then they may diffuse freely in solvent. Near polymer chains, particles could interact with solvent bound to polymer chains or polymer chains themselves. Polymer concentration would affect the frequency with which particles encounter polymer chains. When particles are similar in size to gel structures, then they could appear to have different regimes of motion. For example, particles could become trapped within gel networks if the polymer spacing is smaller than the particle diameter. Alternatively, particles could diffuse through gel networks where the polymer spacing is greater than the particle diameter. When particles are much greater than the mesh size, then they may experience the gel

structure as a continuum viscous or viscoelastic fluid. One caveat, however, is that particle surface properties may confound the expected relationship between particle size and diffusion. For example, one study observed that 500-nm polystyrene particles coated with polyethylene glycol (PEG) diffuse more rapidly in human cervical mucus than 100-nm particles coated with carboxyl groups [173]. Thus, diffusion coefficients are specific to the polymer, solvent, and diffusing particle.

One biological example of a semi-solid gel that acts to modulate the transport of pathogens at mucosal surfaces is mucus [100]. Mucus is a complex, viscoelastic glycoprotein gel consisting of many components. In studies using transmission electron microscopy (TEM), the mesh size of mucus has been observed to be 0.5-2 μm [174]. Mucins, the glycoprotein polymers that form the basis of mucous gel, are long (several microns) and flexible molecules. Mucins are coated with glycans, many of which have negatively-charged carboxyl or sulfate end-groups. Mucins also contain relatively hydrophobic regions that fold into globules stabilized by disulfide bonds. These hydrophilic and hydrophobic regions allow mucus to form multiple low-affinity bonds with particles. On epithelial surfaces in the body such as the gut and respiratory tract, mucus maintains an unstirred layer adjacent to mucosal surfaces. To penetrate through this unstirred layer, particles must diffuse through the gel. Elasticity may play an important role in trapping particles in mucus; elastic recoil prevents particles from diffusing as they would through a purely viscous medium. Mucus has been shown to trap pathogens and particles. For example, it has been shown that HIV virions can be trapped in cervical mucus [36, 37].

The diffusion of HIV virions through synthetic polymers used in microbicide gels has not yet been comprehensively studied. Understanding how gel properties affect transport of HIV virions could inform design topical formulations that act to hinder the transport of virions to tissue surfaces. Transport of HIV virions in semi-solid gels likely depends on the interaction of the virions, synthetic polymers, and water. For HIV, virion properties relevant to diffusion include size and surface properties determined by the lipid bilayer composition and glycoprotein spikes. Relevant properties of semi-solid gels include polymer concentration, polymer molecular weight, flexibility of polymer chains, polymer charge, interaction of polymer chains to form entanglements or crosslinks, and swelling characteristics of the polymer in the solvent. These properties contribute to determining mesh size. The mesh size of typical vaginal gels has not been determined. Previous studies of poly acrylic acid hydrogels suggest that the mesh size is 60-100 nm [175]. Studies of hydroxyethyl cellulose gels for electrophoresis estimate gel mesh size of 5-100 nm [176]. Another study of hydroxyethyl cellulose tablets swollen by water found that the equilibrium mesh size was approximately 26 nm [177]. This suggests that the mesh sizes of current vaginal gels are similar to the size HIV virions. Thus, semi-solid polymer gels are likely to hinder virion diffusion.

3.1.3 Methods for quantifying diffusion coefficients

We quantified the diffusion coefficients of HIV virions and HIV-like particles in two vaginal gels. The diffusion coefficient provides an objective means of comparing HIV transport in different materials. In Fickian diffusion, the diffusion coefficient relates diffusive flux and concentration gradient for particles within a given medium (Equation

4). The purpose of measuring the diffusion coefficient here is to help quantify the transport of HIV virions in scenarios relevant to HIV prevention. The first step in HIV infection is the contact of HIV and an infectable target cell. Assuming that transport occurs due to diffusion, it would be desirable to reduce the diffusion coefficient of HIV and thus reduce the flux of HIV to target cells.

There are many experimental methods for measuring the diffusion coefficient [178]. However, all methods derive from two basic approaches: (1) tracking the motion of individual particles to find the mean squared displacement and (2) fitting concentration profiles to diffusion equations. Our lab employs both of these approaches, in two methods that we use to measure diffusion coefficient: (1) particle tracking [179-181] and (2) postphotoactivation scanning [139].

Each of the two methods has advantages and disadvantages for measuring diffusion coefficients within the context of HIV transmission (Table 11). One advantage of particle tracking is that it can easily be applied to quantify transport of fluorescently-labeled HIV virions. Recently, particle tracking has been used to study diffusion of HIV virions in human cervical mucus [36, 37] and a synthetic hydrogel engineered to trap HIV [182]. More generally, particle tracking has also been used to study transport of small particles in various synthetic and biological media, including in living cells [181]. Particle tracking data are affected by microscale spatial heterogeneity, so diffusion coefficients obtained using this microscale method and alternative macroscale measurements may differ. For example, particle tracking may yield particles that appear immobile for the time of observation, perhaps trapped by polymer structures. In contrast,

some particles may appear to diffuse freely within the solvent. Due to spatial heterogeneity, quantitative measures of the diffusion coefficient may depend on the length scale of measurement. Single-particle tracking might not provide relevant diffusion coefficients, especially for gels with heterogeneous macroscale structures and larger particles [153, 183]. Thus, it is important to consider the biological context of the length scale of diffusion when selecting a method of measuring the diffusion coefficient.

Table 11. Comparison of methods for measuring diffusion coefficient (D).

| | Particle tracking | Postphotoactivation scanning |
|----------------------------|--|--|
| Data used to determine D | Root mean squared displacements of single particles over time | Concentration profiles over time |
| Imaging method | Fluorescence microscopy using 100× oil immersion objective | Fluorescence scanner (Genepix 4000B microarray scanner) |
| Length scale | Microns | Hundreds of microns to millimeters |
| Range of measurable D | Approximately 10^{-9} - 10^{-12} cm ² /s (Upper limit determined by movement of particles out of frame of observation; Lower limit determined by motion or noise) | Approximately 10^{-6} - 10^{-9} cm ² /s (Upper limit determined by time required to acquire fluorescence image; Lower limit determined by total length of experiment) |
| Diffusing particle | HIV virions labeled with fluorescent proteins | HIV-like liposomes encapsulating caged fluorescent label |
| Level of dilution | Minimal | Significant (Liposomes are extruded in PBS solution, Extent of dilution is limited by fluorescence of liposomes and detection of scanner) |
| Label | Any fluorescent label | Caged fluorophore (e.g., CMNB-caged fluorescein) |

The major advantage of postphotoactivation scanning is that it measures the diffusion coefficient over a length scale of hundreds of microns or millimeters, which is biologically relevant to microbicide gels. Topical microbicide gels are deployed in the

body in layers of approximately 50-500 μm [184, 185]. However, the major disadvantage of postphotoactivation scanning is that we have not yet been able to adapt the method for use with HIV virions. In collaboration with Dr. Thomas Hope's lab at Northwestern University, we evaluated HIV-1 virions labeled with photoactivatable green fluorescent protein (GFP) [186] fused with the viral protein gag for use in postphotoactivation scanning. We found that the fluorescent signal was not adequate for the macroscale imaging technique used in postphotoactivation scanning.

Our current solution for this obstacle is to use HIV-like liposomes as surrogates for HIV virions. These are liposomes with formulation based on the lipid composition of the HIV-1 envelope. Use of liposomes in the assay requires significant dilution of the test medium because the HIV-like liposomes are extruded within an aqueous medium, phosphate-buffered saline (PBS).

Finally, an important limitation of postphotoactivation scanning is that the time course of the experiment determines the lower limit of detection for the range of diffusion coefficients that can be measured. For very low diffusion coefficients, the intensity profiles will appear identical over the typical experimental time points. Furthermore, experimental noise can cause diffusion coefficients to appear higher than the actual values. For practical purposes, the time course of an experiment is limited by the maintenance of the sample quality over time. To prepare samples for experiments, we seal a small quantity (10-15 μl) within a chamber on a glass slide. The edges of the sample are surrounded by air. In experiments using vaginal gels, samples tend to dry out over time, causing the original photobleached line to shift. Approximately 3-4 hours is

the realistic maximum length of experiment. This corresponds to a lower limit of detection for diffusion coefficient of approximately 10^{-9} cm²/s (see Appendix). As a result, postphotoactivation scanning has thus far only been appropriate for quantifying the diffusion coefficient of HIV-like liposomes in gels with relatively high levels of dilution.

In our experiments here, we used the two methods to measure diffusion coefficients of HIV and HIV-like liposomes in various concentrations of gels (Table 12). We used particle tracking to measure the diffusion coefficients of fluorescently-labeled HIV virions in placebo gels that were undiluted, diluted to 50% (v/v) in PBS, and diluted to 20% (v/v) in PBS. We used postphotoactivation scanning to measure diffusion coefficients of HIV-like liposomes in placebo gels diluted to 10% (v/v), 5% (v/v), and 2% (v/v) in PBS. We also used postphotoactivation scanning to measure the diffusion coefficient of HIV-like liposomes in PBS alone.

Table 12. Concentrations of gels for which diffusion coefficients (*D*) were measured.

| Concentration | Ratio gel:PBS | Method used to measure <i>D</i> |
|---------------|--------------------|---------------------------------|
| 100% (v/v) | No dilution by PBS | Particle tracking |
| 50% (v/v) | 1:1 | Particle tracking |
| 20% (v/v) | 1:4 | Particle tracking |
| 10% (v/v) | 1:9 | Postphotoactivation scanning |
| 5% (v/v) | 1:19 | Postphotoactivation scanning |
| 2% (v/v) | 1:49 | Postphotoactivation scanning |

3.2 Materials and Methods

3.2.1 Microbicide placebo gels from clinical trials

We tested two placebo gels, 2.7% (w/w) hydroxyethyl cellulose (HEC) (Study No. C03-090, Batch 03724326, CONRAD, Arlington, VA) [166] and 2.5% methylcellulose (MC) (Batch 100306, Population Council, New York, NY) [187].

HEC is known as the “universal placebo” for microbicide clinical trials [166]. The HEC gel used in our experiments the placebo in the Phase III clinical trial of Ushercell, or cellulose sulfate [160, 188, 189]. Variations of HEC gels have also been used in other clinical trials [95, 161, 190, 191]. HEC is an uncharged linear polymer that has been shown to lack anti-HIV activity in *in vitro* assays and macaque models [166]. HEC has also been shown to be safe and acceptable to humans [192]. HEC has been presumed not to provide “the physical barrier protection of high-yield strength gelling agents” [166]. However, the actual barrier functioning of HEC has not been previously characterized.

MC was used as the placebo in clinical trials of the microbicide candidate Carraguard [159]. MC has been shown to lack anti-HIV activity *in vitro* [193] and does not protect macaques from SHIV infection [112, 163].

3.2.2 Particle tracking

3.2.2.1 Preparation of fluorescently-labeled HIV-1

HIV-1 virions fluorescently-labeled with Alexa Fluor 488 C5 maleimide were generously provided by Dr. Jeffrey D. Lifson (HIV-1 BAL/SUPT1-CCR5 CL.30 [Alexa 488 labeled /NEM Tx], Lot SP1551A, NIH, Frederick, MD). Treatment with the

fluorophore, which is an N-Ethylmaleimide (NEM) analog, eliminates infectivity of virions by cross-linking zinc finger structures needed for viral replication [194]. Envelope glycoproteins are unaffected by NEM treatment, retaining their structure and function. Virions prepared using these methods have been used previously in fluorescence correlation spectroscopy and microscopy studies of HIV transport in human cervical mucus [37]. Virions were stored at -80°C and thawed immediately before use.

For validation experiments, we used fluorescently-labeled latex beads of similar size to HIV virions (F-8801, red fluorescent (580/605) $0.1\ \mu\text{m}$ carboxylate-modified FluoSpheres® beads, Invitrogen, Carlsbad, CA).

3.2.2.2 Sample preparation

Gels were undiluted (100%), diluted to 50% (v/v) in $1\times$ phosphate-buffered saline (PBS) (from OmniPur $10\times$ PBS concentrate, EMD chemicals, Darmstadt, Germany) or to 20% (v/v) in PBS (Table 12).

For validation experiments, we used glycerol (G7757, Glycerol Reagent Plus, Sigma-Aldrich, St. Louis, MO), which is a Newtonian fluid. We also diluted the glycerol to 95% (w/w) and 90% (w/w) in distilled water. The viscosities of glycerol and glycerol dilutions were measured using a controlled-strain cone-and-plate viscometer (Brookfield Digital Rheometer model LV DV-III with CP52 cone, Brookfield, Middleboro, MA). Measurements were taken at 37°C , using 5 shear rates. Mean values of viscosity were reported (Table 16).

Samples of virions and gels were prepared by combining 1 μ l solution of HIV-1 virions (32.8 μ g/ml p24, 0.239 mg/ml estimated total protein concentration) and 100 μ l gel. Samples of fluorescent beads and gels were prepared by combining 1 μ l fluorescent bead solution at approximately 0.02% solids and 100 μ l gel. Samples were mixed by pipetting. Slides were prepared by placing a Secure Seal Spacer (Electron Microscopy Sciences, Hatfield, PA) on a glass slide, applying approximately 11.1 μ l of sample, and sealing with a coverslip. The thickness of the sample is determined by the spacer, which is 120 μ m thick.

3.2.2.3 Microscopy

Fluorescence microscopy (Zeiss Axio Observer with 100x/1.46 oil Plan Apochromat DIC objective, QuantEM backthinned EM-CCD camera) was used to image the position of diffusing particles over time. Images were acquired using MetaMorph 7.5 Stream Acquisition. Images of 100-nm beads were acquired using 1 ms exposure and 0.037 s between frames for 1000 frames. Images of HIV virions required greater exposure times of 5 ms and were acquired with 0.041 s between frames for 1000 frames. The number of particles observed varied depending on the concentration of particles and the medium. Typically, approximately 2-10 particles were observed in each stack. For each sample, 10 image stacks were acquired from different areas of the sample. Care was taken to ensure that the z-position during imaging was sufficiently above the coverslip, where particles may stick to the glass. For each condition, independent experiments were

performed on 3 different days using separate samples to obtain $n = 3$. All experiments were performed at 37°C .

3.2.2.4 Analysis

We analyzed images to obtain the diffusion coefficient (Figure 41). We found the x and y position of a given particle using the software Video Spot Tracker developed by the Center for Computer Integrated Systems for Microscopy and Manipulation at the University of North Carolina, Chapel Hill [195]. Image stacks where directional drift of all particles was observed were excluded from analysis. This was determined visually by watching the time-lapse images and noting when all particles in the field moved in the same direction. Directional drift was likely caused by convective flow in the sample or movement of the slide or microscope.

Coordinates for x and y positions were used to calculate the mean-square displacement (MSD), $\langle \Delta r^2(\tau) \rangle$ as follows [179-181]:

$$\langle \Delta r^2(\tau) \rangle = \langle \Delta x^2 + \Delta y^2 \rangle .$$

Equation 44

Here τ is the time interval, or time lag, over which the displacement was calculated.

Figure 41 illustrates how displacement values were obtained from combinations of individual images within an image stack. For example, for a particle that was observed for the entire length of imaging, 1000 frames, we would obtain 1000 coordinates for the position of the particle, one from each image. We could calculate the MSD for the time interval equal to the time between successive images (i.e., $\tau = 41$ ms)

by applying Equation 44 to the position coordinates for successive images. This would provide 999 values for MSD for time interval equal to the time between successive images. Values for MSD were averaged for each particle for each τ . Next, to find the average MSD for the time interval equal to two times the time between successive images (i.e., $\tau = 82$ ms), we would use the position coordinates from images from every other frame. This would provide 998 values for MSD. We used this technique to find the MSDs for all possible values of the time interval. The greatest time interval is equal to the total time of imaging, 40,959 ms, for which we would be able to obtain only one value of MSD using the position coordinates from the first and last image.

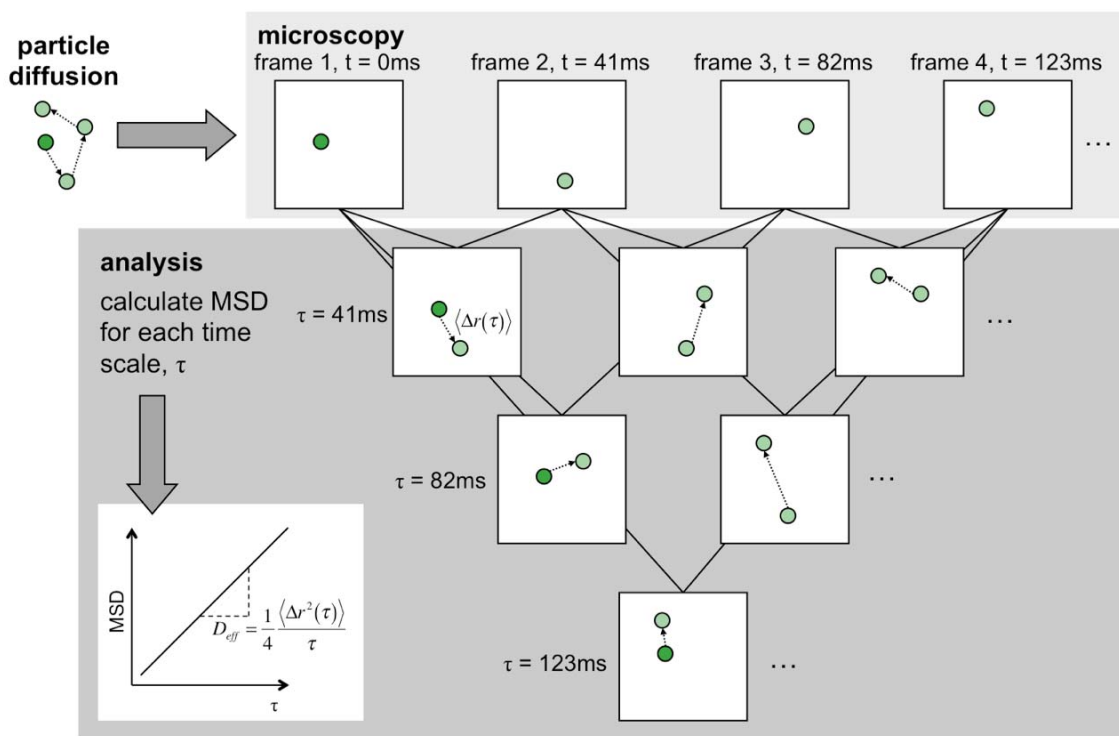


Figure 41. Scheme for calculating the diffusion coefficient from single-particle tracking.

For two-dimensional diffusion in a Newtonian fluid, the effective diffusion coefficient is related to the MSD as follows:

$$\langle \Delta r^2(\tau) \rangle = 4D_{eff} \tau .$$

Equation 45

Thus, we obtained the diffusion coefficients by plotting MSD with respect to τ and using a linear regression to find the slope, which is equivalent to $4D_{eff}$. We fitted MSD values to a linear regression in MATLAB using the linear least squares method (using MATLAB function “fit” with method “LinearLeastSquares”). Values were weighted using the inverse of the variance [180]:

$$\text{weight} = \frac{1}{\text{var} \langle r^2(\tau) \rangle} .$$

Equation 46

In MATLAB, each residual was multiplied by the weight. The best-fit line is the one that minimizes the sum of the square of the weighted residuals.

We used the function for calculating the variance for successive determinations of MSD developed by Qian et al. [179, 180]:

$$\text{var} \langle r^2(\tau) \rangle = \frac{\langle r^2(\tau) \rangle^2 F}{n_p} .$$

Equation 47

Here, n_p is the number of particles used to calculate the MSD for a given time interval and F is the coefficient of covariance:

$$F = \begin{cases} \frac{4n^2N_A + 2N_A + n - n^3}{6nN_A^2} & \text{for } N_A \geq n \\ 1 + \frac{N_A^3 - 4nN_A^2 + 4n - N_A}{6nN_A^2} & \text{for } N_A < n \end{cases}$$

Equation 48

Here, n is the interval over which the MSD values were calculated in terms of the number of images. This value can be calculated using the time interval (τ) such that

$$n = \tau \times \text{framerate}$$

Equation 49

and N_A is the number of possible intervals of length n that can be observed for a particle that appears in a given total number of images (T) such that

$$N_A = T - n$$

Equation 50

The coefficient of determination, R^2 , was calculated using MATLAB:

$$R^2 = 1 - \frac{\sum (MSD_{observed} - MSD_{fit})^2}{\sum (MSD_{observed} - \overline{MSD})^2}$$

Equation 51

Here, $MSD_{observed}$ is each observed data point for mean MSD for a given value of τ , MSD_{fit} is the corresponding value on the best-fit line, and \overline{MSD} is the mean of all observed data points.

Statistical analyses were performed using JMP 8 software (SAS, Cary, NC).

ANOVA was used to compare diffusion coefficients for all conditions; post-hoc t-tests

were then used to make comparisons of diffusion coefficients of HIV virions and 100-nm beads. Values for $p < 0.05$ were considered statistically significant.

3.2.3 Postphotoactivation scanning of HIV-like liposomes

Postphotoactivation scanning is a method of quantifying the diffusion coefficient that was developed previously by our group [139]. The method measures diffusion coefficients over the length scale of hundreds of microns or millimeters using fluorescent profiles.

3.2.3.1 Preparation of HIV-like liposomes

Thus far, we have not been able to adequately label HIV virions for use in postphotoactivation scanning, so it has become necessary to develop surrogate particles. Surrogate particles offer some advantages: Working with surrogate particles is safer than handling infectious virus, and the development of particles that mimic the transport properties of HIV can provide some insight to the components of HIV-1 envelope (Env) that determine its behavior. In choosing a surrogate for HIV virions, we considered the factors that would likely determine the diffusive properties of a particle, namely size and surface properties.

Liposomes were chosen as surrogates for HIV virions because these lipid vesicles can be extruded to approximate the size of HIV virions, and the lipid formulation can be designed to replicate properties of the HIV Env, which is comprised of a lipid membrane budded from the membranes of infected cells. Liposomes can be easily labeled with caged-fluorescein for use in postphotoactivation scanning (Figure 42).

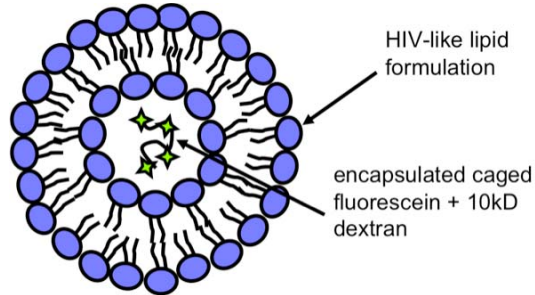


Figure 42. Liposome labeled for use in postphotoactivation scanning.

The lipid composition of HIV has been characterized previously (Table 13), and was used to create a synthetic lipid formulation for HIV-like liposomes (Table 14). HIV virions bud from the membranes of infected cells, typically T cells. The virus likely buds from a lipid raft formed by the clustering of viral structural proteins. Compared to host T cell membranes, the HIV-1 virion is enriched in saturated lipids, phosphatidyl serine (PS), plasmogen-phosphatidyl ethanolamine (plasm-PE), cholesterol, and sphingolipids.

Table 13. Lipid composition of HIV, from [101].

| Lipid | Mol % |
|--|-------|
| Cholesterol (Chol) | 45.2 |
| Plasmogen-phosphatidyl ethanolamine (plasm-PE) | 14.8 |
| Sphingomyelin (SM) | 12.5 |
| Phosphatidyl choline (PC) | 8.8 |
| Phosphatidyl serine (PS) | 8.4 |
| Dihydrosphingomyelin (DHSM) | 5.7 |
| Phosphatidyl ethanolamine (PE) | 4.4 |
| Mono-hexosylceramide (HC) | 0.2 |
| Ceramide (Cer) | 0.1 |

Table 14. Synthetic liposome formulation based on composition of HIV-1 Env (designed by Dr. Patrick Kiser, University of Utah).

| Lipid | Mol % |
|---|-------|
| Cholesterol (Chol) | 45 |
| Sphingomyelin | 18 |
| 1-O-1'-(Z)-octadecenyl-2-arachidonoyl-sn-glycero-3-phosphoethanolamine (Plasm-PE) | 15 |
| 1-oleoyl-2-palmitoyl-sn-glycero-3-phosphocholine (POPC) | 9 |
| 1,2-distearoyl-sn-glycero-3-phospho-L-serine (DSPS) | 9 |
| 1-palmitoyl-2-oleoyl-sn-glycero-3-phosphoethanolamine (POPE) | 4 |

It is debatable to what extent the lipid composition of HIV affects its diffusive properties compared to other components of Env. HIV-1 Env also contains glycoprotein spikes: The transmembrane glycoprotein gp41 and the external envelope glycoprotein gp120 form trimeric complexes on the surfaces of virions. HIV-1 gp120 has multiple, variable sites for N-linked glycosylation, where large glycans function to shield antigenic sites. The trimers function to mediate viral fusion and entry. The spikes also elicit host antibody responses, and have often been the target of vaccines. Recent cryo-electron microscopy tomography studies have shown that each HIV-1 virion has 14 ± 7 (range 4 to 35, $n = 40$ virions) Env spikes (Figure 43) [102]. Each spike is approximately 10.5 nm in diameter and 13.7 nm in height [102]. Assuming that the diameter of each HIV-1 virion is approximately 110 nm and each virion has 14 10.5-nm spikes, only about 3% of the surface area of each virion is “covered” with glycoprotein spikes. This would leave a significant portion of the lipid membrane surface exposed. Therefore, it is conceivable that the lipid portion of HIV-1 Env is a major determinant of the surface properties of HIV virions.

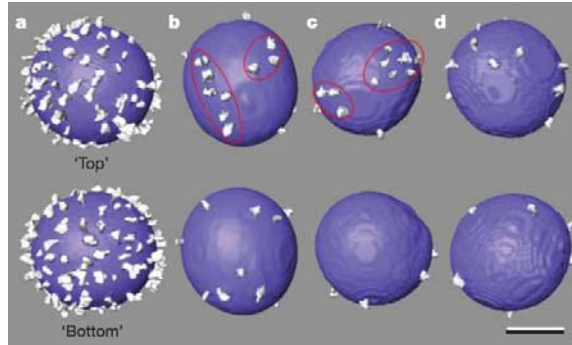


Figure 43. Cryo-electron microscopy tomography characterizing the spatial distribution of Env spikes on (a) SIV and (b-d) HIV-1. These surface-rendered models of virions suggest that spikes cover only a small portion of the HIV-1 virion surface, leaving much of the lipid portion exposed. Scale bar = 50 nm. Reproduced with permission from Macmillan Publishers Ltd: *Nature* from Ref. [102] © (2006).

Liposomes (Figure 42) were prepared using membrane extrusion as described previously [144] using the Avanti® Mini-Extruder (Avanti Polar Lipids, Inc., Alabaster, Alabama). Lipids of the amounts listed in Table 14 were dissolved in chloroform. Using a desiccator and vacuum, the chloroform was allowed to evaporate overnight. Liposomes were labeled with caged-fluorescein by rehydrating the lipid film with a solution of 10-kD dextrans conjugated with CMNB-caged fluorescein via succinimidyl ester in PBS; this mixture was incubated for 45 minutes in a water bath at 50° C prior to extrusion. Dextrans were conjugated with caged fluorophore using 10 mg/ml amino 10-kD dextrans (Cat. No. D-1860, Invitrogen, Carlsbad, CA) and CMNB-caged fluorescein, succinimidyl ester (Cat. No. C-20050, Invitrogen, Carlsbad, CA) according to the manufacturer's instructions. Fluorescent label was conjugated to dextrans to improve solubility in PBS. Liposomes were formed by extrusion through 400-nm, 200-nm, and 100-nm nucleopore membranes in succession. Free label was subsequently removed using gel filtration columns (Sephadex G75, GE Healthcare, Piscataway, NJ). Liposomes were sized using

dynamic light scattering (DLS) (ZetaPlus Zeta Potential Analyzer with Model B1-9000AT Digital Correlator, Brookhaven Instruments, Holtsville, NY).

3.2.3.2 Sample Preparation

Mixtures of HIV-like liposomes and gels were prepared for postphotoactivation scanning by combining solutions of HIV-like liposomes in PBS, HEC or MC, plus additional PBS. The final concentration of the HIV liposome solution in all mixtures was 50% (v/v). The final concentrations of either HEC or MC gel tested were 50% (v/v), 20% (v/v), 10% (v/v), 5% (v/v), and 2% (v/v). We also tested the HIV-like liposomes diluted to 50% (v/v) with PBS alone.

Slides were prepared by placing a Secure Seal Spacer (Electron Microscopy Sciences) on a glass slide, applying 11.1 μ l of sample, and sealing with a coverslip (Figure 15). The depth of the sample is the thickness of the spacer, 120 μ m. For each condition, we prepared 4 replicates for each experiment. Results from replicates were averaged. We then performed 3 independent experiments on different days, using separate batches of liposomes. These were summarized using the mean and standard error.

3.2.3.3 Imaging fluorescent profiles

The postphotoactivation scanning method analyzes fluorescence profiles over time to determine diffusion coefficients. Here, the particles of interest, HIV-like liposomes, were labeled using CMNB-caged fluorescein conjugated via succinimidyl ester to amino 10-kD dextrans (Invitrogen, Carlsbad, CA), which becomes fluorescent

after exposure to UV light (Figure 17). A line is uncaged by UV light (using 500 W mercury arc lamp, Oriel, Stratford, CT and UV filter, 255-425 nm, Edmund Scientific, Barrington, NJ) using a metal stencil with a slit of width 200 μm (Figure 16).

The fluorescent profiles were imaged over time using a microarray scanner with 532 nm laser and 20- μm pixel resolution (Genepix 4000B, Molecular Devices, Sunnyvale, CA). A single image was obtained prior to uncaging to provide background information for image analysis. After uncaging, images were obtained approximately every 25 minutes for 3.5 hours. Experiments were performed at room temperature, approximately 24-25°C.

3.2.3.4 Analysis

Image analysis was performed using MATLAB (The MathWorks, Inc., Natick, MA). For each slide, a portion of the image containing the fluorescent region was selected for analysis. The user selected the portion for analysis visually, using the computer cursor to highlight an area that (1) contained the entirety of the fluorescence as it diffused outward in the x direction so that the fluorescence at the boundaries was equal to the background level of fluorescence and (2) had the minimal amount of experimental noise due to spots on slide or bubbles in the sample. Slides in which the gel had moved within the chamber were excluded from analysis. Background intensity values were subtracted from the intensity profiles so that the intensity values at the boundaries were zero. Intensity values were normalized to the highest intensity value in the first image taken after uncaging.

We analyzed postphotoactivation scanning profiles to account for multiple diffusing species, each with a distinct diffusion coefficient. This method of analysis was useful for experiments using HIV-like liposomes, in which free label is often present in solution, even after column filtration. Using this method, we were able to resolve distinct diffusion coefficients for liposomes and free label.

Our analysis followed one developed by Periasamy et al. [145] for analysis of Fluorescence Recovery After Photobleaching (FRAP) diffusion profiles. We assumed that diffusion profiles could be described by a distribution of diffusion coefficients, $\alpha(D)$. The observed intensity profile ($I_{observed}$) at any given time is the sum of intensity profiles (I_i) for the multiple diffusing species:

$$I_{observed}(x,t) = \sum_i \alpha_i I_i(D_i, x, t)$$

Equation 52

Here, the index, i , refers to each species, for which α_i is the relative amplitude of the diffusing species with diffusion coefficient D_i .

To analyze the observed diffusion profiles, we discretized D at equal intervals in log space between D_{min} and D_{max} . For the experiments in this chapter, we selected $D_{min} = 10^{-12}$ cm²/s, $D_{max} = 10^{-6}$ cm²/s, and performed analyses using 100 points. We numerically solved the diffusion equation for all D_i assuming that the intensity at the boundaries was zero and using the experimental initial condition (I_0):

$$\frac{dI_i}{dt} = D_i \frac{\partial^2 I_i}{\partial x^2}, \quad I_i(\pm\infty, t) = 0, \quad I_i(x, 0) = I_0(x)$$

Equation 53

We then used the MATLAB optimization function “lsqnonlin” to find the distribution $\alpha(D)$ that minimizes sum of the squares of residuals:

$$\sum_i (I_{observed} - I_{computed})^2$$

Equation 54

Here, $I_{computed}$ is the sum of intensity profiles I_i with distribution α . Refer to the Appendix for examples, validation experiments, and characterization of the lower limit of detection and resolution.

3.3. Results

3.3.1 Particle tracking of HIV virions in HEC and MC

We performed particle-tracking experiments to measure diffusion coefficients of fluorescently-labeled HIV virions in HEC and MC. To examine the effect of dilution on the diffusion coefficient, we also performed particle-tracking experiments using HEC and MC diluted to 50% (v/v) gel in PBS, and diluted to 20% (v/v) gel in PBS. Figure 44 shows examples of particle tracks obtained over the time of observation, approximately 41 s. Qualitatively, we observed that particle motion increased with increased dilution by PBS. Undiluted HEC and MC appeared to trap the HIV virions. Tracks for undiluted HEC and MC appeared similar to tracks for 100-nm beads dried to the glass slide.

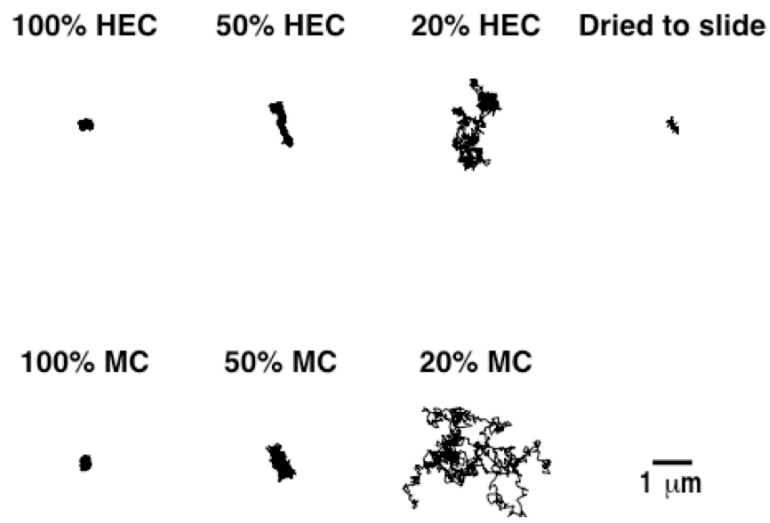


Figure 44. Examples of tracks obtained for fluorescently-labeled HIV virions in HEC and MC, and for 100-nm bead dried to glass slide. Particles were tracked for 41s.

Tracks were used to calculate mean squared displacements (MSD). Figure 45 shows representative plots of MSD vs. timescale (τ) from single experiments. These data were weighted by the inverse of their variance and fitted to a linear regression. The diffusion coefficient was computed as one-fourth of the slope.

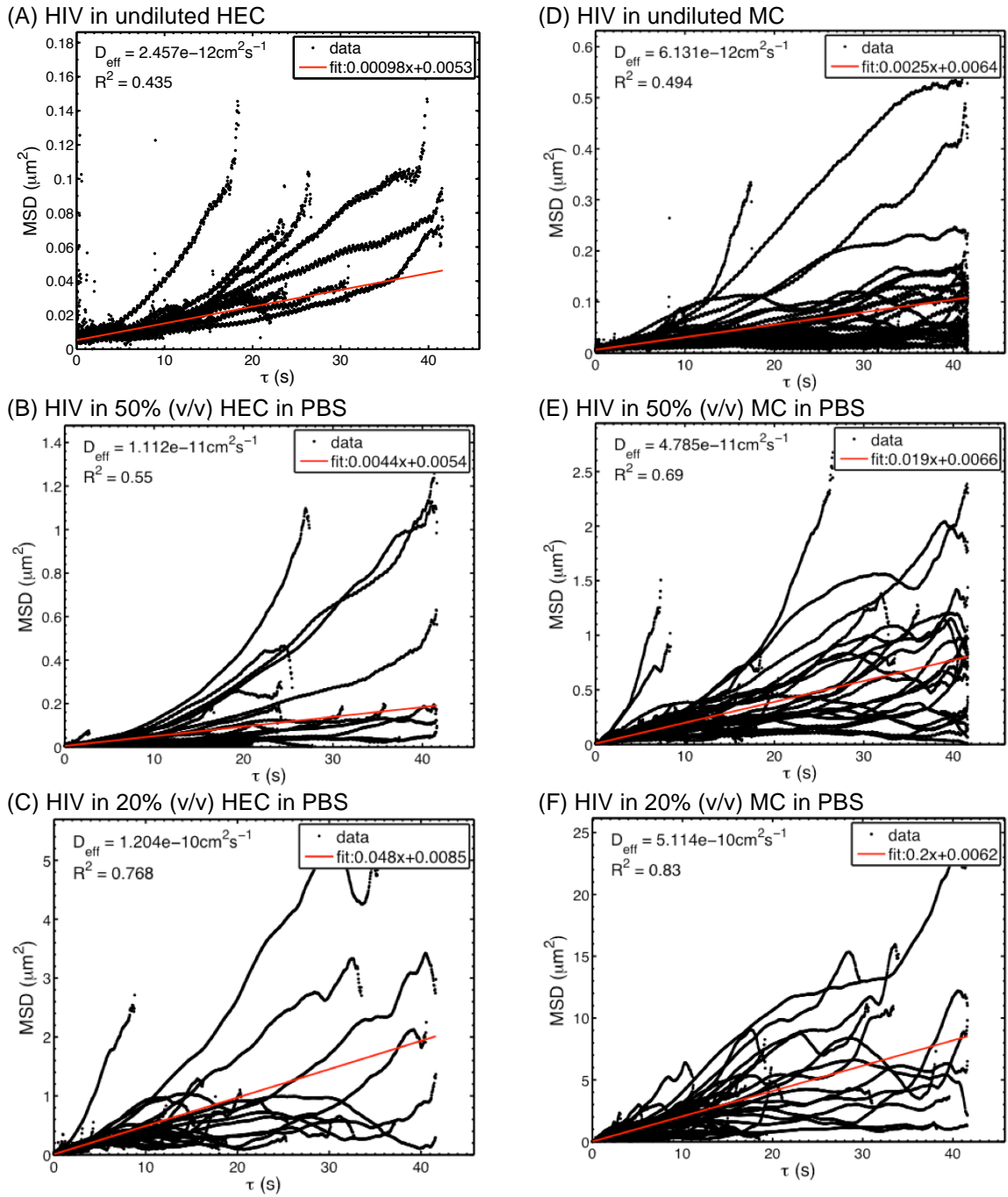


Figure 45. Examples of plots for MSD vs. τ for HIV in HEC and MC. Data represent different virions within single experiments.

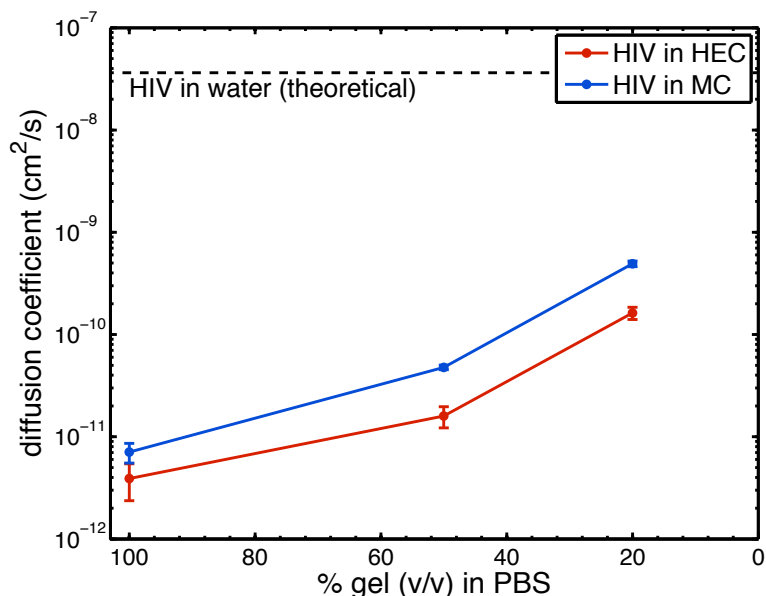


Figure 46. Diffusion coefficients (mean \pm SE, n = 3 independent experiments) obtained using particle tracking of fluorescently-labeled HIV in HEC and MC undiluted, diluted to 50% (v/v) in PBS, and diluted to 20% (v/v) in PBS. Values are given in Table 15.

Figure 46 summarizes diffusion coefficients obtained from three independent experiments for particle tracking of HIV virions in HEC and MC, with and without dilution by PBS. Values are listed in Table 15. Diffusion coefficients for HIV virions in undiluted HEC and MC were $4 \pm 2 \times 10^{-12}$ cm²/s and $7 \pm 1 \times 10^{-12}$ cm²/s, respectively. These are approximately 10,000 times lower than the diffusion coefficient for HIV in water predicted by the Stokes-Einstein equation, 3.6×10^{-8} cm²/s at 37° C. Diffusion coefficients in HEC and MC were not significantly different (t-test, $p > 0.05$).

Diffusion coefficients increased with increasing level of dilution by PBS. However, HIV-virion diffusion was still hindered in diluted gels when compared to water. Diffusion coefficients in 50% (v/v) dilutions of HEC and MC were approximately

3 orders of magnitude lower than in water, whereas diffusion coefficients in 20% (v/v) dilutions of gels were approximately 2 orders of magnitude lower than in water.

3.3.2 Accuracy of diffusion coefficients obtained via particle tracking

To verify that diffusion coefficients measured for HIV were reasonable, we also measured diffusion coefficients of fluorescently-labeled beads of similar size to HIV virions. The diameter of the beads is approximately 126 ± 2 nm (characterized by DLS). The diameter of HIV is approximately 125 ± 14 nm [103]. Values of the diffusion coefficients for 100-nm beads and HIV virions were similar (Figure 47). Comparison of diffusion coefficients using a t-test showed that the diffusion coefficients for HIV virions and 100-nm beads were not significantly different, except for in 20% HEC ($p < 0.05$). These data suggest that the diffusion coefficients we obtained from particle tracking of HIV virions were indeed reasonable, and that we did not observe significant aggregation of virions.

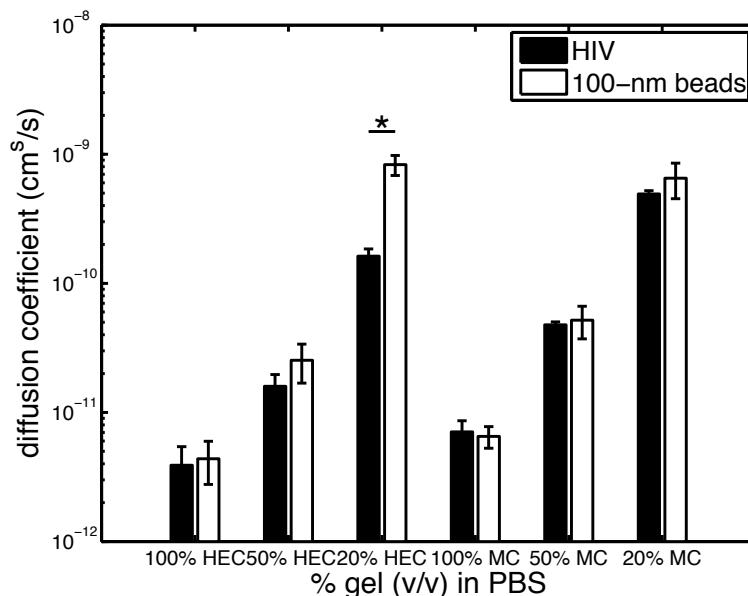


Figure 47. Comparison of diffusion coefficients (mean ± SE) for HIV and 100-nm beads in HEC and MC (n = 3). Diffusion coefficients were not significantly different except for in 20% HEC (t-test, p < 0.05)

Table 15. Values of diffusion coefficient for HIV virions and 100-nm beads in HEC and MC.

| Sample | Diffusion coefficient (cm ² /s) | |
|----------------------|--|-------------------------------|
| | HIV virions | 100-nm beads |
| 100% HEC | $4 \pm 2 \times 10^{-12}$ | $4 \pm 2 \times 10^{-12}$ |
| 50% (v/v) HEC in PBS | $1.6 \pm 0.4 \times 10^{-11}$ | $2.5 \pm 0.8 \times 10^{-11}$ |
| 20% (v/v) HEC in PBS | $1.6 \pm 0.2 \times 10^{-10}$ | $8 \pm 1 \times 10^{-10}$ |
| 100% MC | $7 \pm 2 \times 10^{-12}$ | $7 \pm 1 \times 10^{-12}$ |
| 50% (v/v) MC in PBS | $4.8 \pm 0.3 \times 10^{-11}$ | $5 \pm 1 \times 10^{-11}$ |
| 20% (v/v) MC in PBS | $4.9 \pm 0.3 \times 10^{-10}$ | $7 \pm 2 \times 10^{-10}$ |

We also performed validation experiments measuring diffusion coefficients of particles in Newtonian fluids of known viscosity, namely glycerol and glycerol dilutions (Table 16). Our diffusion coefficient measurements tended to over-estimate the diffusion coefficient of 100-nm beads by approximately 30% compared to theoretical values predicted by the Stokes-Einstein equation (Equation 6). In contrast, the experimental

value of diffusion coefficient for HIV virions in glycerol was lower than the theoretical value. Nevertheless, the experimental diffusion coefficients were consistently within one order of magnitude of the expected value.

The media selected for these validation experiments did not adequately represent the range of diffusion coefficients measured in gels, 10^{-9} - 10^{-12} cm²/s. Future validation experiments should use media with viscosities that would allow particle tracking of 100-nm beads to span the range of diffusion coefficients in gels, 35-35,000 cP.

Table 16. Diffusion coefficients (mean \pm SE, n = 3) in glycerol solutions. Experiments were performed at 37° C. Theoretical values for diffusion coefficient were calculated using Stokes-Einstein, assuming spherical particle of 126-nm diameter.

| Particle | Medium | Viscosity (cP) | Diffusion coefficient (cm ² /s) | | Error |
|-------------|--|----------------|--|------------------------|------------|
| | | | Experimental | Theoretical | |
| HIV virion | 100% Glycerol | 369 | $5.6 \pm 0.4 \times 10^{-11}$ | 9.8×10^{-11} | (-) 39-47% |
| 100-nm bead | 100% Glycerol | 369 | $13.5 \pm 0.2 \times 10^{-11}$ | 9.8×10^{-11} | (+) 36-40% |
| 100-nm bead | 95% (w/w) Glycerol in H ₂ O | 148.6 | $3.19 \pm 0.05 \times 10^{-10}$ | 2.42×10^{-10} | (+) 30-34% |
| 100-nm bead | 90% (w/w) Glycerol in H ₂ O | 78.4 | $5.6 \pm 0.3 \times 10^{-10}$ | 4.6×10^{-10} | (+) 15-28% |

To characterize the level of noise in our particle tracking methods, we performed particle-tracking experiments for 100-nm beads that had been dried to the glass slide. Ideally, we would expect to observe no motion and obtain a diffusion coefficient of zero. Figure 48 shows a representative plot of MSD vs. τ for beads dried to the slide. The computed diffusion coefficient was $1.9 \pm 0.4 \times 10^{-12}$ cm²/s (mean \pm SE, n = 11). This represents the lower limit of detection for our particle tracking methods. This lower limit is determined by thermal motion and noise in detection and analysis. Diffusion

coefficient measurements for HIV virions in undiluted HEC and MC were of the same order of magnitude as for the immobilized 100-nm beads.

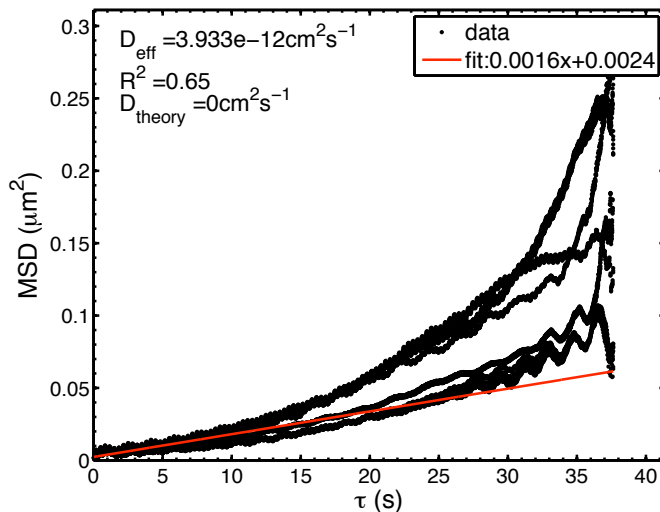


Figure 48. Example plot of MSD vs. τ for 100-nm beads dried to glass slide from one experiment. Data represent MSDs of different particles.

3.3.3 Postphotoactivation scanning of HIV-like liposomes in HEC and MC dilutions

We were also interested in applying postphotoactivation scanning to measure diffusion coefficients of HIV-like particles in HEC and MC dilutions. Postphotoactivation scanning using HIV-like liposomes requires significant dilution of the gel tested because high concentrations of liposomes are required to obtain the level of fluorescence necessary for macroscale imaging. In our experiments, we tested 50%, 20%, 10%, 5%, and 2% (v/v) dilutions of the gels in PBS. We also measured the diffusion coefficient of liposomes in PBS alone. Unfortunately, we found that postphotoactivation scanning was appropriate for measuring diffusion coefficients only in the highest dilutions, namely 10% (v/v) gel in PBS, 5% (v/v) gel in PBS, 2% (v/v) gel in PBS, and PBS alone. For lower dilutions, i.e., 50% and 20% (v/v) gel in PBS, the

diffusion coefficient was below the lower limit of detection (See Appendix for details about characterizing the lower limit of detection).

Extrusion of the liposomes using the formulation based on the composition of HIV Env (Table 14) appeared to be successful. The sizes of the HIV-like liposomes, $132 \pm 3 \text{ nm}$ ($n = 5$, measured using DLS), were similar to that of HIV-1 virions, $125 \pm 14 \text{ nm}$ [103].

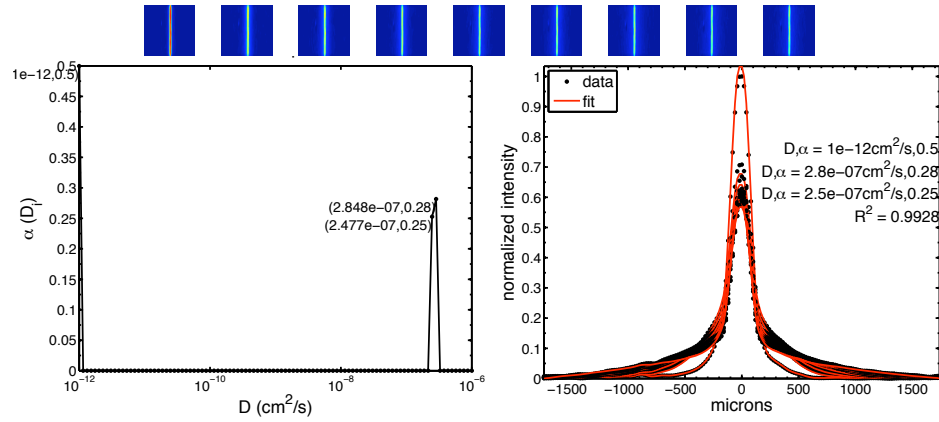
Figure 49 shows examples of postphotoactivation scanning results for HIV-like liposomes in MC dilutions. For each experiment, we acquired 9 images approximately every 25 minutes, over the course of approximately 3.5 hours. From the intensity profiles, we observed that the photobleached line became diffuse more rapidly in samples with higher dilution (Figure 49).

The distributions of $\alpha(D)$ typically showed two peaks, with one consistently near $3 \times 10^{-7} \text{ cm}^2/\text{s}$. This high peak represents free label, which was not encapsulated within liposomes and not adequately removed by column filtration. The dextrans did not appear to be hindered by placebo gels, even at the highest concentration of 50% (v/v) gel in PBS. The peak with the lower diffusion coefficient represents the HIV-like liposomes. In the 50% and 20% (v/v) gel, it was not possible to accurately obtain the diffusion coefficient because the diffusion coefficients were lower than the limit of detection. For the highest dilutions to 10%, 5%, and 2% (v/v) gel in PBS, diffusion coefficients were of the same order of magnitude as in PBS.

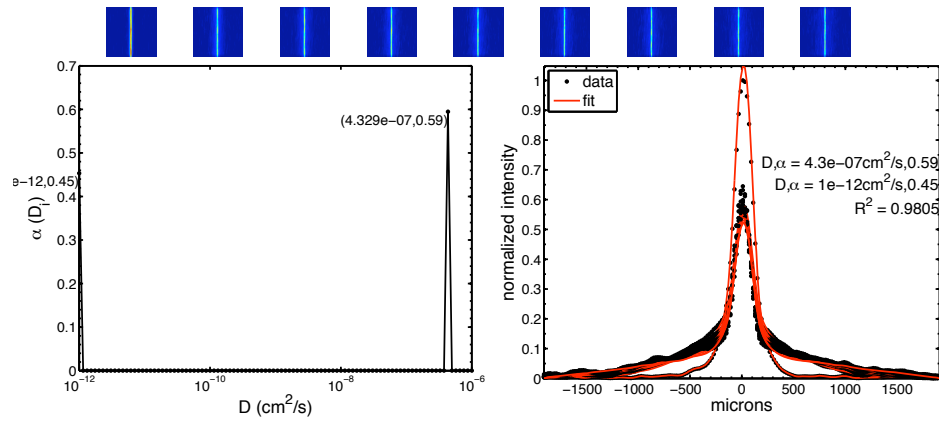
When fitted to solutions of the diffusion equation, intensity profiles yielded high R^2 values. This suggests that Fickian diffusion adequately describes transport of the

HIV-like liposomes in the diluted placebo gels. In samples with higher concentrations of gels, we observed more noise, perhaps due to heterogeneity in the sample preparation or because gels were autofluorescent.

(A) HIV-like liposomes in 50% (v/v) MC



(B) HIV-like liposomes in 20% (v/v) MC



(C) HIV-like liposomes in 10% (v/v) MC

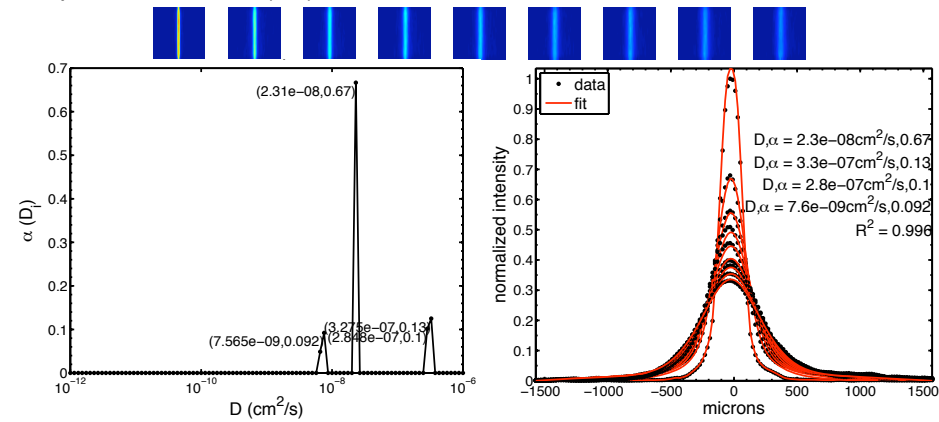


Figure 49. Examples of results from postphotoactivation scanning of HIV-like liposomes in MC dilutions (A-E) and PBS (F). For each condition, top: images over time (red = high intensity, blue = low intensity), bottom left: plot of $\alpha(D)$, and bottom right: intensity profiles fit to diffusion model.

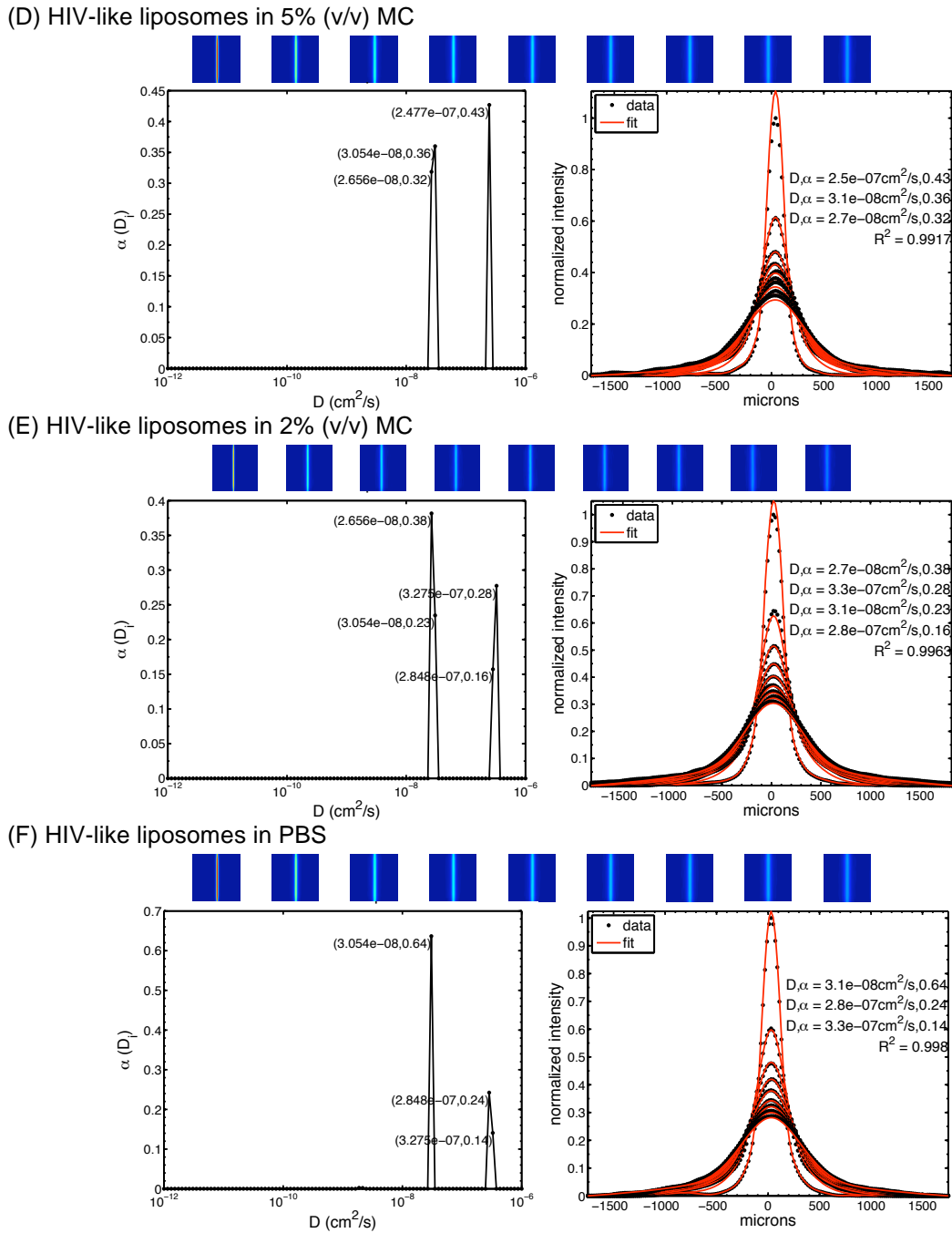


Figure 49. Examples of results from postphotoactivation scanning of HIV-like liposomes in MC dilutions (A-E) and PBS (F). For each condition, top: images over time (red = high intensity, blue = low intensity), bottom left: plot of $\alpha(D)$, and bottom right: intensity profiles fit to diffusion model.

Figure 50 summarizes diffusion coefficients obtained from postphotoactivation scanning. There was a trend of increasing diffusion coefficients with increasing dilution.

However, diffusion coefficients in these dilute solutions of gels were similar – all were within one order of magnitude of the diffusion coefficient in HIV-like liposomes in PBS.

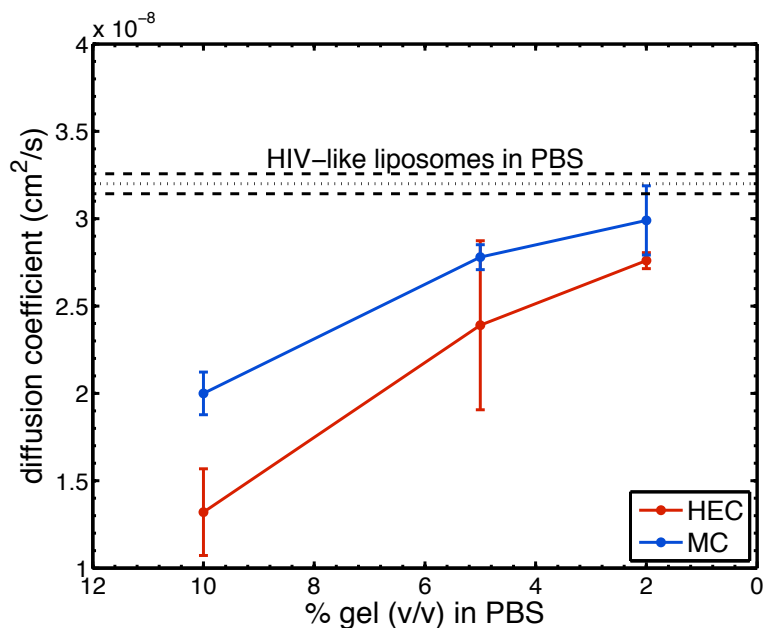


Figure 50. Diffusion coefficients (mean ± SE) obtained from postphotoactivation scanning of HIV-like liposomes in HEC and MC dilutions, and PBS. See Table 17 for detailed results.

Table 17. Diffusion coefficients obtained (mean ± SE) from postphotoactivation scanning of HIV-like liposomes in HEC and MC dilutions, and PBS.

| Medium | Diffusion coefficient (cm ² /s) |
|---------------|--|
| 50% (v/v) HEC | Below limit of detection |
| 20% (v/v) HEC | Below limit of detection |
| 10% (v/v) HEC | $1.3 \pm 0.2 \times 10^{-8}$ (n = 2) |
| 5% (v/v) HEC | $2.4 \pm 0.5 \times 10^{-8}$ (n = 3) |
| 2% (v/v) HEC | $2.76 \pm 0.05 \times 10^{-8}$ (n = 3) |
| 50% (v/v) MC | Below limit of detection |
| 20% (v/v) MC | Below limit of detection |
| 10% (v/v) MC | $2.0 \pm 0.1 \times 10^{-8}$ (n = 2) |
| 5% (v/v) MC | $2.78 \pm 0.07 \times 10^{-8}$ (n = 3) |
| 2% (v/v) MC | $3.0 \pm 0.2 \times 10^{-8}$ (n = 3) |
| Control (PBS) | $3.15 \pm 0.07 \times 10^{-8}$ (n = 8) |

The diffusion coefficient obtained for HIV-like liposomes in PBS, $3.15 \pm 0.07 \times 10^{-8} \text{ cm}^2/\text{s}$ (mean \pm SE, $n = 8$), was close to the value predicted by the Stokes-Einstein equation, $3.3 \times 10^{-8} \text{ cm}^2/\text{s}$ (assuming $d = 132 \text{ nm}$, $\mu = 1 \text{ cP}$, $T = 24.5^\circ\text{C}$).

3.4 Discussion

3.4.1 Summary of measured diffusion coefficients

Our experiments quantifying the diffusion coefficients of HIV virions and HIV-like particles suggest that typical vaginal gels can indeed hinder diffusion of HIV. HEC has been previously presumed not to provide “the physical barrier protection of high-yield strength gelling agents” [166]. In contrast, the diffusion coefficients measured here were relatively low. We found that the diffusion coefficient for HIV virions in undiluted HEC and MC were $4 \pm 2 \times 10^{-12} \text{ cm}^2/\text{s}$ and $7 \pm 1 \times 10^{-12} \text{ cm}^2/\text{s}$, respectively. These are almost 10,000 times lower than the diffusion coefficient for HIV in water predicted by the Stokes-Einstein equation, $3.6 \times 10^{-8} \text{ cm}^2/\text{s}$. Virions were effectively trapped in the placebo gels, with movement similar to that of 100-nm beads that had been dried to the glass slide. The diffusion coefficient has a central role in characterizing times required for diffusion. The characteristic length scale for one-dimensional diffusion in a semi-infinite medium is $\delta = \sqrt{4Dt}$ [107]. Diffusion coefficients can be input to mathematical models to interpret the flux of virions to vulnerable tissues.

3.4.2 Comparison to diffusion coefficients of HIV in other gels

The diffusion coefficients measured here for HIV in placebo gels are similar to those previously documented for HIV virions in human cervicovaginal mucus. Cervical

mucus likely evolved to function, in part, as a physicochemical barrier to pathogens [100]. A recent study using particle tracking of HIV virus-like particles (VLPs) found that diffusion coefficients of HIV VLPs in fresh, human cervicovaginal mucus (from six different donors) were less than 10^{-11} cm²/s [36]. Another study, using time-resolved confocal microscopy particle tracking and fluorescence correlation spectroscopy to examine movement of fluorescently-labeled HIV virions, found a more modest effect: Virions were slowed by approximately 200 times in mucus compared to water [37]. Thus, the diffusion coefficients measured here for HEC and MC were similar or lower than those previously measured for human cervicovaginal mucus, a natural physical barrier to HIV.

Diffusion coefficients measured here were also similar to those for HIV virions in a reversibly crosslinked hydrogel engineered to hinder HIV transport [182]. That gel was designed using phenylboronic acid (PBA) and salicylhydroxamic acid (SHA) crosslinks that respond to changes in pH, hindering virion diffusion at vaginal pH. Diffusion coefficients from particle tracking experiments of fluorescently-labeled HIV-1 virions in the hydrogel ranged from 6×10^{-10} cm²/s at pH 4.3 to below 2×10^{-12} cm²/s at pH 4.8. These diffusion coefficients roughly correspond with the diffusion coefficients measured in this study for HIV in 20% (v/v) HEC in PBS and undiluted HEC, respectively.

3.4.3 Comparison to theoretical predictions for diffusion coefficients

To place diffusion coefficients measured here within the context of theoretical expectations, we compared our results with mathematical models of particle diffusion in polymer solutions. The simplest relation for the diffusion coefficient of a particle in a

viscous medium is the Stokes-Einstein relation (Equation 6). Generally, the Stokes-Einstein relation does not accurately describe diffusion coefficients in complex, structured media like polymer solutions. However, for particles much larger than the mesh size of the gel, the particle may experience the medium as a continuum viscous fluid.

Our lab has previously characterized the rheology of HEC and MC using cone-and-plate viscometry (D.F. Katz, unpublished results). Both gels are shear-thinning fluids: Their viscosity decreases as shear rate increases. Here, we calculated the effective viscosities of undiluted HEC and MC using diffusion coefficients measured for HIV virions and 100-nm beads in HEC and MC (Table 15). The calculated viscosities corresponded to cone-and-plate viscosities for HEC at 18.75 s^{-1} and for MC at approximately $3.2\text{-}4.5 \text{ s}^{-1}$ (Figure 51).

It is unlikely that the Stokes-Einstein relation can be used to consistently estimate the diffusion coefficients of particles like HIV because it unclear what shear rate is appropriate. Polymer gels have complex, non-Newtonian rheology that precludes the use of a single value for viscosity. Furthermore, viscosities from macroscale measurement techniques, like cone-and-plate viscometry, do not necessarily represent the viscosities experienced by particles on the micro- or nano-scale.

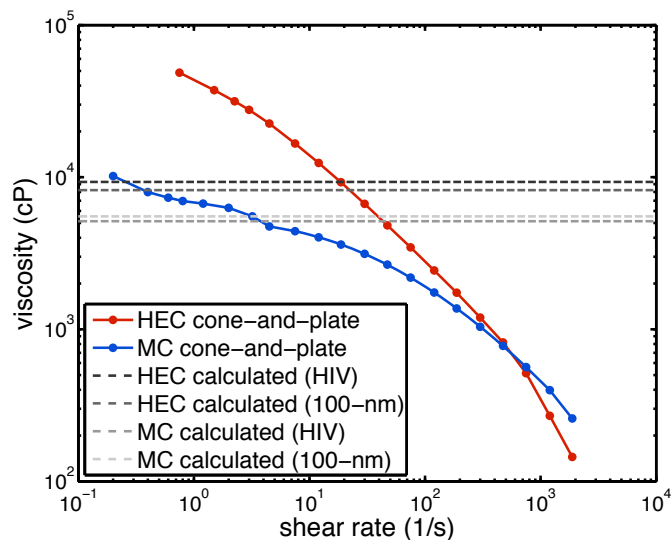


Figure 51. Comparison of cone-and-plate viscosities for undiluted HEC and MC and effective viscosities calculated from measured diffusion coefficients of HIV virions and 100-nm beads in HEC and MC (Table 15). To calculate the effective viscosity, we used the Stokes-Einstein relation (Equation 6), temperature of 37° C, and particle diameters of 125 nm and 126 nm for HIV and 100-nm beads, respectively. Cone-and-plate viscometry data were collected by Jennifer Peters.

Other mathematical models require greater knowledge of the physical parameters of the gel. For example, obstruction models typically input dimensions for the polymer structure, such as fiber radius and mesh size, or pore size [172, 196]. Previous models have used the following geometries: array of regularly-spaced fibers; overlapping fibers; network of interconnected pores; or array of hollow cylinders [196]. To our knowledge, the mesh size of MC has not yet been characterized. However, the polymer used as the gelling agent in the HEC placebo has been previously characterized. Peppas et al. analyzed the equilibrium swelling of hydroxyethyl cellulose discs in water [177]. They found that the equilibrium mesh size was 51 times the monomer unit. Assuming that the length of the anhydroglucose monomer unit is 0.514 nm [172], this corresponds to a mesh size of approximately 26 nm. While the concentration of hydroxyethyl cellulose polymer

swollen to equilibrium in water may not be the same concentration found in the HEC placebo gel, we used this mesh size as an approximation for the mesh size of HEC in calculations below.

Most obstruction models assume that the diffusing particle is smaller than the mesh size or pore size, and would poorly predict diffusion coefficients of HIV virions in HEC because HIV virions are larger than the average mesh size of HEC. However, an obstruction model developed by Amsden [151] has been used to describe the diffusion coefficients of antibodies, human papiloma virus (HPV, $d = 55$ nm), and Herpes Simplex Virus (HSV, $d = 180$ nm) in human cervical mucus [152]. Although the mesh size of human cervical mucus is larger than that of HEC, we applied the model to diffusion of HIV virions in HEC here.

The diffusion coefficient of a particle in a polymer solution can be expressed as follows [172]:

$$D = D_0 \exp \left[-\pi \left(\frac{R_{particle} + R_{polymer}}{\xi + 2R_{polymer}} \right)^2 \right]$$

Equation 55

Here, D_0 is the diffusion coefficient of the particle in water, $R_{particle}$ is the radius of the particle (125 nm [103]), ξ is the mesh size (26 nm [177]), and $R_{polymer}$ is the radius of the polymer chain. To estimate the diffusion coefficient of HIV in water, we used the Stokes-Einstein equation (Equation 6), temperature of 37° C, and viscosity of 1 cP. The radius of the polymer chain can be estimated as follows:

$$R_{polymer} = \left(\frac{M_m \nu}{l \pi N_{Av}} \right)^{1/2} + R_{water}$$

Equation 56

Here, M_m is the molecular weight of the monomer (272 g/mol [177]), ν is the specific volume (0.73519 cm³/g [177]), l is the length of the monomer unit (0.514 nm [172]), N_{Av} is Avogadro's number, and R_{water} is the radius of a water molecule (0.185 nm [172]).

Using the literature values above, we found the predicted diffusion coefficient, $D = 2.3 \times 10^{-15}$ cm²/s. This is much lower than the value we measured using particle tracking, $4 \pm 2 \times 10^{-12}$ cm²/s. The model likely underestimates the diffusion coefficient here because the particle is larger than the average mesh size, and the model assumes that particles are physically obstructed by the polymer chains. Given the poor correspondence between theoretical and experimental values of diffusion coefficients for HIV in semi-solid gels, it is advisable to measure the diffusion coefficient directly rather than relying on theoretical estimates.

3.4.4 Effect of dilution

For a gel to serve as an effective topical barrier to HIV transmission *in vivo*, it is not sufficient for it to trap virions. The gel must also comprehensively coat the surface of epithelial tissue and retain its barrier properties upon dilution with fluids such as vaginal transudate and semen. Here, we performed preliminary studies of the effects of dilution, using PBS as the diluent. The gels tested here are not sensitive to the pH of the diluent,

so dilutions here are relevant to scenarios of dilution observed *in vivo*. More comprehensive studies on deployment are described in Chapter 5.

Vaginal gels may experience a range of dilutions after topical application. Current clinical trials of microbicide gels typically use 2-5 ml of gel. After insertion, vaginal gels come in contact with fluid in the vagina, consisting of vaginal transudate and cervical mucus, typically 0.5-0.75 ml in volume [57]. The volume of human ejaculate is 2-5 ml [75]. Considering these volumes, a gel may be maximally diluted to 26% (v/v). In this study, we were able to obtain diffusion coefficients using particle tracking of HIV virions for a biologically-relevant range of dilutions, from undiluted to 20% (v/v). Additionally, we used postphotoactivation scanning to investigate even higher levels of dilution. These high levels of dilution may be relevant to studies where cervicovaginal lavage is used to obtain samples of gels that have been applied topically and also regions of thin gel layers applied *in vivo*. Cervicovaginal lavage typically further dilutes gels by introducing 10 ml of PBS to the lower female reproductive tract [34]. In recent studies of the microbicide candidate PRO 2000, gel samples obtained from cervicovaginal lavage contained approximately 2-7% the original concentration of PRO 2000 gel [197].

Figure 52 summarizes diffusion coefficients we obtained for the range of gel dilutions. We found that diffusion coefficients of virions increased with increasing dilution of the gel. However, virions were hindered in the range of typical biological dilutions of gel, from undiluted to 20% (v/v). In 50% (v/v) HEC and MC, diffusion coefficients of HIV virions were $1.6 \pm 0.4 \times 10^{-11}$ cm²/s and $4.8 \pm 0.3 \times 10^{-11}$ cm²/s, respectively. These were approximately 1000 times lower than diffusion coefficients of

HIV in water. Diffusion coefficients in 20% (v/v) gels were still approximately two orders of magnitude lower than those of HIV in water: $1.6 \pm 0.2 \times 10^{-10} \text{ cm}^2/\text{s}$ and $4.9 \pm 0.3 \times 10^{-10} \text{ cm}^2/\text{s}$ for HEC and MC, respectively. Diffusion coefficients of HIV-like liposomes in gels diluted to 10, 5, and 2% (v/v) gel in PBS were of the same order of magnitude as HIV-like liposomes in PBS alone. This suggests that samples obtained from cervicovaginal lavage are unlikely to retain the barrier functioning of gels.

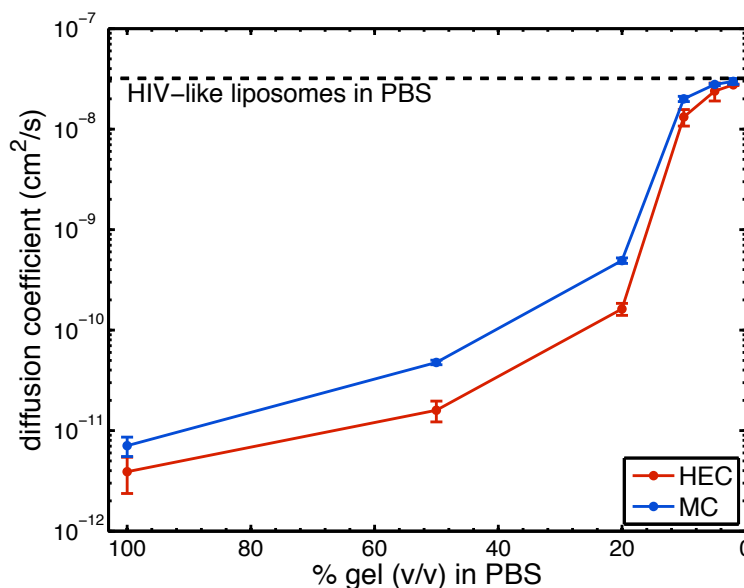


Figure 52. Summary of diffusion coefficients of HIV-like liposomes and HIV virions in HEC and MC. Values for undiluted, 50%, and 20% (v/v) gel in PBS were obtained using particle tracking. Values for 10%, 5%, 2% (v/v) gel in PBS were obtained using postphotoactivation scanning of HIV-like liposomes.

Future studies should examine effect of dilution more carefully, using biological fluids as diluents. For example, it has been previously shown that pH of the diluent can affect HIV diffusion in mucus – HIV virions are trapped in native mucus, but diffuse more rapidly when buffered to pH 6 or 7 [36].

3.4.5 Interpretation using mathematical model of virion diffusion

To provide biological context, we inputted measured diffusion coefficients to a mathematical model in which virions diffuse from semen, through a layer of gel, to reach the tissue compartment (Figure 53). The model is described in detail in Chapter 5. Here, we assumed that the epithelium was completely coated with gel of 100- μm thickness. We examined the percentage of virions to reach the tissue compartment within 48 hours.

We found that there were notable differences in the diffusion of virions to the tissue, depending on dilution. Undiluted HEC and MC presented a robust barrier to HIV – over 48 hours were required for virions to reach the tissue surface. Even with 50% (v/v) dilution of the gel, fewer than 1% of virions reached the tissue surface within 48 hours.

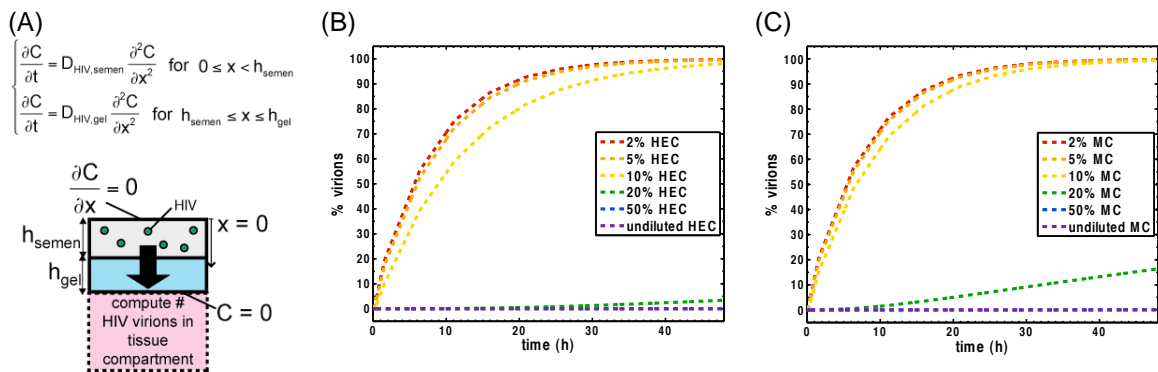


Figure 53. Interpretation of experimentally-measured diffusion coefficients using mathematical model of diffusion of HIV virions from semen, through microbicide layer, to tissue compartment. (A) Schematic of mathematical model. Measured diffusion coefficients were input to the model. Plots show percent of virions in the tissue compartment, as a function of time, for various concentrations of (B) HEC and (C) MC.

In contrast, nearly all of the virions reach tissue for dilutions to 2%, 5%, and 10% (v/v) gel in PBS. Diffusion coefficients for 20% (v/v) gel in PBS produced intermediate results: For 20% (v/v) HEC, 3% of virions reached tissue within 48 hours, and for 20%

(v/v) MC, 16% of virions reached tissue within 48 hours. According to this mathematical model, log reductions in diffusion coefficients are necessary to achieve a noticeable effect on HIV diffusion through a gel layer of typical thickness found *in vivo*. Diffusion coefficients 1000-10,000 times lower than diffusion coefficients in water are needed for a gel layer to function as a barrier to HIV diffusion over the time period of 48 hours.

3.4.6 Context of placebo gels *in vivo*

Our findings here suggest that gels used as placebos in microbicide clinical trials may actually have some function in HIV prevention, by acting as physical barriers to HIV-virion diffusion. The fact that placebos may function in HIV prevention is a known disadvantage of using placebos in blinded clinical trial design [17, 198]. Much uncertainty remains as to the clinical efficacy of these placebo gels for preventing HIV infection (Discussed in §6.2.3). Some studies in macaque models show that HEC (8/8 animals infected using 10^3 TCID₅₀ SHIV-162p3) [166] and MC (3/3 animals infected using 300 TCID₅₀ SHIV-162P4) [112] alone do not protect from SHIV infection. One study of MC in macaques found that the number of macaques infected varied with RT-SHIV concentration: 66.7% (6/13), 83.3% (5/6), and 46% (2/3) of macaques were infected using 10^3 TCID₅₀, 10^4 TCID₅₀, and 10^5 TCID₅₀ RT-SHIV, respectively. However, all of these models introduced virus in concentrations much higher than those experienced in scenarios of HIV infection in humans [88]. In these animal models, the high HIV concentration gradient introduced during the viral challenge may overwhelm the semi-permeable physical barrier of the gel.

Our studies here are certainly limited, as well. We assume that diffusion of HIV virions is the primary mode of transport in HIV transmission. However, it is certainly possible that cell-associated HIV and convective transport of HIV are significant. Furthermore, each of the two methods used here for measuring the diffusion coefficient has its limitations. Ideally, we would have been able to compare results from the two methods, but we found that the ranges of diffusion coefficients over which these methods could be used did not overlap. Particle tracking measures diffusion coefficients of the order of 10^{-12} - 10^{-9} cm²/s whereas postphotoactivation scanning works well for diffusion coefficients of the order of 10^{-6} - 10^{-9} cm²/s.

Finally, it is important to keep in mind that the diffusion coefficient of HIV virions in gels is merely one parameter in a complex problem. When gels are applied topically *in vivo*, their abilities to function as physical barriers to HIV also depend on distribution and response to dilution. Values for diffusion coefficients measured here provide proof of concept that typical vaginal gels can hinder HIV diffusion. Numbers presented here provide a baseline for future efforts to design materials that act as physical barriers to HIV transmission. In the future, materials designed to function as physical barriers to HIV should out-perform the placebo gels tested here, particularly under the conditions of use *in vivo*. Also, the barrier functioning of topically-applied gels can be combined with active agents that act against HIV using other mechanisms of action to develop more effective microbicide products.

3.5 Conclusions

We performed experiments to provide proof of concept that typical vaginal gels can hinder HIV-virion diffusion. We measured diffusion coefficients in two gels that have previously been used as placebos in microbicide clinical trials, HEC and MC. We found that HIV diffusion coefficients in these gels were $4 \pm 2 \times 10^{-12}$ cm²/s and $7 \pm 1 \times 10^{-12}$ cm²/s, respectively. These values were very low, approximately 10,000 times lower than the diffusion coefficient of HIV in water. This suggests that these vaginal gels may indeed act as barriers to HIV transport.

We also performed preliminary studies of the effect of dilution on HIV diffusion coefficients. We found that the diffusion coefficient increased with increased dilution of the gel. However, diffusion coefficients of HIV in 50% (v/v) gel in PBS and 20% (v/v) gel in PBS were still approximately 3 and 2 orders of magnitude lower, respectively, than the diffusion coefficient of HIV in water.

Numbers here provide a baseline for the future design of gels that act as topical barriers to HIV. The potential barrier function of vaginal gels should also be considered in the design and interpretation of microbicides clinical trials.

4. Evaluation of physical barrier functioning of semi-solid gels using experimental model of HIV transmission

4.1 Introduction

In Chapter 3, we found that diffusion coefficients of HIV virions in microbicide placebo gels are approximately 10,000 times lower than the diffusion coefficient of HIV in water. In this chapter, we were interested in the related problem of determining whether thin layers of these semi-solid gels, applied topically, could reduce the flux of infectious virions to vulnerable tissue over a given period of time.

We developed an experimental model to simulate the spatial configuration of HIV transmission in the presence of topical gel. During male-to-female sexual transmission, HIV is introduced to the lower female reproductive tract via semen. If a topical gel has been applied to the epithelium, then HIV must move through these gel layers before reaching vulnerable tissue. Previous studies in our lab have found that vaginal gels are deployed *in vivo* in layers approximately 100-500 μm thick [184, 185, 199]. We used Transwell plates to simulate this scenario of HIV transmission and evaluated the barrier functioning of thin layers of semi-solid gels. We hypothesized that the reduced diffusion coefficient of HIV in gels would translate to reduced levels of HIV in the bottom compartment. We considered a reduction in the levels of infectious HIV in the bottom compartment to be a measure of efficacy in HIV prevention. Considering that the first step in HIV infection is contact of HIV and infectable cells, any strategy that would inhibit this step could contribute to HIV preventing infection.

4.1.1 Experimental models of HIV transmission

Our understanding of sexual transmission of HIV-1 at mucosal surfaces has been shaped by a variety of experimental systems. Early studies using immortalized cell lines suggested that cervical epithelial cells could be productively infected by HIV [200]. Since then, experiments using primary epithelial cell cultures from the female genital tract have shown that epithelial cells are not productively infected and, instead, likely act as physical barriers to HIV transmission [22] or to sequester virions [23]. Some experimental systems have used cervicovaginal tissue cultured *ex vivo* [22, 38, 201-203]. These studies show HIV-1 virions penetrating epithelial tissue through gaps between cells [38]. Virions then come in contact with and productively infect CD4⁺ T cells [202] and perhaps also Langerhans cells [203] and macrophages [203]. Both cell and explant culture systems have been adapted for evaluating activity of anti-HIV compounds.

Cell-based assays used to evaluate the efficacy of microbicide candidates typically incubate the test compound, HIV, and target cells for a given amount of time, and then quantify levels of HIV. A myriad of configurations are used, with different forms of HIV, cell lines, and incubation protocols (Table 18). Cell-based assays are advantageous for screening microbicide candidates because they use standardized cell lines and allow for high-throughput testing. Cell-based assays can be mechanism-specific, isolating one mechanism of HIV infection, and examining the effects of compounds on this specific mechanism. One disadvantage of cell-based assays is that they often do not replicate the spatial configuration of HIV transmission *in vivo*, where

HIV target cells are found within much more complex systems of tissues, organs, and organ systems.

Table 18. Examples of cell-based assays used in evaluation of microbicide candidates.

| Assay | HIV strain | Target cell line | Endpoint | Incubation protocol |
|--|--|---|--------------|---|
| HIV-1 binding to epithelial cells [204] | HIV-1 BaL, LAI, primary isolates | A431 epithelial cells | RT PCR | Incubation of compound, virus, and cells overnight |
| HIV-1 transfer from epithelial cells to PBMCs [204] | HIV-1 BaL, LAI, primary isolates | A431 epithelial cells, PBMCs (primary cells) | p24 | Incubation of compound, virus, and epithelial cells for 18 h, then culture of epithelial cells with PBMCs |
| CD4-dependent cell-free HIV-1 entry assay [205] | HIV-1 IIIB (X4) or BaL (R5) | MAGI or MAGI-CCR5 | Luminescence | Incubation of cells with diluted compound for 15 minutes, then with addition of virus for 2-3 h |
| CD4-dependent cell-associated HIV-1 transmission assay [205] | SK-1(X4)-infected H9 or JR-CSF(R5)-infected MOLT4/CCR5 cells | GHOST(3) CD4-X4/R5 | p24 | Incubation of diluted compound and cells for 4 h |
| CD4-independent HIV-1 transmission assay [205] | SK-1(X4)-infected H9 cells | ME-180 | p24 | Incubation of diluted compound and cells for 4 h |
| HIV-1 cell-to-cell fusion assay [205] | None | HL2/3 cells(X4) fused with MAGI or HeLa R5-16 cells (R5) fused with MAGI-CCR5 | Luminescence | Incubation of cells and diluted compound for 40-48 h |

Explant models have also been adapted for evaluating microbicide candidates [22, 206-211]. There are also several variations in explant systems. Excised tissues from the cervix may be cultured in a polarized [206, 207] or non-polarized fashion [22, 208-210]. Explant tissues are typically incubated with the microbicide compound diluted in culture medium and inoculated with HIV-1. Explants are cultured for varying periods of time to allow infection to occur. Levels of infection are often quantified using levels of p24, but

alternate endpoints have been developed [211]. The advantage of using tissue samples is that they more accurately capture the complex biological interactions of HIV with tissue during HIV infection. Target cells, such as CD4⁺ T cells, are incorporated within complex tissue architecture and interact with surrounding cells including epithelial, Langerhans, and dendritic cells. Disadvantages of explant culture systems include high variability [211], limited viability of tissues over time [201], and limited sample availability [206].

The goal of our experiments here was to evaluate the barrier function of thin gel layers, so we wanted to reproduce the spatial configuration of HIV transmission in the presence of gel layers. We also wanted our experimental system to give consistent, quantitative measures of HIV infection so that we could mathematically study the kinetics of transport over time. We chose to use a Transwell system, which allowed us to simulate the spatial configuration of HIV transmission with high throughput and consistency.

Transwell systems are used commonly in drug delivery research to assess the permeability of polarized cell monolayers to drugs or nanoparticulate drug carriers [212-218]. Transwell systems have also been used in microbicide development to create models of HIV infection [85, 219, 220]. For example, Van Herrewege et al. developed an experimental model for cell-associated HIV transmission [85]. Cervical epithelial cells were cultured on the Transwell membrane, and HIV-infected PBMCs were introduced to the top compartment. Target cells in the bottom compartment consisted of dendritic cells and T-cells. Transwell models have been used to study vaginal epithelial

permeability to HIV-1 [219, 220] and paracellular transport [33]. Transwell systems have also been used to culture tissue explants in a polarized configuration [206, 207]. In general, Transwell systems are useful for replicating the spatial configuration of barriers that modulate the transport of a substance from one compartment to another.

4.1.2 Assay for testing physical barrier function of thin gel layers

Gels that are applied to the vagina before intercourse form layers hundreds of microns thick on the epithelium [184, 185, 199]. Virions introduced in semen must diffuse through these semi-solid gel layers before reaching epithelial tissue (Figure 54A). We recreated this configuration within a Transwell system (Figure 54B). Transwell plates contain upper and lower chambers separated by a porous membrane. A thin layer (100-300 μm) of gel was applied to the membrane. A suspension of HIV virions was added to the top compartment. After incubation for a given period of time, a sample of the medium in the bottom compartment was assayed for infectious HIV using the TZM-bl assay. A reduction in the number of infectious virions in the bottom compartment of the Transwell was taken as an indicator of efficacy in HIV prevention.

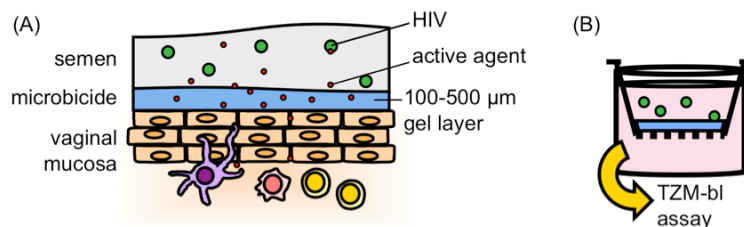


Figure 54. (A) Idealized scenario of HIV transmission in the presence of a microbicide. (B) Transwell system for evaluating barrier function of topical gels.

Thus far, methods for testing microbicide gels do not apply the gels as they are deployed in the body. Instead, most assays use active agents that have not been

formulated or mix the active agent thoroughly with cell culture medium. These methods ignore the spatial configuration of topical gels and the possible barrier function of semi-solid gels. There are technical challenges associated with applying gels in thin layers – vaginal gels are typically highly viscous materials. The thicknesses of gel layers observed in the body are small, and difficult to consistently replicate. Here, we have developed methods for creating and testing thin gel layers.

Our Transwell experiments allowed us to study kinetics of HIV transport through gel layers within a controlled environment. In this chapter, we describe experiments testing the barrier functioning of 2 gels, HEC and MC. These were the gels in which diffusion coefficients of HIV virions were measured in Chapter 3. The experimental system can be extended to test other semi-solid materials in the future, aiding in the evaluation and development of materials that act as physical barriers to HIV.

This chapter further develops preliminary research conducted working with Anthony Geonnotti [221]. The work here extended preliminary research by conducting experiments with additional incubation times, comprehensively characterizing gel layers applied to membranes, characterizing the lifetime of HIV in the Transwell system, and analyzing results in the context of diffusion coefficients measured in Chapter 3.

4.2 Materials and Methods

Our *in vitro* assay used 96-well Transwell plates (HTS Transwell®-96 Well Plate, Cat. No. 3388, Corning Incorporated, Corning, NY), which have an insert that forms upper and lower chambers separated by a porous membrane (polycarbonate membrane, pore size = 5 μm) (Figure 55). In each Transwell, we applied a gel layer of characterized

thickness (100-300 μm) to the membrane or no gel for the control condition. A solution of HIV was then added to the top chamber. The insert was placed in the bottom plate, which contained cell culture medium. The plate was incubated for a given time, then samples from the top and bottom chambers were assayed for infectious HIV using the TZM-bl assay. Details of the assay are described below.

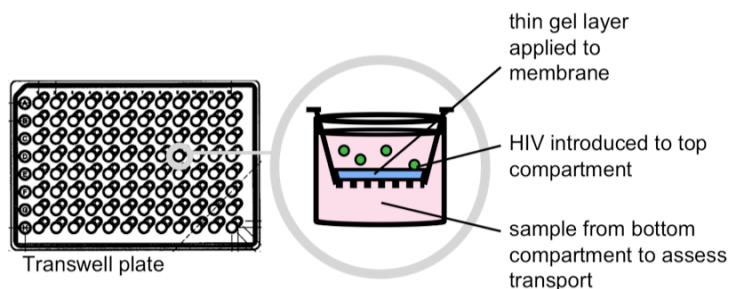


Figure 55. Transwell system to evaluate barrier functioning of thin gel layers.

4.2.1 Gels

In this study, we tested the two gels for which diffusion coefficients were measured in Chapter 3: 2.7% (w/w) hydroxyethyl cellulose (HEC) (Study No. C03-090, Batch 03724326, CONRAD, Arlington, VA); and 2.5% methylcellulose (MC) (Batch 100306, Population Council, New York, NY). These polymers are commonly used in vaginal formulations [155, 156] and have been used as placebos in microbicide clinical trials [159, 188, 222]. Here, we hypothesized that these gels would reduce levels of infectious HIV in the bottom compartment of the Transwell compared to experiments where no gel was applied to the membrane.

4.2.2 Thin gel layers

Layers of each gel were applied by custom-designed applicators (Figure 56A). Each applicator consisted of a steel cylindrical rod (Part Number 98378A936, McMaster-Carr, Atlanta, GA) with diameter slightly smaller than the diameter of the Transwell membrane. Each rod was fitted with an adjustable collar (Part Number 6436K413, McMaster-Carr) to set the depth of insertion into the Transwell insert. The collar was wider than the well diameter, allowing the collar to rest on the top of the Transwell insert during gel application.

To apply gel layers, a small volume (2.8-11.1 μl , see Table 19) of gel was placed on the tip of the applicator (Figure 56B) and inserted into the Transwell insert to transfer the gel to the membrane. Gel layer thickness was varied by adjusting gel volume and collar depth (Figure 56C). Controls consisted of chambers in which no gel was applied to the membrane.

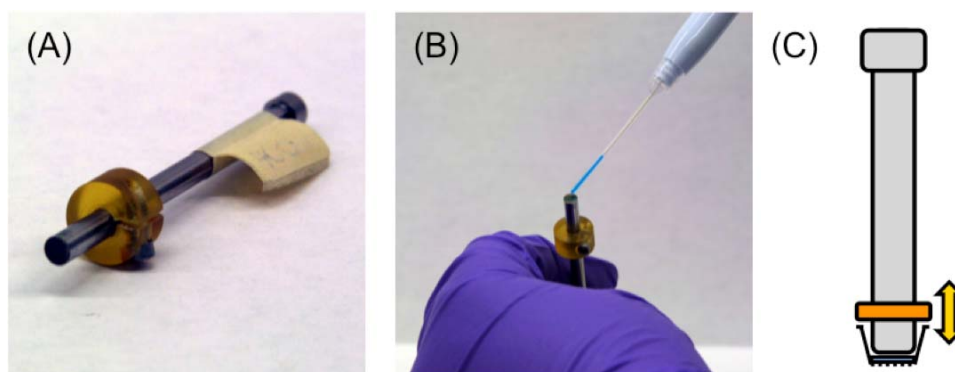


Figure 56. (A) Applicator used to apply thin gel layers to Transwell membrane. (B) Gel is applied to tip of rod. (C) Gel layer thickness is controlled by adjusting gel volume and collar depth.

Gel layers were characterized independently from the Transwell experiments of HIV transport (§4.3.3). Gels were labeled with a fluorescent dye, fluorescein. A

standard curve relating fluorescence to gel thickness was generated by finding the fluorescence intensity of gel layers of defined thickness, created by placing fluorescent gel in chambers of defined height (Figure 59). Chambers were created using Secure Seal Spacers (Electron Microscopy Sciences, Hatfield, PA). The thicknesses of gel layers applied to Transwell membranes were then quantified: A fluorescent plate reader was used to determine the fluorescence intensity of gels applied Transwell membranes, and the standard curve was used to relate intensity to thickness (Table 19).

4.2.3 Viruses

We used two CCR5-tropic, well-characterized, reference strains of HIV-1 isolated from acute, sexually transmitted infections: HIV-1 DU156 (Clade C, 500 TCID₅₀) and HIV-1 TRO (Clade B, 1000 TCID₅₀). Viruses were grown in peripheral blood mononuclear cells (PBMCs) so that virions had surface properties relevant to sexually transmitted virus. HIV virions were budded from cells in the infected host, most commonly PBMCs.

4.2.4 Transwell experiment

In the Transwell model, each gel layer was challenged by a solution of 75 µl of HIV-1 virions, added to the top chamber. The bottom compartment of each Transwell contained 235 µl of cell culture medium. Cell culture medium consisted of D-MEM with 10% heat-inactivated fetal bovine serum (Cat. No. SH30071.03, Hyclone, Logan, UT), 25 mM HEPES (Cat. No. 15630, Gibco, Grand Island, NY), and 50 µg/ml gentamicin (Cat. No. G1272, Sigma, St. Louis, MO).

Transwell plates were incubated in a 37°C, 5% CO₂ incubator for 0, 4, 8, or 12 hours. After the specified incubation time, the Transwell plate was removed from the incubator and samples of solutions from the top and bottom chambers were removed for quantification of infectious HIV using the TZM-bl assay.

4.2.5 TZM-bl assay

To quantify levels of infection, we used the TZM-bl assay developed in Dr. David Montefiori's laboratory at Duke University [120, 223]. TZM-bl cells are a CXCR4-positive HeLa cell clone that has been engineered to express CD4 and CCR5 as well as integrated reporter genes for firefly luciferase and *E. coli* β -galactosidase under control of an HIV long-terminal repeat sequence [120, 224]. Luciferase reporter gene expression is induced by the viral Tat protein soon after single round infection. The level of infection is quantified by incubating the cells with the luciferin substrate. Luciferase, generated by infected cells, cleaves the luciferin substrate to generate luminescence. Luminescence is quantified using a luminometer. There is a linear range in which luminescence is directly proportional to levels of HIV infection.

In our experiments, samples from the top and bottom chambers of the Transwell plate were incubated with TZM-bl cells to quantify levels of HIV. For the top compartment, 50- μ l samples were transferred to the TZM-bl assay plate and mixed with 100 μ l additional cell culture media. For the bottom compartment, 150- μ l samples were transferred to the TZM-bl assay plate. Then, 100 μ l of TZM-bl cell suspension (10^5 cells/ml in culture medium with 15 μ g/ml DEAE dextran) was added to the assay plate.

TZM-bl cells were suspended using treatment with trypsin-EDTA (Cat. No. 25200-056, Invitrogen): Cells were incubated at room temperature with 2.5 ml 0.25% trypsin-EDTA for 30 s. The trypsin-EDTA solution was then removed and cells were incubated for an additional 4 minutes at 37° C. Cells were then suspended in 10 ml growth medium for counting. Cells were further diluted with growth medium to 10⁵ cells/ml. Plates were incubated for 48 hours at 37°C, 5% CO₂.

To read plates, we removed 150 µl medium from each well. The remaining 100 µl was incubated with 100 µl luciferin substrate for 2 minutes (Britelite Reagent, PerkinElmer, Waltham, MA). Samples were mixed by pipetting and transferred to 96-well black plates for reading (Corning 3915, Corning, NY). Luminescence was quantified in Relative Luminescence Units (RLUs) using a plate reader (Wallac 1420 Victor3, PerkinElmer, Waltham, MA).

Controls were used to ensure the proper functioning of the TZM-bl assay for quantifying levels of infectious virus. Negative controls consisted of cells without virus: 150 µl cell culture medium and 100 µl of TZM-bl cells solution were mixed in the assay plate at the time of sampling from the Transwell. Positive controls consisted of cells and virus solution applied to the top compartment of the Transwell: Upon initiation of the Transwell assay, 50 µl of virus solution was mixed with 100 µl cell culture medium in the TZM-bl assay plate. These positive controls were incubated for the length of incubation of the Transwell plate, and 100 µl of TZM-bl cells solution was added at the time of sampling from the Transwell.

We characterized the linear range of the assay for the two strains of HIV-1 used, in which the total number of infectious virions is directly proportional to the luminescence of the sample (Figure 61). In performing our experiments, all RLU values were within the linear range of the TZM-bl assay (Figure 62).

We also used the TZM-bl assay in characterization studies of neutralization and HIV-1 viability. We performed neutralization assays to confirm that the placebo gels tested, HEC and MC, do not neutralize virus at the concentrations used within the Transwell, and thus, reductions in the levels of HIV in the bottom compartment were due to hindrance of transport and not viral neutralization. Neutralization studies were performed using start dilutions of 10%, 5%, or 1.25% (v/v) gel in growth medium. Using the 8 rows of a 96-well plate, seven 3-fold serial dilutions were performed to test a range of concentrations. For each condition, 150 μ l of diluted gel was mixed with 50 μ l virus and incubated for 1 hour prior to the addition of 100 μ l suspension of TZM-bl cells and 48-hour incubation. Plates were read according to the protocol above.

4.2.6 Analyses

RLU levels varied from experiment to experiment and over time due to the finite lifetime of HIV, so results were normalized to the control, in which no gel was applied to the Transwell membrane:

$$\% \text{ control} = 100 \times RLU_{\text{bottom,experiment}} / RLU_{\text{bottom,control}} .$$

Equation 57

Statistical analyses were performed using JMP 8 software (SAS, Cary, NC). ANOVA was used to compare results for all conditions; post-hoc Student's *t*-tests were

then used to make individual comparisons of means. Values for $p < 0.05$ were considered statistically significant.

4.3 Results

4.3.1 Evaluation of two commonly-used vaginal gels

In Chapter 3, we measured the diffusion coefficients of HIV in two placebo gels used in microbicides clinical trials, HEC and MC, to provide proof of concept that vaginal gels could hinder HIV-virion diffusion. Here, we applied these gels to the membrane in a Transwell system to test their functioning as physical barriers to HIV. After incubation for 0, 4, 8, or 12 hours, samples from the bottom compartment of the Transwell were tested for levels of infectious HIV using the TZM-bl assay. RLU levels varied from experiment to experiment and over time due to the finite lifetime of HIV, so results were normalized to the control, in which no gel was applied to the Transwell membrane.

Results show that both HEC and MC reduced the amount of infectious virus in the bottom compartment of the Transwell for all of the incubation times tested (Figure 57). There was no statistically significant difference ($p > 0.05$) between the two strains of HIV-1, so we grouped them for analysis.

Levels of HIV in the bottom compartment were significantly different between control (no gel) and gel experiments ($p < 0.05$). Notably, there was a log reduction the amount of HIV in the bottom compartment for HEC and MC at 0, 4, and 8 hours. In neutralization assays, log reductions in HIV are considered biologically significant.

When data were grouped by gel (over all incubation times), MC appeared to be a slightly

superior barrier to HEC, yielding approximately 20% lower levels of HIV in the bottom compartment ($p < 0.05$).

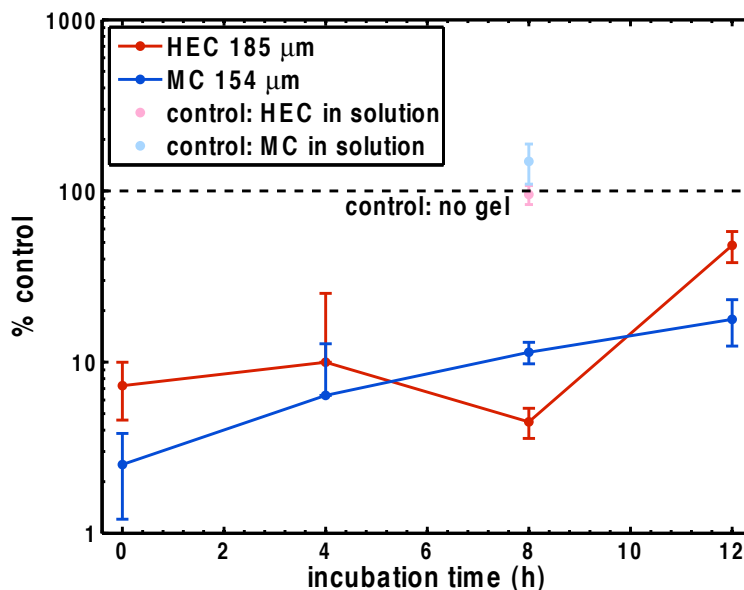


Figure 57. Levels of HIV-1 in bottom compartment of Transwell for two semi-solid gels, HEC and MC ($n \geq 4$ independent experiments). Experimental results are normalized to controls where no gel was applied to the membrane, such that % control = $RLU_{bottom,experiment}/RLU_{bottom,control}$. Additional control experiments were performed in which an equivalent amount of gel was mixed in to solutions. For 0-, 4-, and 8-hour incubations, there was a log reduction in levels of HIV-1 in the bottom compartment.

We also performed control experiments in which gel was mixed into solution and incubated in the Transwell for 8 hours. The volume of gel mixed into solution was equivalent to the volume of gel applied to the Transwell membrane. We found that there was no significant difference in HIV levels in the bottom compartment for this “mixed” condition compared control ($p > 0.05$). However, there was a significant difference between the “mixed” control and the experiments with gel layers ($p < 0.05$). This suggested that reduction of HIV in the bottom compartment was due to reduction of transport, not neutralization by the placebo gels.

Interestingly, levels of HIV in the bottom compartment for $t = 0$ h were significantly different from control. If transport from the top to the bottom compartment occurred due to diffusion alone, we would have observed no HIV in the bottom compartment for all conditions at $t = 0$ h. The observed log reduction suggests that there was some convective transport from the top to bottom compartment, which probably occurred due to hydrostatic pressure differences introduced when the top insert was separated from the bottom plate at the end of the incubation period. This effect may have lessened for longer incubation times, as the gel became more dilute at the time of separation of the top and bottom compartments. Levels of HIV in the bottom compartment appeared to approach the no-gel control as time increased.

4.3.2 Evaluation of gel layers of varying thickness

We also tested various thicknesses of gels, with the hypothesis that increasing gel layer thickness would lead to decreased levels of HIV in the bottom compartment of the Transwell at a given time. We applied gel layers of 3 different thicknesses to the membrane, using HEC (Figure 58).

Results were variable. For 12-hour incubation, levels of HIV trend with layer thickness, as expected: Thicker layers of gel prevent infectious virions from reaching the bottom compartment compared to control. However, results for the different thicknesses were not statistically significant (ANOVA, $p > 0.05$). For 0-, 4-, and 8-hour incubations, levels of HIV in the bottom compartment were similar for all thicknesses, and did not follow the expected trend.

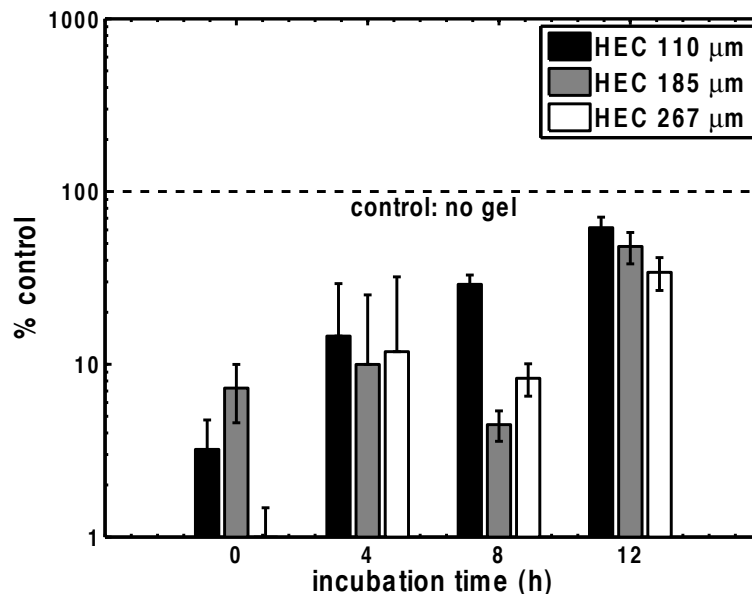


Figure 58. Transwell assay results for various thicknesses of HEC gel ($n \geq 4$ independent experiments). Experimental results are normalized to controls where no gels were applied to the membrane, such that $\% \text{ control} = RLU_{\text{bottom,experiment}}/RLU_{\text{bottom,control}}$. Characterization of gel layer thickness is shown in Table 19 (p. 165).

4.3.3 Characterization studies

4.3.3.1 Thickness and distribution of gel layers

To measure the thicknesses of gel layers applied to the Transwell membrane, we labeled the gel with fluorescent dye and related fluorescence intensity to thickness. For each gel, we generated a standard curve relating fluorescence intensity to thickness (Figure 57). Levels of fluorescence were linearly related to thickness for the range of thicknesses tested.

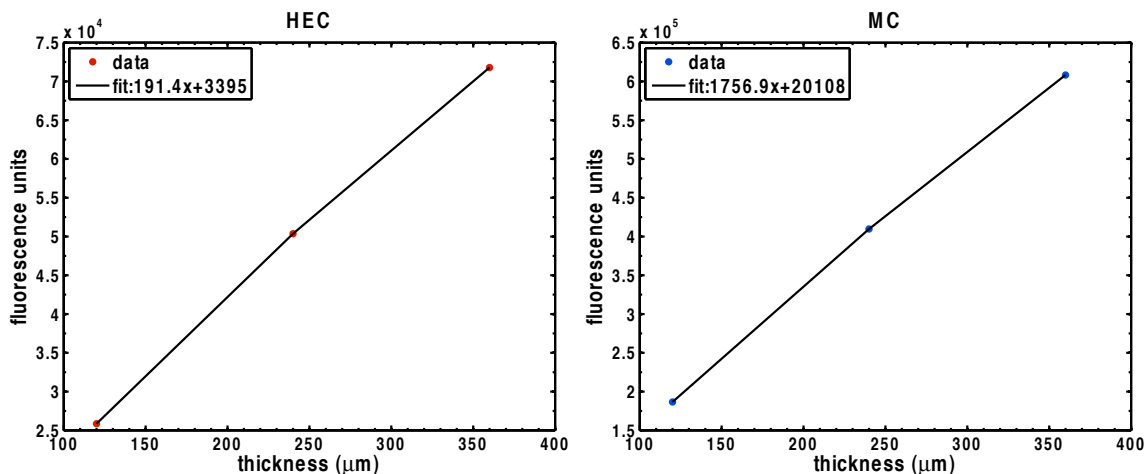


Figure 59. Standard curves relating fluorescence intensity and thickness for Left: HEC and Right: MC labeled with fluorescein.

Gel layers of different thicknesses were produced by varying the height of the collar setting and volume of gel placed on the tip of the applicator (Table 19). Figure 60 shows examples of distributions of the gel on the Transwell membrane. Although gel layers were not uniform, the entire surface of the membrane was covered with at least some gel.

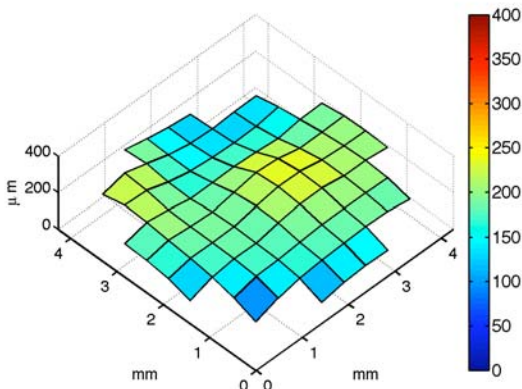
Table 19. Thicknesses of gel layers (mean \pm SE) for different collar heights and gel volumes (n = 12 for HEC, n = 6 for MC).

| Gel | Collar setting | Gel volume (μl) | Arithmetic mean thickness (μm) | Harmonic mean thickness (μm) |
|-----|----------------|-----------------|--------------------------------|------------------------------|
| HEC | 1 | 2.8 | 110 \pm 6 | 65 \pm 4 |
| | 2 | 6.3 | 185 \pm 5 | 167 \pm 6 |
| | 3 | 11.1 | 267 \pm 7 | 225 \pm 7 |
| MC | 2 | 8.4 | 153 \pm 4 | 142 \pm 4 |

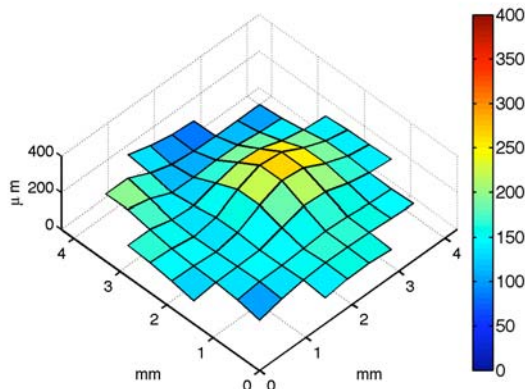
For comparing HEC and MC, we attempted to form gel layers of approximately 150-μm thickness. Actual thicknesses were 185 \pm 5 and 153 \pm 4 μm for HEC and MC, respectively. For comparisons of HEC gel layers of various thicknesses, we used gel

layers 110 ± 6 , 185 ± 5 , and 267 ± 7 μm thick. We also calculated the harmonic mean for use in mathematical models of diffusion (§5.3.5 describes how the harmonic mean is a superior summary of mean thickness for diffusion models).

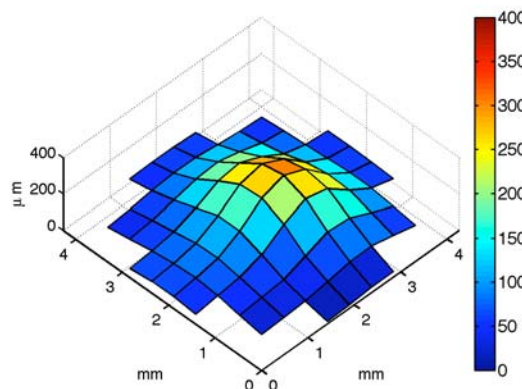
(A) HEC 185 μm



(B) MC 154 μm



(C) HEC 110 μm



(D) HEC 267 μm

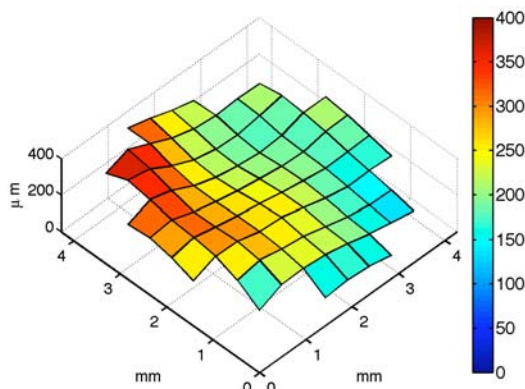


Figure 60. Examples of gel distributions applied to membranes in Transwell system.

4.3.3.2 Linear range of TZM-bl assay

The relationship between luminescence (measured in relative luminescence units, RLU) and HIV concentration in the TZM-bl assay is shown in Figure 61. For the two strains of HIV-1 used in our experiments, luminescence is linearly related to concentration within the range of approximately 1,500 to 170,000 RLU. Figure 62 shows

mean luminescence values from experiments. The negative control, containing only cells had luminescence levels near 920 RLU. The positive control and the media from the top compartments of the Transwell had high levels of virus, near 70,000 RLU. Media from the bottom compartments of the Transwell had intermediate values, near 4,400 RLU. All of our experiments were performed within the linear range of the assay.

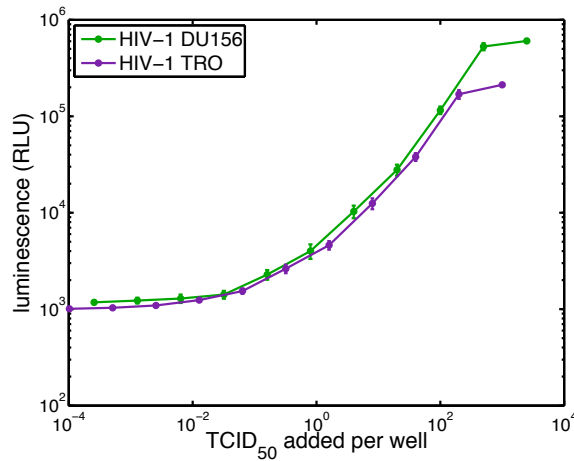


Figure 61. Linear range of TZM-bl assay for HIV-1 strains used in Transwell experiments (n = 4). Levels of luminescence are expressed as Relative Luminescence Units, RLU.

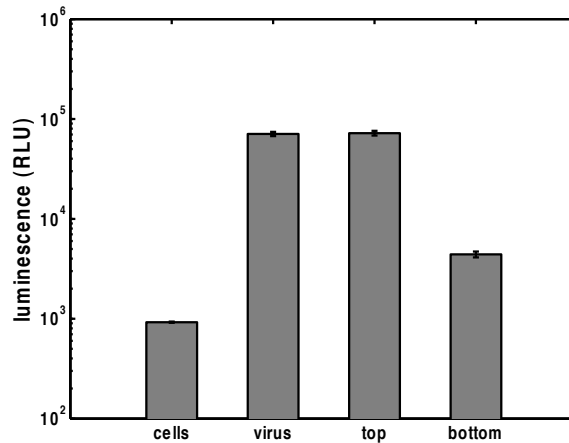


Figure 62. Luminescence values (mean ± SE) for experimental conditions and controls are within the linear range of the TZM-bl assay shown in Figure 61. Data are pooled from various conditions in n = 14 independent experiments. Levels of luminescence are expressed as Relative Luminescence Units, RLU.

4.3.3.3 Dose-dependent neutralization by placebo gels

We also performed neutralization studies for the placebo gels tested, to ensure that the gels were not neutralizing to HIV in the amounts used in the Transwell assay. This assured us that reductions in the amount of virus in the bottom compartment of the Transwell were due to reduction in transport of virus, not neutralization by the gel. We found that HEC and MC did not neutralize HIV at concentrations applied in the Transwell assay (Figure 63).

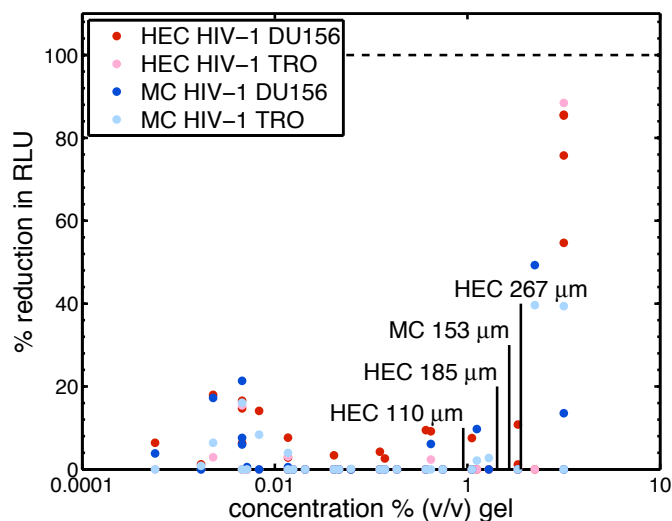


Figure 63. Neutralization of HIV-1 DU156 and TRO by HEC and MC gels (n = 4). Equivalent concentrations used in the Transwell are annotated to the plot. HEC and MC did not neutralize HIV-1 at the concentrations used in the Transwell.

4.3.3.4 HIV-1 viability over time

We analyzed HIV-1 viability over time because we observed that RLU levels of HIV in the bottom compartment of the no-membrane control decreased over time (Figure 64). This was the opposite of our expectation that the amount of virus in the bottom compartment would increase over time due to time-dependent transport from the upper compartment.

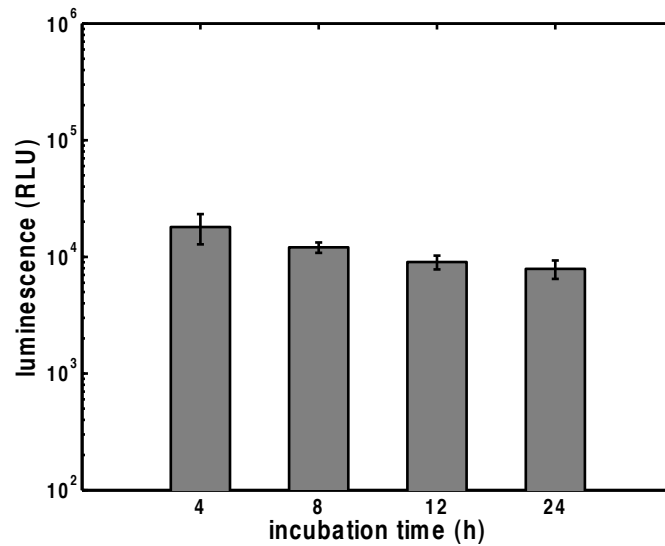


Figure 64. Levels of HIV in the bottom compartment of no-gel controls (mean ± SE, n ≥ 4).

To quantify HIV viability in the Transwell model over time, we fit total levels virus to an exponential curve, and calculated the half-life of each HIV strain. We calculated the total level of HIV in the Transwell by summing the luminescence levels measured in the top and bottom compartments as follows:

$$RLU_{total} = \frac{150}{50} \times \frac{75}{50} \times RLU_{top} + \frac{150}{150} \times \frac{235}{150} \times RLU_{bottom}$$

Equation 58

Coefficients were determined by dilution in the assay plate and portion of the compartment sampled. Figure 65 shows sums of RLU values for the top and bottom compartments of the no-gel control over time. We fit these values to an exponential curve to calculate the half-life. The half-life of DU156 and TRO were 6.8 and 4.4 hours, respectively.

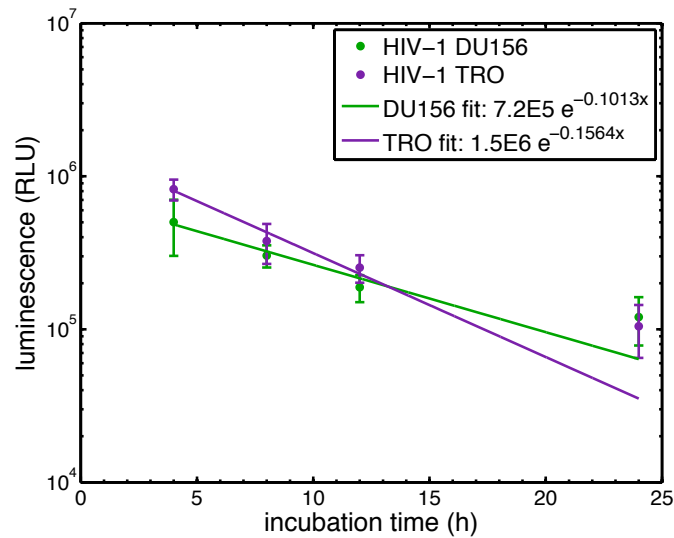


Figure 65. Total levels of HIV in the Transwell (mean \pm SE, $n \geq 4$). RLU values were calculated according to Equation 58. Data were fit to exponential curves to calculate half-life.

Normalization of experimental results to the no-gel control corrects for variations in virus introduced to the top compartment and the decrease in viability of HIV over time.

4.3.3.5 Comparison of experimental results to mathematical model of 1D diffusion

We compared experimental results to 1D mathematical model predictions for (1) no-gel controls and (2) experiments with gel. We used a simple diffusion model [221] (Figure 66), in which the Transwell plate geometry was represented with a slab of area equivalent to the Transwell membrane area, 0.143 cm^2 . The top and bottom compartments were represented with compartments of equal volume to the growth medium applied in the top and bottom compartments of the Transwell. The membrane thickness was $10 \text{ }\mu\text{m}$. For the diffusion coefficient of HIV in culture medium and in the membrane, we used the theoretical diffusion coefficient for HIV in water as predicted by Stokes-Einstein. We also included transport due to sedimentation, assuming that the

specific gravity of HIV was 1.2 times that of water. Convection due to sedimentation contributed minimally to transport. The Peclet number, which is used to estimate the ratio of diffusion time to convection time [107], was 7×10^{-4} here.

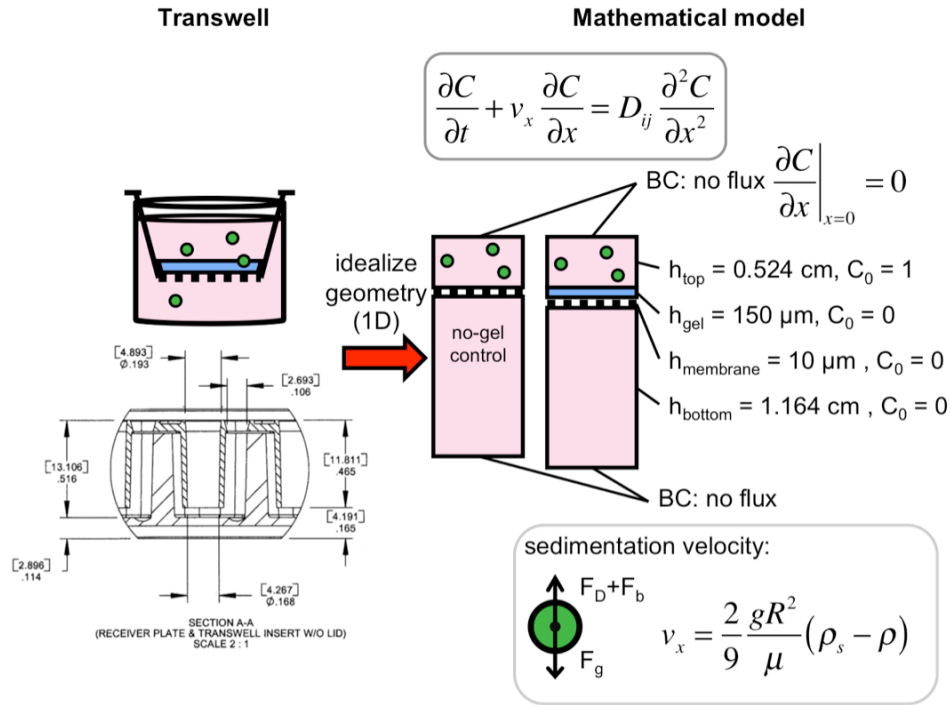


Figure 66. Mathematical model of HIV transport in Transwell experiments.

First, we compared results from no-gel controls to theoretical predictions for the portion of HIV in the bottom compartment (Figure 67). The portion of HIV in the bottom was calculated from luminescence values as follows:

$$\% \text{ of total in bottom compartment} = 100 \times \frac{\frac{150}{150} \times \frac{235}{150} \times RLU_{bottom}}{\left(\frac{150}{50} \times \frac{75}{50} \times RLU_{top} + \frac{150}{150} \times \frac{235}{150} \times RLU_{bottom} \right)}$$

Equation 59

Again, coefficients were determined by the level of dilution in the assay plate and the portion of the Transwell compartment volume sampled.

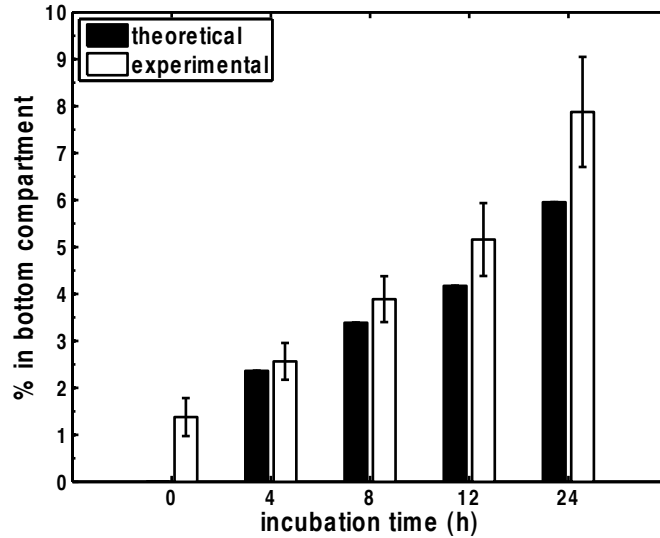


Figure 67. Comparison of theoretical predictions and experimental results (mean \pm SE, $n \geq 4$) for portion of HIV in the bottom compartment of no-gel controls.

We found that there was agreement between control results and theoretical predictions (Figure 67). Results for $t = 4, 8, 12,$ and 24 were not statistically significantly different from theoretical predictions. The portion of HIV in the bottom compartment at $t = 0, 1.4 \pm 0.4\%$, was greater than the predicted. The mathematical model assumed that transport occurred by diffusion and sedimentation alone. The experimental results suggest that there may have been some additional convective transport, transferring HIV from the top compartment to the bottom compartment. This likely occurred due to hydrostatic pressure differences when the Transwell insert was separated from the bottom plate.

Second, we also compared results of Transwell experiments with gels to theoretical predictions. We incorporated a gel layer of 150- μm thickness to the mathematical model (Figure 66). We input a range of diffusion coefficients of HIV in gel such that $D_{HIV,gel}/D_{HIV,water} = 1, 0.01, 0.0001$. Values of $D_{HIV,gel}/D_{HIV,water} = 1$ were comparable to diffusion coefficients of HIV-like liposomes in highly diluted gels, i.e., 2-10% (v/v) gel, measured in Chapter 3. Values of $D_{HIV,gel}/D_{HIV,water} = 0.01$ and 0.0001 were comparable to diffusion coefficients of HIV-virions in 20% (v/v) gel and undiluted gel, respectively.

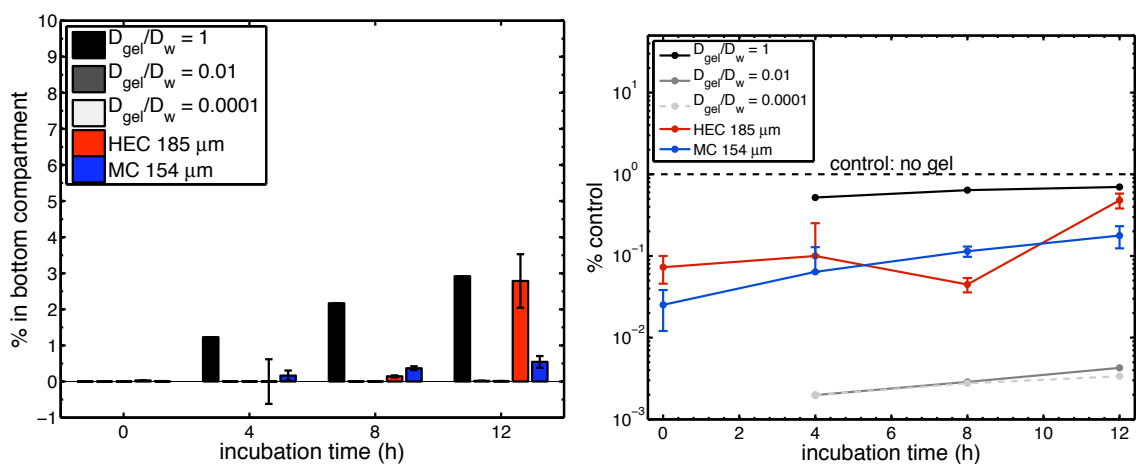


Figure 68. Comparison of theoretical predictions and experimental results (mean \pm SE, $n \geq 4$) for Transwell with approximately 150- μm gel layer. Theoretical predictions are shown in black, gray and white. Experimental results for HEC and MC are shown in red and blue, respectively. Left: Results are expressed in terms of portion in the bottom compartment, calculated according to Equation 59. Right: Results are normalized to no-gel control, according to Equation 57.

Based on diffusion coefficient values of $D_{HIV,gel}/D_{HIV,water} = 0.01$ and 0.0001, theoretical predictions were similar for the incubation times used in the Transwell experiment. The gel acted as a physical barrier to HIV virions, and levels of HIV in the bottom compartment were approximately 2-3 orders of magnitude lower than the no-gel

control. Theoretical predictions using the higher value of diffusion coefficient, $D_{HIV,gel}/D_{HIV,water} = 1$, yielded higher levels of HIV in the bottom compartment. In this scenario, the diffusion coefficient of HIV in gel was equivalent to the diffusion coefficient in culture medium. Reductions in levels of HIV in the bottom compartment were caused by the gel layer introducing additional distance between the top and bottom compartments.

Experimental results were higher than theoretical predictions for $D_{HIV,gel}/D_{HIV,water} = 0.01$ and 0.0001 , but lower than theoretical predictions for $D_{HIV,gel}/D_{HIV,water} = 1$. This suggests that transport in the Transwell model could not be attributed to diffusion alone. Nevertheless, gel layers reduced the levels of HIV in the bottom compartment compared to controls and compared to theoretical predictions for a thin gel layer that did not hinder viral diffusion.

4.4 Discussion

The goal of this study was to provide information about the strategy of using semi-solid gels to reduce the diffusion coefficients of virions, in the context of HIV prevention. We developed an experimental model to simulate the spatial configuration of HIV transmission in the presence of topically-applied gel layers. We tested two gels, HEC and MC, to determine if they acted as physical barriers to HIV.

We found that the vaginal gels tested do indeed act as physical barriers to the transport of HIV in our experimental model. There was a log reduction in levels of HIV after 0-, 4-, and 8-hour incubation where gel layers of approximately 150 μm had been

applied to the Transwell membrane. In HIV neutralization assays, log reductions are typically considered biologically significant.

From our previous work, we expected the level of infectious HIV in bottom compartment to be reduced by semi-solid gels. In Chapter 3, we showed that HEC and MC gels reduce diffusion coefficients of HIV virions, so we would expect that the flux of virions through a layer of gel would be reduced, compared to the control where no gel was applied to the membrane. We would thus expect that the cumulative amount of HIV in the bottom compartment at a given time would be lower than control. And indeed, we measured lower levels of HIV in the bottom compartment of Transwells where gel had been applied to the membrane compared to control.

However, levels of HIV in the bottom compartment were higher than those predicted theoretically by diffusion coefficients measured for undiluted HEC and MC. When we input diffusion coefficients similar to those measured in Chapter 3 to a simple model of 1D diffusion with geometry similar to that of the Transwell (Figure 66), we found that experimental results for levels of HIV in the bottom compartments were higher than theoretical predictions. Theoretical predictions suggest that effective diffusion coefficients of the gels were within the range of diffusion coefficients measured for diluted gels, $D_{HIV,gel}/D_{HIV,water} = 0.0001-1$. Dilution of the thin gel layers may have led to higher levels of HIV in the bottom compartment. Gels applied to the Transwell membrane were likely diluted by the surrounding culture medium over time. The volume ratio of gel to culture medium in the Transwell ranged from 0.9% - 3.6%. Furthermore,

convective transport from the top compartment to the bottom compartment may have also contributed to increasing levels of HIV in the bottom compartment of the Transwell.

Experimental results also suggest that MC is a slightly superior barrier to HEC. This was unexpected given the higher diffusion coefficients measured for HIV virions in MC compared to HEC. This was also unexpected considering that the thicknesses of MC layers were less than those of HEC layers. This phenomenon may be explained by different reactions of the gels to dilution. Perhaps MC is less prone to dilution when placed in contact with tissue culture medium. Differences in HEC and MC are probably not biologically significant.

Another unexpected result was the low level of HIV observed in the bottom compartment at $t = 0$ h. If HIV transport could be explained diffusion and sedimentation alone, then we would expect that no HIV would be detected in the bottom compartment at $t = 0$ h. The small amount of HIV observed in the bottom compartment of no-gel controls (1.4 ± 4 % of total) is likely due to convection from the top compartment to the bottom compartment during separation of the Transwell insert and bottom plate. This was probably caused by hydrostatic pressure differences in the top and bottom fluid compartments of the small Transwells (96-well plate) as separation occurs. This effect appears to have become more negligible with longer incubation times. At $t = 0$ h, differences between gel experiments and the no-gel control were exaggerated by the small levels of HIV measured in the bottom compartments and the fresh application of undiluted gel. With longer incubation times, the gel likely became more dilute, and convective transport through no-gel and gel experiments were similar. To reduce

convection, future experiments could use larger Transwell plates to reduce hydrostatic pressure differences or to allow sampling without separation of the Transwell insert and the bottom compartment, using smaller volumes relative to the compartment. In the 96-well plate format, we could not sample by pipetting from the bottom compartment, without drawing fluid through the membrane, to the bottom compartment. If the Transwell model were to be adapted for larger plates, the gel application method would also require modification.

Additional improvements to the experimental system could include standardization of gel application and optimization of incubation time. We observed variation in results of experiments when gel layers of the same volume had been applied to the membrane. Further work standardizing gel layers could reduce this variability. Gel application methods could also be improved to allow for application of gel to multiple Transwells at once. Currently, the 96-well format is conducive to high-throughput screening of gels. However, gel layers must be applied to wells individually. An applicator analogous to the multi-channel pipette would allow for greater efficiency in experiments. The optimal incubation time depends on the trade-off between decreasing levels of HIV due to finite viral lifetime and increasing levels of HIV in bottom compartment due to transport over time. These will depend on the strains of HIV used, and the gels tested.

In summary, we developed an experimental model for evaluating the barrier function of semi-solid gels in preventing HIV transmission. During HIV infection, transport of HIV at mucosal surfaces occurs on time scale of minutes to hours [18].

Reducing the contact of HIV and vulnerable target cells may aid in HIV prevention. Our studies here suggest that topically-applied gels may act as physical barriers to HIV transport. In particular, our findings for HEC and MC suggest that gels that have been used as placebos in microbicide clinical trials may function as physical barriers in HIV prevention. The experimental system described here could provide a valuable high-throughput tool for the future evaluation and development of gels that act as physical barriers to HIV.

4.5 Conclusions

We evaluated the barrier function of 2 typical vaginal gels, HEC and MC, in a Transwell model for HIV transmission in the presence of thin gel layers. Gel layers were applied to the membranes in 96-well Transwell plates and challenged by a solution of HIV added to the top compartment. After 0-, 4-, 8-, or 12-hour incubation, we quantified levels of HIV in the bottom compartment. We indeed observed that these semi-solid gels could act as physical barriers to HIV – levels of HIV in the bottom compartment of the Transwell were lower than no-gel controls. This experimental system could serve as a tool in high throughput evaluation of topical semi-solid gels, and thus aid in the development of materials that act as physical barriers to HIV.

5. Mathematical model for kinetics of HIV diffusion to tissue surfaces in the presence of realistically deployed semi-solid gels

Chapter material reprinted from Biophysical Journal, 97(9), B.E. Lai, M.H.

Henderson, J.J. Peters, D.K. Walmer, D.F. Katz, Transport theory for HIV diffusion through in vivo distributions of topical microbicide gels, p. 2379-2387, © (2009), with permission from Elsevier.

5.1 Introduction

We have suggested that semi-solid gels can be used to hinder transport of HIV virions to tissue surfaces for HIV prevention. In Chapters 3 and 4, we demonstrated that it is possible to use semi-solid gels to reduce the diffusion coefficients of HIV and to reduce the levels of HIV in the bottom compartment of a Transwell system. However, for semi-solid gels to function in this manner *in vivo*, gels must be sufficiently deployed at epithelial surfaces. From optical imaging studies conducted by our group, we know that vaginal gels do not coat the epithelium completely or evenly after application [184, 199, 225]. Thus, an important aspect of evaluating semi-solid gels for HIV prevention is considering how realistic deployment of gels affects this function. For this purpose, we have developed a deterministic mathematical model of HIV diffusion to tissue surfaces in the presence of realistically deployed gel layers.

5.1.1 Pharmacokinetic and pharmacodynamic models in HIV/AIDS

Mathematical models of pharmacokinetics (PK) and pharmacodynamics (PD) have provided insights for the development of HIV/AIDS antiretroviral therapy [226,

227] and informed our understanding of HIV/AIDS pathology and the immune system [228-230]. However, there have been few attempts to create analogous mathematical models for topical microbicides for HIV prevention. This is probably due to the fact that sexual transmission of HIV is complex and poorly understood. Furthermore, topical microbicides often deliver drugs locally rather than systemically, so the analyses used in traditional pharmacokinetic modeling, where entire organs are treated as single compartments, are less relevant. There is also a lack of experimental pharmacokinetic data for topical microbicides from humans or animal models – biopsies of vaginal tissue are invasive, and there can be high variability in collection and analysis of cervicovaginal lavages and cytobrush specimens. Without these pharmacokinetic data, mathematical models cannot be validated. Additional collaborations between researchers using experimental and mathematical approaches are needed.

New mathematical models of microbicide functioning have the potential to contribute to microbicide development and evaluation. To date, two approaches have been employed for mathematically describing the functioning of microbicides: stochastic models of infectivity and deterministic transport models.

5.1.2 Stochastic model of microbicide functioning

Tuckwell et al. developed a stochastic approach [99] derived from clinical data relating semen viral load and likelihood of infection [231]. The probability of infection, P_{inf} , can be described as follows:

$$P_{inf} = p_E \left(1 - e^{-n(1-q)} \right)$$

Equation 60

Here p_E is the probability that the viral population in the host persists, n is the number of virions transferred to the non-infected partner, γ is a coefficient relating probability of infection and the number of virions transferred, and q is the efficacy of the microbicide (where $q = 1$ implies a 100% efficacious microbicide). Using data obtained from clinical studies [231], the model predicts that probability of infection is high in scenarios where the number of virions transferred is 10^5 - 10^7 , regardless of microbicide efficacy. This suggests that researchers should account for semen viral load in microbicide efficacy trials.

An advantage of the stochastic approach is that it can incorporate data for rates of infection provided by epidemiological studies and clinical trials. Model predictions can provide insights for clinical trial design. However, one limitation of stochastic modeling is that it provides limited insight to microbicide product functioning and biological mechanisms underlying HIV infection. Parameters describing microbicide efficacy and likelihood of infection are empirically derived, and condense complex underlying phenomena.

5.1.3 Deterministic model of microbicide functioning

An alternative modeling approach, taken by our group, has been to develop deterministic models of HIV and microbicide transport and neutralization processes [232-234]. These models consider parameters relevant to development of topical microbicide formulations such as rates of drug release, rates of HIV diffusion, and spatial deployment of drug delivery vehicles. The advantage of this approach is that these mathematical models can serve as tools to microbicide developers, helping them to interpret product

characteristics. However, this approach is hampered by limited experimental data linking model parameters to clinical outcomes.

In this study, we have used transport theory to describe HIV virions diffusing from semen through microbicide gel to vulnerable vaginal epithelial surfaces. The biological context of our analysis is the time interval following ejaculation when HIV virions introduced in semen are deposited in the lower female reproductive tract (Figure 69). We were interested in the functioning of microbicide gels as semi-permeable barriers to HIV and how the spatial deployment of gels *in vivo* affects this function.

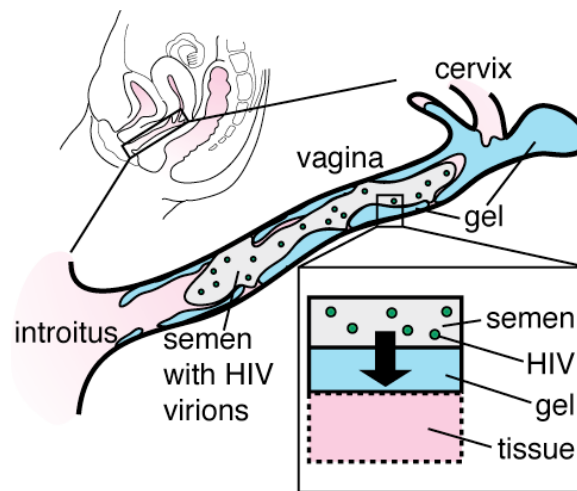


Figure 69. Idealized scenario of HIV transmission in the female reproductive tract in the presence of a microbicide gel. A microbicide gel is applied before coitus to partially coat the vaginal epithelium. Semen containing HIV virions is deposited in the lower female reproductive tract. HIV virions must diffuse from semen, through the gel layer, to reach tissue surfaces.

To date, the functional significance of hindering HIV transport through semi-solid microbicide products has not been comprehensively studied. Barrier methods, e.g., condoms, are known as an effective means of preventing HIV transmission [7].

Moreover, biological physical barriers, e.g. epithelial tissue and mucus, comprise a first

line of an imperfect innate immune defense. However, it is less clear how semi-solid microbicide products could contribute to preventing HIV transmission by acting as physical barriers. A mathematical model previously developed in our lab suggested that hindrance of virion diffusion is crucial to allowing APIs the time necessary to neutralize virions in the vaginal lumen before they reach vulnerable tissue surfaces [232].

Furthermore, HIV has a finite infectious lifetime *in vitro* and presumably *in vivo*: Thus, hindering HIV transport rates could reduce the infectious viral inoculum arriving at vulnerable tissue surfaces. This might also provide innate host defenses extended time in which to neutralize virus. Overall, hindering HIV transport could potentially reduce the inoculum of infectious virions that reaches tissue surfaces *in vivo*; this motivates further studies of potential barrier effects of microbicide products.

We used here the time required for a threshold number of virions to reach the tissue compartment as a metric for comparing different scenarios. This allowed us to study the barrier function of gels without limiting ourselves to specific microbicide active pharmaceutical ingredients. So, while this model does not address neutralization, it provides a foundation for future models that include specific mechanisms of action by pharmaceutical agents. Results here provide a useful first approximation of the lower bound of time required for virions to diffuse from infectious semen, through vaginal gels, to tissue.

In this study, we have also considered realistic deployment of vaginal gels *in vivo*. Previously, our lab developed a mathematical model with an idealized geometry in which vaginal tissue was coated completely by a layer of constant thickness [232]. However,

optical imaging experiments performed by our lab have shown that vaginal coating by gels in women is not so uniform: Coating thickness varies spatially, and not all tissue is covered [199, 235, 236]. Depending upon factors such as gel properties and a woman's posture and activity after gel application, as much as one third of the epithelial surface area has been found to be devoid of detectable coating [199, 235]. The distribution of coating thickness likely affects transport and interactions between HIV virions and active agents, and thus the prophylactic functioning of the gel. Algorithms based upon how coating details impact HIV transport kinetics and neutralization would enhance the biological interpretations of imaging studies.

The goal of this study was to define and understand parameters salient to the functioning of a semi-solid microbicide gel as a barrier to HIV diffusion. We developed a mathematical model for the role of *in vivo* measured gel coating in HIV transport kinetics from semen to vaginal epithelial surfaces, where early events of infection occur. Results provide insights about the time required for virions to contact vaginal epithelium, and how that is influenced by viral mobility in epithelial coating by a gel and details of that coating.

5.2 Materials and Methods

The biological context of our mathematical model is the time following ejaculation when HIV virions introduced in semen are deposited in the lower female reproductive tract (Figure 69). We assumed that the microbicide gel has been applied topically to the vaginal epithelium before challenge by semen containing HIV. We developed a mathematical model of diffusion of HIV virions from semen, through the

microbicide gel, to the tissue compartment (Figure 70). To accommodate realistic gel deployment, we discretized gel coating, assuming that gel deployment could be approximated by regions of constant coating thickness with corresponding fractional areas coated.

We modeled diffusion of HIV in each of these regions using one-dimensional diffusion. The number of virions to reach the tissue compartment for each discretized thickness and fractional area coated was summed to determine the total number of virions in the tissue compartment. The time to reach a threshold number of virions in the tissue compartment was used as a metric for comparing different scenarios.

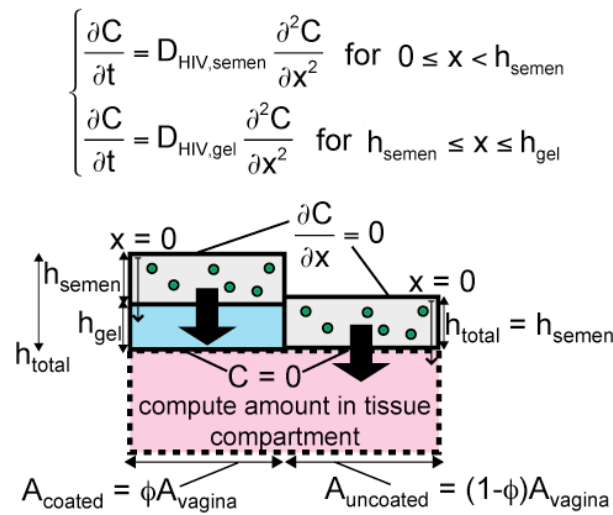


Figure 70. Diagram of mathematical model for HIV diffusion from semen, through topical microbicide, to tissue.

We explored different deployment scenarios in three stages. First, we modeled scenarios where the vaginal epithelium is completely coated with a gel layer of constant thickness. Results were used to validate that the model was behaving as expected. Second, we explored different scenarios of deployment where a fraction of the epithelium

was coated and the remainder of the epithelium was not coated. We used these scenarios to understand the interaction of fractional area coated, coating thickness, and viral restriction. Third, we inputted data from experiments measuring gel deployment *in vivo* to the mathematical model to understand viral restriction in realistic scenarios of gel deployment *in vivo*.

5.2.1 Governing equations

Transport of HIV virions from semen through microbicide gel, where present, was modeled as a 1D diffusion process. Governing equations of transport were applied to HIV diffusion in the semen layer and the gel layer:

$$\frac{\partial C_{HIV}}{\partial t} = D_{HIV,semen} \frac{\partial^2 C_{HIV}}{\partial x^2} ,$$

Equation 61

$$\frac{\partial C_{HIV}}{\partial t} = D_{HIV,gel} \frac{\partial^2 C_{HIV}}{\partial x^2} .$$

Equation 62

Here, C_{HIV} represents the concentration of HIV virions and $D_{HIV,semen}$ and $D_{HIV,gel}$ are diffusion coefficients of HIV in semen and gel, respectively. The assumption of one-dimensional diffusion was justified because the thickness of gel and semen layers (i.e., hundreds of microns) is much smaller than the length scale of area coated (i.e., centimeters).

5.2.2 Boundary conditions

The vagina was treated as a collapsed flat tube [71, 237] with symmetry about $x = 0$. The symmetry boundary condition at $x = 0$ is the following:

$$\frac{\partial C_{HIV}(0,t)}{\partial x} = 0$$

Equation 63

At the interface of the semen and gel layers, we applied standard concentration and flux boundary conditions:

$$C_{HIV}(h_{semen}^+, t) = \Phi_{HIV} C_{HIV}(h_{semen}^-, t),$$

Equation 64

$$D_{HIV,gel} \frac{\partial C_{HIV}(h_{semen}^+, t)}{\partial x} = D_{HIV,semen} \frac{\partial C_{HIV}(h_{semen}^-, t)}{\partial x}$$

Equation 65

Here, h_{semen}^+ and h_{semen}^- refer to positions infinitesimally above and below the semen-gel interface, respectively; Φ_{HIV} is the partition coefficient between the semen and gel layers.

The boundary condition between the gel and tissue compartments is not well understood. Virions likely accumulate on the surface of the vaginal epithelium because the epithelial cells form a physical barrier [238]. Recent work by Hope et al. suggests that HIV virions can diffuse through intact epithelial tissue *in vivo* [31]. The permeability of tissue to HIV has not been quantified. Given this current lack of quantitative understanding, we chose to apply a zero-concentration boundary condition at the gel-tissue interface:

$$C_{HIV}(h_{total}, t) = 0$$

Equation 66

This boundary condition maximizes the flux into the tissue compartment, and provides the most conservative estimates for the times needed to reach threshold levels of virions at the tissue surface.

5.2.3 Initial conditions

In the model, HIV is introduced at concentration C_0 in the semen at time zero:

$$C_{HIV}(x,0) = C_0 \text{ for } 0 \leq x < h_{semen} .$$

Equation 67

The concentration of HIV within the microbicide gel layer is initially zero:

$$C_{HIV}(x,0) = 0 \text{ for } h_{semen} \leq x < h_{total} .$$

Equation 68

5.2.4 Parameters

Parameters used in the model are summarized in Table 20. These values were used to generate results unless otherwise noted.

Table 20. Parameters used in model of HIV-virion diffusion from semen through microbicide gel.

| Variable | Definition | Reference condition |
|------------------|--|--|
| C_{HIV} | Concentration of HIV | - |
| $D_{HIV, semen}$ | Diffusion coefficient of HIV in semen | $3.63 \times 10^{-8} \text{ cm}^2/\text{s}$ |
| d_{HIV} | Diameter of HIV virion | 125 nm |
| μ_{semen} | Viscosity of semen | 1 cP |
| T | Temperature | 37° C |
| $D_{HIV, gel}$ | Diffusion coefficient of HIV in microbicide gel | $0.5 D_{semen}$ |
| Φ_{HIV} | Partition coefficient between semen and gel layers | 1 |
| C_0 | Initial concentration of HIV in semen | $5 \times 10^4 \text{ virions/ml} = 8.3 \times 10^{-17} \text{ M}$ |
| h_{semen} | Thickness of semen layer | 340 μm |
| h_{gel} | Thickness of microbicide gel layer | 300 μm |
| h_{total} | Total thickness of semen and microbicide gel layers, $h_{semen} + h_{gel}$ | 640 μm |
| M_{tissue} | Amount of HIV in tissue compartment | - |
| V_{semen} | Volume of semen | 3.4 ml |
| V_{gel} | Volume of microbicide gel | 3.0 ml |
| A_{vagina} | Surface area of vaginal epithelium | 100 cm^2 |
| ϕ | Fractional area coated by gel of given thickness | 1 |
| threshold | Threshold number of virions in tissue compartment | $1.7 \times 10^4 \text{ virions}$ |

5.2.4.1 Diffusion coefficients

The diffusion coefficient of HIV in semen ($D_{HIV,semen}$) was estimated using the Stokes-Einstein equation [107]. HIV was treated as a sphere with diameter of 125 nm [239]. Semen was treated as a Newtonian fluid with viscosity of 1 cP. Given these assumptions, the value $D_{HIV,semen} = 3.6 \times 10^{-8} \text{ cm}^2\text{s}^{-1}$. Human semen is a heterogeneous material, and measurements of its viscosity have produced results typically within the range of 3-7 cP [75]. This may be due in part to differences in the viscometric methods employed. Our use of the viscosity 1 cP simulates water-like semen properties and thus

provides the highest, and therefore most conservative, value for $D_{HIV,semen}$. That is, it leads to the lowest estimates of times at which threshold numbers of virions contact vaginal tissue.

For the diffusion coefficient of HIV in gel, we inputted a range of conservative values relative to the diffusion coefficient of HIV in semen: $D_{HIV,gel} = D_{HIV,semen}$, $0.5D_{HIV,semen}$, or $0.1D_{HIV,semen}$. To illustrate a range of possible values for viral hindrance in our model, the diffusion coefficient of HIV in vaginal gels ($D_{HIV,gel}$) was varied relative to the diffusion coefficient of HIV in semen ($D_{HIV,semen}$). These levels of viral restriction are much lower than those measured in Chapter 3 for HIV virions in semi-solid gels. For undiluted gel, we found that $D_{HIV,gel} \approx 0.0001D_{HIV,PBS}$. For gels diluted to 20% (v/v) in PBS, viral restriction of $D_{HIV,gel} \approx 0.01D_{HIV,PBS}$ was observed. We chose to use low levels of viral restriction in our mathematical model here because they yielded threshold times that were more biologically relevant, i.e., hours instead of days. In §5.3.4, we explored a more comprehensive range of gel diffusion coefficients to determine deployment scenarios where viral restriction is relevant.

5.2.4.2 Geometry

Volumes of microbicide gels used in clinical trials range from 2-5 ml [165, 240-242]. In our model, we used an intermediate volume of 3 ml.

The average volume of the human ejaculate (V_{semen}) is 3.4 ml [75]. If the volume of semen is distributed relatively evenly over the area of the vagina, then an effective semen layer thickness is $h_{semen} = \frac{V_{semen}}{A_{vagina}}$. The shape and surface area of the vagina vary

between individuals. Using vinyl polysiloxane casts, Pendergrass et al. found that the surface area of the human vagina ranged from 65.73 to 107.07 cm² [243]. Here, an intermediate value for the surface area of the vagina (A_{vagina}) of 100 cm² was used. This yielded an effective value for h_{semen} of 340 μm .

5.2.4.3 HIV viral load and threshold

HIV viral load in semen varies with stage of infection, antiviral treatment, and co-infection with genital tract infections [34]. Risk of HIV transmission is the highest during acute HIV infection, during which the level of HIV RNA in semen can reach 5 log₁₀ to 6 log₁₀ copies/ml [244, 245]. HIV RNA levels were found to be the highest in men within 1 month of infection: In a recent study quantifying HIV RNA levels in seminal plasma, the median HIV RNA level in nine acutely infected men was 5.0 log₁₀ copies/ml [79]. In our mathematical model, we used this value of 10⁵ copies/ml for HIV RNA in semen. There are two copies of RNA per HIV virion, so this is equivalent to an initial concentration of 5×10^4 virions/ml.

The number of virions needed for HIV infection to occur is unknown. It is not possible to translate HIV RNA copy number to measures of infectiousness (e.g., TCID₅₀) because attempts to isolate HIV from semen are typically unsuccessful [88]. However, Klasse et al. [246] have noted that the highest risk of transmission from man to woman per coital act is 10%, which likely reflects the scenario of highest infectiousness of the transmitter and highest susceptibility of the recipient. For our mathematical model, we use a conservative threshold number of virions in the tissue compartment of 1.7×10^4

virions. This is one-tenth of the virions introduced in semen, assuming that semen volume is 3.4 ml and an initial concentration of 5×10^4 virions/ml. We calculated the times, $t_{threshold}$, needed to reach this threshold number of virions in the tissue compartment. These times were used to compare different scenarios in the model.

5.2.5 *In vivo* imaging studies

Our group developed an optical probe for imaging deployment of vaginal gels in women *in vivo* [199, 235, 247]. The imaging technique outputs the spatial distribution of gel coating thickness over vaginal epithelial surfaces, as illustrated in Fig. S1. Gels were fluorescently labeled with US Pharmacopeia (USP)-grade injectable fluorescein powder (typical concentration 0.1% w/w). Coating thickness is linearly related to fluorescence for layers less than 1.5-mm thick. The resolution of the device is 15-25 μm for gel thickness measurements.

Vaginal coating data were obtained for two commercial vaginal gels: K-Y Jelly (Personal Products Company, Skillman, NJ), a hydroxyethyl cellulose based lubricant, termed gel K; and Replens (Lil' Drug Store Products, Cedar Rapids, IA) a Carbopol based moisturizer, termed gel R. These were chosen as surrogates for microbicide products. They have different rheological properties, which give rise to different flow rates in fluid mechanical models of vaginal coating [248-252]. Imaging studies were performed in the clinic of the Department of Obstetrics and Gynecology, Duke University Medical Center, in a group of women of child-bearing age with no abnormalities of anatomy or physiology of the reproductive tract. The group included

both parous and nulli-parous women; measurements were performed throughout the menstrual cycle, excepting menses.

Experiments were performed for 2 protocols for a woman's activity after gel application, without (-) and with (+) simulated coitus. In both, a 3.5 ml bolus of gel was applied by a syringe-type applicator to the vaginal fornix while the woman was in a supine posture. In the first protocol, the woman remained supine for 20 min before imaging measurements commenced. This simulated pre-coital conditions of gel use. In the second protocol, the woman simulated coitus: after gel application, she assumed a sitting position (1 min), a standing position (1 min), a sitting position (1 min), and a supine position during which coitus was simulated by applying 30 strokes using an artificial phallus (approx. 1 min). Imaging measurements were performed 10 min after gel application. These protocols have been followed in a number of prior imaging studies of vaginal gel distributions [253].

A total of 8 experiments in different women were performed, with duplicate experiments in each treatment combination [gel \times activity]. This relatively small sample size is not sufficient to identify statistically significant differences across each combination [gel \times activity]. However, it is sufficient to exercise our new model of intravaginal HIV transport kinetics, providing initial quantitative insights about HIV transport times *in vivo*.

5.2.6 Numerical methods

The partial differential equations were solved using the MATLAB partial differential equation solver "pdepe" to obtain concentration profiles of HIV in the semen

and gel compartments over time from the onset of semen-gel contact. These concentration profiles were integrated throughout the layers and multiplied by corresponding fractional area coated to determine the total number of virions in the semen and gel compartments. The time-dependent amount of HIV in the tissue compartment, $M_{tissue}(t)$, was calculated by a mass balance, subtracting the number of virions in the semen and gel compartments from the initial number of virions in the semen. Using results for $M_{tissue}(t)$, we found the times necessary for a defined threshold number of virions to migrate to the tissue compartment. These times were used as a metric for evaluating effects of different parameters in the model.

5.2.6.1 Modeling of surface entirely coated at constant thickness

First, the model was used to examine HIV diffusion through a topical gel layer of constant thickness that completely coats the vaginal epithelium. To calculate the number of virions that have entered the tissue compartment (M_{tissue}), we used a mass balance. The number of virions in the tissue compartment was obtained by subtracting the number of virions in the gel and semen at a given time from the original number of virions introduced in the semen:

$$M_{tissue}(t) = C_0 V_{semen} - A_{vagina} \int_0^{h_{total}} C_{HIV}(x,t) dx .$$

Equation 69

Here, C_0 is the initial concentration of HIV virions in semen, V_{semen} is the volume of semen, A_{vagina} is the surface area of the vaginal epithelium, h_{total} is the total height of gel and semen, and C_{HIV} is the concentration of HIV. Modeling the simple scenario of

constant thickness and complete coating provided initial validation that the model behaves as expected. We expected that time to threshold would increase with increasing layer thickness and decreasing diffusion coefficient.

5.2.6.2 Using model to evaluate trade-offs between coating thickness and fractional area coated

Next, we explored time to threshold for a conserved volume of gel (V_{gel}), such that gel height (h_{gel}) and fractional area coated (ϕ) are related as follows:

$$h_{gel} = \frac{V_{gel}}{\phi A_{vagina}} .$$

Equation 70

Here, A_{vagina} is the total area of the vaginal epithelium. In this scenario, there was transport of virions over coated and uncoated tissue. The number of virions in the tissue compartment (M_{tissue}) can again be obtained by subtracting the number of virions in the gel and semen at a given time from the original number of virions in semen:

$$M_{tissue}(t) = C_0 V_{semen} - A_{vagina} \left[\phi \int_0^{h_{total}} C_{HIV,coated}(x,t) dx + (1-\phi) \int_0^{h_{semen}} C_{HIV,uncoated}(x,t) dx \right] .$$

Equation 71

Examining this scenario allowed us to answer the question of whether it is better to have a gel that coats more of the tissue or a gel that is deployed in thicker coating layers.

We further explored the sensitivity of the model to fractional area coated and thickness of coating by generating a contour plot of threshold times for combinations of ϕ and h_{gel} . We also determined deployment scenarios where viral restriction affected the

time to threshold by generating a contour plot of threshold times for combinations of ϕ and D_{gel}/D_{semen} .

5.2.6.3 Application to data from *in vivo* experiments

Finally, we applied the mathematical model to deployment data from *in vivo* experiments (Figure 71). We used data previously collected by our group of *in vivo* distributions of two commercially-available vaginal gels, KY Jelly (Personal Products Company, Skillman, NJ) and Replens (Lil' Drug Store Products, Cedar Rapids, IA). The polymer gelling agents used in these products are hydroxyethyl cellulose and Carbopol, respectively. These gels have been used by our group previously in fluid mechanical analyses [254, 255]. We also examined data from two protocols of application, without (-) and with (+) simulated coitus [256].

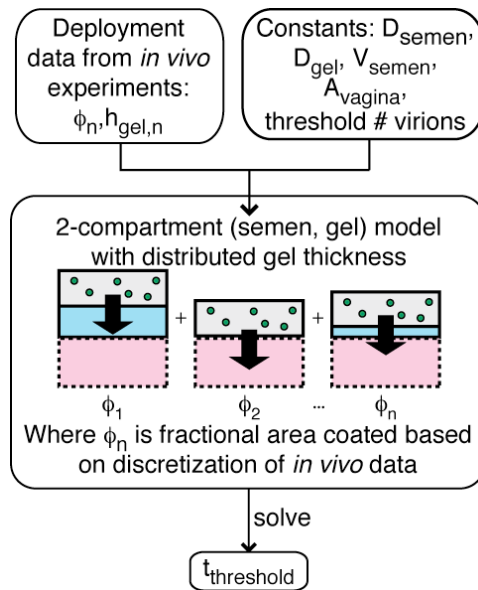


Figure 71. Schematic showing how mathematical model is used to interpret data from *in vivo* deployment experiments.

Vaginal coating data were discretized for application to the HIV transport model. Gel thicknesses were divided into twelve bins: 0 μm (areas in which no gel was detected), 0-50 μm , 50-100 μm , 100-150 μm , 150-200 μm , 200-250 μm , 250-300 μm , 300-350 μm , 400-450 μm , 450-500 μm , and over 500 μm . An approximate value of the thickness was input for h_{gel} for each of these bins: 0 μm , 25 μm , 75 μm , 125 μm , 175 μm , 225 μm , 275 μm , 325 μm , 375 μm , 425 μm , 475 μm , and 525 μm , respectively. The areas coated by gel layers of these thicknesses was normalized to total area, in order to determine fractional area (ϕ_n) coated by a given thickness. The total area of tissue input to the model is 100 cm^2 . The amount of virus in the tissue compartment (M_{tissue}) is calculated as follows:

$$M_{tissue}(t) = C_0 V_{semen} - \sum_{n=1}^m \phi_n A_{vagina} \int_0^{h_{gel,n} + h_{semen}} C_{HIV,n}(x,t) dx, \quad \sum_{n=1}^m \phi_n = 1.$$

Equation 72

Here, m is the number of bins, 12. The time to reach the threshold amount of virus in tissue, $t_{threshold}$, was determined and used as a metric for comparison.

5.3 Results

5.3.1 Initial modeling of complete coating with constant thickness

We initially applied the model to a surface fully coated by a gel layer of constant thickness. This illustrated the primary interaction between HIV diffusion coefficients and gel thickness in governing HIV transport times. Figure 72 and Figure 73 show amount of virus in the tissue compartment as a function of time. Different combinations of gel

thickness (Figure 72) and HIV diffusion coefficients were compared (Figure 73). Note that the presence of a gel layer did not provide an absolute barrier to HIV diffusion, i.e., the curves converge at the same maximum, where all of the virions entered the tissue compartment. However, the presence of a gel layer delayed entry of HIV into the tissue compartment. Increasing the gel layer thickness shifted the curve to the right and increased time to threshold (Figure 72). Decreasing the diffusion coefficient for virus in gel shifted the curve to the right and increased time to threshold (Figure 73).

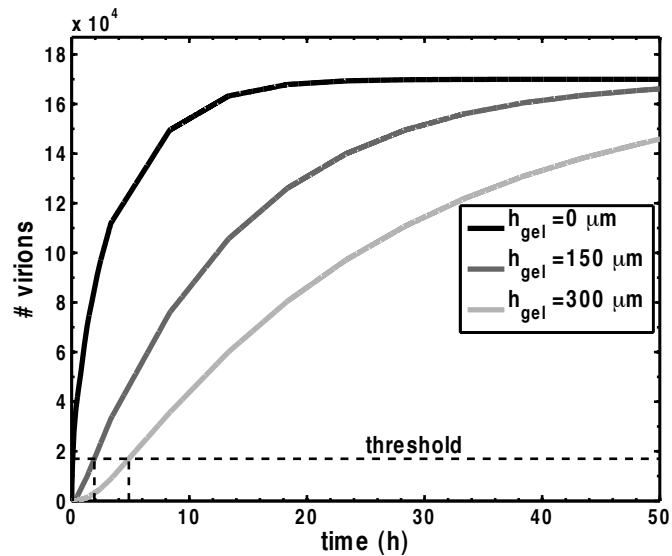


Figure 72. Accumulation of virions in tissue compartment over time for varying thickness of gel layer. Time to threshold is calculated by finding the time for which the number of virions in the tissue compartment is equal to the threshold value. Increasing the thickness of the gel layer increases the time to threshold. $D_{HIV,gel} = 0.5 D_{semen}$ (Table 20).

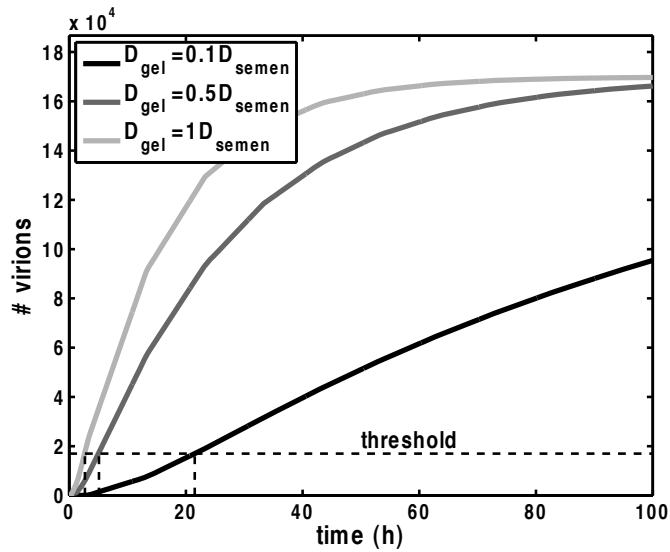


Figure 73. Accumulation of virions in tissue compartment over time for varying levels of viral restriction. Time to threshold is calculated by finding the time for which the number of virions in the tissue compartment is equal to the threshold value. Decreasing the diffusion coefficient of virus in gel increases the time to threshold. Here, $h_{gel} = 300 \mu\text{m}$ (Table 20).

5.3.2 Modeling of conserved volume of gel

To investigate trade-offs between the thickness of coating (where it exists) and the area of tissue with coating, we applied a schema in which the volume of gel was conserved ($V_{gel} = 3 \text{ ml}$). Here, the gel coating thickness and fractional area coated are inversely related as described in Equation 70.

Figure 74 shows the time to threshold vs. fractional area coated. Note that time to threshold increases as fractional area coated increases, even though coating thickness decreases (to conserve gel volume). Figure 74 also illustrates how delay of HIV diffusion to the tissue surface can be attributed to the physical presence of the gel layer, which distances semen and the tissue. This is represented by the scenario $D_{gel} = 1 D_{semen}$, as compared to the scenario in which there is no gel coating. For gel layers a few

hundred microns thick, such distancing delays time to threshold up to 3 hours. When the gel layer hinders viral diffusion (vs. diffusion in semen), the time to threshold is further increased. For $D_{gel} = 0.1D_{semen}$ (i.e., the greatest degree of reduction in viral diffusion in gel vs. semen), there is a pronounced increase in slope of this curve for $f \geq 0.85$. When $D_{gel} = 0.1D_{semen}$, the time to threshold increases to as much as 22 hours.

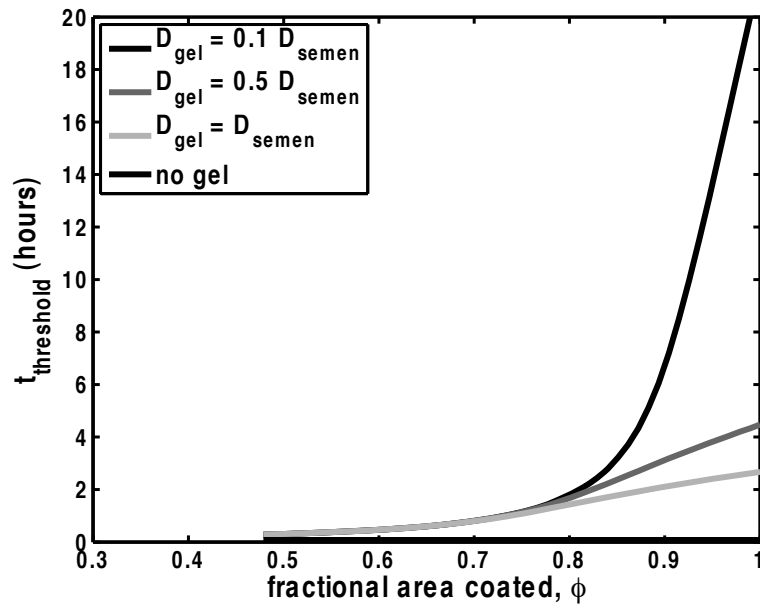


Figure 74. Trade-offs between gel layer thickness and area coated when the volume of gel is conserved as described in Equation 70, for different values of viral restriction. As the fractional area coated increases, time to threshold increases.

5.3.3 Trade-offs between thickness and area coated

To further explore trade-offs between coating thickness and fractional area coated, we generated a contour plot for time to threshold, in which coating thickness, h_{gel} , and fractional area coated, f , are varied (Figure 75). The curves in the contour plot exhibit a notable bend at approximately 100 μm . This means that, for deployment scenarios where coating thickness is less than 100 μm , threshold time remains relatively

constant for a range of areas coated. For deployment scenarios where coating thickness is greater than 100 μm , fractional area coated is the primary determinant of time to threshold. Above fractional area coated of 0.8, both gel thickness and fractional area coated contribute to increasing the time to threshold. When we generated results (not shown) for increased semen viscosity (and therefore decreased D_{semen}), the shapes of the curves were qualitatively the same, but they are shifted to the right. That is, trends were similar but time to threshold increased.

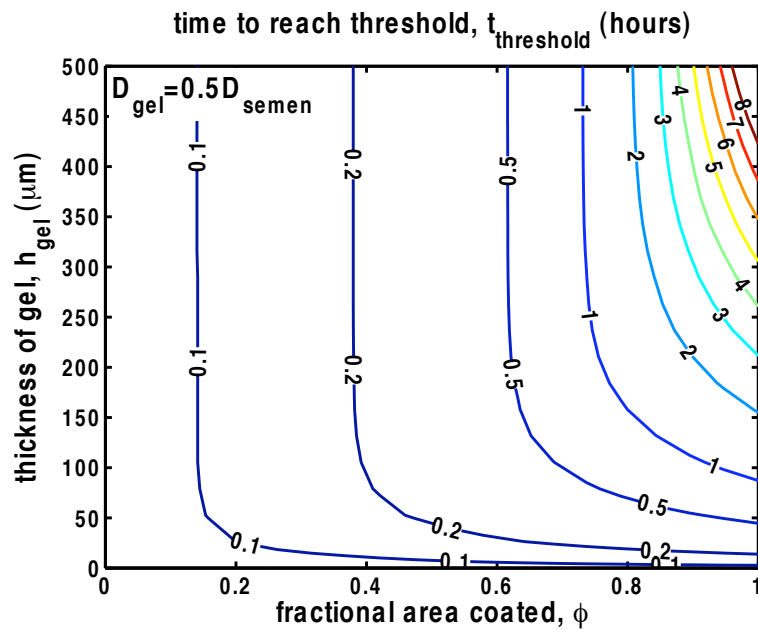


Figure 75. Contour plot showing values of threshold time for different gel thicknesses and fractional areas coated. Note that fractional area coated is the more important factor for all but the thinnest gel layers.

5.3.4 Effect of reducing virion diffusion coefficient

We also generated a contour plot to explore conditions in which viral hindrance significantly affects time to threshold (Figure 76). Recognizing from the trends shown in Figure 75 that the area coated is important in determining time to threshold, we plotted

time to threshold varying level of viral hindrance (D_{gel}/D_{semen}) and fractional area coated for 300- μm coating layer (Figure 76). We find that for $f \geq 0.80$, the level of viral hindrance contributes to determining time to threshold. For $f \geq 0.95$, increasing viral hindrance rapidly increases time to threshold. These results suggest that a significant portion of the tissue must be coated for levels of viral hindrance to contribute to the barrier function of a microbicide gel.

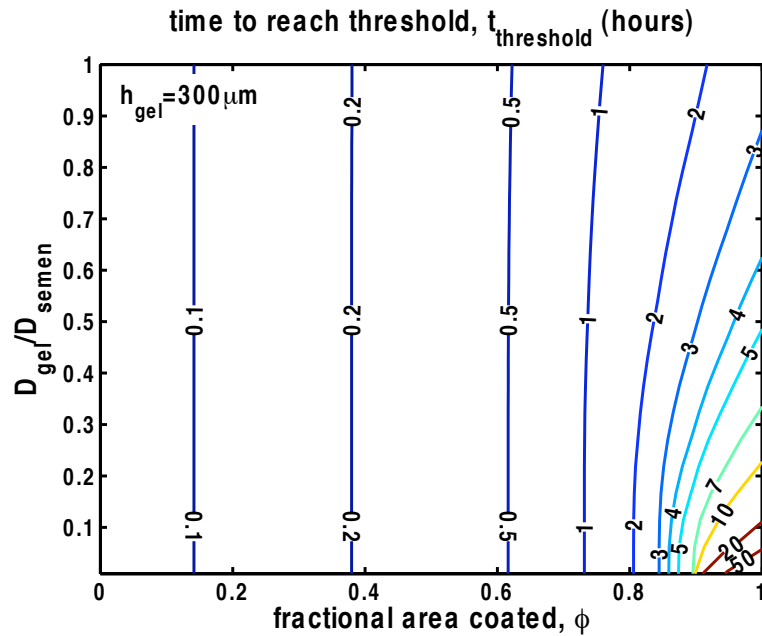


Figure 76. Contour plot showing values of threshold time for different levels of viral restriction and fractional areas coated. When fractional area coated is greater than 0.80, then levels of viral hindrance contribute significantly to threshold time.

5.3.5 Application of model to *in vivo* data

To examine how gels would act to hinder viral diffusion *in vivo*, we input experimental deployment data to the mathematical model (Figure 71). Deployment data for a small sample of *in vivo* data for vaginal coating thickness distributions were selected (Figure 77). These provided a range in fractional areas with detectable coating, and in

the distributions of thicknesses within that coating (Table 21). The deployment data were summarized as discretized thicknesses and corresponding fractional areas coated. These experimental inputs and other model parameters were used to calculate the time to threshold for different vaginal gels, application protocols, and levels of viral hindrance by the gel.

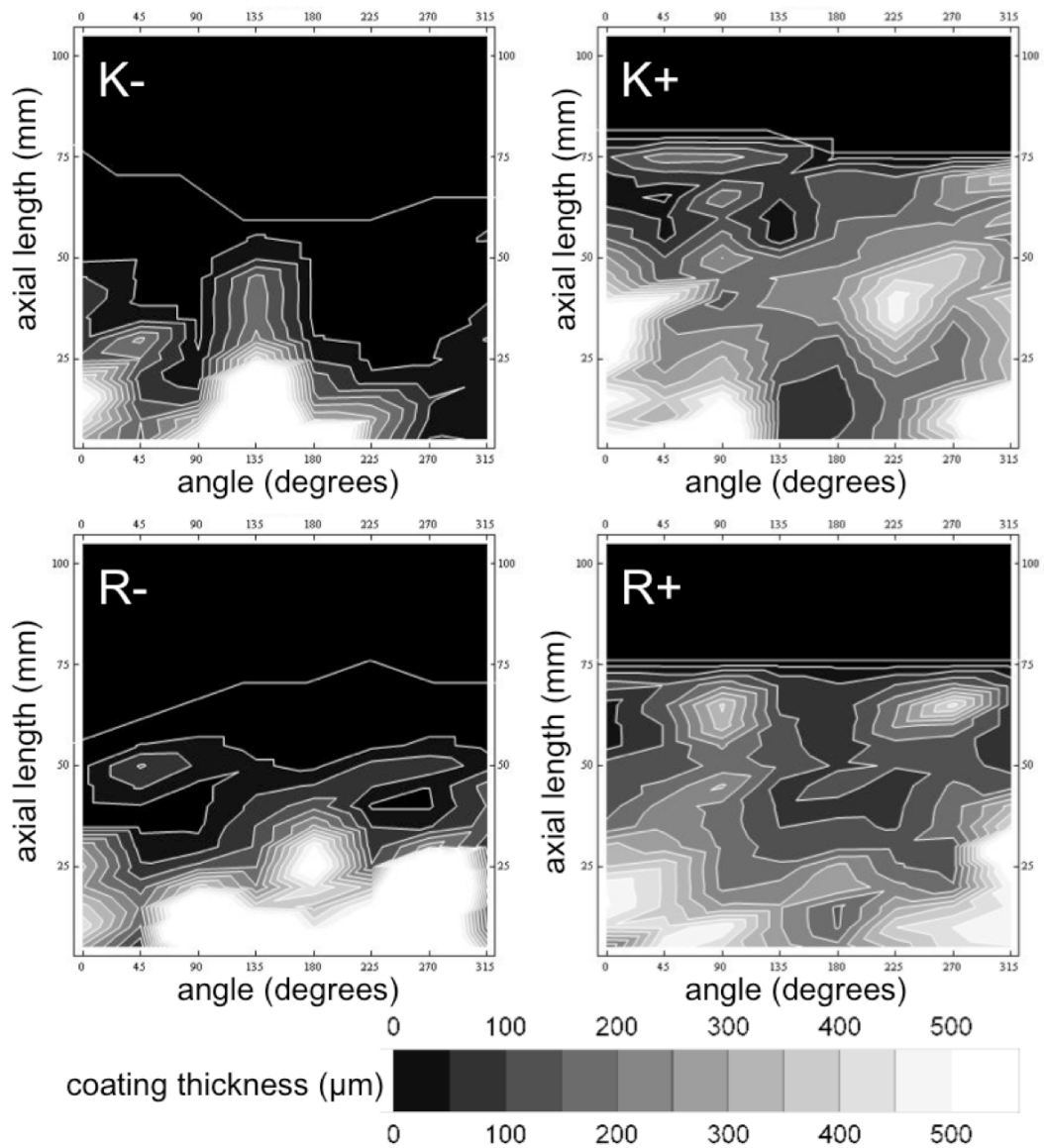


Figure 77. Contour plots depicting deployment data from selected *in vivo* experiments. Black represents undetectable coating (thickness $\sim 0 \mu\text{m}$), white represents coating thickness $> 500 \mu\text{m}$, and gray areas represent coating thicknesses between 0-500 μm . Axial length indicates distance from the end of the probe tube, which is placed in the fornix of the vagina. Angle indicates the position of the endoscope during imaging. Data represent the first (prefix “1”) of two independent experiments for each gel/ protocol listed in Table 21. K = KY Jelly, R = Replens. +/- simulated coitus. Note that simulated coitus increased the fractional area coated for both gels.

Table 21. Summary measures for *in vivo* deployment data. The numbers “1” and “2” represent data from two independent experiments for each gel/ protocol. K = KY Jelly, R = Replens. +/- simulated coitus.

| Gel/ protocol | % area coated | Arithmetic mean thickness (μm) | Harmonic mean thickness (μm) |
|---------------|---------------|---|---|
| 1K- | 72 | 170 | 10 |
| 2K- | 74 | 280 | 20 |
| 1K+ | 99 | 260 | 130 |
| 2K+ | 99 | 310 | 110 |
| 1R- | 80 | 290 | 10 |
| 2R- | 58 | 190 | 30 |
| 1R+ | 100 | 220 | 140 |
| 2R+ | 99 | 290 | 110 |

Figure 78 shows the resulting model outputs of $t_{threshold}$. There was little difference in $t_{threshold}$ between gels K and R. Gel application protocol (+ or - simulated coitus) more significantly affected time to threshold. Simulated coitus increased fractional area coated from ~ 60-87% to nearly 100% (Table 21). Shearing forces of simulated coitus spread the gels over tissue surfaces, and calculated time to threshold increased as a result. For deployment data from experiments without simulated coitus, there was little difference in $t_{threshold}$ for different reductions in viral diffusion coefficient; time to threshold was < 1.5 hours, regardless of the reduction. In contrast, for experiments with simulated coitus, a higher level of viral hindrance ($D_{gel} = 0.1 D_{semen}$) added hours to $t_{threshold}$ compared to cases in which diffusion was not hindered ($D_{gel} = 1D_{semen}$). For gels with $D_{gel} = 0.1 D_{semen}$, calculated time to threshold was nearly 8 hours.

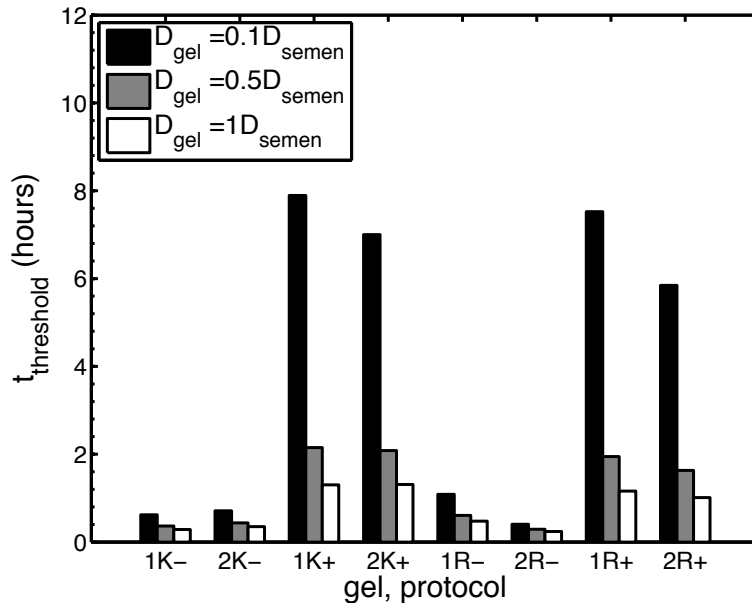


Figure 78. Resulting threshold times for application of mathematical model to experimental data obtained from deployment of vaginal gels in women. The numbers “1” and “2” represent data from two independent experiments for each gel/ protocol. K = KY Jelly, R = Replens. +/- = with/ without simulated coitus. Three levels of viral hindrance were input ($D_{gel}/D_{semen} = 0.1, 0.5, 1$).

We also sought to identify a summary measure for gel thickness distribution that can be used in estimating viral transport times. Use of such a measure would effectively reduce the problem to two partial differential equations corresponding to coated and uncoated regions rather than the set of 12 equations corresponding to multiple discretized thicknesses. This would simplify practical computational estimates of viral transport kinetics, e.g., in analyzing data sets from large imaging studies.

Since steady state 1D diffusion through a slab of material gives a flux inversely proportional to layer thickness, we computed the harmonic means of the coating distributions (as well as the arithmetic means) for use in computations of viral transport times (Figure 79). There was less than a two-fold range in values of the arithmetic mean thickness of coating over all experiments. However, as seen in Table 21, there were

much more conspicuous differences in values of the harmonic means, with a clear trend for higher values after simulated coitus.

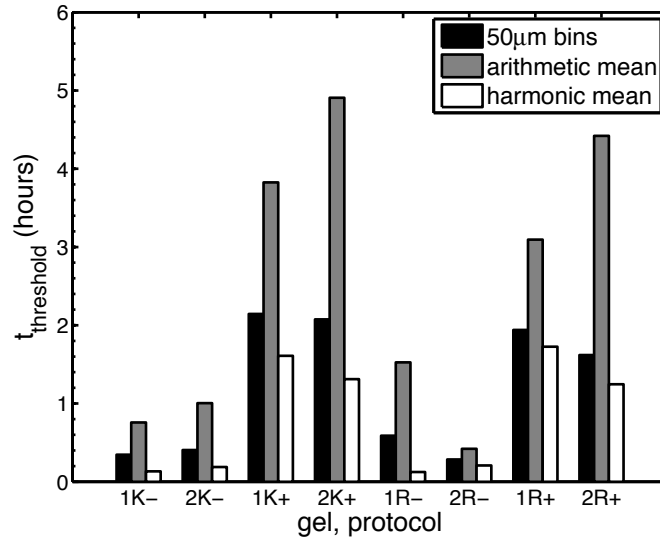


Figure 79. Comparison of the use of arithmetic and harmonic means to approximate thickness of gel coating in the mathematical model. The arithmetic and harmonic means of the thicknesses were calculated from experimental data. The calculated means and experimental fractional area coated were input to the HIV transport model to determine $t_{threshold}$. The harmonic mean better approximated the results derived from discretizing the thickness data into 50-µm bins. The numbers “1” and “2” represent data from two independent experiments for each gel/ protocol. K = KY Jelly, R = Replens. +/- = with/ without simulated coitus.

We compared the time to threshold resulting from inputting these mean values to the time to threshold resulting from inputting the twelve 50-µm bins for thickness distribution (Figure 79). The time to threshold was reasonably well approximated using the harmonic mean in a single diffusion distance computation. Using the arithmetic mean overestimated times to threshold. This suggests that a reasonable estimate of HIV transit times can be obtained in a constant thickness model in which the harmonic mean is used, together with fractional area coated. This would simplify analyses of *in vivo* data,

eliminating the need for binning of coating thickness data and performing separate transport computations for each bin.

5.4 Discussion

We developed a mathematical model for HIV-virion transport in the presence of a microbicide gel. The model uses transport theory to describe diffusion of HIV virions from semen to tissue in the presence of a biologically realistic vaginal gel coating, with incomplete coverage and non-uniform thickness. Our goal was to use the model to understand how deployment affects the ability of a topical gel to function as a barrier to HIV. To compare different scenarios, we used the metric of time required for a threshold number of virions to enter the tissue compartment.

Our results indicate that comprehensive coating by microbicide gels is crucial to increasing time to threshold. For example, for a conserved volume of gel, we found that time to threshold increases with increasing fractional area coated, even as the thickness of gel layers decreases accordingly. Analyzing different deployment scenarios, we also found that there is a cutoff in effective coating thickness: Below about 100 μm , time to threshold was brief (< 1 hour), regardless of fractional area coated. However, for thicknesses above approximately 100 μm , increasing fractional area coated increased time to threshold. When coating was incomplete, HIV transport to epithelium occurred primarily over surfaces in which there was direct contact of semen and uncoated tissue. When fractional area coated was above approximately 0.8, both gel thickness and fractional area coated contributed to increasing the time to threshold. Scenarios of comprehensive coating were needed for level of the viral hindrance (i.e., reduced

diffusion coefficient of HIV in gel) to contribute to increasing time to threshold. Below 0.8 fractional area coated, the time to threshold was determined largely by fractional area coated. However, above 0.8 fractional area coated, the level of viral hindrance contributed significantly to increasing the time to threshold. Taken together, these results suggest the importance of comprehensive coating in determining the ability of a topical gel to function as a barrier to HIV.

The model was also used to provide an objective context for interpreting *in vivo* data for the extent and thickness of vaginal coating. Our human imaging study was relatively small ($n = 8$), but it provided insights about differences in vaginal coating and about how to consolidate coating data. Previous work in our lab has suggested that the two gels tested, K and R, would have different deployment *in vivo* due to differing rheological properties [255]. However, there was little difference in the fractional areas coated by the two gels when measured optically *in vivo*. As a result, threshold times (assuming the same diffusion coefficient) were similar for the two gels. In contrast, the protocol after application appeared to have a more significant effect. The protocol involving simulated coitus (+) produced a larger coated surface area than remaining supine after gel application (-), and the calculated threshold times were longer as a result.

Microbicide formulators should consider the importance of deployment as they design products. Products formulated as gels may function, in part, by preventing or delaying the contact of HIV virions and vulnerable tissue. The deployment of vaginal gels *in vivo* depends on several factors: gel physical properties and changes in these properties over time due to change in temperature or dilution by other fluids; surface

interactions; surrounding tissue properties; posture changes and activities of the user [254]. Our group has been active in studying deployment of vaginal gels *in vivo* [184, 225] and *in vitro* [248-250, 254, 255, 257]. Others have also studied rheological properties of vaginal gels [258] and imaged their deployment *in vivo* [199, 259]. Another innovative approach to achieving more comprehensive coverage of the vaginal epithelium is modifying the design of the gel applicator. For example, one study compared the distribution of the microbicide candidate Invisible Condom® using standard commercially-available applicators and a new applicator designed to provide more comprehensive gel deployment [260].

The results of this study are somewhat paradoxical for gel design: Material properties conducive to gel distribution may be opposed to properties needed to restrict viral diffusion. For example, for simple materials, low viscosity may be conducive to gel spreading and deployment whereas high viscosity may be more effective in restricting viral transport. Thus, the mathematical model here may provide a valuable tool for developers who are evaluating the trade-offs between different formulations. Parameters related to deployment and transport can be input to the model to compare and rank formulation functioning.

In the state of development presented here, our model has several limitations. The greatest limitation is the uncertain relationship between our model predictions and clinical outcomes. To evaluate different scenarios, we used the time needed for a threshold number of virions to enter the tissue compartment. Currently, there is a lack of experimental data needed to relate this value to infection. Also, the functioning of topical

gels needs to be further investigated. To our knowledge, there has not yet been a study linking topical gel deployment to barrier function of a microbicide product. A stochastic model may be needed to link HIV infection to the number of virions because HIV transmission is a complex and variable process that is often unsuccessful: The likelihood of male-to-female sexual transmission of HIV per exposure event is 1/200 – 1/2000 [3]. Thus, it may be helpful to incorporate our approach, which addresses the spatio-temporal distributions of virions, with a stochastic approach, which incorporates data from clinical trials. This could provide increased understanding of the relationship between product characteristics (e.g., pharmaceutical agent potency, concentration, and delivery system) and clinical efficacy.

Another caveat of our study is that some input parameters were approximations. Parameters were derived from literature values when available, and we used conservative estimates for parameters for which previous measurements were not available. For example, we estimated the diffusion coefficient in semen based on the Stokes-Einstein equation. We then explored a range of diffusion coefficients for HIV in gel assuming that diffusion of virions would be restricted by the gel compared to semen. Diffusion coefficients of HIV in gel used here were higher than those measured in Chapter 3. We assumed that diffusion coefficients of virions in semen and gel were constant over time, thereby neglecting possible changes due to dilution of gel with semen and vaginal fluid. Because of these approximations, results here are best interpreted relative to each other and in terms of trends, rather than as absolute quantities.

In our model, we also assumed that HIV infection occurs via cell-free virus. However, cell-associated virus may play a role in HIV transmission [66, 87]. For example, infected immune cells such as lymphocytes or macrophages may introduce HIV to the female reproductive tract. Such cells are much larger than free virions – their diameters are of the order of 10-20 μm – whereas the diameter of a HIV virion is approximately 125 nm. Thus, we would expect cell transport via simple diffusion to be much slower than that for free HIV virions. However, unlike free virions, at least some of these cells are motile. The analog to diffusion coefficient for motile cells, the motility coefficient, is likely similar to or greater than the diffusion coefficient of free virus. For example, Saltzman et al. found motility coefficients of monocytes in synthetic polymer gels mixed with mucus to be approximately 10^{-9} - 10^{-10} cm^2s^{-1} [93]. While further studies will continue to elucidate the roles of cell-associated and cell-free virus, our approach here considering cell-free transmission is consistent with animal models used currently to evaluate microbicide products and conduct HIV/AIDS research [87, 88].

Our model also assumed that HIV transport is the result of simple diffusion and did not consider the possible role of convective transport. Convection in the female reproductive tract likely arises from the clearance of fluids from the vagina. It is unclear how these convective processes would affect transport of HIV at mucosal surfaces. Clearance of vaginal fluids could reduce the number of virions reaching tissue surfaces. Indeed, clearance of significant portions of intravaginally-applied viral inocula has been observed in macaques [39]. Since this convective clearance would likely reduce the

number of virions in the vagina, we believe that our model provides an estimate of the upper bound of the number of virions that could reach tissue surfaces.

We also assumed that topical gels and semen could be modeled as discrete layers. In the body, it is possible that semen or vaginal fluids dilute topical gels, making them indistinct. Also, it may be possible for mixing of these materials to occur due to changes in posture or other activities. Mixing could reduce the effective thickness of gel layers, reducing the calculated time to threshold.

Finally, this study did not account for HIV neutralization by pharmaceutical agents. We made this choice because there are currently over 10 microbicides in clinical trials and several agents in the pipeline [261], with several different mechanisms of action and dosage forms. This study focused on exploring how gel deployment and transport properties could affect the barrier functions of a microbicide gel. A logical follow up to the modeling here will be to incorporate the simultaneous transport of specific anti-HIV pharmaceutical agents for a specific microbicide product.

Future work can incorporate additional microbicide product characteristics and knowledge of HIV transmission and infection processes, as they become available. For example, future work will address simultaneous HIV transport and neutralization by microbicide active pharmaceutical agents. Also, additional experimental data is needed to validate model assumptions and link results to relevant clinical outcomes like infection. Ultimately, an approach combining deterministic and stochastic elements may be appropriate, where a deterministic model is used to describe efficacy of the

microbicide in reducing the number of infectious virions transferred to the non-infected partner, and the probability of infection is determined stochastically.

In summary, a number of transport processes interact in the functioning of vaginal microbicide gels, including movement of active ingredients and virions. Understanding these processes will contribute to fundamental understanding of the functioning of microbicide gels, and to the design of gels with improved performance. Mathematical models for topical microbicides could serve as valuable tools in understanding of mucosal HIV transmission, development of new prevention technologies, and design of clinical trials.

5.5 Conclusions

This study suggests that gel distribution in layers of thickness $> 100 \mu\text{m}$ and fractional area coated > 0.8 is critical in determining the ability of a gel to serve as a physical barrier to HIV diffusion. With comprehensive coating of sufficient thickness, viral restriction contributes to increasing the time required for virions to reach tissue surfaces. The model developed here can serve as a tool for microbicide formulators who are seeking to evaluate the interactions of multiple parameters of microbicide functioning.

6. Conclusions

6.1 Summary

We explored strategies for hindering HIV-virion transport and evaluated the potential of these strategies in HIV prevention. Hindering transport of HIV to mucosal surfaces could serve as an important component of microbicide and vaccine functioning by improving the opportunity for active pharmaceutical agents or host defenses to neutralize virions before they reach vulnerable cells. Two strategies for decreasing virion diffusion coefficients were studied here: (1) use of antibodies to increase the effective radius of virions; and (2) introduction of a viscous, semi-solid gel through which virions must diffuse. We developed mathematical and experimental methods to evaluate these strategies in the context of HIV prevention.

First, we quantified the effects of antibodies on diffusion coefficients using postphotoactivation scanning and a model system of liposomes with 2F5 epitope peptides and 2F5 antibodies of isotypes IgG, IgA, and IgM. We hypothesized that polyvalent antibodies would aggregate liposomes, increasing their effective radii and decreasing their diffusion coefficients. In preliminary experiments, we did not observe the expected reductions in diffusion coefficients. To better understand the kinetics of aggregation and the resulting distribution of aggregated species, we developed a mathematical model. Using model results and simulations of postphotoactivation scanning, we determined that is theoretically possible to experimentally detect changes in diffusion coefficients caused by aggregation using postphotoactivation scanning. Taken together, these results suggest that the aggregation effects in our experiments were small and/or that experimental noise

confounded accurate measurements of the diffusion coefficients. As reagents become available, future studies could use polymeric antibodies that are shown to be better aggregators of HIV than the 2F5 antibodies tested here.

Second, we explored the potential for semi-solid gels to hinder diffusion of HIV and therefore increase transport times. We hypothesized that diffusion coefficients of HIV virions in semi-solid gels would be lower than those in water. We tested two gels that were used as placebos in microbicide clinical trials, HEC and MC. These gels were composed of generally recognized as safe (GRAS) polymers typically used in vaginal formulations. To measure diffusion coefficients, we used particle tracking of fluorescently-labeled HIV virions. We found that these two gels did indeed reduce the diffusion coefficient of HIV virions: The diffusion coefficients of HIV virions in gels were almost 10,000 times lower than those in water.

Since we did not observe reductions in diffusion coefficients in experiments with antibodies, we proceeded to evaluate the potential for semi-solid gels to prevent HIV transmission at mucosal surfaces. From previous experiments in our lab that characterized the topical deployment of vaginal gels *in vivo*, we know that vaginal gels form an uneven coating on the epithelium with gel layer thicknesses of hundreds of microns [184, 185, 199]. Thus, we sought to determine whether semi-solid gels could function as physical barriers to HIV when deployed as thin, incomplete layers on the epithelium.

We created an experimental system to test the physical barrier functioning of thin gel layers. We used Transwell plates that contain upper and lower chambers separated by

a porous membrane. A thin layer (100-300 μm) of HEC or MC gel was applied to the membrane of each Transwell and HIV was added to the top compartment. After incubation for 0, 4, 8, or 12 hours, samples of the medium in the bottom compartment was assayed for infectious HIV using the TZM-bl assay. A reduction in the number of infectious virions in the bottom compartment of the Transwell was taken as an indicator of efficacy in HIV prevention. We found that thin gel layers indeed reduced levels of HIV in the bottom compartment of the Transwell system compared to controls where no gel had been applied: There was a log reduction in levels of HIV where gel layers of approximately 150 μm had been applied to the Transwell membrane after 0-, 4-, and 8-hour incubation. Thus, it is possible for gel layers of thicknesses found *in vivo* to function as physical barriers to HIV over biologically-relevant time scales.

We also created a mathematical model to explore the effect of nonuniform deployment on the ability of a topical gel to function as a physical barrier to HIV. We used mass transport theory develop a deterministic model of HIV diffusing from semen, through gel layers where present, to tissue. We examined scenarios with different fractional area coated, layer thickness, and viral restriction by gel. We used the time required for a threshold number of virions as a metric for comparing different scenarios. Our findings suggest that comprehensive coating of over 80% tissue surface area coated and gel layer thicknesses over 100 μm is crucial to the barrier functioning of topical gels. Under these conditions, the level of viral restriction makes a significant contribution to increasing the threshold time.

Overall, our work here shows how transport theory can be applied to understand phenomena during HIV transmission and prevention. We used fundamental transport theory to design two strategies for reducing HIV transport and developed experimental and mathematical tools for evaluating these strategies within the context of HIV prevention.

6.2 Context

6.2.1 Significance of hindering HIV transport at mucosal surfaces

Several researchers have pointed to the importance of intervening at early events in mucosal HIV transmission to prevent infection [14, 39, 64]. In this regard, the biological significance of hindering virion transport at mucosal surfaces is poorly understood. There are several mechanisms by which hindering virion transport could contribute to HIV prevention.

Clinical studies have shown that likelihood of infection in male-to-female sexual HIV transmission is related to blood viral load [96, 262, 263], which is likely also related to the viral inoculum in semen [78]. Hindering virion transport at mucosal surfaces could reduce the effective viral inoculum that reaches target cells by trapping virions. Trapped virions could then be cleared from the lower reproductive tract with other vaginal fluids. Hindering virion transport could also allow microbicide active agents or innate defense factors a greater opportunity to neutralize virus. Furthermore, because HIV has a finite lifetime, delaying viral contact may reduce the number of infectious virions that reach target cells. On the other hand, it is possible that gels that trap virions might enhance infection by allowing viable virions prolonged access to vulnerable tissues. Further

studies are needed to elucidate the time- and space-dependent viability of HIV within the lower female reproductive tract and the time required for HIV to traverse mucosal barriers to reach targets for infection.

The strategies for hindering HIV transport presented in this dissertation are unlikely to be effective for HIV prevention when used alone. For example, we tested the barrier functioning of gels used as placebos in clinical trials to provide proof of principle that gels could hinder HIV diffusion. Those gels, comprised of polymers typically used in vaginal formulations, have been shown to be less efficacious than other microbicide candidates *in vitro* and in animal models [166]. However, strategies of hindering virion transport may be used in combination with other strategies for HIV prevention. For example, a combination microbicide could be designed to act as a physical barrier to HIV and while delivering small-molecule HIV-neutralizing agents. Indeed, a previous study in our lab constructed a mathematical model that demonstrates how a formulation that restricts virion diffusion can contribute to the efficacy of the microbicide candidate Cyanovirin-N [232]. Hindrance of virion diffusion by gels can also be used in combination with active pharmaceutical agents that act in tissues, allowing for delivery of agents to tissue prior to the arrival of virions. Combinations of strategies are likely to be more effective than a single strategy, particularly against the range of HIV variants encountered [9].

6.2.2 Trends in microbicides development

The microbicides field has changed rapidly over the past decade [8]. First-generation microbicide candidates acted through non-specific mechanisms of action and

targeted virions within luminal fluids. These included surfactants, acidifying agents, and anionic polymer entry inhibitors. In recent years, the microbicides field has shifted to focus on HIV-specific agents, including CCR5 entry inhibitors, fusion inhibitors, and reverse transcriptase inhibitors (RTIs) that act in the lumen and in the epithelium. In particular, RTIs are currently being tested in phase I and II clinical trials [261].

RTIs block viral replication by inhibiting the reverse transcription of DNA from viral RNA. These inhibitors have been used in combination therapy for HIV/AIDS and to prevent mother-to-child transmission. RTIs currently being evaluated in microbicides clinical trials include Tenofovir, UC781, and TMC120 (Dapivirine) [8, 9, 261]. Those agents are being formulated for topical application in gels and in intravaginal rings. It remains unknown whether a microbicide that reduces HIV reproductive rate will be sufficient to prevent productive infection or whether it is necessary for a microbicide to completely block all viral entry. Furthermore, use of RTIs prophylactically might lead to selection of drug-resistant strains of HIV.

For RTIs, the possible benefits of simultaneously hindering HIV-virion transport are unclear. A study by Di Fabio et al. of TMC120 in a cell-associated HIV mouse model suggests that gel deployment affects efficacy [264]. TMC120 was tested in two gel formulations, one more viscous than the other. According to qualitative observations, the more viscous gel did not spread to coat the vaginal epithelium whereas the less viscous gel did. Results showed that the more viscous formulation protected 70-80% of mice whereas the less viscous formulation protected 100% of mice. Both formulations were compared to placebo gels that did not contain TMC120. All of the mice were

infected in these control experiments, so the barrier effect of these gels was not efficacious for HIV prevention alone.

Overall, these results suggest that deployment of the TMC120 gel was an important factor in efficacy. From our mathematical model, we know that comprehensive coating is crucial to the ability of a gel to function as a barrier to HIV (Chapter 5). Furthermore, comprehensive coating allows for drug delivery over a greater surface area. The less viscous gel may have had improved efficacy because it (1) more effectively delivered the TMC120 to target sites and/or (2) delayed the kinetics of HIV transport to tissues to allow for distribution and accumulation of adequate concentrations of drugs in target cells prior to the arrival of virus.

Another emerging trend in microbicide development is the use of alternative drug delivery vehicles. First-generation microbicide candidates were formulated as gels. Intravaginal rings are now also being tested clinically for microbicide delivery [261, 265]. Other delivery forms such as tablets and films are in preclinical development [12]. Thus far, gels have been used to formulate active pharmaceutical agents (APIs) that act in either the lumen or the tissue, whereas intravaginal rings have been used to formulate APIs that act in the tissue.

These next-generation delivery systems might not provide the physical barrier functioning provided by semi-solid gels. The barrier functioning of gels depends on the physical structure of the entangled polymers and comprehensive deployment over the epithelium. These will likely be absent in alternative delivery vehicles. However, one of the advantages of intravaginal rings is the continuous, controlled release of microbicide

drugs locally. Thus, adequate concentrations of the drug will be present in tissues prior to challenge by HIV. This may provide some advantage over coitally-dependent gels, for which the barrier functioning may be more important to allow for drug delivery prior to contact with virus.

6.2.3 Efficacy of placebo gels in microbicides clinical trials

One of the unexpected findings of this research was the extent to which placebo gels used in microbicides clinical trials can hinder the diffusive transport of HIV virions. For example, the universal placebo gel, HEC, was previously presumed to have no physical barrier properties [166]. Thus we expected that the placebo gels that we tested would lead to modest reductions in the diffusion coefficients of virions. Surprisingly, the diffusion coefficients of virions in HEC and MC were almost 4 orders of magnitude lower than those of virions in water. These values of diffusion coefficient were similar to those previously observed for virions in cervical mucus [36] and in a hydrogel engineered to reduce HIV transport [182]. We also found that thin layers of these gels could reduce levels of HIV found in the bottom compartment of a Transwell system. Thus, it may be possible for placebo gels used in clinical trials to function in HIV prevention by acting as physical barriers to virus. The barrier functioning of topically-applied gels is also determined by *in vivo* deployment. The *in vivo* distributions of HEC and MC have not yet been studied.

The actual efficacy of placebo gels used in microbicide clinical trials is unknown, but is likely low. A recent clinical trial, HPTN 035, included a “no gel” arm in which condom use was promoted but no gel was used [95, 161]. This “no gel” arm was

compared to arms with condoms plus placebo gel and condoms plus microbicide candidate gel. The placebo gel used was a hydroxyethyl cellulose-based gel. Similar numbers of HIV infections were observed in the placebo and no gel arms: 51/771 and 53/772, respectively. However, although condom use was promoted in all arms of the trial, condom use was significantly higher in the no gel arm compared to the placebo gel arm. Thus, it is difficult to accurately quantify the efficacy of the HEC placebo, but it is likely to be less than 10% [162]. Taking the findings of this dissertation into account, the low efficacy of placebo gels in clinical trials may be partially explained by incomplete deployment of the gel *in vivo*.

The possible efficacy of placebo gels in clinical trials is recognized as a deficiency of blinded, placebo-controlled clinical trial design for microbicides [17, 198]. A recent study characterized the effect of placebo efficacy on the observed effectiveness in clinical trials [162]. The expected effectiveness (E_b), or expected value of the observed effectiveness, is related to the true efficacy (E_T) of the microbicide product and the efficacy of the placebo gel (E_p) as follows [162]:

$$E_b = 1 - \frac{1 - E_T}{1 - E_p} .$$

Equation 73

Figure 80 shows the expected effectiveness for ranges of microbicide product efficacy and placebo gel efficacy. Placebo gel efficacy can reduce the effectiveness observed in microbicide clinical trials. Other factors that may reduce observed effectiveness in microbicides clinical trials include poor adherence, time off-product due

to pregnancy or adverse reactions, and anal intercourse contributing to HIV infections [162].

Thus far, none of the microbicides clinical trials have demonstrated product effectiveness. This could be explained by poor product efficacy and/or poor ability to detect effectiveness in clinical trials. HIV prevention trials require large numbers of participants because the rate of HIV seroconversion tends to be low, approximately 5-10%. Sample sizes from previous clinical studies have ranged from approximately 1000-10,000 women [162]. The number of HIV infections observed in each arm of the clinical trial has varied from approximately 10-150 [162]. If factors like placebo efficacy reduce the observed effectiveness in a clinical trial, it may become impossible to detect moderate product efficacy.

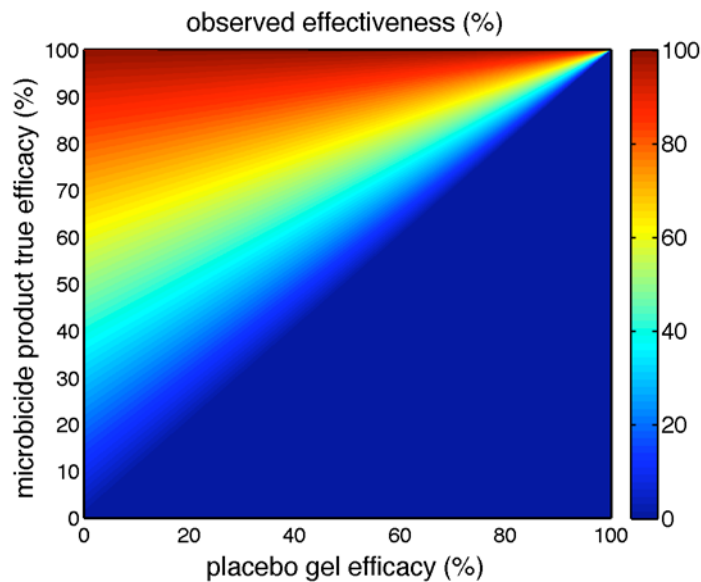


Figure 80. Observed effectiveness for different values of microbicide and placebo efficacies calculated using Equation 73 [162].

For example, the Carraguard clinical trial was designed to detect 33% reduction in HIV risk with 93% power [159]. However, poor adherence may have compromised trial results: With the rates of adherence observed, the trial was actually underpowered to detect efficacy of less than 70% [159]. Thus, it is possible for factors that reduce observed effectiveness to confound the design and interpretation of clinical trials. It is important to understand how factors such as placebo efficacy affect the power of clinical trials, so that future studies may be improved.

6.3 Future directions

6.3.1 Recommendations for preclinical testing of microbicide gels

The methods presented in this dissertation for quantifying transport in semi-solid gels may be useful tools for optimizing future formulations of microbicide gels. Ideally, microbicide formulation development should be an iterative process. Microbicide developers may vary several parameters: gelling agent; molecular weight; concentration; level of cross-linking; and other excipients. These parameters determine the physical properties of the gel, which determine product behavior during use. Several variations of gels may be created and evaluated preclinically to select the optimal formulation. Formulations may be evaluated with respect to several performance attributes, including drug release, shelf life, and acceptability. We suggest that microbicide gel formulations should also be evaluated for functioning as physical barriers to HIV.

Methods used in this dissertation to measure diffusion coefficients of HIV in placebo gels could easily be applied to evaluate other gels. Particle tracking of fluorescently-labeled HIV virions in various formulations can be used to rank order

barrier function, allowing for selection of formulations with the lowest diffusion coefficient of virions. We found that the lower limit detection, $1.9 \pm 0.4 \times 10^{-12} \text{ cm}^2/\text{s}$, was limited by the level of noise due to motion in our system. Improvements in particle tracking methods could conceivably decrease the limit of detection, allowing for comparison of materials with lower virion diffusion coefficients [266-268].

The Transwell system may also be used to preclinically evaluate the barrier functioning of gels, but it will likely be more difficult to make comparisons due to variations in the gel layers applied and the small differences in levels of HIV in the bottom compartment between different materials. Our lab has also considered improving the Transwell assay by incorporating more realistic substrates, such as epithelial cells or tissue. These biological substrates could help account for transport rates in mucosal tissues.

The barrier functioning of semi-solid gels appears to be highly dependent on comprehensive gel deployment over the epithelium. Thus, it is important to consider the trade-offs between gel properties that hinder virion diffusion and properties that are conducive to comprehensive deployment. The mathematical model presented in Chapter 5 for HIV transport in the presence of a nonuniform gel layer may be combined with deployment data from *in vivo* imaging or deployment predictions from other mathematical models developed by our lab. Ongoing research in our lab inputs rheological measurements of gels to mathematical models of fluid flow to predict area coated [248-250, 254, 255, 257]. For future formulation development, the transport

model may be combined with fluid flow models to output a measure of efficacy, such as the predicted number of virions to reach the tissue compartment after a given time.

6.3.2 Pharmacokinetic and pharmacodynamic models for microbicide functioning

Future applications of the mathematical model presented in Chapter 5 could also further develop the pharmacokinetic and pharmacodynamic analyses to incorporate the delivery of anti-HIV active pharmaceutical agents (APIs). A mathematical model of the simultaneous diffusion of HIV virions and APIs could be used to estimate the numbers of infectious vs. neutralized virions that reach tissue. The model could also be used to explore how gel deployment affects drug delivery and the kinetics of HIV transport and neutralization.

Mathematical models have been useful tools in developing HIV/AIDS therapeutics and in understanding disease processes and the immune system. Mathematical models that account for parameters relevant to development of prevention technologies could aid in design and evaluation of these technologies. Distinct mathematical models will be required for different delivery vehicles and agents with different mechanisms of action. Our group has previously developed a pharmacokinetic model of drug delivery by an intravaginal ring [234]. Experimental data will be required as inputs to the model and also to validate the accuracy of model predictions.

6.3.3 Design of advanced materials that act as topical barriers to HIV

The work in this dissertation contributes to quantitative understanding of the potential for antibodies and semi-solid gels to hinder HIV transport. Follow-up work

could further explore these strategies. For example, it would be interesting to evaluate combinations of the two strategies, perhaps designing a microbicide with freely-diffusing active agents that bind and crosslink virions within a semi-solid gel. If these active agents bound to both virions and the gel network, then they could act synergistically within the environment of the topical gel. The binding of active agents to HIV virions would increase the valency of these aggregate particles in binding to the semi-solid gel. This phenomenon of multi-valent binding is observed in mucus at epithelial surfaces [100].

6.3.4 Design of a true placebo for microbicides clinical studies

There is a need for a true placebo for microbicides clinical trials [198]. Five different placebo gels have been used in microbicides clinical trials thus far [162]. Placebo gels may unintentionally function in HIV prevention by acting as physical barriers, providing lubrication, and affecting vaginal pH. In a blinded study, a placebo should have no efficacy and be identical to the microbicide product in appearance, consistency, and odor.

The methods used in this dissertation could be used to select gels that minimally function as physical barriers to HIV. For example, methods used to quantify the diffusion coefficients of HIV virions in gels could be used to identify materials that do not hinder viral diffusion. These materials might have larger polymer mesh sizes that allow for greater mobility of virus while still appearing similar to other semi-solid gels. Furthermore, gels must comprehensively coat the epithelial tissue to function as effective

topical barriers. Thus, a gel that does not provide comprehensive coverage could also be used as a placebo.

6.3.5 Furthering understanding of mechanisms of transport and relationship between viral inoculum and infection

Ultimately, our work here is limited by an incomplete understanding of the sexual transmission of HIV. Further research is needed to clarify the modes of transport relevant to HIV transmission and infection.

For example, researchers have used microscopy to examine events in mucosal HIV infection using explant models [38] and rhesus macaque models [18, 31]. Qualitative observations have suggested that HIV virions diffuse through gaps between cells to penetrate epithelial tissue [31]. Image analysis could be used to quantitatively determine the number of virions that penetrate tissue and their penetration distances. These data could then be compared to predictions from various theoretical models of particle transport to help elucidate which modes of transport play a role in HIV transmission, and to generate empirical models of HIV transport.

The relationship between the viral inoculum and successful HIV infection is also unclear. Experimental data are needed to clarify the relationship between viral load in semen and likelihood of HIV transmission. These data could help link mathematical model predictions to the clinical outcome of HIV infection.

6.4 Theoretical and experimental methods for HIV/AIDS research

Overall, the work in this dissertation contributes to an understanding of how principles from transport theory and tools from drug delivery research can be used to

inform our thinking about HIV transmission. HIV infection occurs over time and space and is affected by physical phenomena. The development of theoretical and experimental frameworks for understanding these phenomena can ultimately contribute to the design of more effective strategies for HIV prevention.

Appendix. Postphotoactivation scanning with multiple diffusing species

A.1 Example of analysis assuming multiple diffusing species

We developed a method of analysis for postphotoactivation scanning profiles that accounts for multiple diffusing species. Our analysis follows one developed by Periasamy et al. [145] for analysis of Fluorescence Recovery After Photobleaching (FRAP) diffusion profiles. We assumed that diffusion profiles could be described by a distribution of diffusion coefficients, $\alpha(D)$. The observed intensity profile ($I_{observed}$) at any given time is the sum of intensity profiles (I_i) for the multiple diffusing species:

$$I_{observed}(x,t) = \sum_i \alpha_i I_i(D_i, x, t)$$

Equation 74

Here, the index, i , refers to each species, for which α_i is the relative amplitude of the diffusing species with diffusion coefficient D_i .

To provide an example, we generated a set of simulated diffusion profiles for two diffusing species with diffusion coefficients of 3×10^{-9} cm²/s and 3×10^{-7} cm²/s present in equal amounts ($\alpha = 0.5$). We began with a Gaussian curve to describe the initial condition:

$$I_0(x) = e^{-\left(\frac{x}{w}\right)^2}$$

Equation 75

Here, we chose $w = 200$ so that the width of the resulting curve resembles the initial images that we observe in postphotoactivation scanning experiments. Intensity values

were normalized to the maximum intensity, as for experimental images. This curve is plotted in Figure 81.

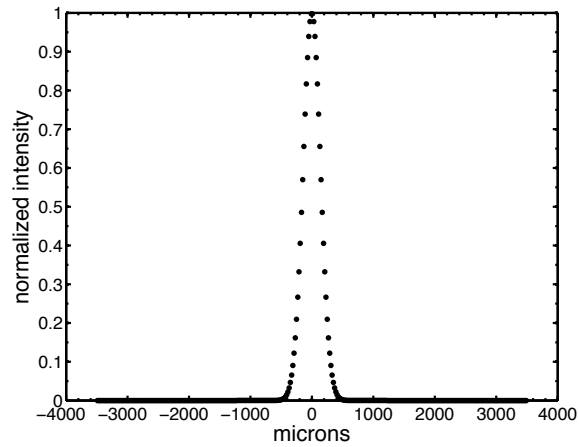


Figure 81. Simulated initial condition using Gaussian curve described by Equation 75.

We then proceeded to create simulated diffusion profiles. For each of the diffusing species, we simulated diffusion for 9 time points equally spaced over 3.5 hours using the solution of the diffusion equation for all D_i assuming that the intensity at the boundaries was zero and using the experimental initial condition (I_0):

$$\frac{\partial I_i}{\partial t} = D \frac{\partial^2 I_i}{\partial x^2}, \quad I_i(\pm\infty, t) = 0, \quad I_i(x, 0) = I_0(x) .$$

Equation 76

Figure 82 shows the resulting intensity profiles for each diffusing species.

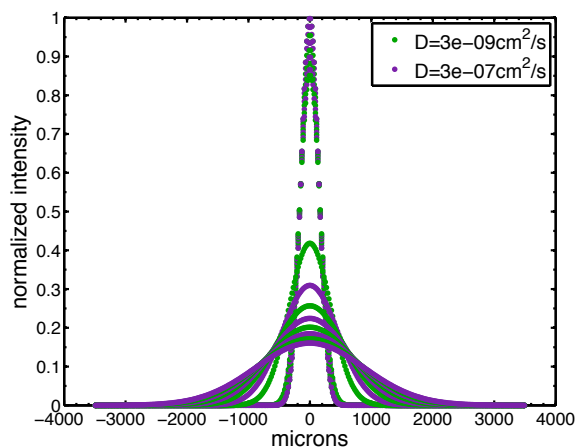


Figure 82. Simulated intensity profiles for 2 diffusing species.

We then summed the diffusion profiles as described in Equation 74 to generate our set of simulated postphotoactivation scanning data (Figure 83).

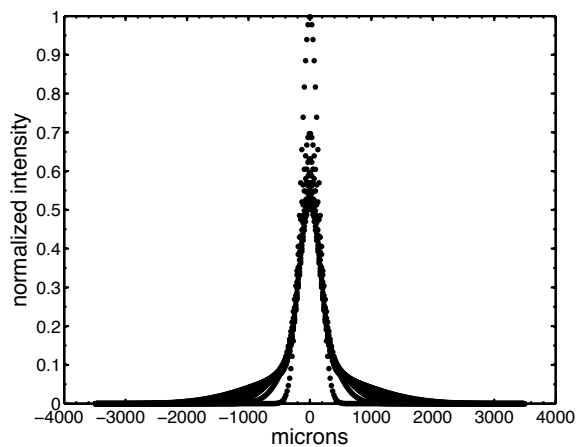


Figure 83. Simulated postphotoactivation scanning data.

To analyze postphotoactivation scanning data, we began by selecting a range of diffusion coefficients. The range encompassed the expected values of the diffusion coefficients for the diffusing species. We then discretized D at equal intervals in log space between D_{min} and D_{max} .

To examine the data from our simulated example, we selected $D_{min} = 10^{-12} \text{ cm}^2/\text{s}$, $D_{max} = 10^{-6} \text{ cm}^2/\text{s}$, and performed analyses using 100 points. We numerically solved the diffusion equation for all D_i assuming that the intensity at the boundaries was zero and using the experimental initial condition (I_0):

$$\frac{\partial I_i}{\partial t} = D \frac{\partial^2 I_i}{\partial x^2}, I_i(\pm\infty, t) = 0, I_i(x, 0) = I_0(x) .$$

Equation 77

This results in sets of intensity profiles for each D_i . Figure 84 shows examples of diffusion profiles generated for D_{min} and D_{max} . One set of intensity profiles is generated for each D_i .

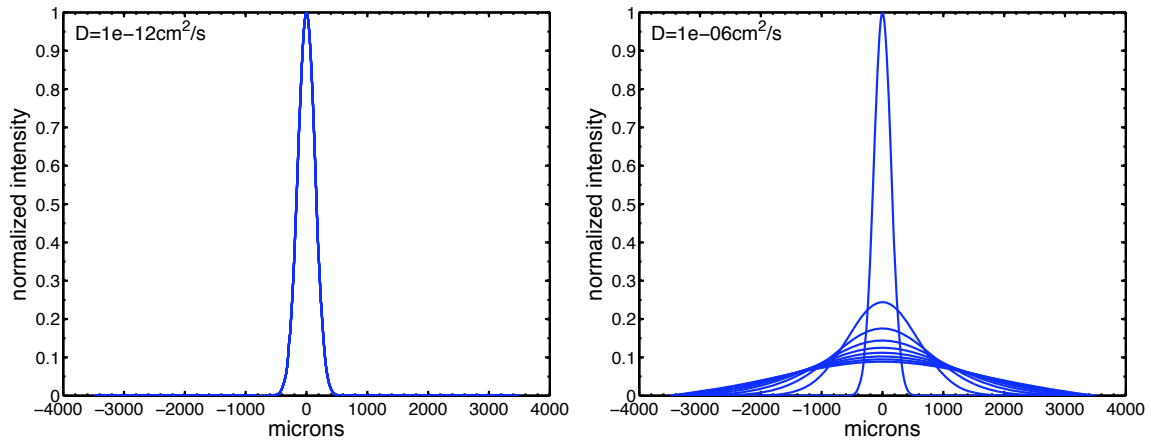


Figure 84. Examples of sets of diffusion profiles used in analysis. Left: Set of diffusion profiles generated for D_{min} . Right: Set of diffusion profiles generated for D_{max} .

We use the MATLAB optimization function “lsqnonlin” to find the distribution $\alpha(D)$ that minimizes the square of the difference between the observed and computed intensity profiles:

$$\sum_i (I_{observed} - I_{computed})^2$$

Equation 78

Here $I_{computed}$ is the sum of intensity profiles I_i with distribution α .

Figure 85 shows results from the analysis of data from our simulated example. There were 2 peaks in α , representing the 2 diffusing species. We were able to accurately identify the diffusion coefficients of the 2 diffusing species: The distribution of α shows that the diffusion coefficient of one species is between $2.8-3.2 \times 10^{-9}$ and the diffusion coefficient of the other is between $2.8-3.2 \times 10^{-7}$. The amplitudes of the two peaks were similar. Predictions for the amplitudes of peaks in α were not strictly accurate because the distribution of diffusion coefficients was discretized, so the output diffusion coefficients were approximated by the sum of curves with diffusion coefficients within the discretized distribution closest to the input values. Thus, the input α values of 0.5 can be obtained by summing the α values of the components, i.e., $0.33+0.17$ and $0.32+0.18$ in this example.

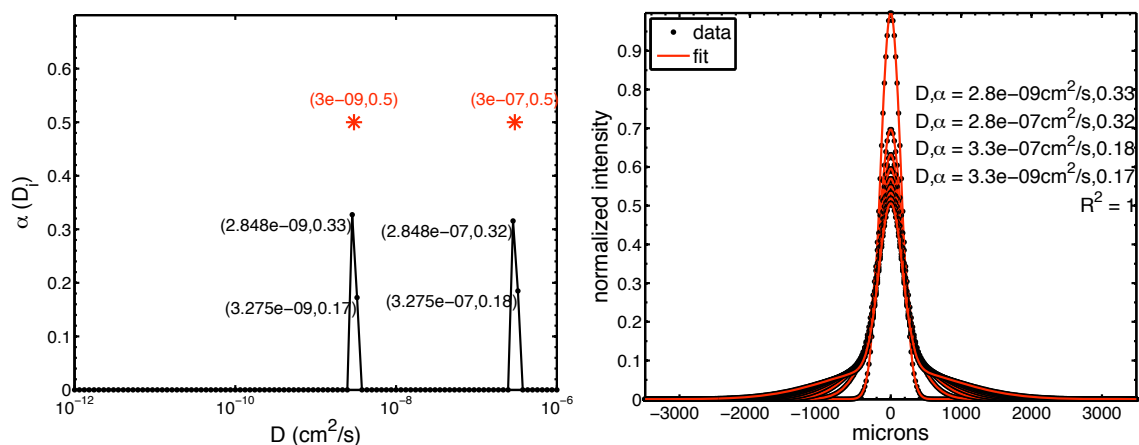


Figure 85. Results from analysis of simulated postphotoactivation scanning data. Left: $\alpha(D)$. Red asterisks indicate diffusion coefficients used to generate simulated data. Right: intensity profiles fit to diffusion model.

A.2 Experimental validation using a solution with multiple diffusing species

We used postphotoactivation scanning to measure the diffusion coefficients of molecules of a variety of sizes. Results are summarized in Table 22. Our goal was to validate the accuracy of the determinations of diffusion coefficients using our new methods for analyzing postphotoactivation scanning data assuming multiple diffusing species. We were also interested in determining how many diffusing species we could reliably detect in experiments.

Table 22. Comparison of diffusion coefficients measured here to values published in the literature. Diffusion coefficients ($D_{\text{experiment}}$) of fluorescein and dextrans in PBS were measured by postphotoactivation scanning. All experiments were performed at room temperature, approximately 24-25° C. Literature values for the diffusion coefficient were obtained using FRAP or *diffusion into slab.

| Particle | M_w (Da) | $D_{\text{experiment}}$ (cm^2/s) | $D_{\text{literature}}$ (cm^2/s) |
|----------------|------------|--|--|
| Fluorescein | 332 | $4.2 \pm 0.1 \times 10^{-6}$ (n = 3) | $2.6\text{-}5.7^* \times 10^{-6}$ [145, 269] |
| 3-kD dextran | 3,000 | $3.0 \pm 0.2 \times 10^{-6}$ (n = 3) | $9.8 \pm 0.6 \times 10^{-7}$ [270] |
| 10-kD dextran | 10,000 | $4 \pm 1 \times 10^{-7}$ (n = 3) | $7.6 \pm 0.3 \times 10^{-7}$ [270] |
| 70-kD dextran | 70,000 | $2.1 \pm 0.2 \times 10^{-7}$ (n = 5) | $4.4 \pm 0.2 \times 10^{-7}$ [271] |
| 500-kD dextran | 500,000 | $2.0 \pm 0.3 \times 10^{-7}$ (n = 3) | $2.3 \pm 0.1 \times 10^{-7}$ [272] |

A.2.1 Fluorescein

Literature values for the diffusion coefficient of fluorescein range from $2.6\text{-}5.7 \times 10^{-6} \text{ cm}^2/\text{s}$ [145, 269]. Here, we analyzed data obtained previously in our lab [139] for $2.5\text{-}10 \text{ }\mu\text{g/ml}$ fluorescein in DI water or PBS. Figure 86 shows an example of results from one postphotoactivation scanning experiment. The value that we measured for the diffusion coefficient of fluorescein, $4.2 \pm 0.1 \times 10^{-6} \text{ cm}^2/\text{s}$ ($n = 3$), fell within the range of previously reported values. The value was also similar to that obtained previously using the original method of analysis assuming one diffusing species, $4.86 \pm 0.03 \times 10^{-6} \text{ cm}^2/\text{s}$ [139].

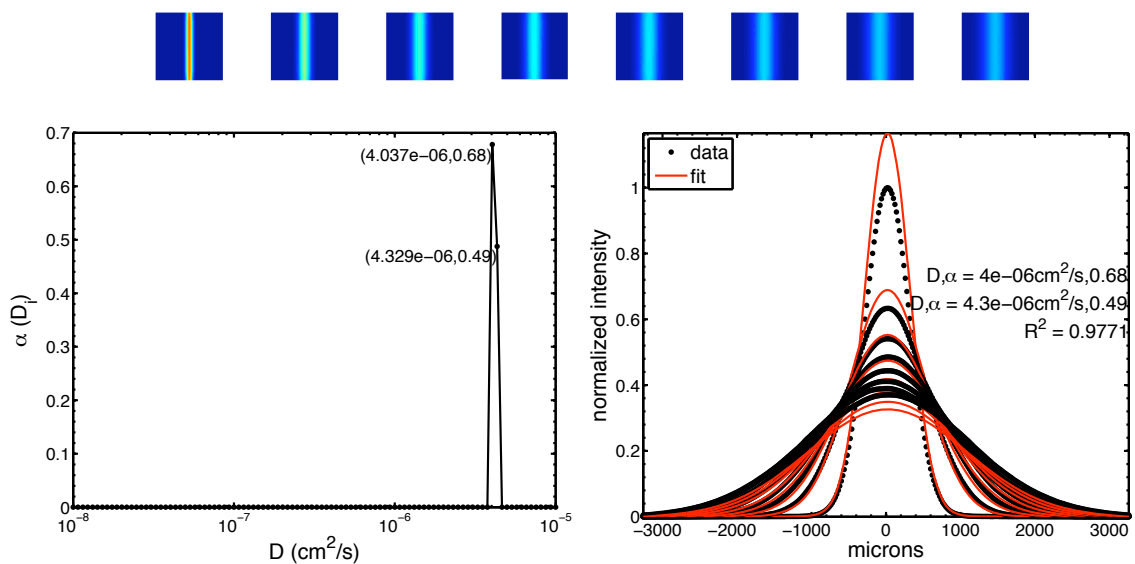


Figure 86. Example of postphotoactivation scanning results for fluorescein diffusing in PBS. Top: images over time (red = high intensity, blue = low intensity); Bottom left: $\alpha(D)$; and Bottom right: intensity profiles fit to diffusion model.

A.2.2 Dextrans

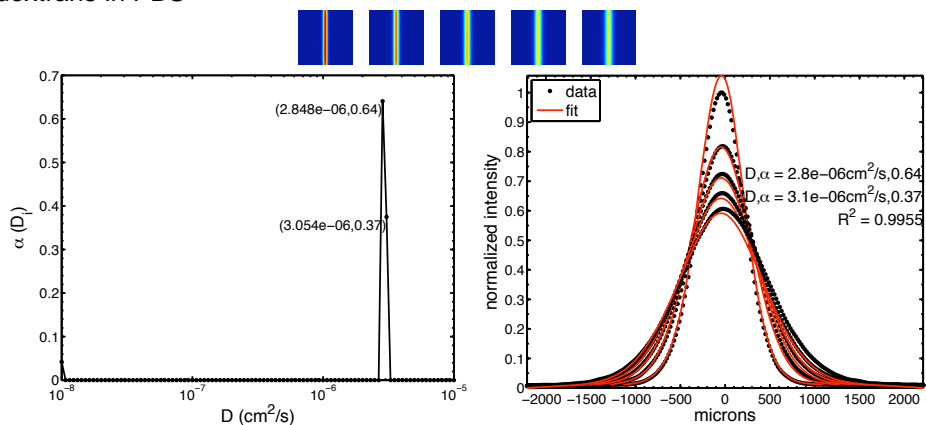
Dextrans are hydrophilic polysaccharides derived from bacteria. They are commonly used as model particles in transport experiments because they can be labeled with fluorescent probes and are commercially-available in a variety of molecular weights. For our experiments, we conjugated 10 mg/ml dextran amino (Invitrogen, Carlsbad, CA) to CMNB-caged fluorescein, succinimidyl ester (Cat. No. C-20050, Invitrogen, Carlsbad, CA) according to the manufacturer's instructions. We then diluted the dextrans 1:100 to a final concentration of approximately 0.1 mg/ml for postphotoactivation scanning experiments.

Examples of postphotoactivation scanning results for 3, 10, 70, and 500 kD dextrans are shown in Figure 87. For dextrans with molecular weights of 10, 70, and 500 kD, we were able to resolve two distinct peaks. The peak with the lower diffusion coefficient represents the labeled dextran. The peak with the higher diffusion coefficient represents free label. For the 3-kD dextrans, we were not able to distinguish dextrans and free label. This is likely due to the fact that the measured diffusion coefficients of the 3-kD dextrans and the unconjugated fluorescent label were similar, $3.0 \pm 0.2 \times 10^{-6}$ and $4.2 \pm 0.1 \times 10^{-6}$ cm²/s (n = 3), respectively. Dextrans are polydisperse, but we were not able to resolve a distribution of diffusion coefficients corresponding to different molecular weights.

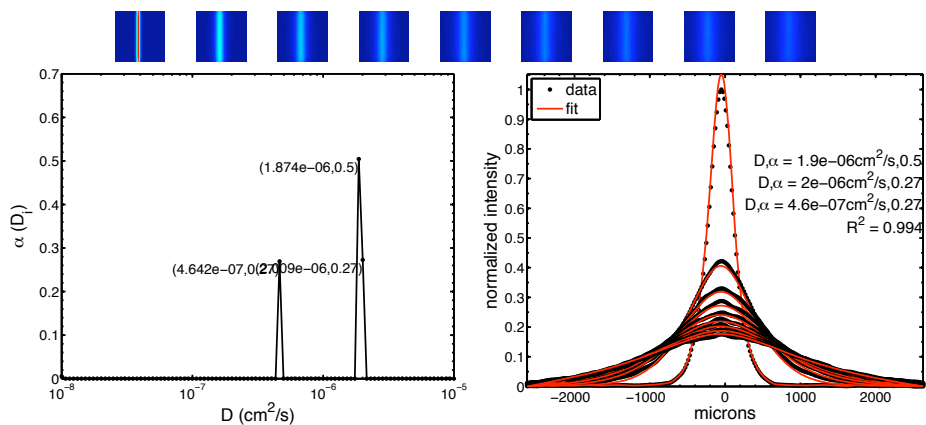
Overall, these results indicated that we could distinguish two diffusing species using the new method of analysis as long as the diffusion coefficients of the two species

were sufficiently distinct. The method of analysis is useful for distinguishing between diffusion coefficients of particles of interest and unconjugated label.

(A) 3 kD dextrans in PBS



(B) 10 kD dextrans in PBS



(C) 70 kD dextrans in PBS

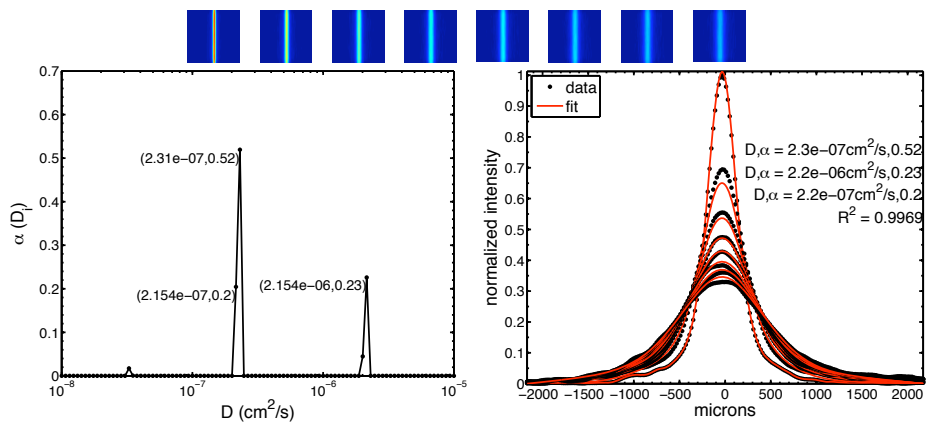


Figure 87. Examples of postphotoactivation scanning results for dextrans of various molecular weights in PBS.

(D) 500 kD dextrans in PBS

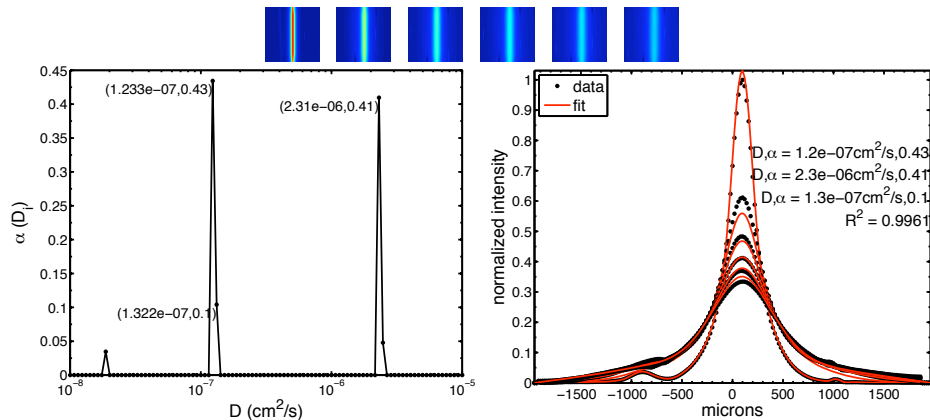


Figure 87. Examples of postphotoactivation scanning results for dextrans of various molecular weights in PBS. Top: images over time (red = high intensity, blue = low intensity); Bottom left: $\alpha(D)$; and Bottom right: intensity profiles fit to diffusion model.

To validate the accuracy of the diffusion coefficients obtained here, we sought to compare our results with previous measurements documented in the literature and theoretical predictions. Diffusion coefficients of dextrans obtained from other suppliers have been measured previously using other experimental methods (Table 22). We found that our measured diffusion coefficients tended to be lower than previous values. The discrepancies between our results and previous values might be explained by the different sources of the dextrans. The degree of branching and polydispersity of dextrans can vary depending on their preparation, and these differences may result in different diffusion coefficients.

Alternatively, the diffusion coefficient can be empirically related to molecular weight. Amu et al. found that the molecular weight (M_w) of dextrans and their diffusion coefficients (D) could be described by a power law expression as follows [273]:

$$D = \alpha M_w^\beta$$

Equation 79

Here, α and β are empirically derived. Amu et al. found $\alpha = 5.5 \times 10^{-5}$ and $\beta = -0.43$ for dextrans ranging from 12 kD to 130 kD [273]. More recently, Gribbon et al. found $\alpha = 2.71 \times 10^{-5}$ and $\beta = -0.37$ for dextrans ranging from 4 kD to 2000 kD using confocal Fluorescence Recovery After Photobleaching (FRAP) [274].

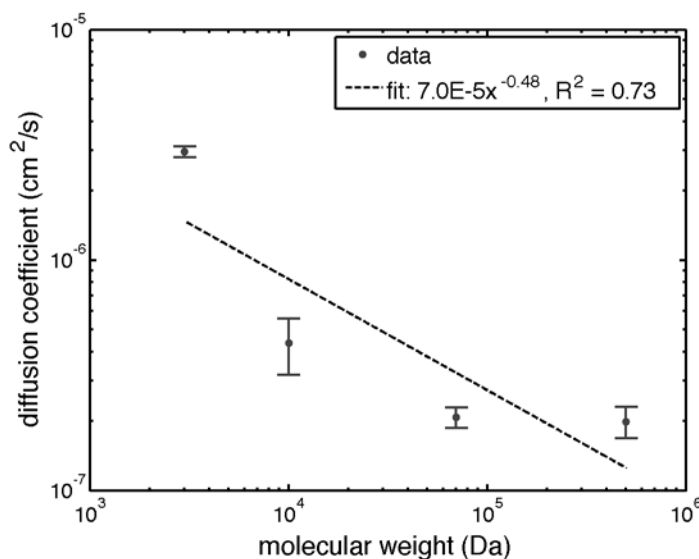


Figure 88. Diffusion coefficients for dextrans of various molecular weights with power law fit.

We fitted our data, for dextrans ranging from 3 kD to 500 kD, to the power law and found similar values of $\alpha = 7.0 \times 10^{-5}$ and $\beta = -0.48$ (Figure 88). However, the power law did not seem to describe the data well, as the R^2 value, 0.73, was low compared to the R^2 value of 0.996 previously obtained by Gribbon et al. Again, differences in the dextrans used may have led to observed differences in diffusion coefficients.

We were not able to make theoretical predictions for the diffusion coefficient based on size or molecular weight. The manufacturer could not provide size

measurements for the dextrans that we used in our experiments. The sizes given are nominal, as dextrans are polydisperse. Literature values of hydrodynamic radii are often calculated from measured diffusion coefficients, using the Stokes-Einstein relation. Thus, using the hydrodynamic radii from these studies would not provide an independent estimate of a theoretical diffusion coefficient.

A.2.3 Multiple diffusing species

To determine if we could resolve more than two diffusing species, we mixed solutions of multiple dextrans. First, we tried mixing dextrans of two different molecular weights. We expected to be able to resolve three peaks from these experiments, two representing the two species of dextrans and one representing free label. Figure 89 shows an example of results from experiments mixing 10- and 500-kD dextrans. As expected, we were able to resolve three distinct peaks representing the two species of dextrans and free label.

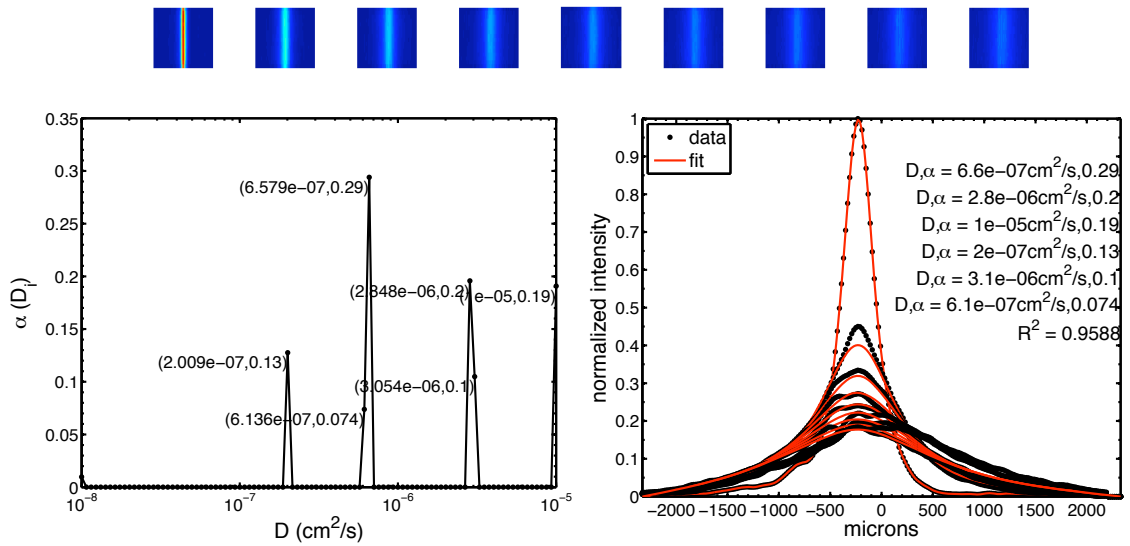


Figure 89. Example of postphotoactivation scanning results for mixture of 10- and 500-kD dextrans in PBS. Top: images over time (red = high intensity, blue = low intensity); Bottom left: $\alpha(D)$; and Bottom right: intensity profiles fit to diffusion model.

We also performed experiments mixing 70- and 500-kD dextrans (Figure 90). In these experiments, we were not able to resolve three distinct peaks. The diffusion coefficients of 70- and 500-kD dextrans are similar, $2.1 \pm 0.2 \times 10^{-7}$ (n = 5) and $2.0 \pm 0.3 \times 10^{-7}$ (n = 3) cm^2/s , respectively. Our methods were not able to distinctly resolve these similar diffusion coefficients.

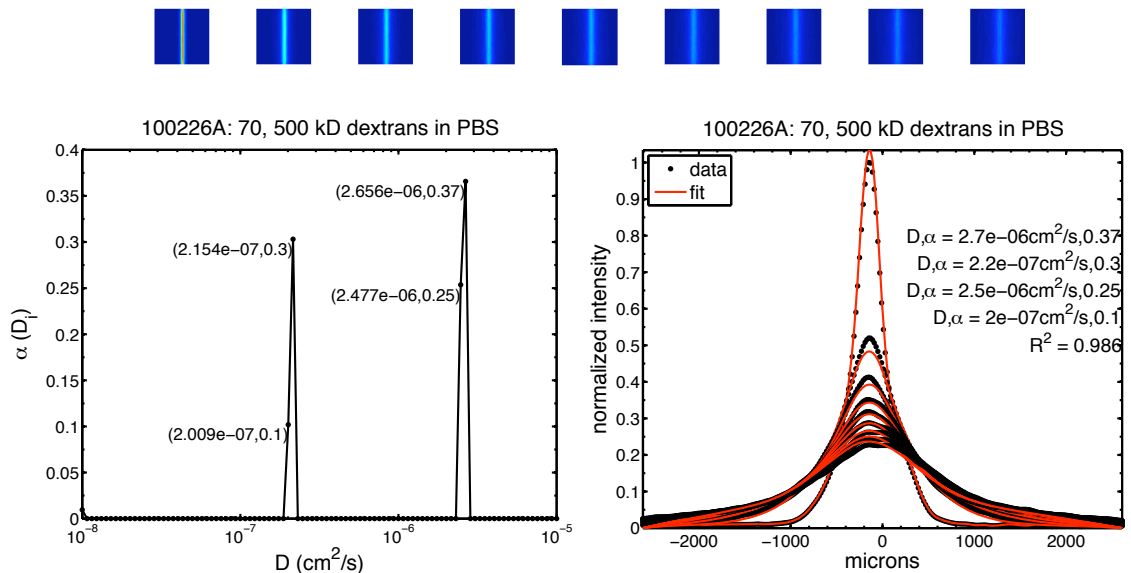


Figure 90. Example of postphotoactivation scanning results for mixture of 70- and 500-kD dextrans in PBS. Top: images over time (red = high intensity, blue = low intensity); Bottom left: $\alpha(D)$; and Bottom right: intensity profiles fit to diffusion model.

Finally, we mixed solutions combining 10-, 70-, and 500-kD dextrans. Based on our findings above, we expected results to yield three peaks: one representing both 70- and 500-kD dextrans; one representing 10-kD dextrans; and one representing free label. Figure 91 shows an example of results from these experiments. Indeed, we observed three peaks representing the four diffusing species. However, we found that these results were not very consistent. The results appeared to be sensitive to experimental noise, and in other replicates, we were only able to resolve two peaks. The following section, §B.3, describes experiments and simulations characterizing noise and its effect on measured diffusion coefficients.

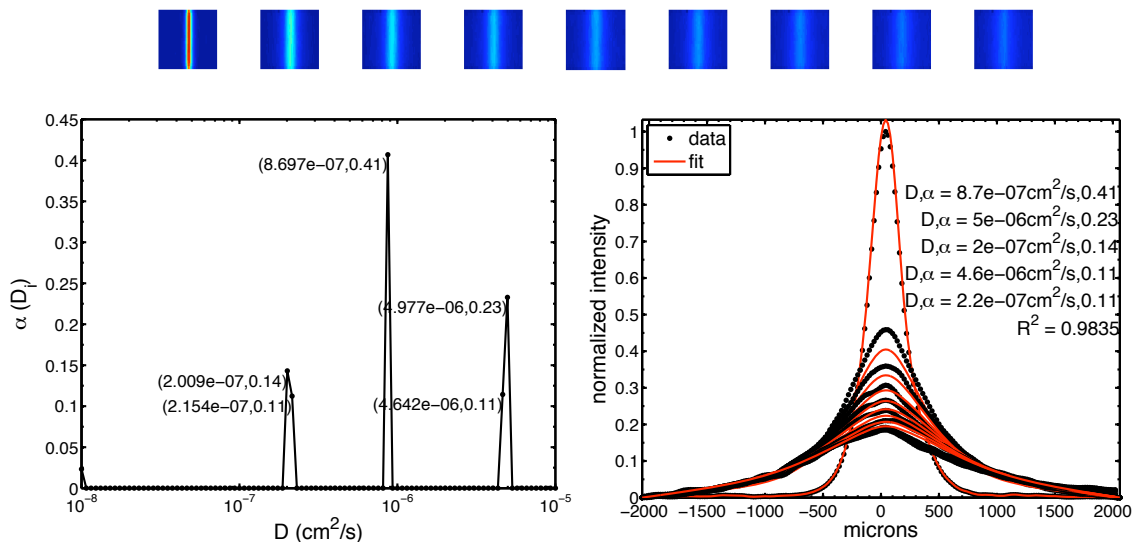


Figure 91. Example of postphotoactivation scanning results for mixture of 10-, 70-, and 500-kD dextrans. Top: images over time (red = high intensity, blue = low intensity); Bottom left: $\alpha(D)$; and Bottom right: intensity profiles fit to diffusion model.

A.3 Characterization of lower limit of detection and resolution

One of the caveats of postphotoactivation scanning is that the total length of the experiment limits the lowest diffusion coefficient that the method can accurately measure. For species with very low diffusion coefficients, intensity profiles may appear to be virtually identical over extended times. For example, profiles shown in Figure 84 for D_{min} over time appear to be superimposed. For short experiments or low diffusion coefficients, it may become impossible to distinguish profiles for one diffusion coefficient from another, particularly in the presence of experimental noise.

Here, we describe experiments and simulations used to characterize the lower limit of detection of our postphotoactivation scanning system. First, we experimentally characterized the variability, or noise in our system. We then incorporated these

measures of variability into simulations to determine the lower limit of detection and the resolution of our experiments.

A.3.1 Experimental characterization of noise

We experimentally characterized the level of noise in our postphotoactivation scanning system by imaging fluorescein immobilized in epoxy. Assuming that the caged fluorescein was completely immobilized by epoxy, the intensity profiles of the images should be identical over time.

Samples were prepared by mixing 80 $\mu\text{g/ml}$ CMNB-caged fluorescein (F-7103, Invitrogen, Carlsbad, CA) in optically transparent epoxy (EPO-TEK® 302-3M, Epoxy Technology, Inc., Billerica, MA). Samples were pipetted on to glass slides with Secure Seal Spacers and sealed with a coverslip as for typical postphotoactivation scanning experiments. The epoxy was allowed to cure at room temperature for 2 weeks (manufacturer's instructions recommended 24 hours at room temperature). We prepared 8 slides.

A mock postphotoactivation scanning experiment was performed for each slide. Fluorescent images were obtained using a microarray scanner with 532-nm laser and 20- μm pixel resolution (Genepix 4000B, Molecular Devices, Sunnyvale, CA). First, a background image was obtained prior to uncaging. Then, a line was uncaged by exposure to UV light using a metal stencil with slit width of 200 μm . We then obtained 9 fluorescent images approximately every 25 minutes over the course of 3.5 hours. The

number of images, interval between images, and total length of the mock experiment were similar to those of experiments performed for HIV-like liposomes.

For each slide, we selected a region of the image for analysis, as we would in a typical postphotoactivation scanning experiment. Intensity profiles are shown in Figure 92.

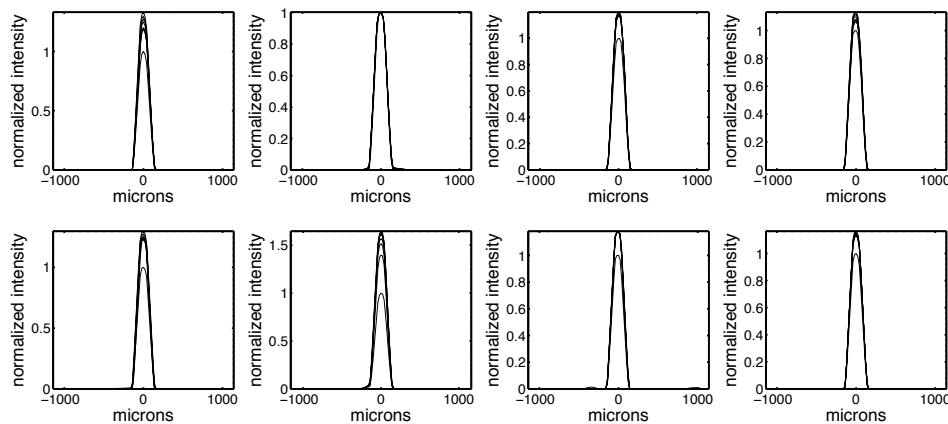


Figure 92. Intensity profiles for caged fluorescein in epoxy. Each plot represents 9 intensity profiles over time for each of the 8 experiments performed.

Ideally, for a given slide, all of the intensity profiles would be identical over time for the immobilized fluorophore. However, the inherent noise in our system results in variability. To find a summary measure for the variability in the intensity profiles, we calculated the variance (σ^2). First, for each slide, we calculated the variance of the intensity profiles over time, for each x position:

$$\sigma^2(x) = \frac{1}{N-1} \sum_{i=1}^N \left(I_i(x) - \overline{I(x)} \right)^2$$

Equation 80

Here, N is the number of images (here, $N = 9$), $I_i(x)$ is the intensity of the image for a given position x , and $\overline{I(x)}$ is the mean of intensity values from all images for a given position x . We then averaged the variances for the different x positions to arrive at a summary measure for the degree to which we expect the intensity profile to vary from image to image. For the $n = 8$ slides tested, we found that the variance ranged from 2.2×10^{-5} to 0.0026. The mean variance for the 8 slides was 5.6×10^{-4} .

A.3.2 Simulations to determine lower limit of detection

We performed simulations similar to the example given in §A.1, incorporating the experimental variances measured in §A.3.1. Again, we generated simulated profiles as shown in Figure 83. We then incorporated random noise at each point in the intensity profiles [145]:

$$I'(x,t) = I(x,t) + \sigma z$$

Equation 81

Where σ is the standard deviation and z is a random number generated from a normal distribution with zero mean and standard deviation of 1. The random number was generated by the MATLAB function “randn”. By multiplying our experimental value for standard deviation, σ , and the randomly generated output of “randn”, z , we arrive at a random number generated from a normal distribution with zero mean and variance equal to the experimentally measured variance. So, essentially, we are adding random variance of the same magnitude observed experimentally to simulated data. Figure 93 shows examples of simulated intensity profiles with varying levels of noise.

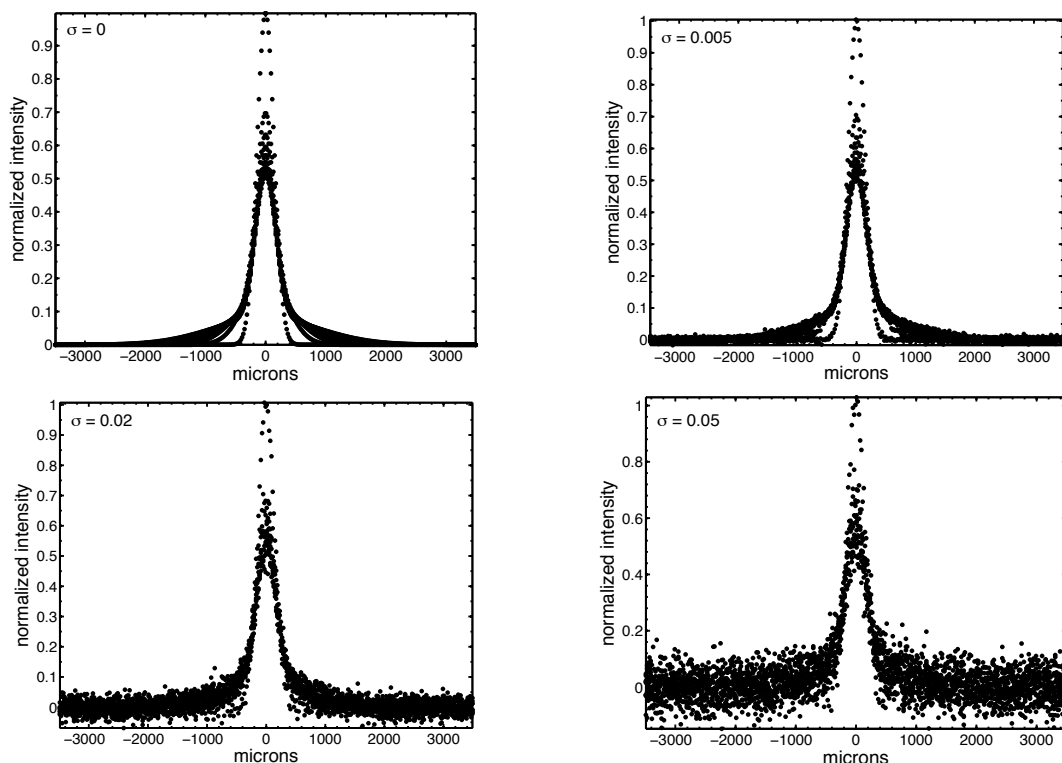


Figure 93. Examples of simulated postphotoactivation scanning intensity profiles with varying levels of random noise added.

We then proceeded to solve for $\alpha(D)$ for various scenarios of multiple diffusing species. We were particularly interested in determining the lower limit of detection for our experiments using HIV-like liposomes, so we selected parameters related to these experiments. We tested a range of diffusion coefficients (D_{input}) from 10^{-12} to 5×10^{-8} cm^2/s . These diffusion coefficients corresponded with the range of diffusion coefficients expected for HIV-like liposomes in gels and dilutions of gels. In each of our simulations, we included a rapidly diffusing species with the diffusion coefficient of 3×10^{-8} cm^2/s . This corresponds to the free label remaining in the liposome solution. We assumed the two species were present in equal amounts so that for each species $\alpha = 0.5$. We also tested different values of noise based on the minimum ($\sigma = 0.005$), mean ($\sigma = 0.02$), and

maximum ($\sigma = 0.05$) of variances observed in the epoxy experiments. For each condition, we simulated $n = 10$ virtual experiments. The total length of each virtual experiment was 3.5 hours with 9 time points evenly distributed over the period of the experiment. We solved for $\alpha(D)$ using postphotoactivation analysis methods and identified the diffusion coefficient (D_{output}) of the peak that corresponded to the slower diffusing species.

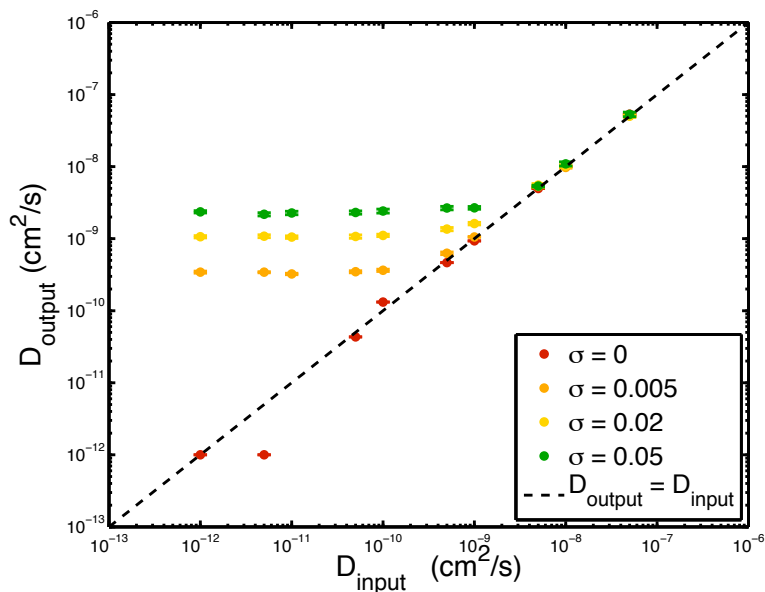


Figure 94. Simulations characterizing the lower limit of detection of postphotoactivation scanning experiments. Intensity profiles were generated using D_{input} and adding random noise with variance σ^2 . We then used postphotoactivation scanning analysis methods to solve for D_{output} (mean \pm SE, $n = 10$ simulations). The plot shows where results diverged from the ideal $D_{output} = D_{input}$.

We found that the lower limit of detection ranged from approximately 5×10^{-11} to 10^{-9} cm^2/s , depending on the level of noise (Figure 94). With no noise added ($\sigma = 0$), the lowest diffusion coefficient that could reliably be detected was approximately 5×10^{-11} cm^2/s . In simulations where $D_{input} = 10^{-11}$ cm^2/s , we were not able to resolve a peak for

the slower-diffusing species (Figure 95). The amplitudes (α) for diffusion coefficients within the range of approximately 3.3×10^{-11} to 10^{-12} (D_{min}) cm^2/s were greater than zero. The intensity profiles produced by these diffusion coefficients were indistinguishable for the time points used in the simulation. The MATLAB nonlinear optimization scheme (“lsqnonlin”) used to determine $\alpha(D)$ was not able to find a unique solution. In simulations where $D_{input} = 10^{-12}$ cm^2/s , the apparent diffusion coefficient (D_{output}) was lower than the expected value. This was the only case where the apparent diffusion coefficient was lower than the expected value.

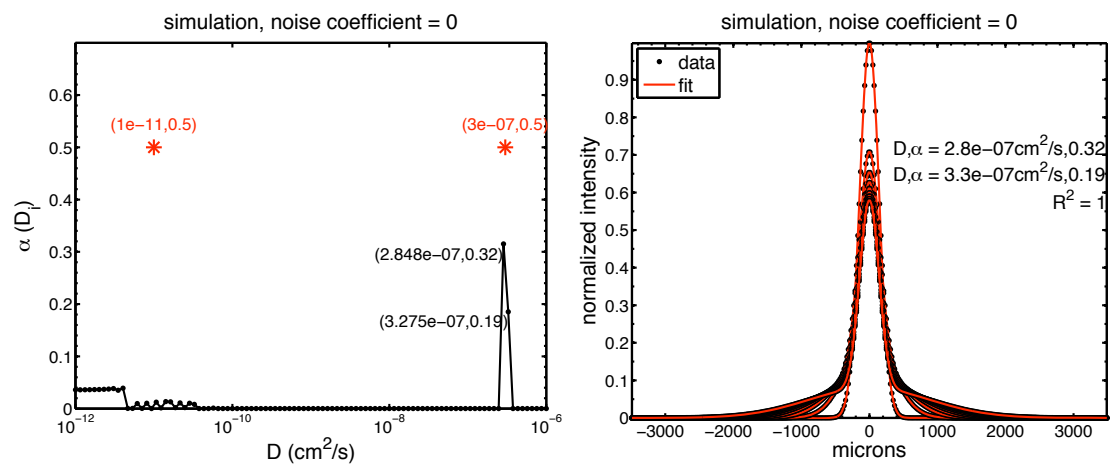


Figure 95. Example of results from postphotoactivation scanning simulations where $D_{input} = 10^{-11}$ cm^2/s . Left: Distribution of $\alpha(D)$. Red asterisks indicate diffusion coefficients used to generate simulated data. Right: Simulated intensity profiles fit to diffusion model.

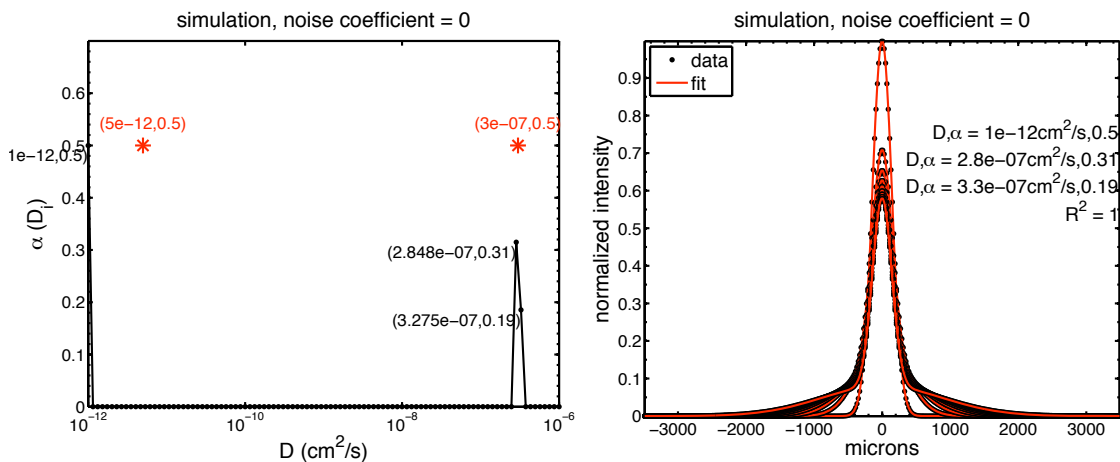


Figure 96. Example of results from postphotoactivation scanning simulations where $D_{input} = 10^{-12} \text{ cm}^2/\text{s}$. Left: Distribution of $\alpha(D)$. Red asterisks indicate diffusion coefficients used to generate simulated data. Right: Simulated intensity profiles fit to diffusion model.

We also found that our postphotoactivation scanning methods were very sensitive to the addition of random noise. Figure 94 shows D_{output} diverging from D_{input} when noise was added. The addition of increasing levels of random noise to the intensity profiles increased the lowest diffusion coefficient that could be reliably detected.

In simulations where noise was added, diffusing species with diffusion coefficient D_{input} beyond a certain lower limit all appear to have similar D_{output} . For example, Figure 97 shows an example of results for simulations where $D_{input} = 10^{-11} \text{ cm}^2/\text{s}$ and $\sigma = 0.02$. D_{output} appears to be $1.2 \times 10^{-9} \text{ cm}^2/\text{s}$, almost two orders of magnitude higher than the actual value. In simulations with $\sigma = 0.02$, species with $D_{input} = 10^{-9} \text{ cm}^2/\text{s}$ to 10^{-12} (minimum value tested) cm^2/s all appear to have diffusion coefficients of approximately $10^{-9} \text{ cm}^2/\text{s}$. Thus, the lowest measurable diffusion coefficient for noise levels $\sigma = 0.02$ is approximately $10^{-9} \text{ cm}^2/\text{s}$.

For $\sigma = 0.005, 0.02,$ and 0.05 the lowest measurable diffusion coefficients were approximately $3.4 \times 10^{-10}, 1.0 \times 10^{-9},$ and $2.3 \times 10^{-9} \text{ cm}^2/\text{s},$ respectively. These levels of noise corresponded to the minimum, mean, and maximum variances observed in the epoxy experiments described in §A.3.1.

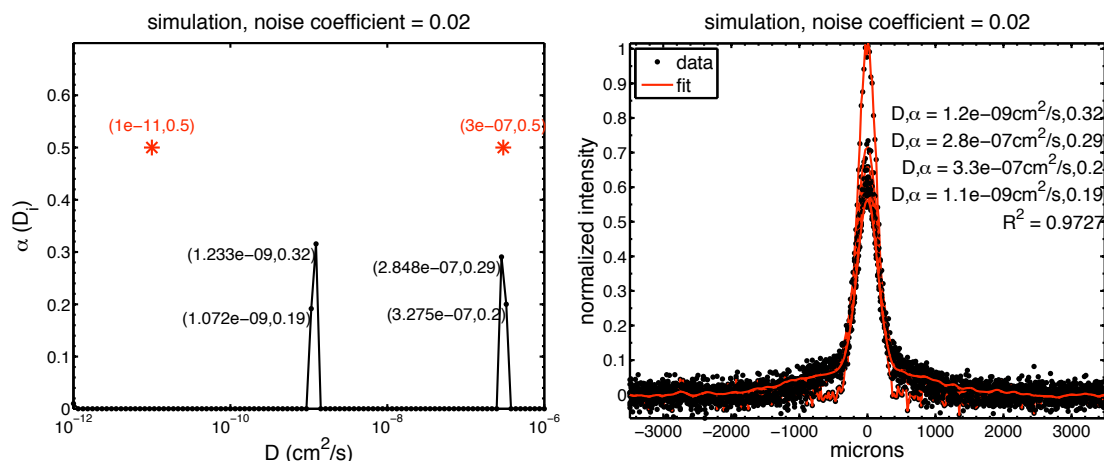


Figure 97. Example of results from postphotoactivation scanning simulations where $D_{input} = 10^{-11} \text{ cm}^2/\text{s}$ and $\sigma = 0.02$. Left: Distribution of $\alpha(D)$. Red asterisks indicate diffusion coefficients used to generate simulated data. Right: Simulated intensity profiles fit to diffusion model.

A.3.3 Comparison of simulated and experimental results

Simulated results help to explain why we were not able to use postphotoactivation scanning to measure the diffusion coefficients of HIV-like liposomes in 20% and 50% (v/v) gel in PBS: Diffusion coefficients of HIV-like liposomes in these media were below the lower limit of detection for the system. Using particle tracking, we found that diffusion coefficients were in the range of 5×10^{-10} to $4 \times 10^{-12} \text{ cm}^2/\text{s}$. We found that the lower limit of detection for the postphotoactivation scanning system ranged from approximately 5×10^{-11} to $10^{-9} \text{ cm}^2/\text{s}$, depending on the level of noise. Diffusion

coefficients of HIV-like liposomes in 20% and 50% (v/v) gel in PBS were likely close to these values, yielding highly variable and unreliable experimental results.

For example, we measured highly variable diffusion coefficients for HIV-like liposomes in 50% (v/v) MC in PBS. The diffusion coefficient obtained through particle tracking of HIV virions was approximately $5 \times 10^{-11} \text{ cm}^2/\text{s}$, so we would expect postphotoactivation scanning results to be similar. This diffusion coefficient was below the lower limit of detection for the postphotoactivation scanning system. According to results from simulations, we would expect the apparent diffusion coefficient to be within the range of 2.3×10^{-9} to $3.4 \times 10^{-10} \text{ cm}^2/\text{s}$ for experiments with some noise (Figure 94). Figure 98 shows an example of results from experiments where the level of noise appeared to be relatively high. The apparent diffusion coefficient is $5.3 \times 10^{-10} \text{ cm}^2/\text{s}$.

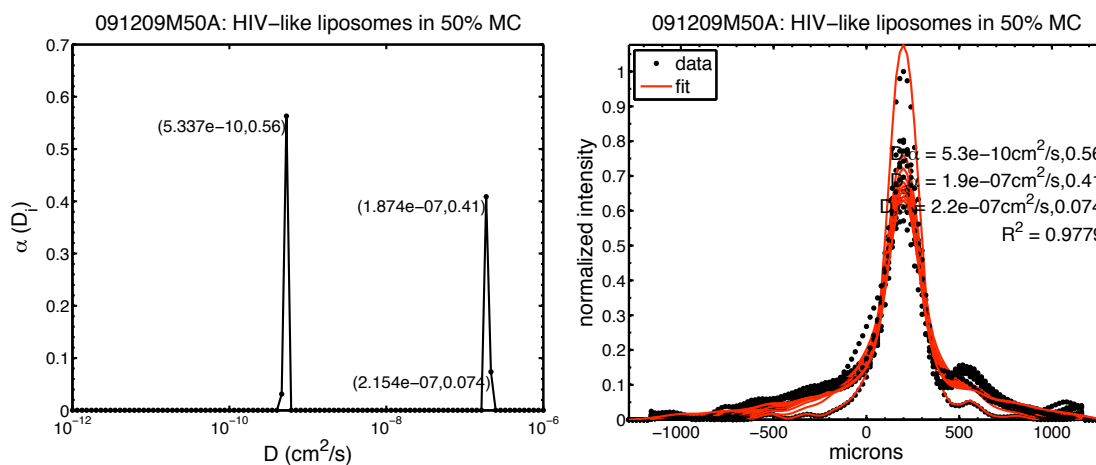


Figure 98. Example of postphotoactivation scanning experimental results for HIV-like liposomes in 50% (v/v) gel in PBS with high levels of experimental noise. Left: $\alpha(D)$; Right: intensity profiles fit to diffusion model.

Results of simulations also suggest that, in cases with low noise, the diffusion coefficient may appear to be lower than the actual diffusion coefficient (Figure 96).

Figure 99 shows an example of an experiment where there were lower levels of noise, and where the apparent diffusion coefficient appeared lower than the expected value.

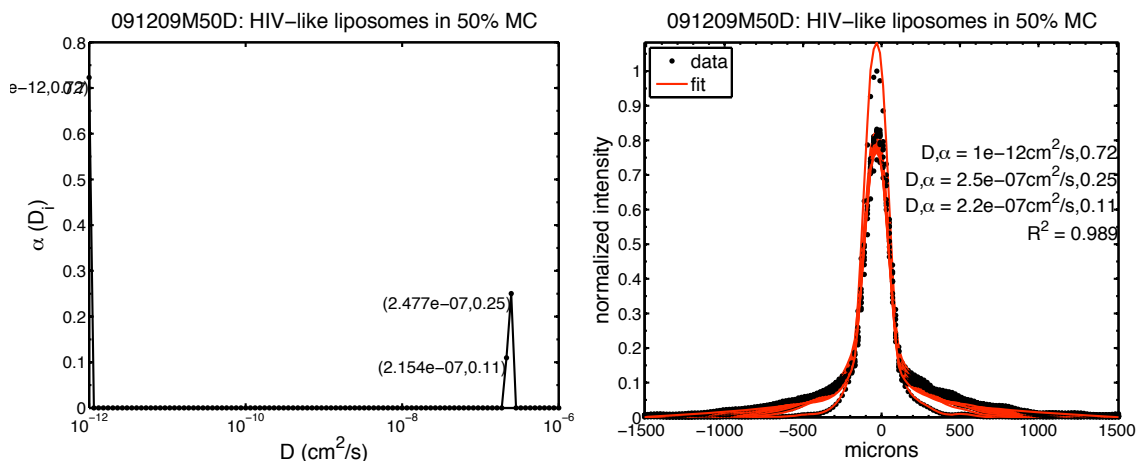


Figure 99. Example of postphotoactivation scanning experimental results for HIV-like liposomes in 50% (v/v) gel in PBS with low levels of experimental noise. Left: $\alpha(D)$; Right: intensity profiles fit to diffusion model.

Thus, simulations can help explain the variable results that we observed for HIV-like liposomes in gel dilutions. In the future, the limit of detection of postphotoactivation scanning experiments should be characterized to aid in interpretation of results.

Simulations are a relatively easy way to characterize the reliability of the system. Here, we input experimental parameters for expected diffusion coefficients, length of experiment, number of time points, and experimental noise. Simulation results helped us to understand the limitations of our measurements.

References

1. Merson, M.H., et al., *The history and challenge of HIV prevention*. Lancet, 2008. **372**(9637): p. 475-88.
2. UNAIDS, *2008 Report on the global AIDS epidemic*. 2008, Joint United Nations Programme on HIV/AIDS: Geneva.
3. Hladik, F. and M.J. McElrath, *Setting the stage: host invasion by HIV*. Nature Reviews Immunology, 2008. **8**(6): p. 447-57.
4. Salomon, J.A., et al., *Integrating HIV Prevention and Treatment: From Slogans to Impact*. PLoS Medicine, 2005. **2**(1): p. e16.
5. Coates, T.J., L. Richter, and C. Caceres, *Behavioural strategies to reduce HIV transmission: how to make them work better*. The Lancet, 2008. **372**(9639): p. 669-684.
6. Gupta, G.R., et al., *Structural approaches to HIV prevention*. The Lancet, 2008. **372**(9640): p. 764-775.
7. Padian, N.S., et al., *Biomedical interventions to prevent HIV infection: evidence, challenges, and way forward*. Lancet, 2008. **372**(9638): p. 585-99.
8. Cutler, B. and J. Justman, *Vaginal microbicides and the prevention of HIV transmission*. The Lancet Infectious Diseases, 2008. **8**(11): p. 685-97.
9. Klasse, P.J., R. Shattock, and J.P. Moore, *Antiretroviral drug-based microbicides to prevent HIV-1 sexual transmission*. Annual Review of Medicine, 2008. **59**: p. 455-71.
10. McGowan, I., *Microbicides: a new frontier in HIV prevention*. Biologicals : journal of the International Association of Biological Standardization, 2006. **34**(4): p. 241-55.
11. Balzarini, J. and L. Van Damme, *Microbicide drug candidates to prevent HIV infection*. The Lancet, 2007. **369**(9563): p. 787-797.
12. Rohan, L.C. and A.B. Sassi, *Vaginal Drug Delivery Systems for HIV Prevention*. The AAPS Journal, 2009. **11**(1): p. 78-87.
13. Ndesendo, V.M., et al., *A review of current intravaginal drug delivery approaches employed for the prophylaxis of HIV/AIDS and prevention of sexually transmitted infections*. Aaps Pharmscitech, 2008. **9**(2): p. 505-20.

14. Johnston, M.I. and A.S. Fauci, *An HIV Vaccine -- Evolving Concepts*. N Engl J Med, 2007. **356**(20): p. 2073-2081.
15. Li, Q., et al., *Glycerol monolaurate prevents mucosal SIV transmission*. Nature, 2009. **458**(7241): p. 1034-1038.
16. Rerks-Ngarm, S., et al., *Vaccination with ALVAC and AIDSVAX to Prevent HIV-1 Infection in Thailand*. N Engl J Med, 2009. **361**(23): p. 2209-2220.
17. Lagakos, S.W., A. Gable, and H.I.V.P.T. Institute of Medicine . Committee on the Methodological Challenges in, *Methodological challenges in biomedical HIV prevention trials*. 2008, Washington, D.C.: National Academies Press.
18. Haase, A.T., *Perils at mucosal front lines for HIV and SIV and their hosts*. Nature Reviews Immunology, 2005. **5**(10): p. 783-792.
19. Wira, C.R., et al., *Innate and adaptive immunity in female genital tract: cellular responses and interactions*. Immunological Reviews, 2005. **206**(1): p. 306-335.
20. Hladik, F. and T.J. Hope, *HIV infection of the genital mucosa in women*. Current HIV/AIDS reports, 2009. **6**(1): p. 20-8.
21. Patton, D.L., et al., *Epithelial cell layer thickness and immune cell populations in the normal human vagina at different stages of the menstrual cycle*. American Journal of Obstetrics and Gynecology, 2000. **183**(4): p. 967-973.
22. Greenhead, P., et al., *Parameters of Human Immunodeficiency Virus Infection of Human Cervical Tissue and Inhibition by Vaginal Virucides*. J. Virol., 2000. **74**(12): p. 5577-5586.
23. Dezzutti, C.S., et al., *Cervical and Prostate Primary Epithelial Cells Are Not Productively Infected but Sequester Human Immunodeficiency Virus Type 1*. The Journal of infectious diseases, 2001. **183**(8): p. 1204-1213.
24. Kawamura, T., et al., *The role of Langerhans cells in the sexual transmission of HIV*. Journal of Dermatological Science, 2005. **40**(3): p. 147-155.
25. Wu, L. and V.N. KewalRamani, *Dendritic-cell interactions with HIV: infection and viral dissemination*. Nat Rev Immunol, 2006. **6**(11): p. 859.
26. Niedecken, H., et al., *Langerhans cell as primary target and vehicle for transmission of HIV*. The Lancet, 1987. **330**(8557): p. 519-520.
27. Ludewig, B., et al., *Transmission of HIV-1 from Productively Infected Mature Langerhans Cells to Primary CD4+ T Lymphocytes Results in Altered T Cell*

- Responses with Enhanced Production of IFN-[gamma] and IL-10.* Virology, 1996. **215**(1): p. 51-60.
28. Blauvelt, A., et al., *Productive infection of dendritic cells by HIV-1 and their ability to capture virus are mediated through separate pathways.* The Journal of Clinical Investigation, 1997. **100**(8): p. 2043-2053.
 29. Kawamura, T., et al., *R5 HIV productively infects Langerhans cells, and infection levels are regulated by compound CCR5 polymorphisms.* Proceedings of the National Academy of Sciences of the United States of America, 2003. **100**(14): p. 8401-8406.
 30. de Witte, L., et al., *Langerin is a natural barrier to HIV-1 transmission by Langerhans cells.* Nature Medicine, 2007. **13**(3): p. 367-371.
 31. Broliden, K., et al., *Introduction: Back to basics: mucosal immunity and novel HIV vaccine concepts.* Journal of Internal Medicine, 2009. **265**(1): p. 5-17.
 32. Wira, C.R., K.S. Grant-Tschudy, and M.A. Crane-Godreau, *Epithelial Cells in the Female Reproductive Tract: a Central Role as Sentinels of Immune Protection.* American Journal of Reproductive Immunology, 2005. **53**(2): p. 65-76.
 33. Gorodeski, G.I., *The cultured human cervical epithelium a new model for studying paracellular transport.* Journal Of The Society For Gynecologic Investigation, 1996. **3**(5): p. 267-280.
 34. Coombs, R.W., P. Reichelderfer, and A.L. Landay, *Recent observations on HIV type-1 infection in the genital tract of men and women.* Aids, 2003.
 35. Lamar, J.K., L.B. Shettles, and E. Delfs, *Cyclic penetrability of human cervical mucus to spermatozoa in vitro.* Am J Physiol, 1940. **129**(2): p. 234-241.
 36. Lai, S.K., et al., *Human Immunodeficiency Virus Type 1 Is Trapped by Acidic but Not by Neutralized Human Cervicovaginal Mucus.* J. Virol., 2009. **83**(21): p. 11196-11200.
 37. Boukari, H., et al., *HIV-virions Appear To Be Trapped By Human Cervical Mucus.* Biophysical Journal, 2009. **96**(3, Supplement 1): p. 35a.
 38. Maher, D., et al., *HIV binding, penetration, and primary infection in human cervicovaginal tissue.* Proc Natl Acad Sci U S A, 2005. **102**(32): p. 11504-9.
 39. Miller, C.J., et al., *Propagation and dissemination of infection after vaginal transmission of simian immunodeficiency virus.* Journal of Virology, 2005. **79**(14): p. 9217-27.

40. Eggert-Kruse, W., et al., *Antimicrobial activity of human cervical mucus*. Human Reproduction, 2000. **15**(4): p. 778-784.
41. Hein, M., et al., *Antimicrobial factors in the cervical mucus plug*. American Journal of Obstetrics and Gynecology, 2002. **187**(1): p. 137-144.
42. Cole, A.M. and A.L. Cole, *Antimicrobial Polypeptides are Key Anti-HIV-1 Effector Molecules of Cervicovaginal Host Defense*. American Journal of Reproductive Immunology, 2008. **59**(1): p. 27-34.
43. Wira, C.R. and J.V. Fahey, *A new strategy to understand how HIV infects women: identification of a window of vulnerability during the menstrual cycle*. AIDS (London, England), 2008. **22**(15): p. 1909-17.
44. Lehner, T., et al., *The emerging role of innate immunity in protection against HIV-1 infection*. Vaccine, 2008. **26**(24): p. 2997-3001.
45. Shugars, D.C., et al., *Endogenous salivary inhibitors of Human Immunodeficiency Virus*. Archives of Oral Biology, 1999. **44**(6): p. 445-453.
46. Chang, T.L. and M.E. Klotman, *Defensins: natural anti-HIV peptides*. AIDS reviews, 2004. **6**(3): p. 161-8.
47. Chang, T.L., et al., *Dual role of alpha-defensin-1 in anti-HIV-1 innate immunity*. The Journal of Clinical Investigation, 2005. **115**(3): p. 765-773.
48. Quinones-Mateu, M.E., et al., *Human epithelial beta-defensins 2 and 3 inhibit HIV-1 replication*. Aids, 2003. **17**(16): p. F39-F48.
49. Lee-Huang, S., et al., *Lysozyme and RNases as anti-HIV components in beta-core preparations of human chorionic gonadotropin*. Proceedings of the National Academy of Sciences of the United States of America, 1999. **96**(6): p. 2678-2681.
50. Harmsen, M.C., et al., *Antiviral Effects of Plasma and Milk Proteins: Lactoferrin Shows Potent Activity against Both Human Immunodeficiency Virus and Human Cytomegalovirus Replication in vitro*. The Journal of infectious diseases, 1995. **172**(2): p. 380-388.
51. Cocchi, F., et al., *Identification of RANTES, MIP-1alpha, and MIP-1beta as the Major HIV-Suppressive Factors Produced by CD8+ T Cells*. Science, 1995. **270**(5243): p. 1811-1815.
52. Sheehy, A.M., et al., *Isolation of a human gene that inhibits HIV-1 infection and is suppressed by the viral Vif protein*. Nature, 2002. **418**(6898): p. 646-650.

53. Chiu, Y.-L., et al., *Cellular APOBEC3G restricts HIV-1 infection in resting CD4+ T cells*. *Nature*, 2005. **435**(7038): p. 108-114.
54. Yap, M.W., et al., *Trim5alpha protein restricts both HIV-1 and murine leukemia virus*. *Proceedings of the National Academy of Sciences of the United States of America*, 2004. **101**(29): p. 10786-10791.
55. Ongradi, J., et al., *Acid Sensitivity of Cell-Free and Cell-Associated HIV-1: Clinical Implications*. *Aids Research and Human Retroviruses*, 2009. **6**(12): p. 1433-1436.
56. Olmsted, S., et al., *Low pH immobilizes and kills human leukocytes and prevents transmission of cell-associated HIV in a mouse model*. *BMC Infectious Diseases*, 2005. **5**: p. 79.
57. Owen, D.H. and D.F. Katz, *A vaginal fluid simulant*. *Contraception*, 1999. **59**(2): p. 91-5.
58. Antonio, M.A.D., S.E. Hawes, and S.L. Hillier, *The identification of vaginal Lactobacillus species and the demographic and microbiologic characteristics of women colonized by these species*. *Journal of Infectious Diseases*, 1999. **180**(6): p. 1950-1956.
59. Boris, S. and C. Barbès, *Role played by lactobacilli in controlling the population of vaginal pathogens*. *Microbes and Infection*, 2000. **2**(5): p. 543-546.
60. Klebanoff, S.J. and R.W. Coombs, *Viricidal effect of Lactobacillus acidophilus on human immunodeficiency virus type 1: possible role in heterosexual transmission*. *The Journal of experimental medicine*, 1991. **174**(1): p. 289-92.
61. Martin, H.L., et al., *Vaginal Lactobacilli, Microbial Flora, and Risk of Human Immunodeficiency Virus Type 1 and Sexually Transmitted Disease Acquisition*. *The Journal of Infectious Diseases*, 1999. **180**(6): p. 1863-1868.
62. Sewankambo, N., et al., *HIV-1 infection associated with abnormal vaginal flora morphology and bacterial vaginosis*. *The Lancet*, 1997. **350**(9077): p. 546-550.
63. Hu, J., M.B. Gardner, and C.J. Miller, *Simian Immunodeficiency Virus Rapidly Penetrates the Cervicovaginal Mucosa after Intravaginal Inoculation and Infects Intraepithelial Dendritic Cells*. *J. Virol.*, 2000. **74**(13): p. 6087-6095.
64. Trapp, S., S.G. Turville, and M. Robbiani, *Slamming the door on unwanted guests: why preemptive strikes at the mucosa may be the best strategy against HIV*. *J Leukoc Biol*, 2006. **80**(5): p. 1076-1083.

65. Miyauchi, K., et al., *HIV Enters Cells via Endocytosis and Dynamin-Dependent Fusion with Endosomes*. Cell, 2009. **137**(3): p. 433-444.
66. Sattentau, Q., *Avoiding the void: cell-to-cell spread of human viruses*. Nature Reviews Microbiology, 2008. **6**(11): p. 815-26.
67. Greene, W.C., *The brightening future of HIV therapeutics*. Nat Immunol, 2004. **5**(9): p. 867-871.
68. Moore, J.P. and M. Stevenson, *New targets for inhibitors of HIV-1 replication*. Nat Rev Mol Cell Biol, 2000. **1**(1): p. 40-49.
69. Greene, W.C., et al., *Novel targets for HIV therapy*. Antiviral Research, 2008. **80**(3): p. 251-265.
70. Lytle, C.D., et al., *An in vitro evaluation of condoms as barriers to a small virus*. Sexually Transmitted Diseases, 1997. **24**(3): p. 161-4.
71. Barnhart, K.T., et al., *Baseline dimensions of the human vagina*. Hum. Reprod., 2006. **21**(6): p. 1618-1622.
72. Saltzman, W.M., *Drug delivery: engineering principles for drug therapy*. Topics in chemical engineering. 2001, New York: Oxford University Press.
73. Masters, W.H. and V.E. Johnson, *Human sexual response*. 1966, Boston: Little, Brown and Company.
74. Zervomanolakis, I., et al., *Physiology of upward transport in the human female genital tract*. Annals of the New York Academy of Sciences, 2007. **1101**: p. 1-20.
75. Owen, D.H. and D.F. Katz, *A review of the physical and chemical properties of human semen and the formulation of a semen simulant*. J Androl, 2005. **26**(4): p. 459-69.
76. Quayle, A.J., et al., *T Lymphocytes and Macrophages, but Not Motile Spermatozoa, Are a Significant Source of Human Immunodeficiency Virus in Semen*. The Journal of infectious diseases, 1997. **176**(4): p. 960-968.
77. Quayle, A.J., et al., *The case against an association between HIV-1 and sperm: molecular evidence*. Journal of Reproductive Immunology, 1998. **41**(1-2): p. 127-136.
78. Kalichman, S.C., G. Di Berto, and L. Eaton, *Human immunodeficiency virus viral load in blood plasma and semen: review and implications of empirical findings*. Sexually Transmitted Diseases, 2008. **35**(1): p. 55-60.

79. Stekler, J., et al., *HIV dynamics in seminal plasma during primary HIV infection*. AIDS Research and Human Retroviruses, 2008. **24**(10): p. 1269-74.
80. Vernazza, P.L., et al., *Effect of antiviral treatment on the shedding of HIV-1 in semen*. Aids, 1997. **11**(10): p. 1249-1254.
81. Ball, J.K., et al., *HIV-1 in semen: Determination of proviral and viral titres compared to blood, and quantification of semen leukocyte populations*. Journal of Medical Virology, 1999. **59**(3): p. 356-363.
82. Butler, D.M., et al., *The Origins of Sexually Transmitted HIV Among Men Who Have Sex with Men*. Science Translational Medicine, 2010. **2**(18): p. 18re1.
83. Khanna, K.V., et al., *Vaginal transmission of cell-associated HIV-1 in the mouse is blocked by a topical, membrane-modifying agent*. Journal of Clinical Investigation, 2002. **109**(2): p. 205-211.
84. Dimitrov, D.S., et al., *Quantitation of human immunodeficiency virus type 1 infection kinetics*. J. Virol., 1993. **67**(4): p. 2182-2190.
85. Van Herrewege, Y., et al., *A dual chamber model of female cervical mucosa for the study of HIV transmission and for the evaluation of candidate HIV microbicides*. Antiviral Research, 2007. **74**(2): p. 111-124.
86. Sowinski, S., et al., *Membrane nanotubes physically connect T cells over long distances presenting a novel route for HIV-1 transmission*. Nat Cell Biol, 2008. **10**(2): p. 211-219.
87. Anderson, D.J., et al., *Targeting Trojan Horse leukocytes for HIV prevention*. Aids. **24**(2): p. 163-187 10.1097/QAD.0b013e32833424c8.
88. Klasse, P.J., R.J. Shattock, and J.P. Moore, *Which Topical Microbicides for Blocking HIV-1 Transmission Will Work in the Real World?* PLoS Medicine, 2006. **3**(9).
89. Anderson, D.J. and E.J. Yunis, *Trojan horse leukocytes in AIDS*. New England Journal of Medicine, 1983. **309**(16): p. 984-985.
90. Kaizu, M., et al., *Repeated intravaginal inoculation with cell-associated simian immunodeficiency virus results in persistent infection of nonhuman primates*. The Journal of infectious diseases, 2006. **194**(7): p. 912-916.
91. Weiler, A.M., et al., *Genital ulcers facilitate rapid viral entry and dissemination following intravaginal inoculation with cell-associated simian immunodeficiency virus SIVmac239*. Journal of Virology, 2008. **82**(8): p. 4154-8.

92. Gail, M.H. and C.W. Boone, *The Locomotion of Mouse Fibroblasts in Tissue Culture*. Biophysical Journal, 1970. **10**(10): p. 980-993.
93. Willits, R.K. and W.M. Saltzman, *The effect of synthetic polymers on the migration of monocytes through human cervical mucus*. Biomaterials, 2004. **25**(19): p. 4563-4571.
94. Willits, R.K. and W.M. Saltzman, *Synthetic polymers alter the structure of cervical mucus*. Biomaterials, 2001. **22**(5): p. 445-452.
95. Microbicide Trials Network. *Fact Sheet: HPTN 035 at a glance*. 2009; Available from:
<http://www.hptn.org/web%20documents/HPTN035/HPTN%20035%20fact%20sheet%20for%20media.pdf>.
96. Quinn, T.C., et al., *Viral Load and Heterosexual Transmission of Human Immunodeficiency Virus Type 1*. N Engl J Med, 2000. **342**(13): p. 921-929.
97. Wilson, D.P., et al., *Relation between HIV viral load and infectiousness: a model-based analysis*. Lancet, 2008. **372**(9635): p. 314-20.
98. Smith, R.J. and S.M. Blower, *Could disease-modifying HIV vaccines cause population-level perversity?* The Lancet Infectious Diseases, 2004. **4**(10): p. 636-639.
99. Tuckwell, H.C., P.D. Shipman, and A.S. Perelson, *The probability of HIV infection in a new host and its reduction with microbicides*. Mathematical Biosciences, 2008. **214**(1-2): p. 81-6.
100. Cone, R., *Barrier properties of mucus*. Advanced Drug Delivery Reviews, 2009. **61**(2): p. 75-85.
101. Brügger, B., et al., *The HIV lipidome: a raft with an unusual composition*. Proceedings of the National Academy of Sciences of the United States of America, 2006. **103**(8): p. 2641-6.
102. Zhu, P., et al., *Distribution and three-dimensional structure of AIDS virus envelope spikes*. Nature, 2006. **441**(7095): p. 847-852.
103. Briggs, J.A., et al., *The mechanism of HIV-1 core assembly: insights from three-dimensional reconstructions of authentic virions*. Structure, 2006. **14**(1): p. 15-20.
104. Briggs, J.A., et al., *Structural organization of authentic, mature HIV-1 virions and cores*. EMBO J, 2003. **22**(7): p. 1707-15.

105. Gentile, M., et al., *Determination of the size of HIV using adenovirus type 2 as an internal length marker*. Journal of virological methods, 1994. **48**(1): p. 43-52.
106. Johnson, W.E. and R.C. Desrosiers, *Viral persistence: HIV's Strategies of Immune System Evasion*. Annual Review of Medicine, 2003. **53**(1): p. 499-518.
107. Truskey, G.A., F. Yuan, and D.F. Katz, *Transport Phenomena in Biological Systems*. 2nd ed. 2009, Upper Saddle River, New Jersey: Pearson Education, Inc.
108. Mascola, J.R. and D.C. Montefiori, *The Role of Antibodies in HIV Vaccines*. Annual Review Of Immunology, 2009.
109. Burke, B. and S.W. Barnett, *Broadening Our View of Protective Antibody Responses Against HIV*. Current HIV Research, 2007. **5**(6): p. 625-641.
110. Parren, P.W.H.I., et al., *Antibody Protects Macaques against Vaginal Challenge with a Pathogenic R5 Simian/Human Immunodeficiency Virus at Serum Levels Giving Complete Neutralization In Vitro*. J. Virol., 2001. **75**(17): p. 8340-8347.
111. Mascola, J.R., et al., *Protection of macaques against vaginal transmission of a pathogenic HIV-1/SIV chimeric virus by passive infusion of neutralizing antibodies*. Nat Med, 2000. **6**(2): p. 207-210.
112. Veazey, R.S., et al., *Prevention of virus transmission to macaque monkeys by a vaginally applied monoclonal antibody to HIV-1 gp120*. Nat Med, 2003. **9**(3): p. 343-346.
113. Mestecky, J., *Humoral immune responses to the human immunodeficiency virus type-1 (HIV-1) in the genital tract compared to other mucosal sites*. Journal of Reproductive Immunology, 2006. **72**(1-2): p. 1-17.
114. Kozlowski, P.A. and M.R. Neutra, *The role of mucosal immunity in prevention of HIV transmission*. Current Molecular Medicine, 2003. **3**(3): p. 217-228.
115. Mestecky, J. and P.N. Fultz, *Mucosal immune system of the human genital tract*. The Journal of Infectious Diseases, 1999. **179** (Suppl 3): p. S470-4.
116. Hirbod, T. and K. Broliden, *Mucosal immune responses in the genital tract of HIV-1-exposed uninfected women*. Journal of Internal Medicine, 2007. **262**(1): p. 44-58.
117. Kindt, T.J., R.A. Goldsby, and B.A. Osborne, *Kuby Immunology*. 6 ed. 2007, New York: W.H. Freeman and Company.

118. Mascola, J.R., *Defining the Protective Antibody Response for HIV-1*. Current Molecular Medicine, 2003. **3**(3): p. 209.
119. Burton, D.R., et al., *HIV vaccine design and the neutralizing antibody problem*. Nat Immunol, 2004. **5**(3): p. 233-6.
120. Mascola, J.R., et al., *Recommendations for the Design and Use of Standard Virus Panels To Assess Neutralizing Antibody Responses Elicited by Candidate Human Immunodeficiency Virus Type 1 Vaccines*. J. Virol., 2005. **79**(16): p. 10103-10107.
121. McMichael, A.J., et al., *The immune response during acute HIV-1 infection: clues for vaccine development*. Nat Rev Immunol, 2010. **10**(1): p. 11-23.
122. Karlsson Hedestam, G.B., et al., *The challenges of eliciting neutralizing antibodies to HIV-1 and to influenza virus*. Nat Rev Micro, 2008. **6**(2): p. 143-155.
123. Yang, X., et al., *Stoichiometry of Envelope Glycoprotein Trimers in the Entry of Human Immunodeficiency Virus Type 1*. J. Virol., 2005. **79**(19): p. 12132-12147.
124. Sagar, M., et al., *Human Immunodeficiency Virus Type 1 V1-V2 Envelope Loop Sequences Expand and Add Glycosylation Sites over the Course of Infection, and These Modifications Affect Antibody Neutralization Sensitivity*. J. Virol., 2006. **80**(19): p. 9586-9598.
125. Wei, X., et al., *Antibody neutralization and escape by HIV-1*. Nature, 2003. **422**(6929): p. 307.
126. Haynes, B.F., et al., *Cardiolipin polyspecific autoreactivity in two broadly neutralizing HIV-1 antibodies*. Science, 2005. **308**(5730): p. 1906-8.
127. Alam, S.M., et al., *The role of antibody polyspecificity and lipid reactivity in binding of broadly neutralizing anti-HIV-1 envelope human monoclonal antibodies 2F5 and 4E10 to glycoprotein 41 membrane proximal envelope epitopes*. J Immunol, 2007. **178**(7): p. 4424-35.
128. Phogat, S. and R. Wyatt, *Rational Modifications of HIV-1 Envelope Glycoproteins for Immunogen Design*. Current Pharmaceutical Design, 2007. **13**(2): p. 213-227.
129. Shibata, R., et al., *Neutralizing antibody directed against the HIV-1 envelope glycoprotein can completely block HIV-1/SIV chimeric virus infections of macaque monkeys*. Nat Med, 1999. **5**(2): p. 204-210.

130. Flynn, N.M., et al., *Placebo-controlled phase 3 trial of a recombinant glycoprotein 120 vaccine to prevent HIV-1 infection*. The Journal of infectious diseases, 2005. **191**(5): p. 654-665.
131. Gilbert, P.B., et al., *Correlation between Immunologic Responses to a Recombinant Glycoprotein 120 Vaccine and Incidence of HIV-1 Infection in a Phase 3 HIV-1 Preventive Vaccine Trial*. The Journal of infectious diseases, 2005. **191**(5): p. 666-677.
132. Scheid, J.F., et al., *Broad diversity of neutralizing antibodies isolated from memory B cells in HIV-infected individuals*. Nature, 2009. **458**(7238): p. 636-640.
133. Montefiori, D., et al., *Antibody-Based HIV-1 Vaccines: Recent Developments and Future Directions*. PLoS Med, 2007. **4**(12): p. e348.
134. Mantis, N.J., et al., *Inhibition of HIV-1 Infectivity and Epithelial Cell Transfer by Human Monoclonal IgG and IgA Antibodies Carrying the b12 V Region*. J Immunol, 2007. **179**(5): p. 3144-3152.
135. Bomsel, M., et al., *Intracellular Neutralization of HIV Transcytosis across Tight Epithelial Barriers by Anti-HIV Envelope Protein dIgA or IgM*. Immunity, 1998. **9**(2): p. 277-287.
136. Bomsel, M., et al., *Natural mucosal antibodies reactive with first extracellular loop of CCR5 inhibit HIV-1 transport across human epithelial cells*. Aids, 2007. **21**(1): p. 13-22.
137. Hessel, A.J., et al., *Fc receptor but not complement binding is important in antibody protection against HIV*. Nature, 2007. **449**(7158): p. 101-104.
138. Dimmock, N.J. and S.A. Hardy, *Valency of antibody binding to virions and its determination by surface plasmon resonance*. Reviews in Medical Virology, 2004. **14**(2): p. 123-35.
139. Geonntotti, A.R., et al., *Measuring macrodiffusion coefficients in microbicide hydrogels via postphotoactivation scanning*. Biomacromolecules, 2008. **9**(2): p. 748-751.
140. Armstrong, J., et al., *The hydrodynamic radii of macromolecules and their effect on red blood cell aggregation*. Biophysical Journal, 2004. **87**(6): p. 4259-70.
141. Björk, I. and E. Lindh, *Gross conformation of human secretory immunoglobulin A and its component parts*. Eur J Biochem, 1974. **45**(1): p. 135-45.

142. Stieh, D., D. King, and R. Shattock, *The Ability of Antibodies to Complex HIV Virions and Implications for Neutralization*, in *Center for HIV/AIDS Vaccine Immunology 4th Annual Retreat*. 2008: Durham, NC.
143. Dennison, S.M., et al., *Stable Docking of Neutralizing Human Immunodeficiency Virus Type 1 gp41 Membrane-Proximal External Region Monoclonal Antibodies 2F5 and 4E10 Is Dependent on the Membrane Immersion Depth of Their Epitope Regions*. *J. Virol.*, 2009. **83**(19): p. 10211-10223.
144. New, R.R.C., *Liposomes : a practical approach*. Practical approach series. 1990, New York: IRL Press.
145. Periasamy, N. and A.S. Verkman, *Analysis of fluorophore diffusion by continuous distributions of diffusion coefficients: application to photobleaching measurements of multicomponent and anomalous diffusion*. *Biophysical Journal*, 1998. **75**(1): p. 557-67.
146. Dolgosheina, E.B., A.Y. Karulin, and A.V. Bobylev, *A kinetic model of the agglutination process*. *Mathematical biosciences*, 1992. **109**(1): p. 1-10.
147. Chandrasekhar, S., *Stochastic Problems in Physics and Astronomy*. *Reviews of Modern Physics*, 1943. **15**(1): p. 1-89.
148. Haynes, B.F. and S.M. Alam, *HIV-1 Hides an Achilles' Heel in Virion Lipids*. *Immunity*, 2008. **28**(1): p. 10-12.
149. Neelamegham, S., L.L. Munn, and K. Zygourakis, *A model for the kinetics of homotypic cellular aggregation under static conditions*. *Biophysical Journal*, 1997. **72**(1): p. 51-64.
150. Nguyen, P. and E. O'Rear, *Temporal aggregate size distributions from simulation of platelet aggregation and disaggregation*. *Annals of Biomedical Engineering*, 1990. **18**(4): p. 427-444.
151. Amsden, B., *An obstruction-scaling model for diffusion in homogeneous hydrogels*. *Macromolecules*, 1999. **32**(3): p. 874-879.
152. Olmsted, S.S., et al., *Diffusion of macromolecules and virus-like particles in human cervical mucus*. *Biophysical Journal*, 2001. **81**(4): p. 1930-1937.
153. Yuan, F., A. Krol, and S. Tong, *Available space and extracellular transport of macromolecules: effects of pore size and connectedness*. *Annals of Biomedical Engineering*, 2001. **29**(12): p. 1150-8.

154. Haynes, B., *Finding a path for design of an HIV vaccine*, in *CHAVI 4th Annual Retreat*. 2008: Durham, NC.
155. Justin-Temu, M., et al., *Intravaginal gels as drug delivery systems*. *J Womens Health (Larchmt)*, 2004. **13**(7): p. 834-44.
156. das Neves, J.J. and M.M.F. Bahia, *Gels as vaginal drug delivery systems*. 2006. **318**(1-2): p. 14.
157. Neurath, A., N. Strick, and Y.-Y. Li, *Anti-HIV-1 activity of anionic polymers: a comparative study of candidate microbicides*. *BMC Infectious Diseases*, 2002. **2**(1): p. 27.
158. Honey, K., *Microbicide trial screeches to a halt*. *Journal of Clinical Investigation*, 2007. **117**(5): p. 1116.
159. Skoler-Karppoff, S., et al., *Efficacy of Carraguard for prevention of HIV infection in women in South Africa: a randomised, double-blind, placebo-controlled trial*. *Lancet*, 2008. **372**(9654): p. 1977-87.
160. Tao, W., C. Richards, and D. Hamer, *Short Communication: Enhancement of HIV Infection by Cellulose Sulfate*. *AIDS Research and Human Retroviruses*, 2008. **24**(7): p. 925-929.
161. Abdool Karim, S., et al., *Safety and effectiveness of vaginal microbicides BufferGel and 0.5% PRO 2000/5 gel for the prevention of HIV infection in women: results of the HPTN 035 Trial*, in *16th Conference on Retroviruses and Opportunistic Infections*. Montreal, QC, CANADA. 2009.
162. Masse, B., et al., *Efficacy dilution in randomized placebo-controlled vaginal microbicide trials*. *Emerging Themes in Epidemiology*, 2009. **6**(1): p. 5.
163. Turville, S., et al., *Efficacy of Carraguard-based microbicides in vivo despite variable in vitro activity*. *PLoS ONE*, 2008. **3**(9): p. e3162.
164. Neurath, A.R., et al., *Cellulose acetate phthalate, a common pharmaceutical excipient, inactivates HIV-1 and blocks the coreceptor binding site on the virus envelope glycoprotein gp120*. *BMC Infectious Diseases*, 2001. **1**(1): p. 17.
165. Low-Beer, N., et al., *Dextrin sulfate as a vaginal microbicide: randomized, double-blind, placebo-controlled trial including healthy female volunteers and their male partners*. *Journal of acquired immune deficiency syndromes (1999)*, 2002. **31**(4): p. 391-8.

166. Tien, D., et al., *In vitro and in vivo characterization of a potential universal placebo designed for use in vaginal microbicide clinical trials*. *Aids Research and Human Retroviruses*, 2005. **21**(10): p. 845-853.
167. Karim, S.A., *Safety and Effectiveness of Vaginal Microbicides BufferGel and 0.5% PRO 2000/5 Gel for the Prevention of HIV Infection in Women: Results of the HPTN 035 Trial*, in *CROI 2009*. 2009: Montreal, Canada.
168. Jespers, V.A., et al., *Dose-ranging phase I study of TMC120, a promising vaginal microbicide, in HIV-negative and HIV-positive female volunteers*. *Journal of acquired immune deficiency syndromes (1999)*, 2007. **44**(2): p. 154-8.
169. Patton, D.L., et al., *Preclinical safety assessments of UC781 anti-human immunodeficiency virus topical microbicide formulations*. *Antimicrobial Agents And Chemotherapy*, 2007. **51**(5): p. 1608-15.
170. Mayer, K.H., et al., *Safety and tolerability of tenofovir vaginal gel in abstinent and sexually active HIV-infected and uninfected women*. *AIDS (London, England)*, 2006. **20**(4): p. 543-51.
171. Rosen, R.K., et al., *Acceptability of tenofovir gel as a vaginal microbicide among women in a phase I trial: a mixed-methods study*. *Journal of women's health (2002)*, 2008. **17**(3): p. 383-92.
172. Amsden, B., *Modeling solute diffusion in aqueous polymer solutions*. *Polymer*, 2002. **43**(5): p. 1623-1630.
173. Lai, S.K., et al., *Rapid transport of large polymeric nanoparticles in fresh undiluted human mucus*. *PNAS*, 2007. **104**(5): p. 1482-1487.
174. Yudin, A., F. Hanson, and D. Katz, *Human cervical mucus and its interaction with sperm: a fine-structural view*. *Biol Reprod*, 1989. **40**(3): p. 661-671.
175. Amende, M.T., D. Hariharan, and N.A. Peppas, *Factors influencing drug and protein transport and release from ionic hydrogels*. *Reactive Polymers*, 1995. **25**(2-3): p. 127-137.
176. Grossman, P.D. and D.S. Soane, *Experimental and theoretical studies of DNA separations by capillary electrophoresis in entangled polymer solutions*. *Biopolymers*, 1991. **31**(10): p. 1221-8.
177. Baumgartner, S., J. Kristl, and N.A. Peppas, *Network Structure of Cellulose Ethers Used in Pharmaceutical Applications During Swelling and at Equilibrium*. *Pharmaceutical Research*, 2002. **19**(8): p. 1084-1090.

178. Serdyuk, I.N., G. Zaccai, and N.R. Zaccai, *Methods in molecular biophysics : structure, dynamics, function*. 2007, New York: Cambridge University Press.
179. Qian, H., M.P. Sheetz, and E.L. Elson, *Single particle tracking. Analysis of diffusion and flow in two-dimensional systems*. Biophysical Journal, 1991. **60**(4): p. 910-21.
180. Saxton, M.J., *Single-particle tracking: the distribution of diffusion coefficients*. Biophysical Journal, 1997. **72**(4): p. 1744-53.
181. Suh, J., M. Dawson, and J. Hanes, *Real-time multiple-particle tracking: applications to drug and gene delivery*. Advanced Drug Delivery Reviews, 2005. **57**(1): p. 63-78.
182. Jay, J.I., et al., *Modulation of Viscoelasticity and HIV Transport as a Function of pH in a Reversibly Crosslinked Hydrogel*. Advanced Functional Materials, 2009. **19**(18): p. 2969-2977.
183. Cavalieri, F., et al., *Water, solute, and segmental dynamics in polysaccharide hydrogels*. Macromolecular Bioscience, 2006. **6**(8): p. 579-89.
184. Henderson, et al., *Optical imaging and analysis of human vaginal coating by drug delivery gels*. Contraception, 2007. **75**(2): p. 142-151.
185. Henderson, M.H., et al., *Optical instrument for measurement of vaginal coating thickness by drug delivery formulations*. Review of Scientific Instruments, 2005. **76**(3): p. -.
186. Patterson, G.H. and J. Lippincott-Schwartz, *A Photoactivatable GFP for Selective Photolabeling of Proteins and Cells*. Science, 2002. **297**(5588): p. 1873-1877.
187. Maguire, R.A., V.R. Zacharopoulos, and D.M. Phillips, *Carrageenan-based nonoxynol-9 spermicides for prevention of sexually transmitted infections*. Sexually Transmitted Diseases, 1998. **25**(9): p. 494-500.
188. Van Damme, L., et al., *Lack of effectiveness of cellulose sulfate gel for the prevention of vaginal HIV transmission*. The New England Journal of Medicine, 2008. **359**(5): p. 463-72.
189. Halpern, V., et al., *Effectiveness of cellulose sulfate vaginal gel for the prevention of HIV infection: results of a Phase III trial in Nigeria*. PLoS ONE, 2008. **3**(11): p. e3784.

190. Peterson, L., et al., *SAVVY (C31G) gel for prevention of HIV infection in women: a Phase 3, double-blind, randomized, placebo-controlled trial in Ghana*. PLoS ONE, 2007. **2**(12): p. e1312.
191. Feldblum, P.J., et al., *SAVVY Vaginal Gel (C31G) for Prevention of HIV Infection: A Randomized Controlled Trial in Nigeria*. PLoS ONE, 2008. **3**(1): p. e1474.
192. Schwartz, J.L., et al., *Fourteen-day safety and acceptability study of the universal placebo gel*. Contraception, 2007. **75**(2): p. 136-141.
193. Phillips, D., *Intravaginal formulations to prevent HIV infection*. Perspectives in Drug Discovery and Design, 1996. **5**(1): p. 213-224.
194. Morcock, D.R., et al., *Elimination of Retroviral Infectivity by N-Ethylmaleimide with Preservation of Functional Envelope Glycoproteins*. J. Virol., 2005. **79**(3): p. 1533-1542.
195. Computer Integrated Systems for Microscopy and Manipulation. *Video Spot Tracker*. 2010 [cited 2010; Available from: <http://cismm.cs.unc.edu/downloads/>].
196. Cu, Y. and W.M. Saltzman, *Mathematical modeling of molecular diffusion through mucus*. Advanced Drug Delivery Reviews, 2009. **61**(2): p. 101-14.
197. Keller, M. and B. Herold, *Understanding Basic Mechanisms and Optimizing Assays to Evaluate the Efficacy of Vaginal Microbicides*. Sexually Transmitted Diseases, 2009. **36**(Supplement): p. S92-S95.
198. Kilmarx, P.H. and L. Paxton, *Need for a true placebo for vaginal microbicide efficacy trials*. The Lancet, 2003. **361**(9359): p. 785-786.
199. Mauck, C.K., et al., *Vaginal distribution of Replens and K-Y Jelly using three imaging techniques*. Contraception, 2008. **77**(3): p. 195-204.
200. Phillips, D.M., et al., *Mechanisms of sexual transmission of HIV: does HIV infect intact epithelia?* Trends in Microbiology, 1994. **2**(11): p. 454-458.
201. Collins, K.B., et al., *Development of an in vitro organ culture model to study transmission of HIV-1 in the female genital tract*. Nature Medicine, 2000. **6**(4): p. 475-479.
202. Gupta, P., et al., *Memory CD4+ T Cells Are the Earliest Detectable Human Immunodeficiency Virus Type 1 (HIV-1)-Infected Cells in the Female Genital Mucosal Tissue during HIV-1 Transmission in an Organ Culture System*. J. Virol., 2002. **76**(19): p. 9868-9876.

203. Hladik, F., et al., *Initial Events in Establishing Vaginal Entry and Infection by Human Immunodeficiency Virus Type-1*. *Immunity*, 2007. **26**(2): p. 257-270.
204. Roth, S., et al., *Effect of Topical Microbicides on Infectious Human Immunodeficiency Virus Type 1 Binding to Epithelial Cells*. *Antimicrob. Agents Chemother.*, 2007. **51**(6): p. 1972-1978.
205. Lackman-Smith, C., et al., *Development of a comprehensive human immunodeficiency virus type 1 screening algorithm for discovery and preclinical testing of topical microbicides*. *Antimicrobial Agents And Chemotherapy*, 2008. **52**(5): p. 1768-81.
206. Gupta, P., et al., *Use of Frozen-Thawed Cervical Tissues in the Organ Culture System to Measure Anti-HIV Activities of Candidate Microbicides*. *AIDS Research and Human Retroviruses*, 2006. **22**(5): p. 419-424.
207. Cummins, J.E., Jr., et al., *Preclinical Testing of Candidate Topical Microbicides for Anti-Human Immunodeficiency Virus Type 1 Activity and Tissue Toxicity in a Human Cervical Explant Culture*. *Antimicrob. Agents Chemother.*, 2007. **51**(5): p. 1770-1779.
208. Hu, Q.X., et al., *Blockade of attachment and fusion receptors inhibits HIV-1 infection of human cervical tissue*. *Journal of Experimental Medicine*, 2004. **199**(8): p. 1065-1075.
209. Fletcher, P., et al., *The nonnucleoside reverse transcriptase inhibitor UC-781 inhibits human immunodeficiency virus type 1 infection of human cervical tissue and dissemination by migratory cells*. *Journal of Virology*, 2005. **79**(17): p. 11179-11186.
210. Fletcher, P., et al., *Candidate polyanion microbicides inhibit HIV-1 infection and dissemination pathways in human cervical explants*. *Retrovirology*, 2006. **3**(1): p. 46.
211. Richardson-Harman, N., et al., *Multi-site comparison of anti-HIV microbicide activity in explant assays using a novel endpoint analysis*. *J. Clin. Microbiol.*, 2009: p. JCM.00673-09.
212. Forbes, B. and C. Ehrhardt, *Human respiratory epithelial cell culture for drug delivery applications*. *European Journal of Pharmaceutics and Biopharmaceutics*, 2005. **60**(2): p. 193-205.
213. Behrens, I., et al., *Nanoparticles in Human Intestinal Cell Lines and Rats: The Effect of Mucus on Particle Adsorption*. *Pharmaceutical Research*, 2002.

214. Behrens, I., et al., *Transport of Lipophilic Drug Molecules in a New Mucus-Secreting Cell Culture Model Based on HT29-MTX* Pharmaceutical Research, 2001.
215. Pontier, C., et al., *HT29-MTX and Caco-2/TC7 monolayers as predictive models for human intestinal absorption: Role of the mucus layer.* Journal of Pharmaceutical Sciences, 2001. **90**(10): p. 1608-1619.
216. Balimane, P.V., S. Chong, and R.A. Morrison, *Current methodologies used for evaluation of intestinal permeability and absorption.* Journal of Pharmacological and Toxicological Methods, 2000. **44**(1): p. 301-312.
217. Cecchelli, R., et al., *In vitro model for evaluating drug transport across the blood-brain barrier.* Advanced Drug Delivery Reviews, 1999. **36**(2-3): p. 165-178.
218. Mathias, N.R., F. Yamashita, and V.H.L. Lee, *Respiratory epithelial cell culture models for evaluation of ion and drug transport.* Advanced Drug Delivery Reviews, 1996. **22**(1-2): p. 215-249.
219. Dezzutti, C.S., et al., *In vitro comparison of topical microbicides for prevention of human immunodeficiency virus type 1 transmission.* Antimicrobial Agents And Chemotherapy, 2004. **48**(10): p. 3834-3844.
220. Guenther, P.C., W.E. Secor, and C.S. Dezzutti, *Trichomonas vaginalis-induced epithelial monolayer disruption and human immunodeficiency virus type 1 (HIV-1) replication: implications for the sexual transmission of HIV-1.* Infection and immunity, 2005. **73**(7): p. 4155-60.
221. Geonnotti, A.R., *Transport Phenomena in Anti-HIV Microbicide Delivery Vehicles,* in *Biomedical Engineering.* 2008, Duke University: Durham, NC.
222. Halpern, V., et al., *Effectiveness of Cellulose Sulfate Vaginal Gel for the Prevention of HIV Infection: Results of a Phase III Trial in Nigeria.* PLoS ONE, 2008. **3**(11): p. e3784.
223. Montefiori, D.C. *Standardized Assessments of Neutralizing Antibodies for HIV/AIDS Vaccine Development.* 2010 [cited 2010; Available from: <http://www.hiv.lanl.gov/content/nab-reference-strains/html/home.htm>.
224. Hammonds, J., et al., *Induction of Neutralizing Antibodies against Human Immunodeficiency Virus Type 1 Primary Isolates by Gag-Env Pseudovirion Immunization.* J. Virol., 2005. **79**(23): p. 14804-14814.

225. Henderson, M.H., et al., *Optical instrument for measurement of vaginal coating thickness by drug delivery formulations*. Review of Scientific Instruments, 2005. **76**(3): p. 034302-7.
226. Rosario, M.C., et al., *A pharmacokinetic-pharmacodynamic disease model to predict in vivo antiviral activity of maraviroc*. Clinical pharmacology and therapeutics, 2005. **78**(5): p. 508-19.
227. Rosario, M.C., et al., *A pharmacokinetic-pharmacodynamic model to optimize the phase IIa development program of maraviroc*. Journal of acquired immune deficiency syndromes (1999), 2006. **42**(2): p. 183-91.
228. Davenport, M.P., et al., *Understanding the mechanisms and limitations of immune control of HIV*. Immunol Rev, 2007. **216**: p. 164-75.
229. Perelson, A.S., *Modelling viral and immune system dynamics*. Nature Reviews Immunology, 2002. **2**(1): p. 28-36.
230. Perelson, A.S., et al., *HIV-1 dynamics in vivo: virion clearance rate, infected cell life-span, and viral generation time*. Science (New York, NY), 1996. **271**(5255): p. 1582-6.
231. Chakraborty, H., et al., *Viral burden in genital secretions determines male-to-female sexual transmission of HIV-1: a probabilistic empiric model*. AIDS (London, England), 2001. **15**(5): p. 621-7.
232. Geonnotti, A.R. and D.F. Katz, *Dynamics of HIV neutralization by a microbicide formulation layer: Biophysical fundamentals and transport theory*. Biophysical Journal, 2006. **91**(6): p. 2121-2130.
233. Geonnotti, A., et al., *Three-dimensional pharmacokinetic modeling of microbicide delivery by intravaginal rings within an MRI-derived finite-element vaginal compartment*, in *Microbicides 2008*. 2008: New Delhi, India.
234. Geonnotti, A.R. and D.F. Katz, *Compartmental transport model of microbicide delivery by an intravaginal ring*. Journal of Pharmaceutical Sciences, 2010(In press).
235. Henderson, M.H., et al., *Optical imaging and analysis of human vaginal coating by drug delivery gels*. Contraception, 2007. **75**(2): p. 142-51.
236. Henderson, M.H., et al., *Optical instrument for measurement of vaginal coating thickness by drug delivery formulations*. Review of Scientific Instruments, 2005. **76**(3).

237. Barnhart, K., E.S. Pretorius, and D. Malamud, *Lesson learned and dispelled myths: Three-dimensional imaging of the human vagina*. *Fertility And Sterility*, 2004. **81**(5): p. 1383-1384.
238. Greenhead, P., et al., *Parameters of Human Immunodeficiency Virus Infection of Human Cervical Tissue and Inhibition by Vaginal Virucides*. *J. Virol.*, 2000. **74**(12): p. 5577-5586.
239. Briggs, J.A., et al., *The mechanism of HIV-1 core assembly: insights from three-dimensional reconstructions of authentic virions*. *Structure*, 2006. **14**(1): p. 15-20.
240. Coggins, C., et al., *Preliminary safety and acceptability of a carrageenan gel for possible use as a vaginal microbicide*. *Sexually transmitted infections*, 2000. **76**(6): p. 480-3.
241. El-Sadr, W.M., et al., *Safety and acceptability of cellulose sulfate as a vaginal microbicide in HIV-infected women*. *AIDS (London, England)*, 2006. **20**(8): p. 1109-16.
242. Kilmarx, P.H., et al., *Safety and acceptability of the candidate microbicide Carraguard in Thai women: Findings from a phase II clinical trial*. *Journal of Acquired Immune Deficiency Syndromes*, 2006. **43**(3): p. 327-334.
243. Pendergrass, P.B., M.W. Belovicz, and C.A. Reeves, *Surface area of the human vagina as measured from vinyl polysiloxane casts*. *Gynecologic and Obstetric Investigation*, 2003. **55**(2): p. 110-113.
244. Cohen, M.S., et al., *Narrative review: antiretroviral therapy to prevent the sexual transmission of HIV-1*. *Annals of internal medicine*, 2007. **146**(8): p. 591-601.
245. Cohen, M.S. and C.D. Pilcher, *Amplified HIV transmission and new approaches to HIV prevention*. *The Journal of Infectious Diseases*, 2005. **191**(9): p. 1391-3.
246. Klasse, P.J., R.J. Shattock, and J.P. Moore, *Which topical microbicides for blocking HIV-1 transmission will work in the real world?* *PLoS Medicine*, 2006. **3**(9): p. e351.
247. Henderson, M.H., et al., *Optical instrument for measurement of vaginal coating thickness by drug delivery formulations*. *Review of Scientific Instruments*, 2005. **76**(3): p. 034302.
248. Kieweg, S.L., A.R. Geonnotti, and D.F. Katz, *Gravity-induced coating flows of vaginal gel formulations: in vitro experimental analysis*. *J Pharm Sci*, 2004. **93**(12): p. 2941-52.

249. Kieweg, S.L. and D.F. Katz, *Squeezing Flows of Vaginal Gel Formulations Relevant to Microbicide Drug Delivery*. Journal of Biomechanical Engineering, 2006. **128**(4): p. 540.
250. Kieweg, S.L. and D.F. Katz, *Interpreting properties of microbicide drug delivery gels: Analyzing deployment kinetics due to squeezing*. Journal of Pharmaceutical Sciences, 2007. **96**(4): p. 835-850.
251. Lai, B.E., et al., *Dilution of microbicide gels with vaginal fluid and semen simulants: Effect on rheological properties and coating flow*. J Pharm Sci, 2007. **97**(2): p. 1030-8.
252. Szeri, A., et al., *A model of transluminal flow of an anti-HIV microbicide vehicle: Combined elastic squeezing and gravitational sliding*. Physics of Fluids, 2008. **20**(8): p. 083101.
253. Pretorius, E.S., et al., *Magnetic resonance imaging to determine the distribution of a vaginal gel: before, during and after both simulated and real intercourse*. Fertility And Sterility, 2002. **78**(3): p. S24-S24.
254. Kieweg, S.L., *Mechanical Analysis of Vaginal Gels Intended for Microbicide Application*, in *Biomedical Engineering*. 2005, Duke University: Durham, NC.
255. Lai, B.E., et al., *Dilution of microbicide gels with vaginal fluid and semen simulants: Effect on rheological properties and coating flow*. Journal of Pharmaceutical Sciences, 2008. **97**(2): p. 1028-1036.
256. Pretorius, E.S., et al., *Magnetic resonance imaging to determine the distribution of a vaginal gel: before, during and after both simulated and real intercourse*. Fertility And Sterility, 2002. **78**(3): p. S24-S24.
257. Owen, D.H., et al., *Biophysical analysis of prototype microbicidal gels*. Journal of Pharmaceutical Sciences, 2007. **96**(3): p. 661-669.
258. Neves, J.D., et al., *Rheological Properties of Vaginal Hydrophilic Polymer Gels*. Current Drug Delivery, 2009. **6**: p. 83-92.
259. Barnhart, K., et al., *The optimal analysis of MRI data to quantify the distribution of a microbicide*. Contraception, 2006. **73**(1): p. 82-87.
260. Omar, R.F., et al., *Distribution of a vaginal gel Invisible Condom(R) before, during and after simulated sexual intercourse and its persistence when delivered by two different vaginal applicators: a magnetic resonance imaging study*. Contraception, 2008. **77**(6): p. 447-55.

261. Alliance for Microbicide Development. *Microbicide candidates in ongoing clinical trials summary as of September 2009*. 2009 [cited 2009; Available from: <http://www.avac.org/ht/a/GetDocumentAction/i/3109>].
262. Gray, R.H., et al., *Probability of HIV-1 transmission per coital act in monogamous, heterosexual, HIV-1-discordant couples in Rakai, Uganda*. The Lancet, 2001. **357**(9263): p. 1149-1153.
263. Wawer, M.J., et al., *Rates of HIV-1 transmission per coital act, by stage of HIV-1 infection, in Rakai, Uganda*. J Infect Dis, 2005. **191**(9): p. 1403-9.
264. Di Fabio, S., et al., *Inhibition of vaginal transmission of HIV-1 in hu-SCID mice by the non-nucleoside reverse transcriptase inhibitor TMC120 in a gel formulation*. Aids, 2003. **17**(11): p. 1597-1604.
265. Woolfson, A.D., et al., *Intravaginal ring delivery of the reverse transcriptase inhibitor TMC 120 as an HIV microbicide*. International Journal of Pharmaceutics, 2006. **325**(1-2): p. 82-9.
266. Wu, M., J.W. Roberts, and M. Buckley, *Three-dimensional fluorescent particle tracking at micron-scale using a single camera*. Experiments in Fluids, 2005. **38**(4): p. 461-465.
267. Peters, I.M., et al., *Three dimensional single-particle tracking with nanometer resolution*. Review of Scientific Instruments, 1998. **69**(7): p. 2762-2766.
268. Ram, S., et al., *High Accuracy 3D Quantum Dot Tracking with Multifocal Plane Microscopy for the Study of Fast Intracellular Dynamics in Live Cells*. Biophysical Journal, 2008. **95**(12): p. 6025-6043.
269. Saltzman, W.M., et al., *Antibody diffusion in human cervical mucus*. Biophys. J., 1994. **66**(21): p. 508-515.
270. Lang, I., M. Scholz, and R. Peters, *Molecular mobility and nucleocytoplasmic flux in hepatoma cells*. J. Cell Biol., 1986. **102**(4): p. 1183-1190.
271. Pluen, A., et al., *Diffusion of Macromolecules in Agarose Gels: Comparison of Linear and Globular Configurations*. Biophysical Journal, 1999. **77**(1): p. 542-552.
272. Braga, J., J.M.P. Desterro, and M. Carmo-Fonseca, *Intracellular Macromolecular Mobility Measured by Fluorescence Recovery after Photobleaching with Confocal Laser Scanning Microscopes*. Mol. Biol. Cell, 2004. **15**(10): p. 4749-4760.

273. Amu, T.C., *Activation enthalpy of diffusion for well fractionated dextrans in aqueous solutions*. *Biophysical Chemistry*, 1982. **16**(4): p. 269-273.
274. Gribbon, P. and T.E. Hardingham, *Macromolecular Diffusion of Biological Polymers Measured by Confocal Fluorescence Recovery after Photobleaching*. *Biophysical Journal*, 1998. **75**(2): p. 1032-1039.

Biography

Bonnie Lai (born February 4, 1983 in Lansing, Michigan) matriculated at Duke University in August 2005 to pursue a PhD in biomedical engineering. While at Duke, she was the recipient of the National Science Foundation Graduate Research Fellowship (2005-2010), The James B. Duke Fellowship (2005-2009), and the Pratt-Gardner Fellowship (2005-2006). Bonnie was also a member of the Biomedical Engineering Society and the Sigma Xi Scientific Research Society.

Prior to arriving at Duke, Bonnie received her BS from Northwestern University in June 2005, where she majored in both Biomedical Engineering and Art Theory and Practice. During college, Bonnie saw a performance of Eve Ensler's *The Vagina Monologues* that sparked her interest in women's health. Bonnie cultivated this interest by volunteering as a Reproductive Health Educator at Northwestern's Health Services center and by researching methods for culturing ovarian cells *in vitro* in the labs of Professors Lonnie Shea and Teresa Woodruff.

Bonnie was drawn to Duke by the opportunity to study two of her favorite subjects simultaneously: women's health and transport phenomena. While living in North Carolina, Bonnie's hobbies included practicing Ashtanga yoga and visiting the Durham Farmers' Market on Saturday mornings.

Peer-reviewed articles:

Lai, B.E., M.H. Henderson, J.J. Peters, D.K. Walmer, D.F. Katz, *Transport theory for HIV diffusion through in vivo distributions of topical microbicide gels*. Biophysical Journal, 2009. **97**(9): p. 2379-2387.

Lai, B.E., Y. Xie, M.L. Lavine, A.J. Szeri, D.H. Owen, D.F. Katz, *Dilution of microbicide gels with vaginal fluid and semen simulants: Effect on rheological properties and coating flow*. Journal of Pharmaceutical Sciences, 2008. **97**(2): p. 1028-1036.

Jay, J.I., **B.E. Lai**, D.G. Myszka, A. Mahalingam, K. Langheinrich, D.F. Katz, P.F. Kiser, *Multivalent Benzoboroxole Functionalized Polymers as gp120 Glycan Targeted Microbicide Entry Inhibitors*. Molecular Pharmaceutics, 2010. **7**(1): p. 116-129.

Berkholtz, C.B., **B.E. Lai**, T.K. Woodruff, L.D. Shea, *Distribution of extracellular matrix proteins type I collagen, type IV collagen, fibronectin, and laminin in mouse folliculogenesis*. Histochemistry and Cell Biology, 2006. **126**(5): p. 583-592.